The Roles of Cytoplasmic Aspartate Aminotransferase in *Trypanosoma brucei.*

By

Paul Barry

Trinity College Dublin
Coláiste na Tríonóide, Baile Átha Cliath
The University of Dublin

A thesis submitted to the University of Dublin in candidature for the degree of Doctor of Philosophy.

Supervisor: Dr. Derek Nolan.

School of Biochemistry and Immunology,
Trinity College Dublin,
Dublin, Ireland.

Submitted March 2017.

Declaration.

I declare that this thesis has not been submitted as an exercise for a degree at this or any other university and it is entirely my own work, with the following exceptions;

- The generation of the crystal structure of *T. cruzi* cASAT was performed by Dr. Amir Khan, Trinity Biomedical Sciences Institute, Trinity College Dublin.
- Mass spectrometry analysis was performed in collaboration with Glasgow Polyomics.
- Investigations of the roles of *T. brucei* secreted aromatic ketoacids in host inflammation were performed in collaboration with the Inflammation Research (Prof. Luke O'Neill) and Molecular Immunology (Dr. Aisling Dunne) groups of the Trinity Biomedical Sciences Institute, Trinity College Dublin.
- Identification of indolepyruvate breakdown products was performed in collaboration with Dr. Paul Evans, UCD School of Chemistry and Chemical Biology, University College Dublin.

I agree to deposit this thesis in the University's open access institutional repository or allow the Library to do so on my behalf, subject to Irish Copyright Legislation and Trinity College Library conditions of use and acknowledgement.

Name: Paul Barry.

Year: 2017

Abstract.

African trypanosomes cause sleeping sickness (trypanosomiasis), a debilitating disease that affects both humans and wild or domestic animals. Trypanosomiasis is accompanied by alterations in the levels of host circulating aromatic amino acids, and an increased excretion of aromatic ketoacids by the host. Here, the role of a cytoplasmic aspartate aminotransferase (cASAT) in *T. brucei* is investigated using multiple experimental approaches.

Using a combination of RNAi and enzymatic assays, it is shown that cASAT activity is essential for the growth and viability of the bloodstream form of *T. brucei*, but not the procyclic form, and that reduction of of TbcASAT activity leads to a corresponding decrease in parasite-secreted aromatic ketoacids. Preliminary ^{15}N-tryptophan metabolomic analysis suggests that TbcASAT may play an important role in both pyrimidine biosynthesis and purine salvage, which may explain the lethality of cASAT ablation. Purification of recombinant cASAT from *T. brucei* (TbcASAT) and *T. cruzi* (TccASAT) allowed enzymatic assays and crystallisation trials to be undertaken. The enzymatic assays revealed that both enzymes have broad substrate specificities, but have a notable preference for the utilisation of aromatic amino acids in transamination reactions. The preferred α-ketoacid amino acceptor in these transamination reactions appears to be oxaloacetate. It is possible that this preference for oxaloacetate is used to generate aspartate for metabolic purposes, and precludes the possibility of a methionine salvage pathway functioning in *T. brucei*.

The rates of secretion of aromatic ketoacids have been determined for the first time. These rates are significantly high, and suggest that the increase in host circulating aromatic ketoacids is entirely due to secretion by *T. brucei*. Moreover, a combination of ^{13}C-NMR and RNAi techniques has been used to demonstrate that the

aromatic ketoacid indolepyruvate is produced by TbcASAT catalysed deamination of L-tryptophan. Detailed ^{1}H-NMR studies have been performed to clarify the chemical stability of indolepyruvate. Under oxidative conditions, indolepyruvate degrades into other indolic compounds. Two of these breakdown products have been partially identified. Determination of the stability of indolepyruvate proved crucial to the establish the nature of the compound when used in immunological studies.

Aromatic ketoacids secreted by bloodstream form *T. brucei* can modulate portions of the host inflammatory response, as demonstrated with murine BMDMs. This was observed primarily in the decrease of pro-IL-1β production by LPS-stimulated BMDMs in response to treatment with indolepyruvate. Initial data shows that aromatic ketoacids may also modulate other inflammatory responses, such as the glial cells of the CNS. Aromatic ketoacids have been demonstrated to decrease the production of some inflammatory cytokines in these cells and are potent inducers of the anti-inflammatory cytokine, HO-1.

It is hypothesised that the preference for aromatic amino acids as substrates developed as consequence of the need to modulate the host immune system, perhaps at times of high parasitemia, to promote the survival of the host and allow the parasite to be successfully re-transmitted. Thus, the ability of cASAT is used to generate aromatic ketoacids for secretion into the host extracellular environment would be predicted to be a feature of trypanosomes capable of antigenic variation, e.g. *T. brucei*, *T. congolense*, and *T. evansi*, amongst others.

Acknowledgements.

As is the case with any body of research, the work within would not have been possible without the help and support of so many individuals.

I would firstly like to give my sincere thanks to my supervisor, Dr. Derek Nolan. I will always be grateful for his invaluable guidance over the past few years, which has lead me to be a vastly better scientist than I could have ever achieved on my own. He has always maintained the encouragement and understanding that has allowed me to perform this research in an organic manner. Dr. Paul Voorheis also deserves special recognition for providing stimulating conversation, and for allowing me to pester him with questions at any time of the day.

There are many people who have helped me with this research, but Sarah and Glyn deserve a special mention. It has been fun working with both of you to make some of this research possible. A sincere thanks to all the people who I have collaborated with and who gave their time to me, while asking for nothing in return. I would like to thank Glynis Robinson and the teaching staff of the 3rd floor, who have been nothing but helpful and patient, I will miss demonstrating immensely. Thanks also to Liam and Noel, who have managed to repair more things for me than I can count.

The past and current members of the trypanosome lab deserve a prominent nod. Jenni, who taught me almost everything I know and who helped me find my way when I felt lost at the start. Rob, who has been a fine friend and a well of knowledge for many years (and a decent flatmate to boot). And Louise, whose humour and wit made the last year of the PhD more fun than it should have been at times.

I will never forget my time in the 5th floor reading room. The people who have been in and out of its doors (at all hours!) are amongst some of the finest people I have

ever had the privilege of knowing. Thank you all for the laughter and fun! A special thanks to Nidhi for our thought-provoking debates and philosophising, Darren for his casual banter and impish mischief, and Niki for her support and constant friendship. And Nadine, thank you for all chats over fish and chips!

Thank you Mam and Dad, who I'm sure still don't know quite what this research is about, but always asked about it with interest! You have been there for me whenever I needed you. Anna, Louise, and Orlagh have always managed to make me smile when I least expected it. I am so lucky to have such a wonderful family.

Finally, I want to extend my heart-felt gratitude and love to Aoife, without whom I never would have made it this far. Thank you for your encouragement, support, and for always believing in me.

"*It's okay to find the faith to saunter forward*
There's no fear of shadows spreading where you stand
And you'll breathe easier just knowing that the worst is all behind you
And the waves that tossed the raft all night have set you on dry land."

John Darnielle - The Mountain Goats.

Contents

List of Figures

List of Tables

Abbreviations.

AAT ..... Alanine aminotransferase

ASAT ..... Aspartate aminotransferase

ATP ..... Adenosine triphosphate

ADP ..... Adenosine diphosphate

AHADH ..... Aromatic α-hydroxy acid dehydrogenase

APOL-1 ..... Apolipoprotein L1

Avg. ..... Average

BLAST ..... Basic Local Alignment Search Tool

BMDM ..... Bone marrow derived macrophage

BSAT ..... Broad specificity aminotransferase

cASAT ..... Cytoplasmic aspartate aminotransferase

DAPI ..... 4',6-diamidino-2-phenylindole

DCM ..... Dichloromethane

ddH_2O ..... Deionised distilled water

DHICA ..... 5,6-dihydroxyindole-2-carboxylic acid

DMSO ..... Dimethyl sulfoxide

D-dopa ..... D-dopachrome

dsRNA ..... Double-stranded ribonucleic acid

DSS ..... 4,4-dimethyl-4-silapentane-1-sulfonic acid

EDTA ..... Ethylenediaminetetraacetic acid

EtBr ..... Ethidium bromide

FBS/FCS ..... Fetal bovine/calf serum

HEPES ..... 4-(2-hydroxyethyl)-1-piperazineethanesulfonic acid

HMI-9 ..... Hirumi modified Iscove's medium, formulation 9

HPLC ..... High performance liquid chromatography

HPP ..... Hydroxyphenylpyruvate

HRP ..... Haptoglobin-related protein

IDO ..... indoleamine 2,3-dioxygenase

IgG ..... Immunoglobulin G

IgM ..... Immunoglobulin M

IP/IPA ..... Indolepyruvate

LIC ..... Ligation-independent cloning

LPS ..... Bacterial lipopolysaccharide

MITat ..... Molteno Institute Trypanozoon antigen type

mRNA ..... Messenger RNA

MW ..... Molecular weight

ML ..... Molecular ladder

ORF ..... Open reading frame

PBS ..... Phosphate buffered saline

PCR ..... Polymerase chain reaction

PEG ..... Polyethylene glycol

PP ..... Phenylpyruvate

qRT-PCR ..... Quantitative reverse transcription PCR

RNAi ..... Ribonucleic Acid Interference

rRNA ..... Ribosomal RNA

SD ..... Standard deviation

SDS ..... Sodium dodecyl sulphate

SDS-PAGE ..... SDS-Polyacrylamide gel electrophoresis

T. brucei ..... *Trypanosoma brucei brucei*

T. gambiense ..... *Trypanosoma brucei gambiense*

T. rhodesiense ..... *Trypanosoma brucei rhodesiense*

TBS ..... Tris buffered saline

TLF-1/2 ..... Trypanosome lytic factor 1/2

TMS ..... Tetramethylsilane

Tris ..... Tris(hydroxymethyl)aminomethane

v/v ..... volume per volume

w/v ..... weight per volume

Chapter 1

Introduction

The genus Trypanosoma is comprised of several species of parasitic eukaryotic unicellular protozoa, with all species containing a single flagellum and kinetoplast structure [1]. Trypanosomes can be broadly split into two groups; the African trypanosomes, of the Salivarian group, which are the causative agent of African sleeping sickness in mammals in sub-saharan Africa, and the Stercoraria group, which are found in South America and are the causative agent of Chagas' disease [1, 2]. Within these groups two species have been more extensively studied than any other; the African *Trypanosoma brucei* (referred to as *T. brucei* throughout this text), and the South American *Trypanosoma cruzi* (*T. cruzi*). Since *T. brucei* is the focus of the majority of our investigation it will be discussed at length, whereas only a brief overview of *T. cruzi* shall be provided.

1.1 *Trypanosoma brucei.*

1.1.1 *T. brucei*: a brief historical & evolutionary context.

Historical background.

It was Gruby who established the genus *Trypanosoma*, a word derived from the Greek trūpān meaning *'to bore'* and sōma meaning *'body'*, when he first discovered the parasite *T. sanguinis* in frogs in 1843 [3]. There are many records of disease that were likely trypanosome aetiological diseases prior to their initial classification; Steverding notes that trypanosomes were likely influential in breeding and grazing habits of peoples of the Nile valley, and even highlights a suspected case of sleeping sickness in a Malian Emperor in 1373 [4]. There are subsequent reports of sleeping sickness-like symptoms from multiple sources during the 1700s [5]. The period from the 1840s to 1910s was particularly fruitful in establishing multiple species of trypanosomes in various hosts, such as frogs [3], rats, mice, voles, and horses, to name a few [4, 5].

In 1895, Sir David Bruce first discovered *T. brucei brucei* in the blood of horses and also correctly linked the transmission of the parasite from infected animals to healthy ones to the tsetse fly (Fig. 1.1) [6]. Following this discovery, in 1901 Forde and Dutton discovered the first trypanosomes in humans, *T. gambiense* (now *T.b. gambiense*), and in 1910 Stevens and Fantham discovered *T. rhodesiense* (now *T.b. rhodesiense*) [7].

Initially Sir David Bruce believed that *T. rhodesiense* was the human infective form of *T. brucei* [8], but the epidemiological differences in the disease that arose in infectecd hosts (acute vs chronic) helped clarify that it was a distinct subspecies of *T. brucei* [5]. Sir David Bruce also hypothesised that the transmission of *T. brucei* was mechanical [6], which remained the *de facto* viewpoint until experiments by Kline [4, 5] revealed a cyclical transmission cycle for *T. brucei* in the tsetse fly, which Sir David Bruce later expanded upon into a developmental cycle for the parasite [8].

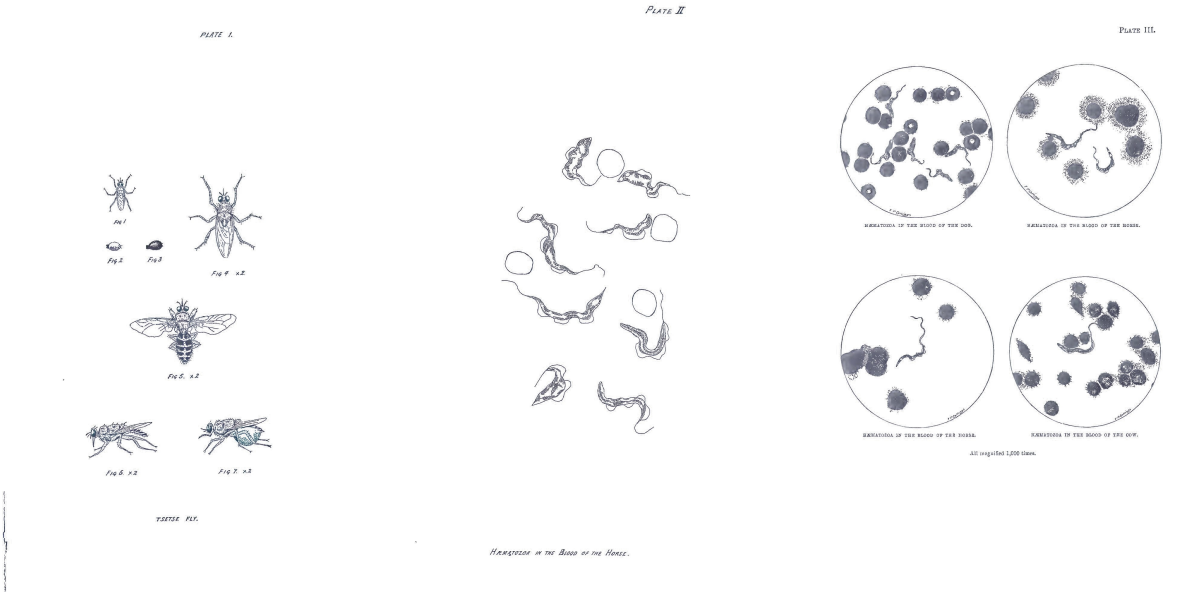

(a) tsetse Fly.

(b) Hematozoa in Horse blood.

(c) Hematozoa in multiple mammals

Figure 1.1. Sketches by Sir David Bruce.
A collection of original sketches by Sir David Bruce, from his report on the prevalence of sleeping sickness in Zululand [6].

Evolution.

The eukaryotic *T. brucei* is a species of the genus *Trypanosoma*, of the family Trypanosomatidae, and the order Kinetoplastida. Two separate studies using 18s rRNA gene comparison estimate the emergence of the species to between 100 million [9] and 300 million [10] years ago, when *T. brucei* and *T. cruzi* diverged into Africa and South America, respectively. *T. brucei* constitutes its own clade, although whether it is monophyletic or polyphyletic in nature continues to be debated [11]. The current view lends support to a monophyletic clade [12]. The debate likely arose in part due to over re-

liance on data from 18s rRNA sampling [13] and biased or skewed taxonomy sampling [2]. Analysis of other molecular markers, such as heat shock protein 70 (HSP70) [14], has expanded the molecular repertoire on which taxonomic relationships can be established. For example, Fraga et al. have concatenated 3 markers (SSU rRNA, GAPDH, and their own HSP70 data) to further establish these relationships, including clear separation of aquatic and terrestrial clades of Trypanosoma (Fig. 1.2) [12]. Despite this progress many tricky taxonomies remain to be clarified, such at the relationships of *T. vivax, T. theileri,* and *T. cruzi* to both Salivarian and Stecorian groups [11, 12].

Given the predicted dating of the emergence of *T. brucei* within Africa, it is generally accepted that the parasite has co-evolved with the species of the *Homo* genus. Indeed, this is evident in the 'arms race' that exists between primates and *T. brucei* subspecies. Humans have evolved two innate mechanisms to prevent systemic trypanosome infection, termed trypanosome lytic factor 1 (TLF-1) and 2 (TLF-2) [15]. Both TLFs confer resistance to the *T. brucei* subspecies through different but similar mechanisms; TLF-1 is primarily composed of high density lipoprotein, whereas TLF-2 is lipid poor and rich in IgM proteins. Considering the similarity of their mechanisms of action it is likely that both TLFs are one and the same when acting to kill the parasite; each TLF type contains a combination of haptoglobin related protein (HRP) and apolipoprotein-L1 (APO-L1) [16]. Once internalised, APO-L1 acts by inserting into the membrane of lysosomes and forming a pore which leads to the disruption of the osmotic balance of the cell. Consequently, either mechanical lysis of the cell due to lysosomal swelling or disruption of the cell due to digestive enzyme leakage occurs [15]. It has been demonstrated more recently that in addition to lysosomal swelling, APO-L1 can cause mitochondrial membrane disruption in *T. brucei* [17]. This is mediated through the transport of APO-L1 from endosomes to the mitochondria by a kinesin motor protein, where APO-L1 then causes the release of an endonuclease from the mitochondria that leads to DNA fragmentation.

Both *T. rhodesiense* and *T. gambiense* have evolved separate mechanisms to evade the action of TLFs. A serum resistance (SRA) gene is expressed by *T. rhodesiense* which encodes for a truncated form of variant surface glycoprotein (VSG) [15]. This truncated VSG can bind internalised APO-L1, preventing its pore forming function. Interestingly, the *T. brucei* species is the only known member of the kinetoplastid class

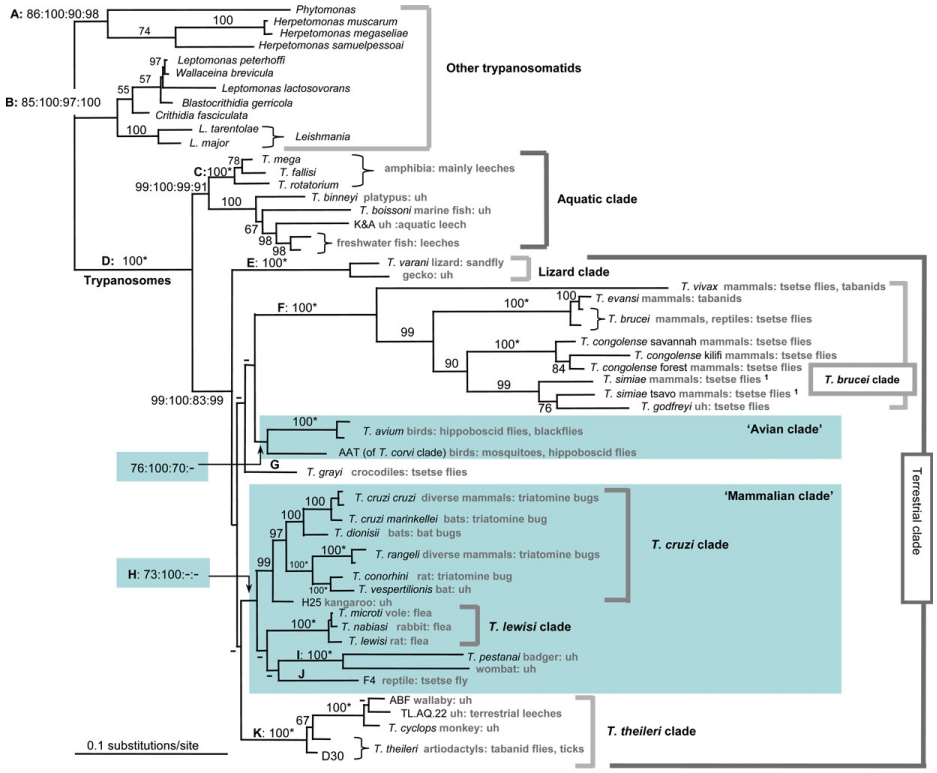

Figure 1.2. Phylogeny of Trypanosoma. Phylogenetic relationships of Trypansoma based on SSU rRNA and GAPDH concatenation. *T. brucei* can be seen to form its own distinct clade. Taken from Hamilton et al [21].

that can undergo genetic exchange (although binary fission is the method of reproduction) [18]. It has been suggested that genetic exchange could actively occur between *T. brucei* subspecies - it is possible to transfer the SRA gene from *T. rhodesiense* into *T. brucei* and confer resistance to human serum [15]. A different mechanism is utilised by *T. gambiense* to negate the activity of TLFs. Again, a VSG-related protein is used (unrelated to SRA), termed *Tgs*GP, in combination with other processes [15]. The *Tgs*GP acts by stiffening the cell membranes of *T. gambiense* which prevents APO-L1 insertion, while cysteine proteases aid the removal of APO-L1 [19]. Finally, it is evident that this arms race is continually active. There is speculative evidence that some human populations in Africa may be expressing novel APO-L1 variants associated with kidney disease that seem to allow the hosts to lyse *T. rhodesiense*. The authors postulate that while the homozygous carriers of this variant suffer from debilitating kidney disease, heterozygous carriers do not [20]. It is possible that heterozygous carriers of the APO-L1 variant have an advantageous resistance to *T. rhodesiense*, while also having a normal risk of kidney disease, in a manner similar to that of malaria and sickle-cell anaemia.

1.1.2 *T. brucei* epidemiology.

T. brucei is endemic to mammals of sub-Saharan Africa, where its subspecies cause the disease trypanosomiasis, also termed sleeping sickness. In humans trypanosomiasis is resultant from infection with *T. gambiense* or *T. rhodesiense*, the former causing a slow onset, chronic form of the disease, whereas the latter causes a faster onset, acute disease progression [22]. The presence of circulating APO-L1 within the blood of humans confers resistance to infection by *T. brucei* [23, 24]. The parasite can still cause large socio-economic problems as it negatively affects the health of livestock such as cattle, in which the disease is termed Nagana [25, 26]. While subspecies other than *T. gambiense* or *T. rhodesiense* are considered non-infective to humans, there have been few documented cases of atypical infections by these subspecies in humans, including infection with *T. brucei* – a sign perhaps, of emerging pathogenicity [27]. African trypanosomiasis is considered a neglected tropical disease due to its low infection and mortality rates when compared to other parasitic diseases such as malaria, with just under 10,000 cases of the disease reported in 2009 [16] and 2012 [25]. However, significant under reporting has led to estimates of 20,000 – 70,000 cases of the disease occuring per year in Africa [16, 22, 25]. Whilst not currently not a major human disease then, it remains a highly important veterinary disease due its massive economic impacts from losses in animal productivity [28].

African trypanosomiasis is a vector born disease of the tsetse fly of the *Glossina* genus, which is geographically located across sub-Saharan Africa [29]. The different subspecies of *T. brucei* are transmitted by different species of *Glossina*. Of the human pathogens *T. rhodesiense*, which is found primarily in East Africa, is a zoonose which is carried by the 'savannah' species of tsetse, *Glossina morsitans* and *Glossina pallidipes*. In West Africa *T. gambiense* is the major subspecies of *T. brucei* and is transmitted by the 'riverine' species of tsetse, *Glossina palpalis* [30, 31]. Both *T. gambiense* and *T. rhodesiense* share a vector in the *Glossina fuscipes* [31], which may be facilitating the spread of *T. rhodesiense* into Uganda where it has the potential to become co-endemic with the native *T. gambiense* and has complicated treatment efforts [32, 33]. Unlike *T. rhodesiense*, *T. gambiense* is an anthroponotic disease and is considered more suited to eradication since the interruption of *T. rhodesiense* transmission in animal hosts is unlikely to be feasible [34].

The transmission path remains the same in all subspecies of *T. brucei*. The tsetse fly must first take a blood meal from an infected mammal, with the pre-adapted metacyclic form of the parasite entering the gut of the fly. Following further differentiation of the parasite within the fly (section 1.1.3) it can be transmitted to a new host via a bite during feeding [26]. Trypanosomiasis is a disease which has two characteristic stages; stage 1 consists of initial infection and a haemolymphatic phase, while the stage 2 is characterised by the parasites invasion of the central nervous system (CNS) and other internal organs (encephalitic phase) [22]. In stage 1 the parasites utilise the lymph system to enter the bloodstream and other organs, where they can survive and proliferate. Fever, malaise and weight loss are symptomatic features of stage 1, but other more severe symptoms may also be evident, such as cardiac failure. In stage 2 the parasite crosses the blood brain barrier and invades the CNS. More severe symptoms such as disrupted sleep and psychiatric disorders are common, and without treatment death invariably occurs. The duration of the chronic infection with *T. gambiense* has been estimated to be approximately 3 years, divided equally between stage 1 and 2 of the disease [16]. The more acute form of trypanosomiasis is caused by *T. rhodesiense*, which typically lasts a few weeks or months. However, the acute form only accounts for around 2% of all disease cases [22, 34].

Current treatments for trypanosomiasis are not wholly effective and are difficult to administer, while the most suitable method of reducing/eradicating the disease remains undecided. Since a vaccine for trypanosomiasis seems unlikely to be developed due to antigenic variation of the parasites external VSG coat [35, 36], drugs and vector control remain the best prospects for tackling the disease. Drug treatment of diseased hosts is problematic as drugs must be selected that target both the specific subspecies of *T. brucei* infecting the host and for the specific stage of the disease. Identification of the disease form and stage is not ideal either; while a card agglutination test (CATT) can be used to positively identify *T. gambiense* infection, a lumbar puncture and cerebrospinal fluid (CSF) examination must be performed to confirm if it is stage 1 or stage 2 of the disease [16]. Clinical tests do not yet exist to help positively identify a *T. rhodesiense* infection, identification is instead based on symptom presentation. There are currently on-going efforts to develop all-in-one dual species identification tests using PCR techniques which are yielding promising results [16, 37]. The period of drug administration itself can also be difficult – for example, Eflornithine (used for *T. gambiense* stage 2

treatment) must be administered intravenously every 6 hours for 14 days. Nifurtimox, which is used to treat the late stage of African trypanosomiasis and Chagas disease, can have adverse effects on the patients such as neurological toxicity and gastrointestinal upset. The period of treatment and drug dosage for Nifurtimox are also relatively high (8 - 10 mg/kg body weight, for 90 days) [38, 39]. There are, however, a number of promising drugs currently in development, and combination therapies using existing drugs are proving somewhat effective [16, 22, 26]. Of these new developmental drugs, one recent discovery has proved particularly promising. GNF6702, a drug developed by screening 3 million compounds for growth inhibitory activity and then optimising hits, was found to be highly effective at clearing both *T. brucei* and *T. cruzi* infections in mice (in addition to being effective against Leishmaniasis) by non-competitively targeting the parasites proteasome [40]. Research into anti-trypanosomal drugs will continue, with hope that new drugs will help eliminate sleeping sickness by 2020 [41].

In the early 20th century trypanosomiasis was effectively epidemic, being the cause of almost 800,000 deaths in a 10 year period alone [4, 42]. This prompted extensive investment in tsetse control and human population screening for the disease, which almost lead to the eradication of trypanosomiasis by the 1960's [26]. Unfortunately due to unstable governments and economic difficulties, as well as a drop in the vigilance of control programmes, trypanosomiasis has experienced a resurgence in the last 30 years, though not to the epidemic levels previously experienced. While screening human and animal populations for infection has proven effective in reducing trypanosomiasis, it is generally agreed that the main method of future disease prevention should be eradication of the tsetse fly as a parasite vector [28, 43, 44]. Control of the disease has been restricted in recent decades to non-environmentally intrusive methods in preference to the use of harmful pesticides. For example, baiting traps deployed by governments and local communities have proven effective at reducing tsetse prevalence but not in its complete eradication. It has been estimated that complete eradication of the tsetse fly would cost approximately US$ 20 billion, but the economic benefits from doing so could be in the region of US $ 50 billion over a 10 year period [28, 43].

1.1.3 Life cycle.

Due to its obligate nature, the trypanosome undergoes an extraordinarily diverse life cycle involving mass changes in cell morphology, gene, and protein expression. These changes are necessary for its survival in the distinctly different environments of its animal and fly hosts [45]. The life cycle of *T. brucei* can be broadly divided into two distinct stages; the procyclic life stage in the tsetse fly, so named because of the external procyclin coat expressed on its cell body, and the bloodstream stage in its infected animal host (where variant surface glycoprotein is alternatively expressed on the cell surface) [46]. An uninfected male or female tsetse fly must first ingest trypanosomes from a previously infected mammalian host during blood meals. These trypanosomes are typically in their short, stumpy trypomastigote form, which are a non-dividing subset of bloodstream form cells that have been pre-adapted for uptake by the fly [47]. It is thought that temperature changes and proteases in the fly mid-gut trigger differentiation of the trypomastigote form trypanosome into its early procyclic stage [48]. This differentiation can be triggered *in vitro*, by a combination of the addition of cis-aconitate to cultured cells or depletion of glucose, and a lowering of the culturing temperature to 27 ^{o}C [47, 49]. Further differentiation into the mature procyclic form occurs in the gut, followed by mesocyclic form in the anterior gut, and to epimastigote form in the salivary glands, where the trypanosomes proliferate readily. Finally the cells enter a non-proliferative metacyclic trypomastigote form which can infect potential human and animal hosts. Upon biting of the prospective host by the fly, the infectious metacyclic cells enter the bloodstream. Here they are induced to undergo transformation into the long, slender trypomastigote form which proliferates and spreads through the lymph and blood systems [50] (Fig. 1.3). This proliferation is characteristic of stage 1 of trypanosomiasis, while eventual invasion of the organs and CNS by these long, slender forms is characteristic of stage 2 of the disease. Some cells in the animal host will further differentiate back to the stumpy form and will be able to be taken up again during a tsetse fly blood meal. Only these differentiated stumpy form cells will be viable in the fly gut [45, 48].

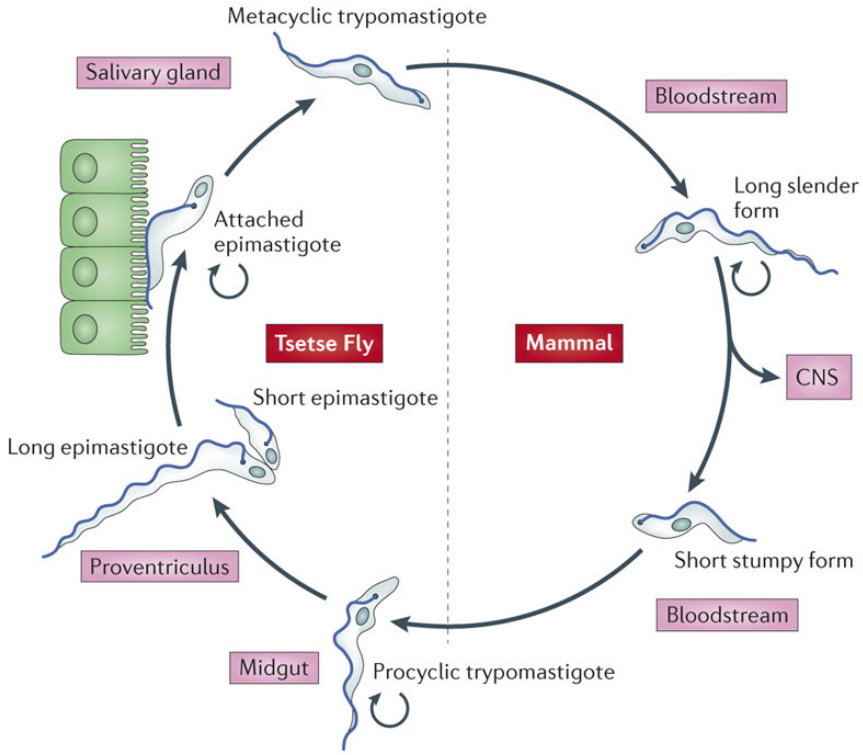

Figure 1.3. The life cycle of *T. brucei*. Figure modified from [51].

1.1.4 Cell structure.

Trypanosomes are unicellular, mono-flagellated eukaryotic cells. They possess single copies of organelles common to all eukaryotic cells such as a nucleus, extensive endoplasmic reticulum, Golgi apparatus, and single mitochondria (Fig. 1.4a). They also contain many unique structures such as basal bodies, which are found at the posterior ends of the flagellum within the cell body, and the kinetoplast, which is attached to the mitochondrion and contains the mitochondrial DNA [52]. The single flagellum of T. brucei is attached to the body of the cell, from the posterior end of the cell extending towards the anterior, culminating in a free, detached distal tip. The body of the cell is supported by a network of polarized 24 nm diameter microtubules in an even helical array, termed the sub-pelicular corset. It is a strong, stable structure which determines cell shape and has an important role in maintaining the relative positions of the organelles within the cell body. Cell size varies depending on the specific life cycle stage, with procyclic cells typically 20 – 25 μm in length. Bloodstream form cells are typically long and slender, and can be anywhere up to 40 μm long (Fig. 1.4b) [53].

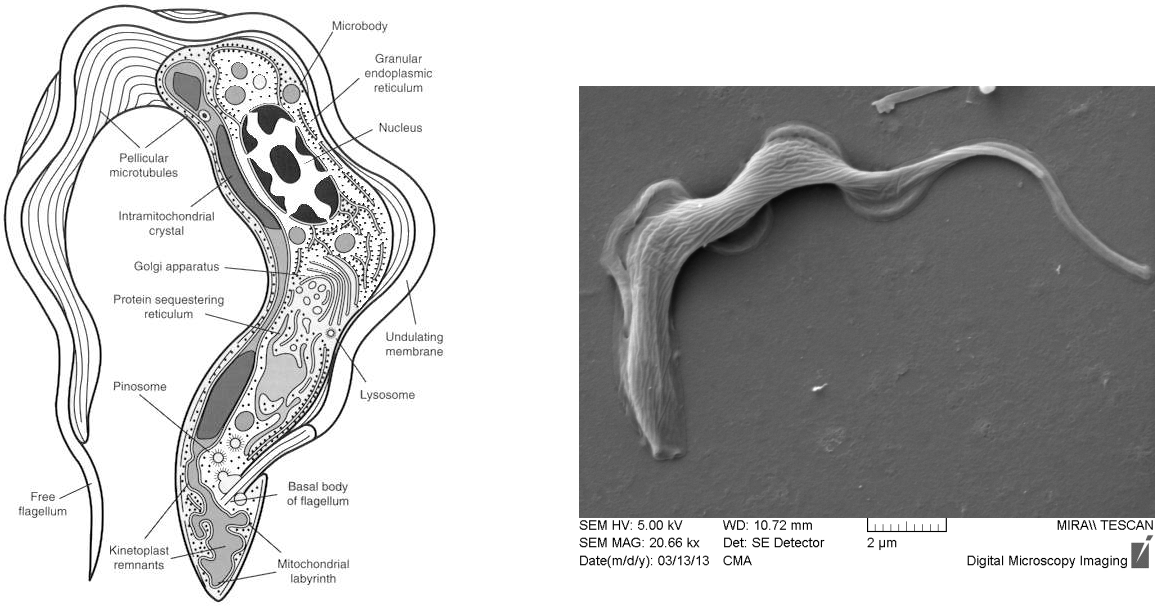

(a) **(b)**

Figure 1.4. The cell structure of *T. brucei*.
(a) Illustrated diagram of the cell structure of *T. brucei*, taken from [54]. **(b)** Scanning electron microscope image of bloodstream form *T. brucei*.

1.2 *Trypanosoma cruzi.*

1.2.1 *T. cruzi* epidemiology.

The *T. cruzi* parasite is found widely distributed in the Central and Southern American continent, where is causes a form of trypanosomiasis termed Chagas' disease [22]. Unlike *T. brucei*, there are no strict subspecies of *T. cruzi* but rather two distinct lineages as defined by molecular typing, type 1 and type 2 [55]. The type 1 lineage is predominantly found in non-domestic, sylvatic mammals, whereas type 2 is constrained to human habitations in a peridomestic fashion and is the major cause of Chagas' disease [56]. Chagas' disease had a prevalence of approximately 10 million cases in 2005, with 28 million people at risk of infection [57]. In the United States alone more than 100,000 people are chronically infected with *T. cruzi*, largely due to mass Latin American migration into the country [58].

Triatomine insects, commonly referred to as 'assassin bugs', are the natural transmissive vector of *T. cruzi*, although other modes of transmission such as organ donation or blood transfusion from an infected to non-infected individual can occur [59]. Typi-

cally when a Triatomine insect is taking a blood meal at night it deposits faecal matter near the bite site, which contains the infective trypomastigote cells [60]. The trypomastigotes may enter the body through mucosal surfaces or through broken skin, including the site of the original bite [56], which may be aided by host scratching the bite area. Risk of infection remains low, with an estimated risk of infection of 0.1% through a Triatomine route [61], 20% through blood transfusion, and 1 – 10% risk of congenital infection [56]. Like African trypanosomiasis, Chagas' disease is typified by two distinct stages, an acute stage and a chronic stage [22, 56]. In the acute stage symptoms are evident within 6 – 10 days post-infection, although the disease is can often be asymptomatic [62]. Parasites are readily detected in the blood despite low load levels, and PCR testing can be used to successfully confirm a *T. cruzi* infection in a quantitative and qualitative manner [63]. Non-specific symptoms can include malaise, fever, enlarged liver and spleen, and possible oedema. More obvious symptoms can be present if a patient is examined using electrocardiograms (ECG), such as cardiac arrhythmia's and abnormal ECG signals. Cardiac complications are the main cause of death in the acute stage of the disease [64].If the disease is diagnosed correctly the outlook is generally good following treatment, with mortality estimated to be between 5 – 10% [62]. Chronic Chagas' disease may present severe illness in the forms of digestive, cardiac, or cardiodigestive problems. Conversely, chronically infected hosts may be free of any discernible symptoms at all [62, 63]. Individuals infected but not presenting any clinical symptoms (the indeterminate form) may remain unaffected for periods stretching from months to decades [60]. 20 – 30% of infected individuals with the indeterminate form will go on to develop cardiomyopathic or gastrointestinal Chagas', eventually resulting in death if not treated [60, 62, 64].

Diagnosis and treatment of Chagas' disease is less complex than that of its African cousin, but difficulties remain. Diagnosis of acute stage Chagas' is relatively uncomplex; a simple fresh blood smear is usually effective, but serological detection of host IgGs raised against *T. cruzi* may also be used. The chronic stage is more difficult to diagnose, and may even elude initial detection if in the indeterminate stage that exhibits a lack of symptoms. Diagnosis by blood smear or IgG detection is not possible in chronically infected hosts, due to low latent levels of parasites. Often dual tests, such as ELISA and indirect haemagglutination, are used to confirm chronic stage infection [62, 65]. Despite these combined tests, many samples are of an inconclusive diagnosis,

and even new techniques such as PCR which can be up to 70% accurate, are not wholly suitable [59, 65]. Overall, there is a lack of a standardised chronic stage disease test. The extracellular membrane coat of *T. cruzi* is comprised of mucins that are expressed variably, in a similar manner to VSG in *T. brucei* [66]. As a consequence, development of a vaccine against the parasite currently remains unviable. Treatment of Chagas' disease is performed with one of two drugs available; benzidazole or nifurtimox. Both nifurtimox and benzidazole are an effective treatment for acute stage Chagas', and while side effects are common (approx. 40 - 50% of patients) they are rarely deemed severe. Treatments are lengthy with treatment periods typically lasting 30 – 90 days, with cure rates of between 60% - 80% [59, 63]. There is no well established method for drug treatment for chronic stage Chagas', since drug efficacy is not easy to establish given the lack of defined diagnostic tests (above), though benzidazole has been shown to be at least somewhat effective [36, 40]. Clearly new, standardised tests and drugs for the treatment of chronic stage infection need to be developed.

Efforts to control Chagas' disease in South America have been very successful thus far, with the disease practically eliminated in most rural areas. This has been achieved through pesticide spraying, residential housing improvements, active monitoring of infected individuals, and serological testing of blood donations and transplant organs [67, 68]. Through education and active monitoring it's hoped that the disease can be eliminated entirely, although vigilance must be maintained to reach this goal.

1.2.2 Life cycle.

There are many distinct host micro-environments that *T. cruzi* must adapt to in order to thrive and maintain infective viability. Broadly speaking, there are three main forms of the parasite that can be identified morphologically; the amastigote, epimastigote, and trypomastigote forms [57, 69]. When the Triatomine insect takes a blood meal from an infected host it an also take up a pleomorphic population of slender non-replicative trypomastigotes contained within the blood, a proportion of which undergo differentiation in the Triatomine mid-gut into stumpy amastigotes. Further differentiation into the epimastigote form then occurs as this form is more suited to the cooler 20 – 28 ^{o}C temperature of the mid-gut [57]. In the hind-gut of the bug the epimastigote attaches to the gut membrane wall and transforms into the infective metacyclic trypomastigote,

which is then excreted in the insects faecal matter and is capable of infecting a wide number of cells upon entering the new host. Once inside a cell, the trypomastigote will transform into an amastigote which divides and proliferates until a pseudo cyst is formed. A population density sensing mechanism triggers a subset of the amastigotes to differentiate into trypomastigotes, which can escape the pseudocyst and go on to infect other cells, or failing infection, become amastigotes that can infect other cells. This trypomastigote – epimastigote mix may also be taken up by a Triatomine bug, completing the life cycle [22, 57, 69].

1.3 The metabolism of *Trypanosomes*.

Like many of their cellular processes, trypanosomes have adapted their metabolic processes to the vastly varied life cycles and extracellular or host/vector environments they are subjected to. Many of these adaptions, such as the compartmentalisation of glycolysis [70] and the use of an alternative to the citrate/malate shuttle for fatty acid synthesis [71], are unique to trypanosomes. The metabolisms of both *T. brucei* and *T. cruzi* parasites have been and continue to be studied extensively, as outlined here (Fig. 1.5 and 1.6).

1.3.1 Glycolysis.

Upon infecting their mammalian host *T. brucei* reside extracellularly in the bloodstream, which contains a high concentration of glucose (mean of 5 mM in a healthy adult human). The glucose supply is homeostatically regulated and is the main source of *T. brucei* energy metabolism during this life cycle stage. Long slender cells will utilise glucose extensively for energy purposes as it is the sole source of ATP in these cells, with pyruvate excreted as an end product [72]. A previous dogma existed where pyruvate was understood to be the singularly excreted end product from glucose metabolism, although recent research indicates that small quantities of acetate may be produced by long slender trypomastigotes for fatty acid synthesis and alanine and succinate may also be secreted (Fig. 1.6) [73]. Uniquely, the first seven enzymes of glycolysis are compartmentalised within the glycosome, a peroxisome-like organelle, with the last

three enzymes of the pathway existing in the cytosol [70]. This compartmentalisation has been deemed necessary to protect trypanosomes from their very high rate of glycolytic flux and from the generation of excessive amounts of glycolytic intermediates, as trypanosomes lack enzymatic feedback regulation of the glycolytic pathway [74]. For example, the production of glucose-6-phosphate does not negatively regulate trypanosomal hexokinase, as normally found in other eukaryotic organisms [75]. Net production of ATP through glycolysis is only obtained in the cytosol, where phosphoenolpyruvate is converted to pyruvate by pyruvate kinase, generating ATP [72]. Large quantities of reducing equivalents such as NADH are generated during the glycolytic steps, that must be rapidly re-oxidised to maintain a steady glycosomal redox balance. Both bloodstream and procyclic form *T. brucei* utilise a unique glycerol-3-phosphate shuttle and plant-like alternative oxidase for NADH re-oxidation, with bloodstream forms relying solely on this mechanism to maintain the redox balance as they lack a fully functional electron transport chain. Glycerol-3-phosphate is siphoned off from the glycolytic pathway and shuttled into the cytosol and then into the mitochondria. Here the electrons are transferred into the quinone pool and then to molecular oxygen as the final electron acceptor a process facilitated by the SHAM sensitive plant-like terminal oxidase. Dihydroxyacetone phosphate produced from glycerol-3-phosphate then re-enters the glycosome (Fig. 1.6). All trypanosomatids utilise this mechanism as part of their NAD^+ regeneration, and indeed it is a core component of the so called "aerobic fermentation" metabolism that has only been demonstrated in trypanosomatids so far. Substrates used for metabolism in trypanosomatids are not fully oxidised, rather fermentation products such as pyruvate, succinate, and acetate are produced. Despite the production of these partially oxidised products, oxygen is still used as the final electron acceptor in the electron transport chain and both bloodstream cells and procyclic cells require oxygen to grow. It is likely that a fully oxidative Krebs cycle is not required due to the high glycolytic flux of *T. brucei* and the glucose rich environment in which the bloodstream form resides, which together allow the parasite to generate large amounts of ATP such that expression of a Krebs cycle is deemed surplus to requirements [76]. However, reducing equivalents must still be oxidised by some other mechanism.

Pyruvate produced by glycolysis has been demonstrated to account for approximately 85% of the excreted carbon end-product, however, pyruvate and its precursors are metabolised extensively by different branches of the oxidative pathways [77]. Phos-

phoenolpyruvate (PEP) excreted into the cytosol can re-enter the glycosome where ìt is further metabolised to succinate. Phosphoenolpyruvate carboxykinase (PEPCK) converts PEP to oxaloacetate, producing ATP in the process. PEPCK was recently shown to be essential in bloodstream form *T. brucei*, which may indicate that it has a key role in restoring glycosomal ATP levels [77]. Succinate is likely the product of this branch, although a bona fide NADH-dependent fumarate dehydrogenase that would carry out this conversion, as in procyclic *T. brucei*, has not been identified. Excreted pyruvate can be further utilised within the mitochondria as a precursor in fatty acid synthesis [73]. It is converted to Acetyl-CoA by the pyruvate dehydrogenase complex, which is then further converted to acetate by acetyl-CoA thioesterase, and excreted for use in fatty acid synthesis. This path of acetate production has been shown to be active and essential in bloodstream form cells lacking threonine dehydrogenase, normally the source of acetate – although relative contributions to acetate from pyruvate and threonine seem to be split evenly, at least under *in vitro* conditions [78]. It is worth noting that pyruvate derived acetate does not contribute to ATP production in bloodstream form mitochondria as acetate:succinate CoA-transferase is not significantly expressed [73].

1.3.2 The Pentose Phosphate pathway.

A basic pentose phosphate pathway (PPP) exists in both bloodstream and procyclic form cells, in *T. brucei* & *T. cruzi*. It had been previously believed that only the oxidative branch was functional in either parasite to regenerate NADPH, but recent metabolic labelling studies using ^{13}C-glucose have shown that large monosaccharide phosphates can be detected in *T. brucei* cellular extracts [77]. However, the authors note that this activity is likely a consequence of carbon shuffling by the transaldolase of the non-oxidative branch, and no obviously useful roles for these monosaccharide phosphates exist. The absence of transketolase and ribulose 5-phosphate epimerase activity in bloodstream form *T. brucei* further suggests that the non-oxidative branch is not fully functional, and does not serve the classical purpose of feeding useful products back into the glycolytic path (may be redundant) [79]. In contrast, these enzymes are expressed in procyclic form *T. brucei*, allowing for a fully functional non-oxidative branch of the PPP.

The oxidative branch of the PPP does perform an important role in *T. brucei* as the primary source of NADPH and for the production of ribose-5-phosphate, which is used in nucleotide synthesis [77]. Two molecules of NADPH are generated by glucose-6-phosphate dehydrogenase and 6-phosphogluconate dehydrogenase during the 3-step conversion of glycolytically derived glucose-6-phosphate to ribulose-5-phosphate. NADPH generated here is most likely used as a co-substrate for trypanothione reductase, the trypanosomal equivalent of gluthathione in mammals, which acts to protect against oxidative stress [80, 81]. Trypanothione reductase is especially important in protecting *T. brucei* from oxidative damage, as the parasite also lacks catalase [70]. All the enzymes of both branches of the PPP have been reported to be active in *T. cruzi*, and expressed at all stages of the parasites developmental cycle [82]. The study noted the increased activity of the enzymes in the metacyclic versus epimastigote stages of the parasite, speculating that this may due to an increase in the need for protection against oxidative stress during invasion of the mammalian host. Like *T. brucei*, *T. cruzi* express an NADPH-dependent trypanothione [81].

While the oxidative branch has been characterised in many trypanosomatids, and is known to play a key role in nucleotide synthesis and protection against oxidative stress, the non-oxidative branch remains somewhat neglected. In particular, the question of why elements of the branch exist fully in certain life stages or even certain species and not in others has not been answered.

1.3.3 Krebs Cycle and Electron Transport Chain.

The Krebs cycle is not active in bloodstream form *T. brucei*. Pyruvate from glycolysis is partially oxidised to fermentation products which are then excreted by the parasite. The enzymes associated with the Krebs cycle, and complexes typical of the electron transport chain are not expressed, but the plant-like alternative oxidase is [83]. While functioning in an oxygen dependent manner to re-oxidise NADH, this oxidase is not capable of H^+ trans-location and so does not play a role in the generation of ATP. The creation of ATP is instead coupled to substrate level phosphorylations performed by enzymes within the glycosome, such as PEPCK [84]. In contrast, procyclic form *T. brucei* have a much more diverse metabolism downstream of glycolysis. Procyclic form *T. brucei* express an almost complete set of enzymes of the Krebs cycle, as well

as a practically complete set of the classical electron transport chain (ETC) complexes I, II, III, and IV. Interestingly, the alternative oxidase is also expressed in these cells [49, 84]. Electrons from NADH or $FADH_2$ may be transferred to oxygen through the alternative oxidase or enter through the complexes of the ETC, which consequently produces a proton motive force capable of being used for ATP production. Dual inhibition of both complex IV and the alternative oxidase in procyclic form *T. brucei* leads to a rapid onset of cell death, highlighting the need for terminal reducing equivalents in these cells [49]. The presence of two terminal oxidising components is puzzling however, as procyclic form cells have been shown to survive - albeit at reduced rates of growth - upon the oligomycin inhibition of ATP synthase in glucose rich media [85]. It seems that substrate-level phosphorylation in these cells remains the primary supplier of ATP, at least under standard cell culture conditions, and that the ETC may primarily act to re-oxidise glycolytically produced NADH with a minor role in producing ATP. It is likely that the function of the ETC and components of the Krebs cycle would become more prominent under conditions typically experienced in the gut environment of the tsetse fly, where glucose is limited and amino acids such as L-proline are the primary energy source. Interestingly, procyclic form cells cannot grow in the complete absence of glucose (at least in culture), and a functioning oxidative phosphorylation mechanism is required for procyclic form cell viability [72]. This suggests that oxidative phosphorylation is not required by cells when catabolising glucose, but that it becomes essential when switching to an amino acid base catabolism in low glucose environments. Pyruvate produced by glycolysis can be further metabolised to acetate in the mitochondrion, a process that utilises the Krebs cycle enzyme succinyl-CoA synthetase. This enzyme is part of a succinate/succinyl-CoA cycle that generates ATP from acetate. succinyl-CoA synthetase is also utilised as an end point in the metabolism of L-proline to succinate, in addition to the involvement of 2-ketoglutarate dehydrogenase, which converts L-proline derived α-ketoglutarate to succinyl-CoA to be used in the succinate/succinyl-CoA cycle [86]. Substantial evidence that the Krebs cycle as a whole is not involved in energy generation in these cells comes from Weelden et al., who have shown that aconitase knockout procyclic form *T. brucei* grow identically to wild type cells, whilst both cell types require the ETC for survival [87]. Other research has demonstrated that threonine may be used for energy generation by procyclic cells, and that threonine-derived acetyl-CoA can be used for fatty acid synthesis, an anabolic process [88]. The same research also suggests a role for other Krebs cycle enzymes in

gluconeogenesis using succinate. The complexity in PCF metabolism is likely due to the need for these cells to adapt to the transition from a glucose rich environment in mammalian blood to the amino acid rich environments of the fly gut, amongst other unidentified factors.

Both glucose and amino acids can be taken up by *T. cruzi* for metabolic purposes, and it appears to do so at all stages of its life cycle [84, 89]. A full set of Krebs cycle enzymes - bar one - have also been characterised and are expressed in *T. cruzi*, as are a full set of ETC complexes [89]. However, *T. cruzi* lacks an alternative oxidase, as expressed in *T. brucei*. Aerobic fermentation also occurs in *T. cruzi*, with alanine the primary excreted product from pyruvate, in addition to glycolytically derived succinate. It appears that a full Krebs cycle is functional in *T. cruzi*, where succinate is the primary reducing equivalent. It has been suggested that the secretion of reduced products rather than complete oxidation through the ETC may represent a lack of capacity of the respiratory chain to process these substrates, and so they are alternatively excreted [89, 90]. Further metabolic studies have been hampered in *T. cruzi* as it is not susceptible to reverse genetic approaches such as RNAi [90]. Perhaps metabolite labelling studies, such as those performed with ^{13}C-glucose [77], would help elucidate the precise mechanisms of *T. cruzi* metabolism.

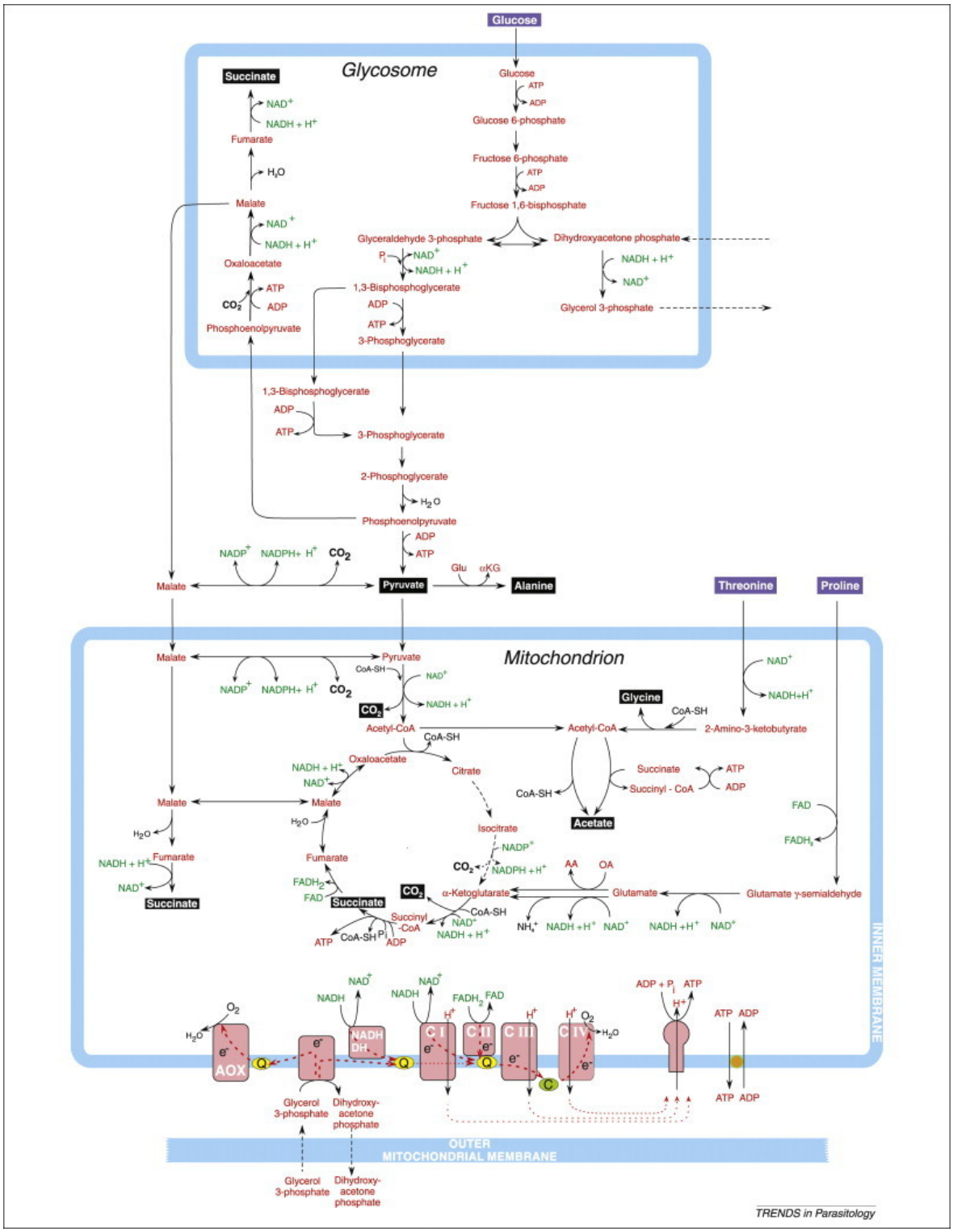

Figure 1.5. Overview of the metabolic pathways of Trypanosomatids.

This diagrammatic representation encompasses the major metabolic pathways of trypanosomatids. Each species expresses some elements, such as procyclic form *T. brucei*, or all elements, such as *T. cruzi*, of these metabolic pathways. Abbreviations: amino acids (AA), α-ketoglutarate (α-KG), alternative oxidase (AOX), cytochrome c (c), ETC complexes I-IV (CI-IV), 2-oxoacids (OA), ubiquinone (Q). Figure taken from [84].

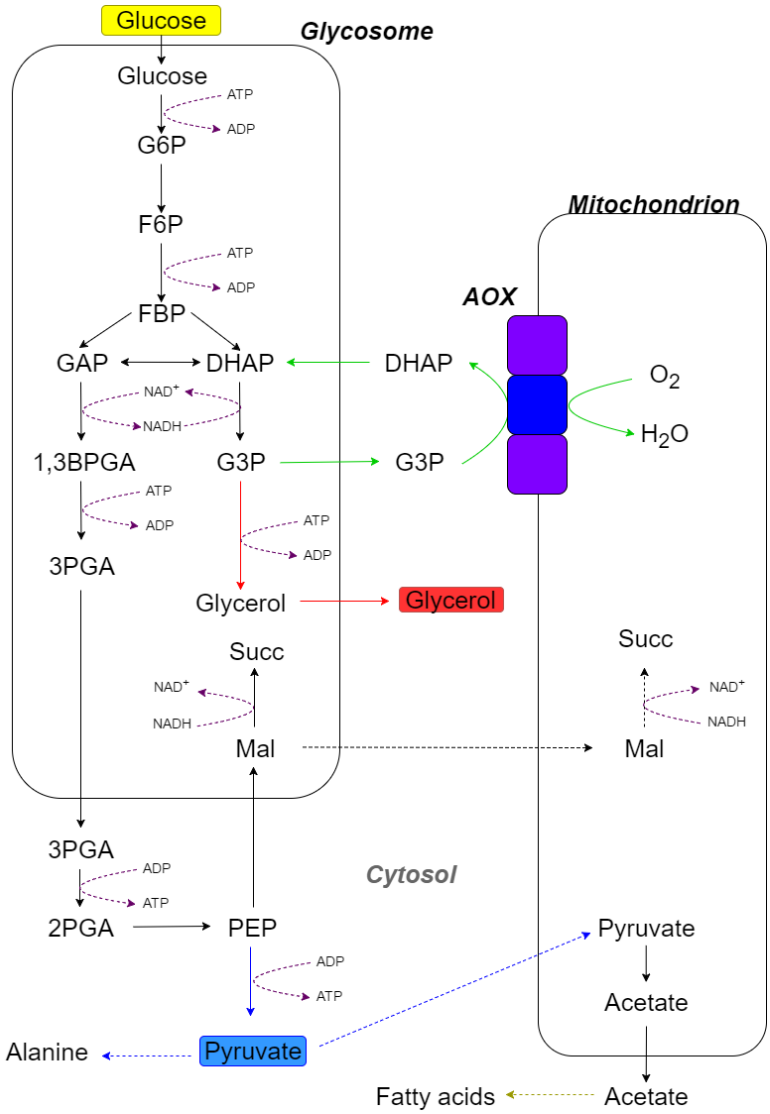

Figure 1.6. Scheme of glucose metabolism in bloodstream form *T. brucei*.
Simplified diagram of the metabolic pathways of glucose metabolism in bloodstream form *T. brucei*. Under aerobic conditions, pyruvate is the primary end-product of glycolysis. Under anaerobic conditions, both pyruvate and glycerol are excreted in equimolar amounts as the AOX can no longer function to reoxidise G6P to DHAP. Pathways believed to have minor metabolic functions are indicated with dashed arrows (except ADP/ATP and NAD^+/NADH). Abbreviations: alternative plant-like oxidase (AOX), dihydroxyacetone phosphate (DHAP), fructose-2,6-bisphosphate (FBP), fructose-6-phosphate (F6P), glyceraldehyde-3-phosphate (GAP), glycerol-3-phosphate (G3P), glucose-6-phosphate (G6P), malate (Mal), succinate (Succ), phosphoenolpyruvate (PEP), 1,3-bisphosphoglycerate (1,3BPGA), 2-phosphoglycerate (2-PGA), 3-phosphoglycerate (3-PGA).
Figure based on [73, 91].

1.4 Amino acid transamination in *T. brucei*.

Amino acid transamination reactions are reversible, and involve the abstraction of the α-amino group from the donor amino acid, to be transferred to an α-ketoacid acceptor. In most eukaryotic metabolic systems this process provides a key link between amino acid and carbohydrate metabolism. It is used to generate intermediates that can enter the Krebs cycle for energetic purposes, for production of precursors in fatty acid synthesis, and as a key part of the glutamate-malate shuttle used for NADH transfer in mitochondria [92].

The use of amino acids as substrates for various cellular processes in *T. brucei* is complicated by its different life cycle stages; bloodstream form *T. brucei* exclusively metabolise glucose for energetic purposes, whereas the procyclic form may utilise amino acids for energy and as a carbon source. Procyclic cells primarily metabolise threonine, glutamate, and L-proline, which is the predominant energy source in a low glucose environment [84]. Amino acid uptake by bloodstream form *T. brucei* has been reported to be minimal for the vast majority of amino acids *in vitro*, though efficient transporters for methionine and the aromatic amino acids have been characterised [93, 94]. Given the vast difference in the metabolisms of these two parasite stages, the aminotransferases they possess may have different functional purposes at each given stage.

1.4.1 Alanine aminotransferase.

Alanine aminotransferase (AAT) functions to catalyse the reversible transfer of an amino group from alanine to α-ketoglutarate, yielding glutamate and pyruvate. It was demonstrated by Coustou et al. that alanine was the primary metabolite secreted by procyclic *T. brucei* under glucose-depleted conditions, with authors suggesting that AAT could play a role in its generation [95]. Further work on AAT suggests that it is an essential gene in both bloodstream and procyclic stages of the parasite, and that in the absence of glucose and presence of L-proline, AAT activity was important for maintaining normal growth rates and levels of alanine excretion comparable to that of wild type cells [96]. Taken together, both reports suggest a key role for AAT in converting L-proline derived glutamate to α-ketoglutarate, the production of which generates NADH that could be further used for oxidative phosphorylation.

That AAT appears to be essential in bloodstream form *T. brucei* remains puzzling. Generation of AAT double gene knockout cells was not possible [96]. Furthermore, AAT is expressed in bloodstream form cells and has high activity (523 nmoles.min^{-1}.mg^{-1}) [97]. These cells do not catabolise L-proline, and only minor amounts of glutamine consumption have been reported in culture [93]. Reduction of the AAT activity to 5% of the activity of the parental cell line had only a minor affect on cell growth rates [96]. It may be that AAT activity is coupled to other, as yet undetermined metabolic functions.

1.4.2 Aspartate aminotransferase.

Aspartate aminotransferase (ASAT) is a PLP-dependent enzyme that normally functions to catalyse the reversible transfer of an amino group from aspartate to α-ketoglutarate, yielding glutamate and oxaloacetate. The genome of *T. brucei* contains two genes for aspartate aminotransferases; a mitochondrial type (TbmASAT) and a cytosolic type (TbcASAT), both of which are expressed by the parasite. The expression of TbmASAT is down-regulated in bloodstream form cells, whereas TbcASAT is expressed throughout the parasites life cycle [98]. In contrast to the narrow substrate specificity of TbAAT [96] and TbmASAT, TbcASAT has been shown to have a much broader substrate specificity [98, 99]. The broad specificity of TbcASAT encompasses an affinity for the three aromatic amino acids - tryptophan, tyrosine, and phenylalanine. Aromatic amino acid transamination was discovered in Trypanosomatida in 1957, initially in *Leishmania donovani* [100]. The reported aromatic amino acid transamination activity in *L. donovani* was likely due to an ASAT homologous to TbcASAT in this organism.

The role of TbcASAT in bloodstream form *T. brucei* remains to be determined. Several studies have acknowledged the ability of TbcASAT to transaminate aromatic amino acids, and have speculated upon this function [101–104]. Berger et al. suggests that TbcASAT could play an important role in methionine recycling in *T. brucei* [99, 101]. Methionine is required as a precursor for the production of trypanothione; the adenylated methionine, S-adenosylmethionine (SAM), acts as a donor of aminopropyl groups to putrescine which generates spermidine to be used for trypanothione synthesis. Methylthioadenosine (MTA) is also produced, which can enter a cycle for conversion

back to methionine (Fig. 1.7). This pathway has been mostly characterised in rat ccells, the final step of which is the regeneration of methionine by the transamination of α-ketomethiobutyrate (KMTB) [105]. Berger et al. have provided kinetic evidence that both TbcASAT and TbmASAT could effectively use KMTB and the aromatic amino acids as substrates for methionine regeneration [99], and that TbcASAT preferred to deaminate aromatic amino acids over other substrates whereas TbmASAT did not. Additionally, earlier work by the same group demonstrated that ^{15}N-methionine was produced by *C. fasciculata*, a related trypanosomatid, incubated with ^{15}N-tyrosine [101]. More recent data casts this purported methionine recycling pathway in *T. brucei* into doubt however. A transporter with a high affinity for methionine has been characterised in both life cycle stages of *T. brucei* [106], and methionine has been shown to be taken up from culture media by bloodstream form cells [93]. Most tellingly, carbon derived from ^{13}C-glucose was not found to be present in intracellular methionine, suggesting methionine requirements are satisfied by uptake from culture media [77]. It could be possible that a partially active methionine recycling pathway functions *in vivo*, where methionine concentrations are at least 7 times lower in the mammalian bloodstream compared to standard *T. brucei* culture media [93], but this remains to be established.

Many studies have noted that as a consequence of aromatic amino acid deamination, aromatic ketoacids are produced [101, 103, 104]. Berger et al. had suggested that these aromatic ketoacids are merely a waste byproduct of the conversion of KMTB to methionine [101]. It could be possible that aromatic ketoacids play a role in suppressing the host immune response during *T. brucei* infection. Tryptophan was reported to be metabolised to tryptophol by enzyme extractions from *T. gambiense*, by an enzyme that appeared to be PLP-dependent [107]. Tryptophol was subsequently shown to have immune suppressive effects when mice were orally treated with the substance [108]. Similarly, both tyrosine and phenylalanine were metabolised to aromatic ketoacids and further derivatives by *T. gambiense* cell extracts, which was again suggested to be the function of an unidentified aminotransferase [103]. Using recombinant TbcASAT, it has been demonstrated that the enzyme can effectively and preferentially convert aromatic amino acids to aromatic ketoacids [98]. It has also been demonstrated that aromatic amino acid pools are severely depleted in *T. brucei* infected hosts [109], and that there is a marked increase in ketoacids secreted by the infected host, corresponding

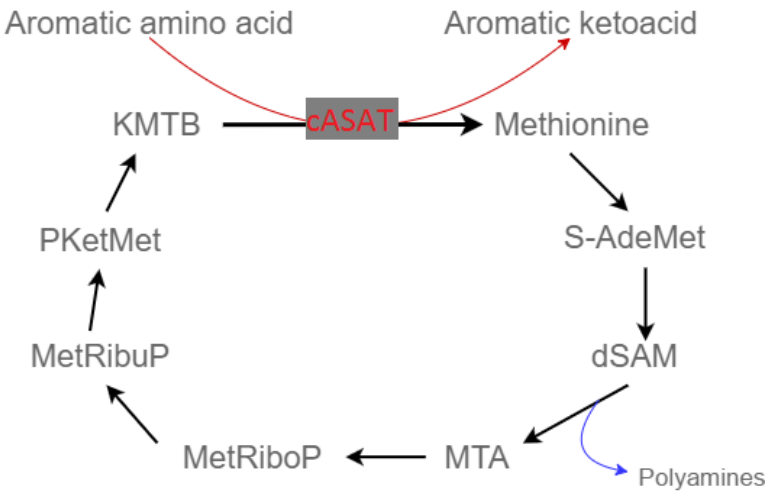

Figure 1.7. The proposed methionine recycling pathway in *T. brucei*.
Simple representation of the methionine recycling pathway proposed by Berger et al. in *T. brucei* [101]. Aromatic amino acids donate their amino group to KMTB, regenerating methionine and producing aromatic ketoacid byproducts. Abbreviations: S-adenosylmethionine (S-AdeMet), decarboxylated S-adenosylmethionine (dSAM), methylthioadenosine (MTA), methylthioribose phosphate (MetRiboP), methylthioribulose phosphate (MetRibuP), phosphodiketomethiopentane (PKetMet), α-ketomethiobutyrate (KMTB). Figure based on [101].

to parasitemia [110, 111] - yet a unifying role for all three functions together has not been put forward. Therefore, a role for the aromatic ketoacids possibly produced by TbcASAT deamination of aromatic amino acids in host immune regulation needs to be examined. In the absence of a methionine recycling pathway, a metabolic function for TbcASAT is not obvious. TbcASAT also has some alanine aminotransferase activity, but this activity has been shown to be almost negligible, being unable to rescue AAT knockdown lethality in procyclic *T. brucei* [96]. Interestingly, the same authors suggest that TbAAT and TbcASAT may function in conjunction with on another, with TbAAT providing directional drive to aromatic amino acid deamination to TbcASAT by coupling it to the high rate of pyruvate production through a glutamate/α-ketoglutarate cycle between the two enzymes. This does not explain the necessity of AAT in bloodstream cells however, as aromatic ketoacids are not further metabolised, but excreted into the extra-cellular environment.

1.5 Immune evasion strategies of *T. brucei*.

1.5.1 Antigenic variation and VSG.

The interplay between the immune responses of the host to a *T. brucei* infection, and the parasites defences against these responses are vastly complex, and are the subject of much of our current studies. *T. brucei* survives exclusively in an extra-cellular environment in the vascular system of its host, meaning it is constantly exposed to the robust immunogenic machinery of the host. Perhaps the most novel and well documented mechanism the parasite employs to evade total destruction is the expression of a dense, homologous, VSG coat, and the periodic swapping of this coat through an antigenic variation mechanism [35]. *T. brucei* possesses a library of over 1,000 *vsg* genes, the majority of which are situated primarily on subtelomeric regions of large chromosomes [112]. Only one VSG is expressed at a given time, despite the presence of at least 20 expression sites (ES), being transcribed in a sub-nuclear site termed the expression site body (ESB) [113]. The mechanisms surrounding the selection and use of only one copy of VSG are still being elucidated, as well as how the control and timing of VSG switching occurs [35, 112]. Nonetheless, how VSG functions is remarkable; a single parasite expressing a unique VSG coat will continually grow and divide, and an expansive population of cells expressing this VSG will arise. The host immune system will eventually mount a response to parasites with this foreign antigen, effectively clearing cells with this VSG variant. However, VSG switching is a continual process, that occurs at fast rates, meaning at any given time there can be a small sub-population of cells expressing an alternate VSG that has not yet been recognised by the host immune system [112]. As such, once the previous population has been cleared, a new population of the parasite can grow and expand, until it too is recognised. This expansion, switching, clearing, expansion, etc. is responsible for the characteristic waves of parasitemia observed in the host, and can continue indefinitely given the vast repertoire of VSG variants *T. brucei* possesses [35, 112]. Ultimately, this allows the parasite to persist for a lengthy period in the host, such that it can be taken up and be retransmitted by the tsetse fly vector.

1.5.2 The innate immune response.

Upon invasion of the host by *T. brucei* through biological transmission by the tsetse fly, macrophages are amongst the primary responders to initial infection that are primed by detection of parasite derived antigens, such as CpG DNA or cleaved VSG [114]. During early stage infection, type 1 myeloid (M1) cells act in an inflammatory capacity, releasing pro-inflammatory molecules such as IFN-γ, IL-6, and TNF-α, as well as nitric oxide (NO) [115]. IFN-γ and TNF-α have both been shown to be critical in controlling parasitemia for both *T. brucei* and *T. congolense* [116]. In contrast, M2 cells are active at later stages of the infection, and act in an anti-inflammatory capacity in-part by secreting high levels of IL-10. Increase amounts of circulating IL-10 are thought to suppress an over-active inflammatory response which would be detrimental to the host [114]. How these two opposing effectors regulate each other is not yet clear. Interestingly, it has been observed that a so-called trypanosome suppressive immunomodulatory factor (TSIF) secreted by *T. brucei* can elicit TNF-α and NO production by macrophages, and that these macrophages could act to block T-cell proliferation [117]. Additionally, TSIF reduced the secretion of IL-10 by M2 macrophages. The authors speculate that down-regulation of the adaptive immune response may be purposeful modulation by the parasite [117].

1.5.3 The adaptive immune response.

Infection with *T. brucei* results in the expansion of polyclonal B-cell populations in a T-cell independent manner in the host, which also leads to rapid elevation of circulating antibodies [116, 118]. Because the expansion is poly-clonal the IgM antibodies generated are not *T. brucei* specific, and are cross-reactive. A rapid loss of marginal zone B-cells is associated with *T. brucei* infection, and a collapse of the B-cell population occurs in later stages of the infection [116], resulting in a reduction in the IgM response. More importantly, this B-cell loss prevents the development of a more *T. brucei* antigen specific IgG response. T-cell proliferation is also inhibited, primarily by a reduction in the expression of IL-2 and its corresponding receptor. This inhibition is thought to occur through trypanosome-induced release of NO, TNF-α, and prostaglandins, which mediate T-cell suppression. Conversely, IFN-γ and TNF-α are

believed to stimulate the macrophage to release these factors, yet the large increase in IFN-γ during infection is likely released by T-cells [118]. Whether T-cells mediate their own down regulation, or whether macrophages are solely responsible, or both, remains to be determined. The increase in IFN-γ is associated with an increase in acute inflammation and anaemia development in the host [114]. Early research had also investigated whether macrophage secreted IL-1 was reduced during *T. brucei* infection, which would correspond to observed T-cell suppression. Such a reduction had been observed for *T. congolense* infections [119]. Curiously, a higher release of IL-1 (but not increased synthesis) was observed in LPS-stimulated macrophages of *T. brucei* infected mice [120]. There are thus many mechanisms that remain to be determined in the *T. brucei* modulation of both the innate and adaptive immune responses. A basic outline of our current understanding is provided in Fig. 1.8.

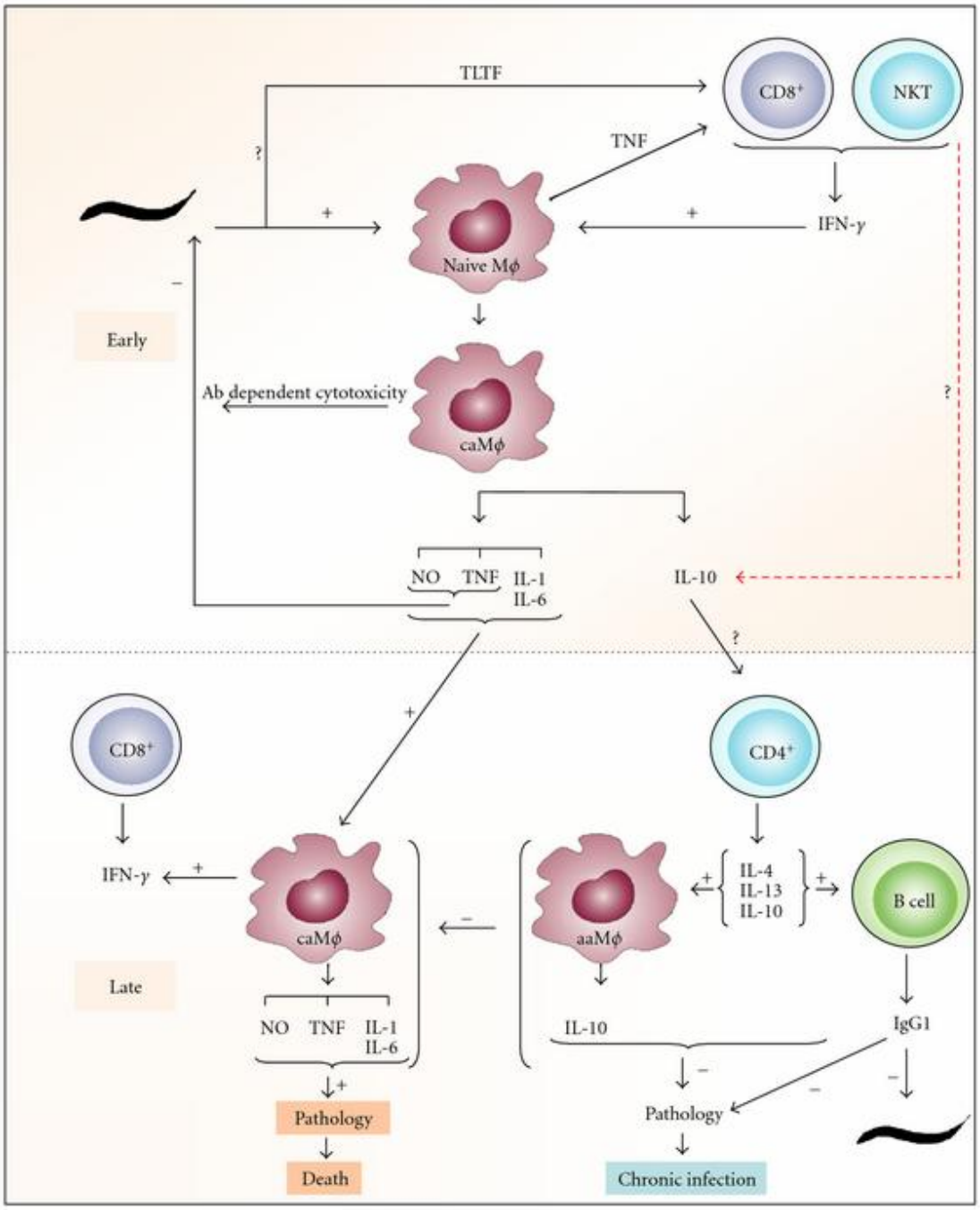

Figure 1.8. Representation of trypanosome-host immune interactions.

Early stage and late stage responses of both classically activated (caMϕ) and alternatively activated (aaMϕ) macrophages, and the corresponding interactions with adaptive immune cells that can display either a pathogenic or protective response. Figure taken from [116].

1.6 Project Aims.

The aim of this study is to investigate the biochemical and cellular functions of *T. brucei* cytosolic aspartate aminotransferase (cASAT). In addition, the possible immunological roles of *T. brucei* derived aromatic ketoacids are investigated. These dual investigations encompassed the following:

- The cloning and expression of recombinant *T. brucei* and *T. cruzi* cASAT.
  - Determination of the kinetic parameters of both enzymes.
  - Crystallisation studies of both enzymes to obtain comparable 3D structures.
- RNAi of *cASAT* in *T. brucei*.
  - Monitoring the effects of *cASAT* RNAi in both bloodstream and procyclic form cells.
  - Attempts to rescue the development of a negative growth phenotype in bloodstream cells.
  - The effects of *cASAT* RNAi on aromatic ketoacid output by bloodstream form cells.
  - Development and characterisation of a tetracycline inducible cell line ($AHADH^{in}$) that alternately secretes aromatic hydroxy-acid derivatives.
  - Establishing a link between aromatic amino acid consumption and aromatic ketoacid output by *T. brucei*.
- Demonstration of indolepyruvate as the product of tryptophan deamination catalysed by TbcASAT via ^{13}C-NMR studies.
- Initial metabolomic analysis using ^{15}N-tryptophan to establish a metabolic role for TbcASAT catalysed aromatic amino acid deamination.
- Treatment of murine macrophage and mixed glial cells with aromatic ketoacids to establish their immunological effects.
  - Establishment of circulating concentration of aromatic ketoacids in the sera of *T. brucei* infected rats.

  - Treatment of innate immune cells with indolepyruvate, phenylpyruvate, and hydroxyphenylpyruvate.
  - Treament of innate immune cells with *T. brucei* produced aromatic ketoacids in spent media.

- NMR investigations of the stability and breakdown of indolepyruvate.

Chapter 2

Materials & Methods.

2.1 Chemicals, equipment, and buffers.

Table 2.1. List of chemicals and equipment.

Chemical/Equipment	Supplier
β-mercaptoethanol	Sigma-Aldrich
2X YT broth	Formedium
5 ml NMR tubes	Wilmad
Absolutely RNA Miniprep Kit	Stratagene
Affinity Script Multiple Temperature cDNA synthesis kit	Agilent
Agarose	Sigma-Aldrich
Amaxa Nucleofactor II	Lonza
Ampicillin powder	Duchefa Biochemie
Aspartic acid	Sigma-Aldrich
Automated fraction collector	Bio-Rad
Bradford assay	Fishcher Scientific
Branson Sonifier S-250A ultrasonic cell disruptor	Emerson Electric Co.
Brilliant II SYBR green qRT-PCR one step kit	Stratagene
Cary 50 Scan UV-Visible Spectrophotometer	Agilent
Consort Mini Electrophoresis Power Supply	Sigma-Aldrich
Creeks Minimal Media (CMM)	Made in house, from [77]
D_2O	Sigma-Aldrich
Dichlorodiphenyltrichloroethane (DTT)	Sigma-Aldrich
EmulsiFlex C5 homogeniser (French Press)	Avestin Inc.
GoTaq DNA Polymerase	Promega
GraphPad Prism version 6.00	GraphPad
HMI-9	Invitrogen
HyperLadder 1 Kb Plus	Bioline
Imidazole	Sigma-Aldrich
Isopropyl β-D-1-thiogalactopyranoside (IPTG)	Melford
JB screen Classic	Jena Bioscience
Kanamycin	Fischer Scientific
LB agar, low salt	Duchefa Biochemie
Malate dehydrogenase (MDH)	Sigma-Aldrich
Midas Screen	Molecular Dimensions

Continued on the next page

Table 2.1 – *Continued from the previous page*

Chemical/Equipment	**Supplier**
Mikro 200 R centrifuge	Hettich Lab Technology
Morpheus Screen	Molecular Dimensions
Multitron Standard Incubation Shaker	Infors HT
Mx3000P qPCR System	Stratagene
Nanodrop ND-1000 Spectrophotometer	Thermo Fisher Scientific
Nickel resin	Quiagen
β-Nicotinamide adenine dinucleotide (NADH)	Sigma-Aldrich
peqGOLD Gel Extraction Kit	PeqLab
PfuUltra II Fusion DNA polymerase	Stratagene
Phenylpyruvate	Sigma-Aldrich
Phenylalanine	Sigma-Aldrich
Plasmid DNA Sequencing	Source Bioscience
Primers	Bioline
Protogel	National Diagnostics
PureLink Kit	Invitrogen
Pyridoxal 5'-phosphate (PLP)	Sigma-Aldrich
QIAprep Spin Miniprep Kit	Qiagen
Restriction enzymes	Thermo Scientific & NEB
Rotanta 460 R benchtop centrifuge	Hettich Lab Technology
SBH130 Block Heater	Bibby Scientific Ltd.
SDM-79	Invitrogen
Sodium chloride	Duchefa Biochemie
Sorvall RC-5C Plus	Kendro Laboratory Products
SSL3 gyro-rocker	Bibby Scientific Ltd.
Superdex200 16/600 column	GE healthcare
T4 DNA Polymerase	Novagen
N,N,N',N'-Tetrametyhlethylenediamine (TEMED)	Sigma-Aldrich
ThermoHybaid PCR Sprint	Thermo Scientific
Tetramethylsilane (TMS)	Sigma-Aldrich
Transilluminator	UVP
Tris-base	Fisher Scientific
Tryptophan	Sigma-Aldrich
Tyrosine	Sigma-Aldrich

Continued on the next page

Table 2.1 – *Continued from the previous page*

Chemical/Equipment	**Supplier**
Urea	BDH
Wizard JB screen	Jena Bioscience

2.1.1 Buffers and solutions.

All buffers are prepared in double distilled H_2O unless otherwise specified.

- 2X YT broth - 900 ml ddH_2O, 16 g bactotryptone, 10 g Bacto yeast extract, 5 g NaCl, pH 7.4
- 5% SDS-PAGE gel (8 ml volume) - 5.5 ml ddH_2O, 1.3 ml 30% acrylamide, 1 ml 1 M Tris pH 6.8, 80 μl 10% (w/v) SDS, 80 μl 10% (w/v) ammonium persulfate, 8 μl TEMED
- 12% SDS-PAGE gel (10 ml volume) - 3.3 ml ddH_2O, 4 ml 30% acrylamide, 2.5 ml 1.5 M Tris pH 8.8, 100 μl 10% (w/v) SDS, 100 μl 10% (w/v) ammonium persulfate, 10 μl TEMED
- Column buffer (1X) - 10 mM Tris, 100 mM NaCl, 5 mM DTT, pH 8.0
- Coomassie Brilliant Blue - 0.1% (w/v) in 50% (v/v) methanol and 10% (v/v) glacial acetic acid
- Destain solution - 40% (v/v) methanol, 10% (v/v) acetic acid, in ddH_2O
- DNA lysis buffer (1X) - 50 mM Tris-HCl (pH 8), 62.5 mM EDTA (pH 9), 2.5 M LiCl, and 4% (v/v) Triton X-100
- Elution buffer (1X) - 20 mM Tris HCl, 250 mM imidazole, 300 mM NaCl, 1 mM β-mercaptoethanol, pH 7.4
- Bacterial lysis buffer (1X) - 20 mM Tris HCl, 20 mM imidazole, 300 mM NaCl, 1 mM β-mercaptoethanol, pH 8
- Phosphate buffered saline glucose (1X PSG) - 44 mM NaCl, 57 mM Na_2HPO_4, 3 mM KH_2PO_4, 55 mM glucose (added fresh before use), pH 8
- Protein sample buffer (2X) - 4% (v/v) SDS, 20% (v/v) glycerol , 10% (v/v) β-mercaptoethanol, 0.05% (w/v) bromophenol blue and 0.125 M Tris-HCl, pH 6.8
- Running buffer (1X) - 300 mM glycine, 80 mM Tris base, 0.1% (v/v) SDS.

- SDS sample buffer (1X) - 125 mM Tris pH 6.8, 10% (v/v) glycerol, 0.02% (v/v) SDS
- Sodium phosphate buffer (1X PBS) - 136 mM NaCl, 3 mM KH_2PO_4, 16 mM Na_2PO_4, 3 mM KCl, pH 7.5
- Transfer buffer (1X) - 25 mM Tris Base, 190 mM glycine, 20% (v/v) methanol, pH 8
- Tris acetate EDTA buffer (1X TAE) - 40 mM Tris-acetate, 2 mM EDTA, pH 8
- Tris buffered saline (1X TBS)- 150 mM NaCl, 25 mM Tris-HCl, pH 7.5
- Tris buffered saline tween (1X TBST) - 2 mM Tris Base, 150 mM NaCl, 1% (v/v) Tween-20, pH 7.6
- Universal buffer (1X) (Britton & Robinson) - 28.6 mM citric acid monohydrate, 28.6 mM KH_2PO_4, 28.6 mM barbital, 28.6 mM boric acid, pH range of 2 - 12, adjusted as as required with 1 M NaOH.

2.2 General experimental methods.

2.2.1 Trypanosome origin and standard culture conditions.

Bloodstream form *T. brucei*.

Bloodstream form *T. brucei* used over the course of these studies were monomorphic, trypomastigote stage *Trypanosoma brucei brucei*. The strain used was MITat 1.2, also termed Lister 427-2, that were modified to express T7 polymerase and Tet repressor elements. These cells were cultured in sterile Hirumis' modified Iscoves' medium, formulation 9 (HMI-9), which was further supplemented with 10% (v/v) FCS, 180 mM $NaHCO_3$, 1 mM β-mercaptoethanol, 50 mg.l^{-1} each of ampicillin and streptomycin, at pH 7.5. Cultures were maintained at 37 ^{o}C in an incubator with 5% CO_2. Cell growth density was always maintained at a range between 1×10^5 cells.ml^{-1} and 2×10^6 cells.ml^{-1}. Cultures were contained in T25, T75, and T175 vented culture flasks.

Procyclic form *T. brucei*.

Procyclic form *T. brucei* used were a cell line generated from the Lister 427-2 strain, that were also modified to express T7 polymerase and Tet repressor elements. Cells were cultured in sterile SDM-79 media which was further supplemented with 10% (v/v) FCS, 25 mM $NaHCO_3$, 50 mg.l^{-1} each of ampicillin and streptomycin, at pH 7.3. Cultures were maintained at 27 ^{o}C in an incubator with 5% CO_2. Cell growth density was always maintained at a range between 1×10^6 cells.ml^{-1} and 2×10^7 cells.ml^{-1}. Cultures were contained in T25, T75, and T175 vented culture flasks.

Cell counting.

The density of cultured cells was measured using an Improved Neubaur haemocytometer, with a silvered stage (Gelman-Hawksley, Lancing, Sussex, UK) and a standard light microscope (Olympus CK2).

Long term storage of cell stocks.

Cell stocks were stored in liquid N_2 when not immediately required. Stocks were prepared by mixing a 1 ml volume of cell culture, when cell density was $\approx 1 \times 10^6$ cells.ml^{-1}, with 1 ml of culture media that was supplemented with 30 % (v/v) glycerol. These samples were cooled to -80 ^{o}C, followed by storage at -80 ^{o}C overnight, before prompt transfer to liquid N_2 for long-term storage.

2.2.2 SDS-PAGE and western blotting.

Preparing SDS-PAGE.

Sodium dodecyl sulfate (SDS) polyacrylamide gel electrophoresis (PAGE) was performed using a modification of the Laemmli method [121]. For our recombinant protein and crystallisation studies 12 % resolving polyacrylamide gels were used, each with a standard 5% stacking polyacrylamide gel (see subsection 2.1.1). The ammonium persulphate solution was prepared freshly prior to use. Resolving gels were loaded between two glass plates following addition of TEMED to induce polymerisation, and covered by a thin layer of isopropanol to prevent the access of air. Once the gel had set ($\approx$ 20 min), the isopropanol was removed before the addition of the 5% stacking gel, and the insertion of a comb to produce wells. After $\approx$ 20 min min the combs were removed and a fine spatula was used to clear the wells of gel fragments. The gels were used immediately or stored for up to a week at 4 ^{o}C in a moist environment prior to use.

Running samples on SDS-PAGE.

10 μl of $\approx$ 2 mg.ml^{-1} protein was loaded per well, with protein concentration assessed roughly with A_{280} absorbance readings. Samples were mixed with an equal volume of 2X protein sample buffer. Samples were boiled for 5 min at 100 ^{o}C and sonicated for 2 min, to ensure homogeneity and to shear genomic DNA. The polyacrylamide gels were docked in a dual slab chamber from Atto Corp, filled with 1X running buffer. The gels were run using a constant voltage of 100 V and 50 mA current per gel, with power supplied by a Bio-Rad power Pac 3000, until the dye front reached the base of

the assembly. The gels were stained with Coomassie Brilliant Blue for 1 - 3 hours or overnight. Following de-staining in destain solution, gels were scanned using an Epson scanner.

Western blotting.

Following treatments, BMDM cells or mixed glial cells isolated from C57BL/6 Harlan UK mice were lysed in 1X SDS sample buffer, and loaded for SDS-PAGE (as described above). Gels were transferred to a PVDF (methanol activated) membrane assembly that had been pre-soaked in 1X transfer buffer. Protein was then transferred from the gel to membrane at 200 mA for 1 hour and 15 min, before being blocked with a 5% (w/v) Marvel milk solution prepared with 1X TBST. Following incubation for 1 hour with gentle shaking on an orbital shaker, the PVDF membranes were transferred into 5% Marvel (w/v)/1X TBST solutions containing either a 1:500 dilution of anti-IL-1β, a 1:100 dilution of anti-HO-1, or a 1:70,000 dilution of Strep-HRP conjugated anti-β-actin, and incubated on a roller overnight at 4 ^{o}C. PVDF membranes were then washed 3 times for 10 min with 1X TBST, then blotted for one hour at room temperature with secondary antibodies; 5% Marvel (w/v)/1X TBST solutions containing either a 1:2000 dilution of anti-rabbit IgG HRP, or a dilution of anti-goat IgG HRP. The membranes were again washed 3 times for 10 min, before being developed with Western Chemiluminescent HRP Substrate, imaged with a Biorad ChemiDoc^{TM} MP Imaging System, and analysed using Biorad Image Lab 5.2.1 software.

2.2.3 Molecular biology procedures.

Agarose gel electrophoresis.

1% (w/v) agarose gels were prepared by dissolving agarose powder in 1X TAE buffer. Solutions were heated in short bursts in a microwave (lidless bottle) with careful swirling, until the agarose was completely dissolved. The solution was allowed to cool to $\approx$ 50 ^{o}C and was then poured into a gel tray containing a separating comb to give a well depth of 6 mm. A solution of 10 mg.ml^{-1} ethidium bromide was added to the gel at a final concentration of 0.5 μg.ml^{-1} while the gel was still hot, and stirred into the

gel to ensure homogeneity. The gel was then allowed to solidify at room temperature, and was transferred to a gel dock (Medical Supply Company) containing 1X TAE. Ensuring the 1X TAE covered the gel completely, samples were prepared in loading buffer and loaded into the lanes once the comb was removed (20 μl maximum per well). After loading, the gel was run at approximately 90 V for 1 h. Stained DNA samples were then visualised using a UV transilluminator.

Polymerase chain reaction.

Restriction enzyme sites were incorporated at the ends of each primer, to aid site specific integration into plasmid vectors. Polymerase chain reaction (PCR) mixtures were composed in a total volume of 50 μl and DNA amplification was achieved using the conditions outlined in the GoTaq® DNA Polymerase kit or the PFUltraFusion II DNA polymerase kit. Genomic DNA extracted from *T. brucei* or *T. cruzi* was used as template DNA. All additions were made to thin walled 0.1 ml PCR tubes (Molecular bioproducts), centrifuged and placed into a ThermoHybaid PCR Sprint machine and set to the required PCR program cycle.

PCR product purification.

PCR products were either extracted straight from a PCR reaction mix, following confirmation of amplification with agarose gel electrophoresis, or were electrophoresed and then extracted directly from the gel. All PCR products were purified by a spin column method using the peqGOLD Cycle-Pure Kit (CLine), or the PureLink™ Quick Gel Extraction and PCR Purification Combo Kit.

Restriction enzyme digest of DNA.

The single or double digest of DNA was carried out in a sterile 200 μl minifuge tube using 1 - 5 U of the restriction enzyme per digest in the appropriate buffer for 1 - 3 h or overnight at the appropriate temperature depending on the amount of DNA being digested - higher amounts required longer digestions. Typically, 1 U of restriction enzyme will digest 1 μg plamid DNA per hour.

Transformation of chemically competent DH5α *E. coli.*

50 μl of DH5α *E. coli* glycerol stock stored at -80 ^{o}C was added to 10 μl of the desired vector (20 ng.μl^{-1} DNA), and incubated on ice for 30 minutes. The bacterium were then subjected to heat shock at 42 ^{o}C for 30 seconds, followed by a 2 minute incubation on ice. The bacterium were then transferred to 250 μl of lysogeny broth (LB broth) and incubated at 37 ^{o}C for 1 hour at 180 RPM in a shaking incubator. Following incubation, the bacterial culture was lawned onto LB agar plates containing 1 mg.ml^{-1} ampicillin, to select for bacterium containing the desired vector, and allowed to grow in an incubator overnight at 37 ^{o}C. A number of colonies were selected from the plate the following day and were added to 7 ml LB broth containing 1 mg.ml^{-1} ampicillin to be grown overnight again, for mini-prep DNA extraction the next day. DNA was extracted from 5 ml of these cultures using the PeqGold plasmid mini-prep kits, and the correct plasmid amplification was confirmed by restriction digest mapping.

The cloning of DNA into the pGEM-T expression vector.

The pGEM®-T Easy Vector was used for the cloning of PCR products, following genomic amplification, to increase the obtainable yields for downstream applications e.g. for inserting desired sequences into expression plasmids. This system utilises a linearised vector with a single 3'-terminal thymidine at both ends to improve ligation efficiency of PCR products generated by thermostable polymerases. The vector has a multiple cloning site flanked by several restriction enzyme sites, as shown in Fig. 2.1. The vector encodes an ampicillin resistance gene to allow for selection in *E. coli*. Typical ligation into pGEM®-T was performed as follows; 5 μl 2X ligation buffer, 1 μl pGEM-T vector, 0.5/1/2 μl DNA, 1 μl T4 DNA ligase, and H_2O, to a final total volume of 10 μl. Samples were incubated overnight at 4 ^{o}C. The ligation mix was then heat shocked into competent *E. coli*, and processed as discussed previously.

Site-directed mutagenesis.

Complimentary primers were designed as required to change a single nucleotide in a given DNA sequence. Firstly, the vector to be changed was subjected to PCR with

the new primers. The reaction mixture contained; 5 μl reaction buffer, 100 pmol.μl^{-1} of each primer, 1 μl dNTPs (10 mM stock), 1 μl 2.5 U.μl^{-1} Pfu polymerase, 50 ng of plasmid DNA, in a total volume of 50 μl H_2O. The PCR cycle was an initial 95 ^{o}C for 1 min, then 18 cycles consisting of 95 ^{o}C for 30 s, 55 ^{o}C for 1 min, 68 ^{o}C for 4 min (1 min per kb), followed by a hold cycle at 4 ^{o}C. The samples were then digested with DpnI - 1 μl 10 U.μl^{-1} DpnI was added to the PCR samples, and allowed to digest for 1 h at 37 ^{o}C. DpnI digests the methylated parental DNA, and leaves the newly generated plasmid, ideally containing the desired mutagenised site. DpnI treated DNA was then heat shocked into *E. coli* to increase yields of the mutagenised vector. Restriction digest was used to confirm if the site-directed mutagenesis had been successful or not.

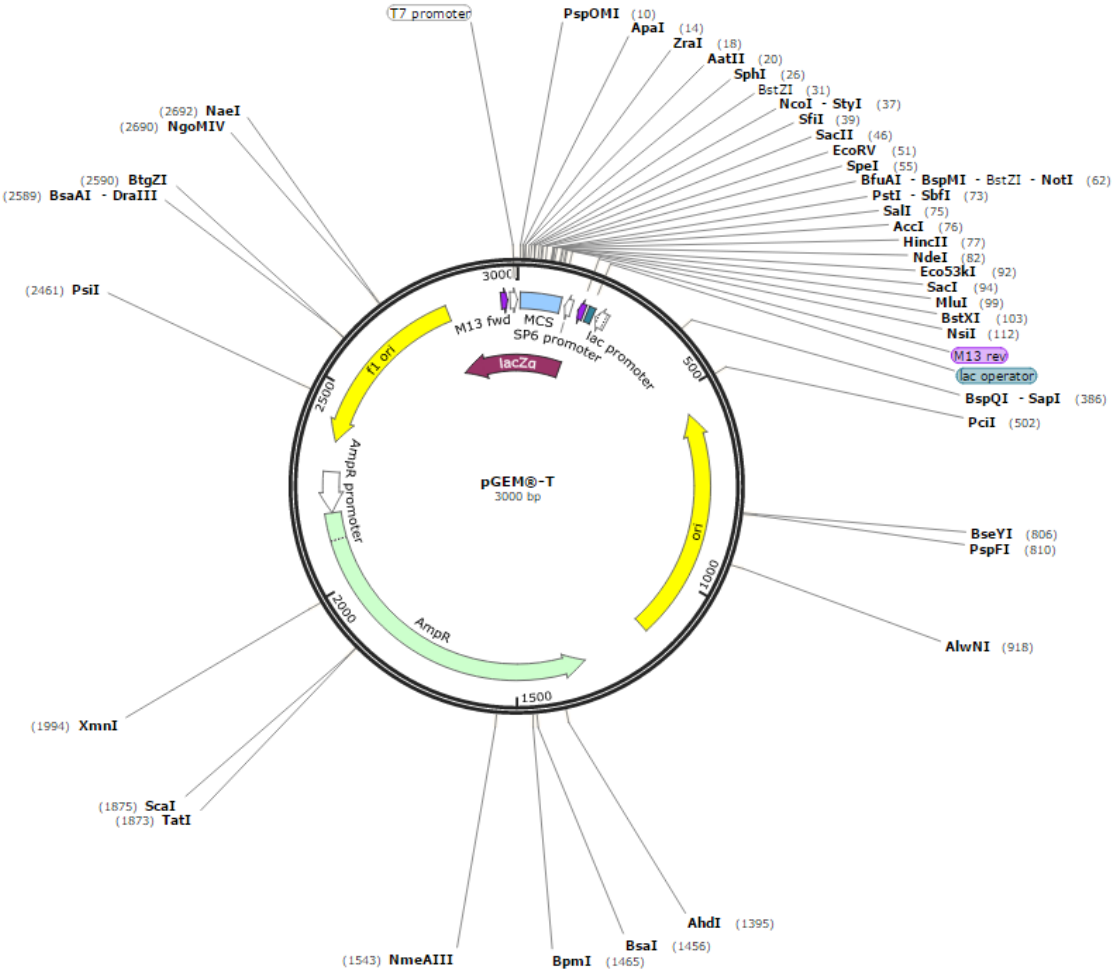

Figure 2.1. The pGEM®-T vector.

Vector map of the pGEM®-T vector, including the locations of the multiple restriction sites. Produced using SnapGene viewer 3.3.1.

Genomic DNA isolation from *T. brucei*.

3×10^8 cells were harvested at by centrifugation at 1,500 g for 10 min, washed once in 1X PBS, centrifuged again, and re-suspended in 150 μl 1X DNA lysis buffer at 37 ^{o}C for 5 min. Next, 150 μl of 1:1 (v/v) phenol/chloroform solution was added and the tube slowly inverted for 5 min. 100% EtOH (300 μl) was added and the mixture was gently swirled for 15 s followed by incubation for 5 min on ice. Centrifugation at 13,000 g for 10 min was used to separate the aqueous layer from the organic layer, and the aqueous layer containing the DNA was transferred into a fresh tube. 300 μl of 100% EtOH was added, the tube was inverted ten times and then incubated at room temperature for 5 min, and centrifuged at 13,000 g for 5 min. The pellet was washed once with 1 ml of 100% EtOH and harvested by centrifugation at 13,000 g for 5 min. The DNA was dried and ethanol removed using a vacuum for 10 min, then the DNA was dissolved in 100 μl of TE-8 (10 mM Tris-HCl (pH 8), 1 mM EDTA (pH 8)). The samples were then stored at - 20 ^{o}C until used. This procedure was based on the method described by Medina-Costa and Cross used to isolate gDNA from bloodstream form *T. brucei* [122].

DNA precipitation (concentration).

50 μl DNA was added to a mixture of 40 μl nuclease-free water, 5 μl linear acrylamide, 10 μl 3 M sodium acetate, and 400 μl chilled 100% ethanol (-20 ^{o}C). This mixture was incubated at -20 ^{o}C for 30 minutes, then centrifuged at 14,000 g for 10 minutes at 4 ^{o}C. The supernatant was removed and the white linearised plasmid pellet was re-suspended in 600 μl chilled 70% ethanol (-20 ^{o}C), and centrifuged at 14,000 g for 30 minutes at 4 ^{o}C. The supernatant was removed and the pellet allowed to dry in a culture hood, then re-suspended in nuclease free water to a final concentration of 1 - 2 $\mu g.\mu l^{-1}$.

DNA transfection of *T. brucei*.

3×10^7 cells were required for both bloodstream form and procyclic form transfections, and were pelleted from culture at 1,000 g for 10 minutes. The supernatant was removed

and the pelleted cells were re-suspended in 100 μl Amaxa Nucleofactor solution, and incubated for 1 minute at room temperature. The linearised and precipitated plasmid was added to an electroporation cuvette, to which the nucleofactor – cell mix was added. Cells were then electroporated using the X-100 setting of the Amaxa Nucleofactor II transfection system, and added to HMI-9 (bloodstream form) or SDM-79 (procyclic form) culture media to be incubated overnight to allow cells to recover. Appropriate selection antibiotics were added the following day, and cells were plated out into individual wells in 2 $\times$ 24 well plates. Successful clones were usually evident after 1 - 2 days incubation, but were cultured and monitored for at least one week to ensure that clones were successfully selected.

2.2.4 Cell fixation and imaging.

Cells were harvested from culture and centrifuged gently at 1,000 g for 15 min at 4 ^{o}C. The supernatant was removed, and the cell pellet was washed with chilled 1X PSG, then centrifuged again at 1000 g for 15 min at 4 ^{o}C. This was repeated twice more, and the pellet was re-suspended in chilled 1X PBS to a concentration of 2×10^7 cells.ml^{-1}. An equal volume of 6% (v/v) para-formaldehyde was added to the suspended cells, for fixation, and the solution was incubated on ice for 10 - 20 min (bloodstream cells were incubated longer than procyclic cells). Following incubation, the cells were washed twice with 1X PBS, with centrifugation at 800 g for 10 min, and re-suspended at 2×10^7 cells.ml^{-1} in 1X PBS containing 0.02 % (w/v) sodium azide (for up to 1 weeks storage at 4 ^{o}C).

Triple-well microscope slides were prepared by bathing in a 10% (w/v) poly-L-lysine solution, for by gentle drying at 80 ^{o}C. 10 μl of the fixed cells were added to well 1, followed by 10 μl of a 1 in 10 dilution of the fixed cells to well 2, and 10 μl of a 1 in 50 dilution of the fixed cells to well 3. Cells were allowed to settle on the slides for 30 min at room temperature. The slides were then dipped gently in 1X PBS to rinse off loose cells, and were left air-dry to semi-dryness. Prolong® Gold reagent containing DAPI stain was then applied to each well, and the wells were carefully sealed with a cover-slip and nail varnish. Finally, cells were imaged using an Olympus IX81-long focal length fluorescent microscope.

2.3 Generation of bloodstream form and procyclic form cASAT RNAi cell lines.

Bloodstream form and procyclic form monomorphic MITat 1.2 cells were used to generate cytoplasmic aspartate aminotransferase (cASAT) specific tetracycline inducible RNAi knockdown cells. These cells had been modified previously to express a stable T7 RNA polymerase and tetracycline repressor protein to allow relatively easy and replicable RNAi induction. This inducible expression system was constructed by Wirtz et al, with the intention of allowing the generation of cells that could contain conditionally expressed toxic components or RNAi knockdown components [123]. Bloodstream form cells were manipulated to stably express both pLEW90 and pLEW13 (termed the 90.13 cell line), whilst procyclic form cells expressed pLEW29 and pLEW13 (termed the 29.13 cell line) (Table 2.2, Fig. 2.2 & 2.3). To introduce the cASAT RNAi component into the cells, the phleomycin selectable p2T7-177 RNAi vector was used, which had been previously generated and contained a 446 bp open reading frame segment of *T. brucei* cASAT (Fig. 2.4). The p2T7-177 vector is advantageous in that it utilises the transcriptionally silent minichromosomes, rather than mega base-sized chromosomes present in trypanosomes, which avoids displacing endogenously expressed genes [124]. Moreover, these mini chromosomes are mitotically stable and so daughter cells maintain the desired RNAi induction levels as parent cells.

Table 2.2. Vectors for generating inducible cell lines.

Plasmid	Main elements	Target loci	Selection marker
pLEW13	T7 RNA polymerase and Tet repressor	Tubulin	G418
pLEW29	T7 promoter-regulated Tet repressor	RNA pol I	Hygromycin
pLEW90	T7 promoter-regulated Tet repressor	Tubulin	Hygromycin

Transfection of the bloodstream 90.13 and procyclic 29.13 MITat 1.2 cells with the cASAT p2T7-177 RNAi vector was performed. A previously generated cASAT p2T7-177 RNAi vector was first transfected into DH5α *E. coli* as outlined previously to generate the required amount of the vector for transfection into trypanosomes, followed by mini-prep of the plasmid DNA, as above. Restriction digest to confirm the presence of the 446 bp insert in the p2T7-177 RNAi vector was performed using a HindIII and BamHI double digest, where both sites were flanking the 446 bp cASAT

insert in the vector. Two bands of 447 bp and 5,274 bp confirmed correct insertion of the fragment. 2 ml of the corresponding bacterial culture was added to 248 ml LB broth containing 1 mg.ml^{-1} ampicillin and cultured overnight at 37 ^{o}C. Successful clones were then DNA midi-prepped using a Promega pureyield plasmid midi-prep kit, with yields and purity of DNA quantified using a Nanodrop spectrophotometer. 10 – 20 μg of the plasmid was then linearised overnight with NotI, as required for transfection into trypanosomes. Following linearisation, plasmid DNA was precipitated to concentrate the plasmid DNA. Both bloodstream form 90.13 and procyclic form 29.13 cells were transfected with the cASAT p2T7-177 RNAi vector. A final concentration of 2.5 μg.ml^{-1} of phleomycin was added to culture as the selection antibiotic for the cASAT p2T7-177 RNAi vector for both bloodstream form and procyclic form cells, then cells were plated out evenly on a 24 well plate and incubated at 37 ^{o}C overnight. Clones that had successfully grown over the next 3 days were deemed suitable for further expansion. These cASAT p2T7-177 RNAi MITat 1.2 bloodstream form 90.13 & procyclic form 29.13 cells, herein referred to as 'cASAT RNAi cells', were therein maintained in HMI-9 (bloodstream form) or SDM-79 (procyclic form) culture media. HMI-9 media was supplemented with 2.5 μg.ml^{-1} phleomycin, 2.5 μg.ml^{-1} G418, and 5 μg.ml^{-1} hygromycin to maintain selective pressure for the transfected constructs. SDM-79 media was supplemented with 2.5 μg.ml^{-1} phleomycin, 25 μg.ml^{-1} G418, and 25 μg.ml^{-1} hygromycin.

Knockdown effectiveness was confirmed by induction of the RNAi using tetracycline, and measuring the resultant effects via cell viability measurements, in combination with qRT-PCR. To monitor the effects of cASAT RNAi on growth and cell viability, cells were grown in their respective cultures at an initial concentration of 2×10^5 cells.ml^{-1}. Tetracycline was added to the media to a final concentration of 1 μg.ml^{-1}, and was absent from the non-induced controls. Cell counts were performed using a hemocytometer at 24 hours intervals for a period of 72 - 96 hours.

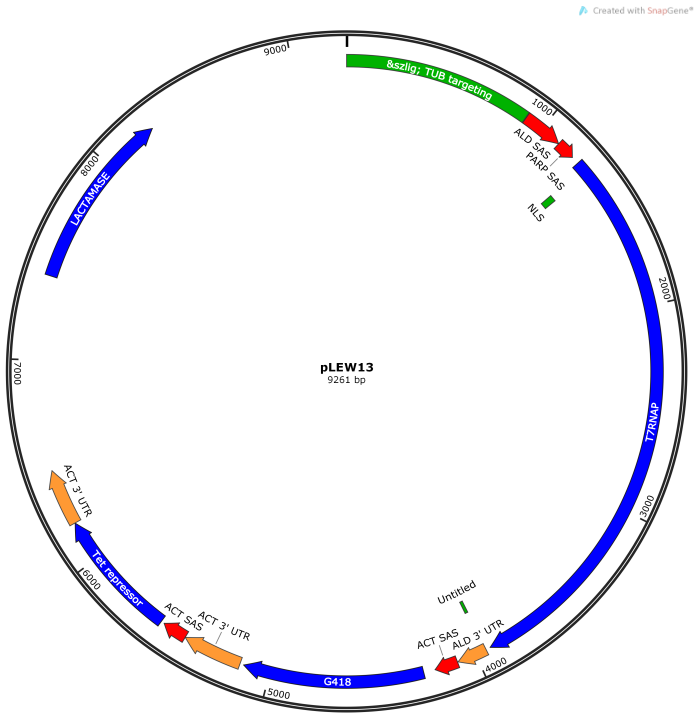

(a)

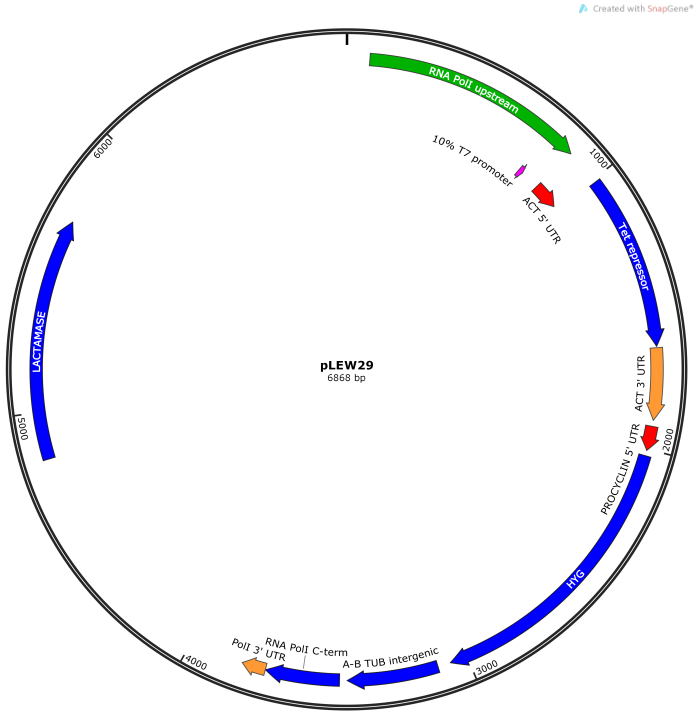

(b)

Figure 2.2. Vector maps of the pLEW13 and pLEW29 constructs.

(a) The pLEW13 construct. **(b)** The pLEW29 construct. These constructs were used to generate a stable T7 polymerase and Tet repressor expressing procyclic form cell line. Vector sequences obtained from http://tryps.rockefeller.edu/trypsru2_plasmids.html, and were generated using SnapGene viewer 3.3.1.

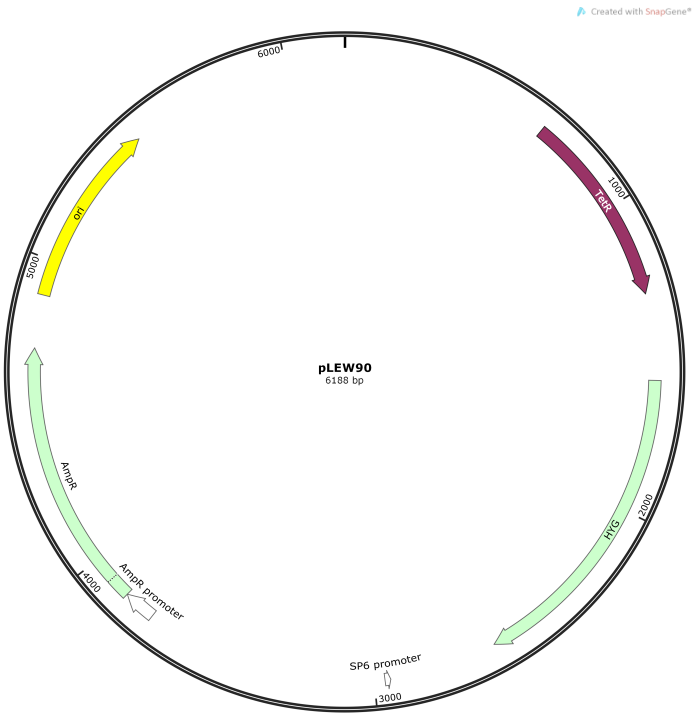

Figure 2.3. Vector map of the pLEW90 construct.

The pLEW90 construct and the pLEW13 construct were used to generate a stable T7 polymerase and Tet repressor expressing bloodstream form cell line. Vector sequence obtained from http://tryps.rockefeller.edu/trypsru2_plasmids.html, and was generated using SnapGene viewer 3.3.1.

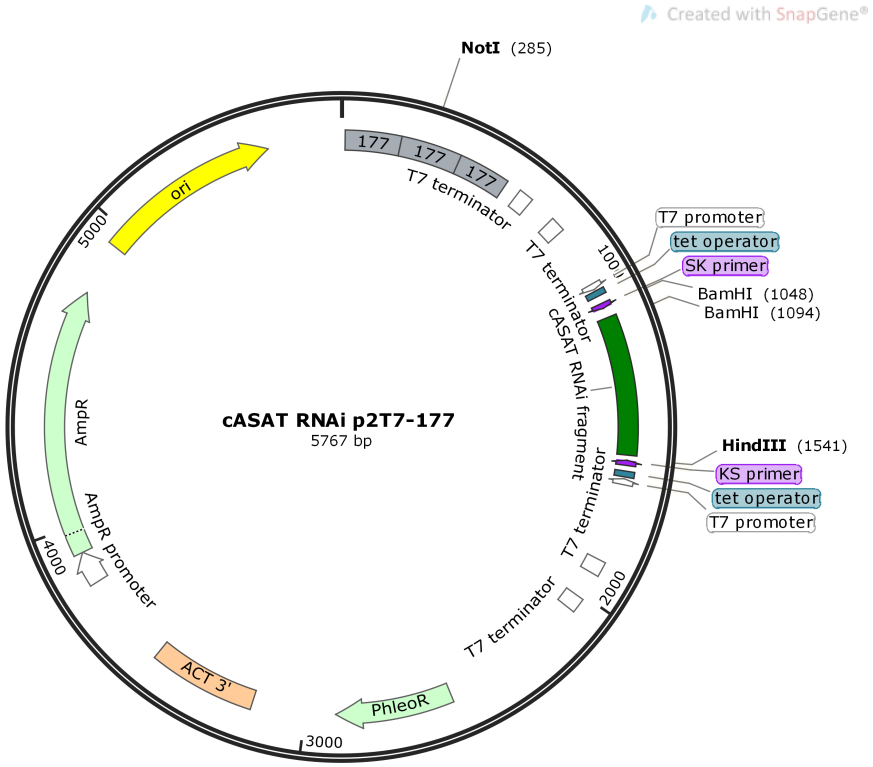

Figure 2.4. The cASAT RNAi p2T7-177 vector.

Vector map of the cASAT RNAi p2T7-177 vector produced using SnapGene viewer 3.3.1.

2.3.1 qRT-PCR of bloodstream and procyclic form cASAT RNAi cells.

RNA extraction.

Cells were isolated in their logarithmic phase of growth, and RNA was extracted from 1×10^8 cells.ml^{-1} using the Absolutely RNA® kit, which uses a spin-cup method for RNA extraction. Care was taken to work in an RNAase free environment in an RNA extraction hood treated with RNaseZap. Purified RNA quality was assessed by the $A_{260/280}$, and concentrations were adjusted to 500 ng total RNA.

Quantitative real time polymerase chain reaction (qRT-PCR).

Relative quantification of the *cASAT* and *mASAT* mRNA transcripts were performed using a Brilliant® II SYBR green qRT-PCR one step kit and an Mx3000P qPCR system. Primers were designed to be optimised for RT and amplification using Beacon 7

designer software (Table 2.3). Specificity was assessed over a range of primer concentrations to have greater than 95% efficiency during amplification. The cycling threshold method ($2^{(\Delta\Delta Ct)}$) was used for relative quantification by comparative method between induced and non-induced RNAi cells [125]. Transcript levels were normalised to the actin RNA transcript level. All measurements were performed in triplicate.

Table 2.3. Primers used for qRT-PCR.

Primer	Sequence	Gene
cASAT.qRTPCR.FP1	5'-ATTTCTGCTGTCGTTTCG-3'	*cASAT*
cASAT.qRTPCR.RP1	5'-ACCATCTCCTTGAGTTCC-3'	*cASAT*
mASAT.qRTPCR.FP1	5'-ACGGCGAGTGCTGAAGAG-3'	*mASAT*
mASAT.qRTPCR.RP1	5'-ACCATAAAGAGGCGGATTGC-3'	*mASAT*
Actin.qRTPCR.FP1	5'-ATGAGCAAGCGATGATGG-3'	*actin*
Actin.qRTPCR.RP1	5'-CAACTCGTTATAGAAGGTATGG-3'	*actin*

2.4 Generation of the bloodstream form AHADH^{in} cell line.

Over the course of the investigations of the secretion of aromatic ketoacids by bloodstream form *T. brucei*, a cell line was created that alternately excreted aromatic hydroxyacids or aromatic ketoacids depending on the tetracycline inducible expression of AHADH. The previously created 90.13 parental line that expressed T7 RNA polymerase and tetracycline repressor protein was used. The blasticidin-selectable p3859 T7 polymerase vector used to ectopically express AHADH was obtained from Mark Carrington [126]. AHADH (EMBL accession number AF112259, TriTrypDB gene ID TcCLB.506937.10) was amplified from *T. cruzi* genomic DNA with the primers shown in Table 2.4, using the standard PCR conditions outlined in the PfuUltra II Fusion DNA polymerase kit. A single 999 bp band was obtained for AHADH, confirming specific amplification (Fig. 2.6a). The p3859 vector was heat shocked into *E. coli*, plasmid DNA was extracted, and p3859 presence was confirmed by BamHI restriction digest (Fig. 2.6b).

Unfortunately, the p3859 vector is linearised NotI, a restriction site that is also

Table 2.4. PCR primers used for the amplification of AHADH.

The HindIII site in the forward primer, and the BamHI site in the reverse primer are underlined.

Primer	Sequence
AHADH FP	5'-GCGAAGCTTATGTTTTTTGAAGGTGCATGCGCGAAGGTG-3'
AHADH RP	5'-CCGGATCCTTACAATGCCAAAGACAGCGACTCCGA-3'

found internally in the AHADH gene sequence (Fig. 2.5). Site-directed mutagenesis was employed to remove the internal NotI site in AHADH. The AHADH gene fragment was first ligated into pGEM®-T, using the standard pGEM®-T protocol. Successful clones containing AHADH were plasmid DNA extracted, and the plasmids were subjected to PCR amplification using new primers designed to mutate a single base of the AHADH NotI site (Table 2.5), followed by DpnI digestion and heat shock into *E. coli*. Successful clones were expanded and DNA extracted via mini-prep. AHADH was then excised from pGEM-T using a BamHI-HindIII double digest, and ligated into p3859 (stuffer removed previously with a BamHI-HindIII double digest). Insertion of AHADH into p3859 and the success of the site directed mutagenesis was confirmed by two separate restriction digests (Fig 2.7a & 2.7b) and by AHADH PCR (Fig. 2.7c). The plasmid was then transfected into bloodstream form *T. brucei* as previously described. Clones were selected for an maintained with a combination of 5 μg.ml^{-1} blasticidin, 2.5 μg.ml^{-1} G418, and 5 μg.ml^{-1} hygromycin added to the culture.

Table 2.5. PCR primers used for site-directed mutagenesis of the NotI site in AHADH.

Underlined nucleotides are at the mutagenesis site (a C/G pair was removed from AHADH).

Primer	Sequence
AHADHNotIMutaFP	5'-TCATTGCCGGAGGCCGCATGTTGG-3'
AHADHNotIMutaRP	5'-CCAACATGCGGCCTCCGGCAATGAGGG-3'

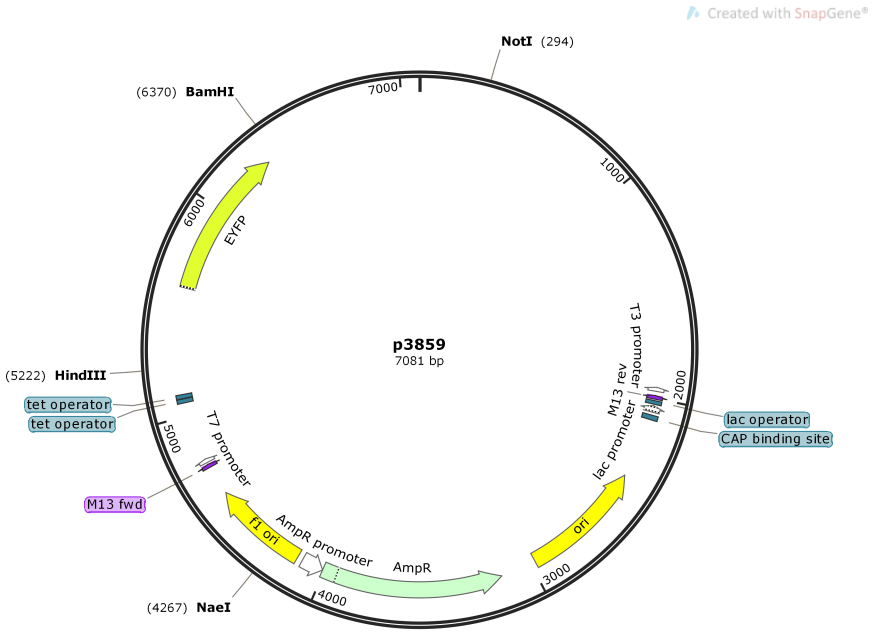

(a)

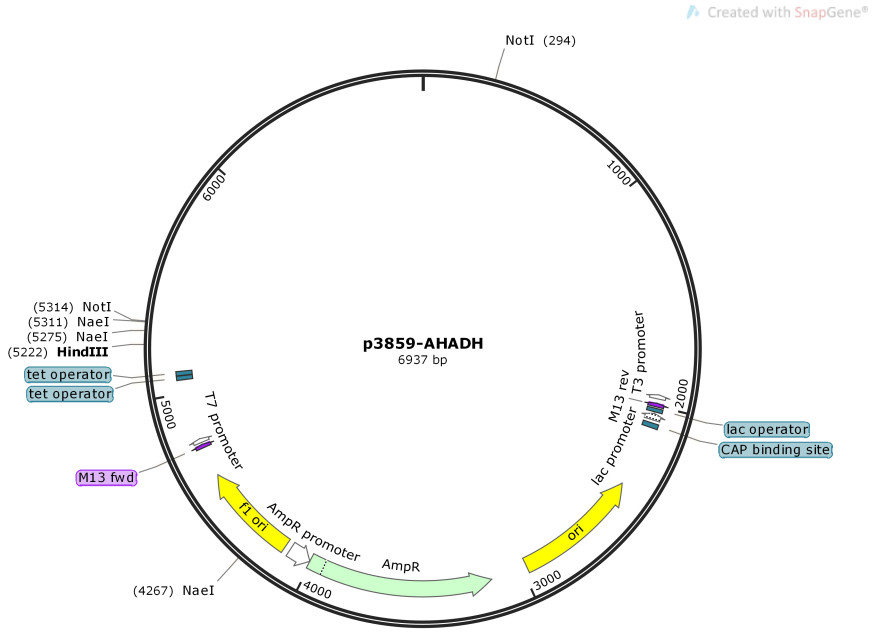

(b)

Figure 2.5. Vector maps of the p3859 and non-mutagenised p3859-AHADH plasmids.

(a) Vector map of the p3859 plasmid. **(b)** Vector map of the non-mutagenised p3859-AHADH plasmid. Produced using SnapGene viewer 3.3.1.

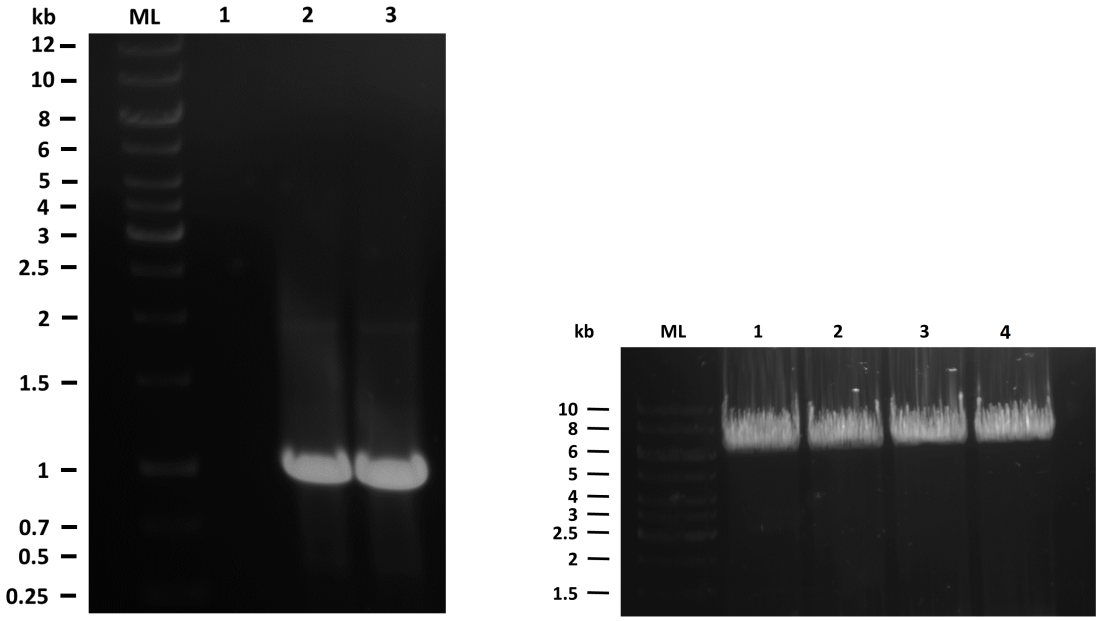

(a) **(b)**

Figure 2.6. DNA agarose gels of PCR amplified AHADH and BamHI digested p3859.

(a) AHADH was successfully amplified from *T. cruzi* genomic DNA, as visualised on an agarose gel at ≈ 1,000 bp. Lane 1 was a negative control, lane 2 and 3 contain amplified AHADH. **(b)** Single site restriction digest with BamHI linearised p3859 to a single ≈ 7,000 bp band, confirming the vector was correct in lanes 1 - 4 (four different bacterial clones, all of which contained p3859). ML = molecular ladder.

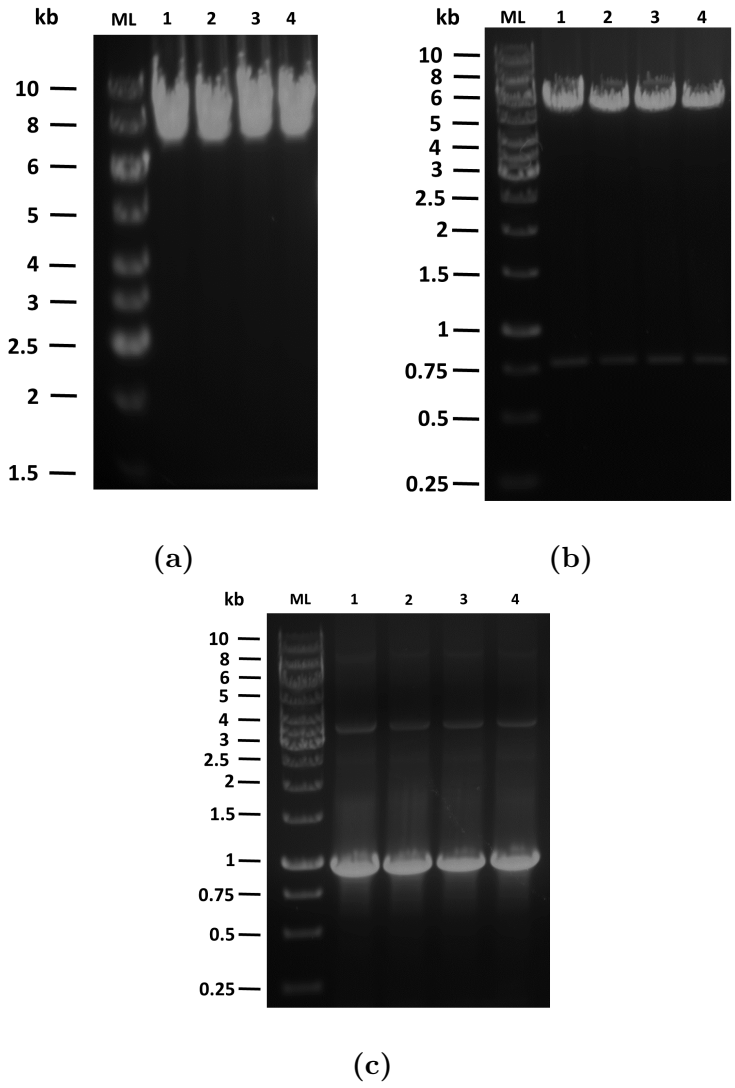

Figure 2.7. DNA agarose gels of restriction digests and PCR amplification of the p3859-AHADH vector.

(a) NotI linearised p3859-AHADH generated a single ≈ 7,000 bp band, confirming at least that some form of p3859 was present in lanes 1 - 4. **(b)** Restriction digest with NaeI yielded two bands as expected (≈ 1,000 bp and ≈ 6,000 bp); there is an NaeI site in both p3859 and AHADH. **(c)** Finally, PCR amplification of AHADH (band at ≈ 1,000 bp) confirmed its presence in the p3859 vector. ML = molecular ladder.

2.5 Generation and purification of *T. brucei* and *T. cruzi* recombinant cASAT.

2.5.1 cASAT expression vector generation.

With the aim of performing kinetic analysis and structural studies of the cASAT proteins, several constructs were designed to be recombinantly expressed and purified. The constructs were designed to amplify segments of *T. brucei* (*Tb*10.70.3710, $XM_8$17522.1, $XP_8$22615) and *T. cruzi* (*Tc*00.1047053503841.70, $XM_8$02695.1, $XP_8$07788.1) cytoplasmic aspartate aminotransferase.

BL21 (DE3) *E. coli* containing a pNIC28-Bsa4 vector expressing T7 RNA polymerase, were chosen for recombinant expression of cASAT. The pNIC28-Bsa4 vector contains an N-terminal hexahistidine epitope tagging site adjacent to the ligation-independent cloning site, to allow for easy downstream purification of cASAT using a Ni^{2+} column, with an internal Tobacco Etch Virus (TEV) cleavage site within the tagging site to allow for hexahistidine tag removal post initial purification (Fig. 2.8). The ligation-independent cloning site is comprised of a 'stuffer' segment that also contains the SacB gene. SacB is used as a negative selection marker for the vector, as it encodes levansucrase which converts sucrose to 2,6-beta-D-fructosyl, a metabolic product that is toxic to the *E. coli*. Consequently, when grown on 5% sucrose supplemented LB agar plates, unsuccessfully transformed cells still containing the SacB gene stuffer would die. Ligation-independent cloning utilises homologous recombination between the single site BsaI linearised pNIC28-Bsa4 vector 5' and 3' ends and the linear cASAT gene insert. Homologous recombination is possible through the generation of sequence specific 5' and 3' ssDNA overhangs on the linearised vector that combine with specifically constructed complimentary overhangs in the insert fragment DNA, using T4 DNA polymerase. Internal nicked ends in the newly circular plasmid are repaired by the host bacterium ligase, which are far more sequence specific than ligations traditionally performed with T4 DNA ligase. Ligation independent cloning is an advantageous technique as it works stably over a broad range of DNA concentrations and is highly specific due to host bacterial ligase activity, leading to reduced levels of shortened assembly products and wrong order assembly [127, 128]. Varying con-

structs were generated for two purposes; full length protein constructs for use in both kinetic studies and for crystallisation purposes, and N-terminally truncated constructs of varying length to aid crystallisation if the full length constructs proved difficult to crystallise [129]. It was postulated that this may be necessary as other cASAT crystal structures contain an extended disordered N-terminal 'arm' segment [130, 131].

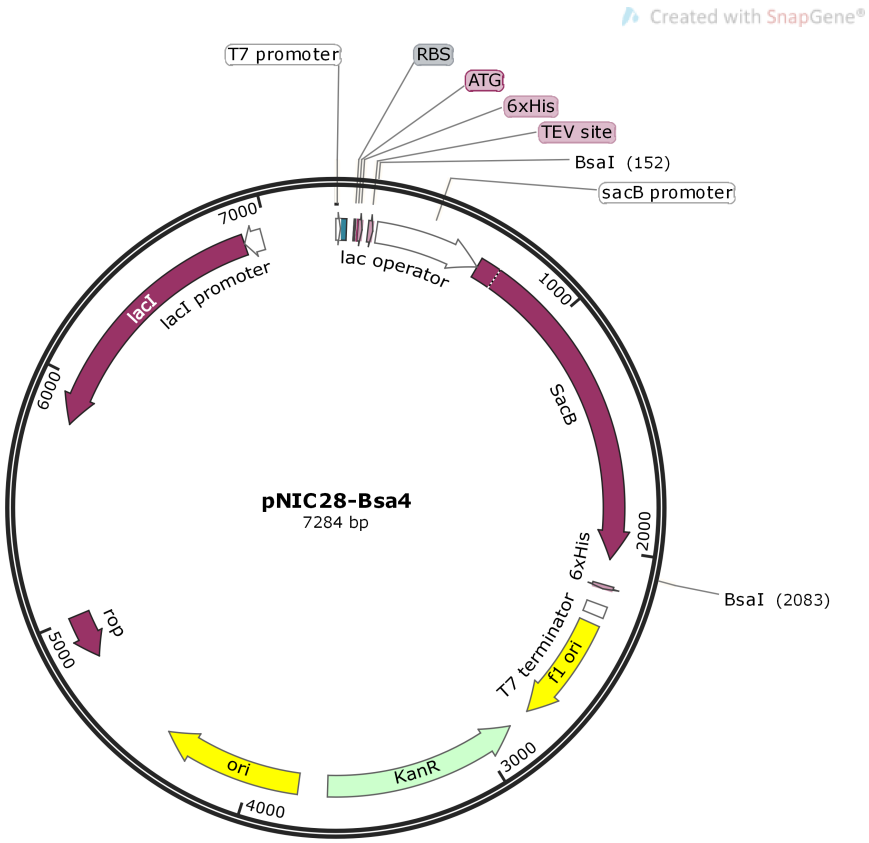

Figure 2.8. The pNIC28-Bsa4 vector.
Vector map of pNIC28-Bsa4 produced using SnapGene viewer 3.3.1.

Gene segments were amplified from *T. brucei* and *T. cruzi* genomic DNA by PCR using LIC specific primers (Table 2.7). A master mix was prepared and the DNA was subjected to the following PCR cycle; 5 min at 95 ^{o}C, followed by 25 cycles at 95 ^{o}C for 45 s, 56 ^{o}C for 45 s, and 72 ^{o}C for 1 min. Then, a final extension step was performed at 72 ^{o}C for 10 min. A single fragment $\approx$ 1.2 Kb was produced for both TbcASAT and TccASAT (Fig. 3.5). The generated DNA fragments were then ligated into the pNIC28-Bsa4 vector. The vector was firstly linearised with BsaI for 3 – 4 hours at 50 ^{o}C in NEBuffer 3, then run on a 1% agarose gel to remove any uncut plasmid, the linearised vector was excised, and then extracted from the gel using a PeqGOLD gel extraction kit. DNA concentration and purity was verified using an

ND-1000 nanodrop spectrophotometer. To add 3' and 5' extensions to the linearised vector making it suitable for LIC, the vector was treated with T4 DNA polymerase and dGTPs (Table 2.6). The use of only a single nucleotide exploits the different rates of exonuclease and polymerase activity of T4 DNA polymerase; in the absence of dNTPs, the exonuclease activity of the enzyme acts in a 3' to 5' direction, removing nucleotides and generating sticky ends on the dsDNA. Sticky end propagation can be controlled by adding a single dNTP, in this case dGTP. When the T4 DNA polymerase reaches a section of G nucleotide repeats, the polymerase activity now out-competes the exonuclease activity, leading to a point where the ssDNA is neither shortened nor extended due to this back and forth activity. By choosing sites or artificially introducing them into the previously produced dsDNA, sticky ends of a desired length are generated [128]. The various inserts were also treated with T4 DNA polymerase to generate complimentary overhangs, using dCTP in place of dGTP (Table 2.6). To ligate the inserts into the vector, both were simply mixed in a 2:1 ratio of insert:vector, typically in 3 μl volumes and incubated at room temperature for 20 min. Following this incubation the 3 μl of insert-vector solutions were added to 50 μl volumes of competent BL21(DE3) *E. coli*, and incubated on ice for 40 min, followed by heat shock at 42 ^{o}C for 30 s, the incubation again on ice for 2 min. These transformed bacteria were then added to tubes containing 1 ml LB broth + 5% Sucrose and incubated at 37 ^{o}C for 1 h. Bacterial cells were then pelleted out of culture at 14,000 g for 20 s, and 950 μl supernatant was removed. The pellet was re-suspended in the remaining supernatant and lawned onto LB Agar + 5% Sucrose w/v plate containing 50 μg.ml^{-1} kanamycin, and incubated overnight at 37 ^{o}C.

Colonies on each plate should contain successfully cloned cASAT inserts. Several clones were selected from each construct plate, to be checked by small scale protein expression and DNA sequencing. DNA was extracted from these clones using a QI-Aprep Spin Miniprep Kit following overnight culture in 50 ml of LB broth + 50 μg.ml^{-1} kanamycin, and DNA quality was assessed using an ND-1000 Nanodrop, before being speed-vacuumed to dryness for shipping. DNA sequencing was performed by Source Bioscience and confirmed cASAT insertions into each plasmid were successful. Difficulties in producing the -47' N-terminal *T. brucei* cASAT clones excluded these constructs from further study.

Table 2.6. Reaction mixture for generation compatible sticky ends on the pNIC28-Bsa4 and DNA insert.

The final concentration of either the vector or insert was dependent on their initial concentration. The vector and DNA inserts were treated with T4 DNA polymerase in the presence of either dGTP or dCTP at 22 ^{o}C for 30 min, followed by extension at 75 ^{o}C for 20 min. Reaction performed in a final volume of 10 μl.

Component	Volume in reaction (μl)
Sterile ddH_2O	X
BsaI digested pNIC28-Bsa4	-
purified DNA insert	-
10X T4 polymerase buffer	1
25 mM dGTP or dCTP	1
100 mM DTT	0.5
10 mg.ml^{-1} BSA	0.1
T4 DNA polymerase	0.1

Table 2.7. PCR primers used for LIC of recombinant cASAT.

Primer	Sequence
TbcASAT.FP	5'-TACTTCCAATCCATGTCCAGGCCCTTTAAGGACTTAGCACCC-3'
TbcASAT.RP	5'-TATCCACCTTTACTGCTACTTGTTACGCACGTGTCGGACAAC-3'
TccASAT.FP	5'-TACTTCCAATCCATGGCGATCCGATGCCTCTGG-3'
TccASAT.FP	5'-TATCCACCTTTACTGTCATTCCGTGACGGTTCTTACC-3'
-47'TbcASAT.FP	5'-TACTTCCAATCCATGCCATTAAAAGTAGTGCGGAAGGCTGAG-3'

2.5.2 Small scale protein expression.

Small scale protein expression was performed concurrently with DNA sequencing preparation. 200 μl of each of the cultures (1-P1C1 to 12-P4C3) used for DNA sequencing had been retained, and 100 μl of each culture was added to 10 ml of 2X YT broth + 50 μg.ml^{-1} kanamycin then cultured at 37 ^{o}C for approx. 3 hours until an OD_{600nm} absorbance of 0.6 was obtained. At this point isopropyl-β-D-thiogalactopyranoside (IPTG) was added to a final concentration of 500 μM to induce cASAT protein expression. The cultures were then incubated at 27 ^{o}C for 6 hours, to ensure optimal expression of stably folded protein. The samples were centrifuged at 4,000 g for 15 min. The pellets were then re-suspended in 3 ml bacterial lysis buffer and sonicated for 5 x

2 min 40% duty cycles at 4 ^{o}C with a Branson Sonifier S-250A. The sonicated mixture was then centrifuged at 14,000 g for 20 min at 4 ^{o}C, to pellet out cell debris. The resultant supernatant was removed and placed in new tubes labelled 'S', whereas the pelleted cell debris was labelled 'P'. Each of the 'S' tubes had 40 μl of 50% v/v Ni^{2+} agarose resin added to them and were incubated on a rotating disc mixer for 5 min at 4 ^{o}C. The resin was then pelleted down at 600 g for 2 min at 4 ^{o}C, the supernatant was removed, and the pellet re-suspended in 1.5 ml lysis buffer, then spun again as previously, and then the supernatant was removed. 20 μl of 2X protein sample buffer was added to the pellet, with an equal volume of ddH_2O. The corresponding pellets were re-suspended in 200 μl 3M urea, then 5 μl of the suspension was removed and added to 15 μl 2X protein sample buffer and 10 μl ddH_2O. Both 'S' and 'P' samples were then boiled at 100 ^{o}C for 5 min, and 10 μl of each was run on a 12% SDS-PAGE gels at 50 mA/gel for approx. 1 hour. The gels were rinsed in ddH_2O, then placed in a Coomassie Brilliant Blue stain for 3 hours. Gels were then treated with destain solution until stained protein bands were clearly distinguishable from one another. The cell lines and constructs were preserved by generating glycerol stocks to be stored at -80 ^{o}C; 500 μl of the respective cell cultures were added to 500 μl 100% v/v glycerol and inverted gently, followed by freezing.

2.5.3 Large scale protein expression.

Stained bands appeared as expected at approx. 40 kDa, corresponding to the recombinant cASAT proteins in the small scale expression. Consequently a large scale expression of the cASAT constructs was undertaken. One construct of *T. brucei* and *T. cruzi* each were chosen based the sequencing results combined with how well they expressed recombinant protein in the small scale expression test. Flame loop inoculations of the stored glycerol cultures of 1-P1C1 and 10-P4C1 used in the small scale expression was used to generate a starter culture by placing them in 10 ml 2X YT media + 50 $\mu g.ml^{-1}$ kanamycin and incubating overnight in a shaking incubator at 180 RPM at 37 ^{o}C. These 10 ml starter cultures were then transferred to 1 L of 2X YT broth + 50 $\mu g.ml^{-1}$ each, and incubated at 37 ^{o}C at 150 RPM on the shaking incubator. The ΔOD_{600nm} was measured periodically until it reached an absorbance of 0.6, at which point IPTG was added to a final concentration of 500 μM and the incubation

temperature was lowered to 27 ^{o}C. Following 18 hour incubation's, *E. coli* cells were pelleted from the culture by centrifugation at 4,000 g for 15 min. The supernatant was removed and the pellets re-suspended in 50 ml 1X PBS each, and centrifuged again as above. The supernatant was removed and the pellets were re-suspended in 50 ml 1X bacterial lysis buffer with 50 μg.ml^{-1} lysozyme at 4 ^{o}C and cells were lysed using a French press homogeniser. Cell debris was removed by centrifugation at 14,000 g for 30 min and a 1% (v/v) protease inhibitor cocktail was added to the supernatant. The resulting supernatants were then run through 5ml of Ni^{2+} resin columns, in a cold room at 4 ^{o}C, which bound the His-tagged protein. For *T. brucei* the elutant was collected in 5 ml fractions; Fractions 1 – 4 (F1-4) contained the 'run through' – unbound contaminant protein and cell debris. The column was then washed with 24 ml bacterial lysis buffer to further remove contaminants, collected as fractions 5 -12 (F5 – F12). The pure recombinant *T. brucei* cASAT bound to the column was then eluted by continuously adding bacterial lysis buffer supplemented with 250 mM imidazole at a constant flow rate, which competitively binds to the Ni^{2+} resin, displacing the recombinant protein [132]. This pure protein was collected in fractions 13 – 16 (F13-F16). A rough Bradford assay was used to assess the protein concentration of the eluted fractions, by adding 2 μl of each fraction to 30 μl volumes of Bradford reagent and mixed, with a deeper blue indicating higher protein concentrations [133]. Based on the Bradford assay, fractions 13, 14, and 15 contained the purified cASAT and were pooled together. The same elution procedure was carried out for the *T. cruzi* recombinant cASAT and its pure fractions were pooled. Regardless of the whether the protein was to be used for kinetic assays or crystallisation purposes, it was dialysed overnight in 3.5K MWCO SnakeSkin Dialysis tubing against 1 L volumes of bacterial lysis buffer, to remove the imidazole. Protein to be used for crystallisation had 50 mg.ml^{-1} rTEV added at this point, to cleave off the histidine tag. Following dialysis, the protein utilised for kinetics was either assayed immediately to mitigate loss of activity due to aggregate formation and protein degradation, or was stored in 20% (v/v) glycerol at -80 ^{o}C for later use. Protein used for crystallisation was re-run through a 2 ml of a Ni^{2+} column, to bind and remove the cleaved His tags. In this case all the protein is eluted as it is run though, as can be seen via rough visual Bradford assay (Fig. 2.9). The fractions were pooled and the protein stored temporarily at 4 ^{o}C until further use. During subsequent purification, problems arose with the solubility of the *T. brucei* protein, as it rapidly formed inclusion bodies and precipitated. Protein aggregates were removed by high

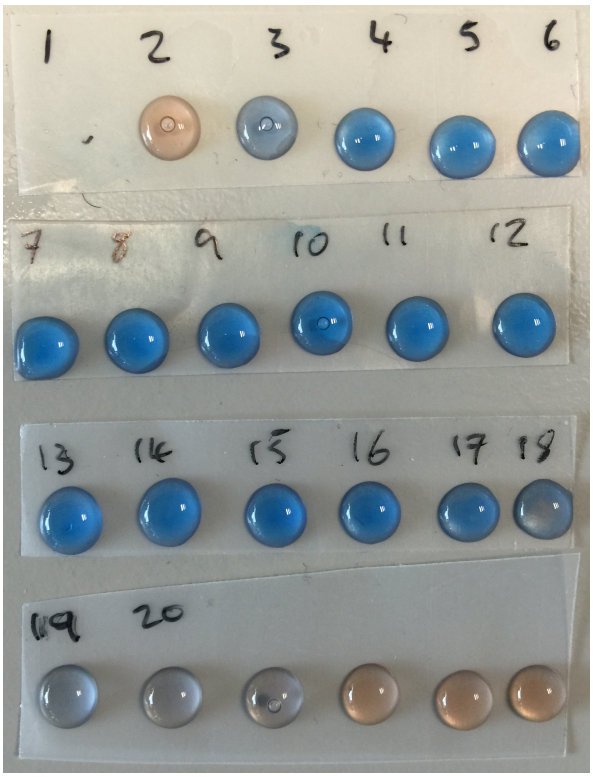

Figure 2.9. Rough visual Bradford assay used to assess protein elution from a Ni^{2+} column.

2 μl of Ni^{2+} column eluted fractions were added to 20 μl of Coomassie Brilliant Blue G-250. Protein content was assessed visually by monitoring the change of the dye from red (no protein) to blue (protein). The deeper blue indicates a higher protein concentration. In this example, fractions 4 - 17 were collected.

speed (24,000 g) centrifugation, protein was diluted to varying degrees, and the pH was raised/lowered in attempts to find stabilising conditions for the protein [134].

2.5.4 cASAT Crystallisation.

rTEV cleaved cASAT protein was passed through a Superdex 200(16/600) gel filtration column equilibrated with column buffer, to purify it further. The protein eluted from the column was then concentrated using 10 kDa MWCO ultri-centrifugal filters, to a final concentration of ≈ 8 mg.ml^{-1}, as assessed by measuring the sample absorbance at 280 nm. Protein purity was confirmed by screening with SDS-PAGE. Crystallisation trials were set up using an automated Mosquito TTP labtech machine, which aliquoted the protein into 96 well plates using the hanging drop method of crystallisation. Protein was diluted in either a 1:1 or 1:2 protein:reservoir ratio. Plates were film sealed and

stored at 18 ^{o}C for a period of 5 - 7 days. The screens used were Midas, Morpheus, Wizard JB screen and JB screen classic. Potential crystal growth in each well was assessed daily using a Nikon bifocal microscope.

Once small crystals were detected, larger scale crystallisation attempts were made using the condition associated with that well in the screens. Hanging drop wells were set up manually on Linbro plates. A total volume of 500 μl H_2O, 1 μl of crystallisation buffer, and 1 μl of 8 mg.ml^{-1} protein was added to each well. Varying conditions were used; TccASAT successfully crystallised in a 50:50 solution of 10 mM tris pH 7.5 and 50 mM acetate pH 4.6, and TbcASAT crystals were obtained in a solution of 1M potassium sodium tartrate and 100 mM MES salt pH 6, after a 1 - 2 week incubation at 18 ^{o}C. Crystals were soaked in 30% (v/v) glycerol combined with their respective crystallisation buffers for 2 min at room temperature and flash frozen in liquid nitrogen. X-ray analysis and molecular modelling was performed by Dr. Amir Khan.

Assessing TccASAT activity in crystallisation buffer.

Recombinant T. cruzi cASAT was incubated in universal buffer at different pH ranges (3 - 12) and crystallisation buffer, each at 37 ^{o}C for 30 - 60 min, then assayed with 25 mM phenylalanine in an AHADH assay as described in section 2.6.1. The crystallisation buffer used was a 50:50 solution of 10 mM Tris pH 7.5 & 50 mM Acetate pH 4.6, and the final pH of this solution was 5.4. The universal buffer was prepared as previously outlined by Britton & Robinson [135].

2.5.5 Expression of recombinant *T. cruzi* L-alpha-hydroxy acid dehydrogenase (AHADH) for enzymatic assays.

Glycerol stocks of recombinant AHADH expressing *E. coli* had previously been prepared by Cecile Cres and Jennifer McFarland [136]. Scrapings from the glycerol stock were taken and incubated overnight at 37 ^{o}C at 180 RPMs in a Bijou tube containing 5 ml of 2X YT broth. This broth was then plated onto LB-agar plates containing 50 μg.ml^{-1} kanamycin and 5% (w/v) sucrose and incubated overnight at 37 ^{o}C. A single colony was selected from one of the plates and was added to a Bijou tube containing

10 ml of 2X YT broth and 10 μl of μg.ml^{-1} kanamycin. The culture was incubated in shaking incubator overnight at 37 ^{o}C. 1 L of 2X YT broth containing 50 μg.ml^{-1} kanamycin was prepared in an Erlenmeyer flask, to which the overnight culture was added. It was then incubated at 37 ^{o}C at 180 RPMs until a ΔOD_{600nm} absorbance of 0.6 was reached. 500 μM IPTG was then added to induce the expression of recombinant AHADH. The culture was incubated overnight in a shaking incubator at 27 ^{o}C at 150 RPMs. The cells were harvested by centrifugation at 4 ^{o}C at 4,000 g for 15 minutes using a Sorvall RC5C plus. The supernatant was discarded and the pellet was re-suspended in 30 ml bacterial lysis buffer. Full lysis of the cells was ensured using an EmulsiFlex-C5 high-pressure cell homogenizer. The post-disruption lysate was then centrifuged at 14,000 g for 30 minutes at 4 ^{o}C. The supernatant was removed and a 1% (v/v) protease inhibitor cocktail was added. Contaminants were removed by dialysis overnight in 3,000 MWCO Snakeskin tubing in 1 L bacterial lysis buffer. The protein was removed and 2.5 ml of Ni^{2+} resin was added, which was then incubated on a roller for 1 hour at 4 ^{o}C. The sample was centrifuged for 5 minutes at 400 g, followed by discarding of the supernatant. The beads were then washed 3 times with 15 ml bacterial lysis buffer, discarding the supernatant each time. Following the last wash, 10 ml of elution buffer was added to each of the falcon tubes and incubated on a roller for 5 minutes at 4 ^{o}C. The tubes were then centrifuged for 10 minutes at 400 g, and the protein-containing supernatant was aliquoted into eppendorfs, snap frozen with liquid N_2, and stored at -80 ^{o}C. Activity was assessed by a simple phenylpyruvate assay with NADH.

2.6 cASAT kinetic assays.

One of the most important investigations carried out was to establish the kinetic abilities of both cASAT enzymes towards aspartate and aromatic amino acid substrates. Full length protein produced in the large scale expressions was used for these purposes. The assays were of a modified design based on the methods of Bergemeyer et al. [137]. Enzyme concentration of the *T. cruzi* and *T. brucei* aliquots were first established via Bradford assay [133], using a Bradford kit supplied by Thermo Scientific Pierce. A standard curve was generated (Fig. 2.10) and enzyme concentrations were extrapolated from this curve by assaying varying dilutions of each enzyme in 1X PBS with

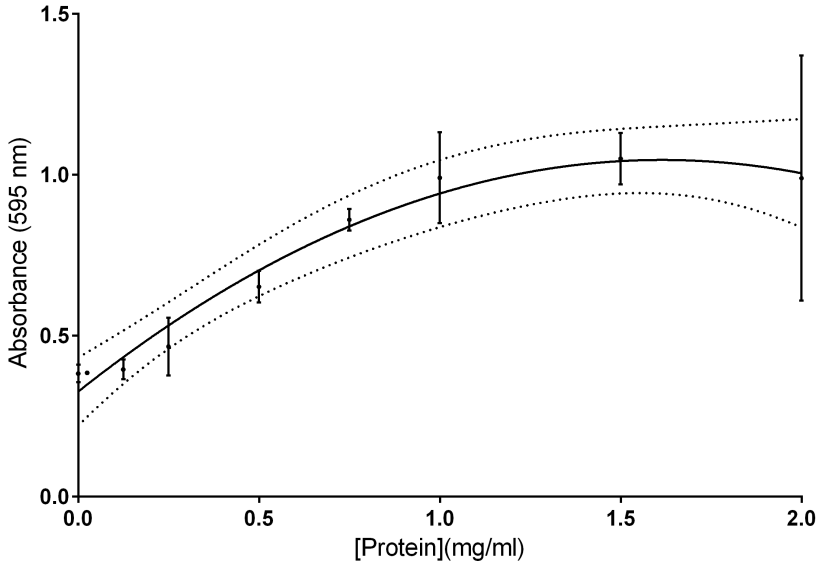

Figure 2.10. Bradford assay standard curve.

Standard curve generated using established methods [133]. The useful range for accurately extrapolating unknown protein concentrations was 0.25 - 0.75 mg.ml^{-1}.

the Bradford assay on a 96 clear well plate. This established that for the *T. brucei* assays there would be 0.0456 mg.ml^{-1} enzyme per 1 μl volume used, and in the *T. cruzi* assays there would be 0.2162 mg.ml^{-1} enzyme per 1 μl volume used.

2.6.1 Aromatic amino acid assays.

cASAT enzymatic affinities and kinetic properties were investigated in a coupled assay. cASAT de-aminates the α-amino group of the aromatic amino acids, in a reversible manner, generating a pyruvyl moiety. As this process is not easily monitored spectrophotometrically, aromatic L-alpha-hydroxyacid dehydrogenase (AHADH) was used to detect the production of the ketoacid derivative produced by cASAT, in a NADH coupled reaction. AHADH converts the ketoacid pyruvyl moiety to its hydroxy acid derivative [138], oxidising NADH to NAD$^+$ (Fig. 2.11), which can be monitored spectrophotometrically. Importantly for these assays, the equilibrium constant heavily favours the reduction of the ketoacid to the hydroxyacid (30 - 60 times more that the reverse reaction) [139]. The decrease in absorbance at 340 nm was used to monitor the reaction, and any change in absorbance correlated directly to ketoacid production due to a 1:1 stoichiometry of the reactions. α-ketoglutarate, pyruvate, and oxaloacetate were used as the amino acceptors.

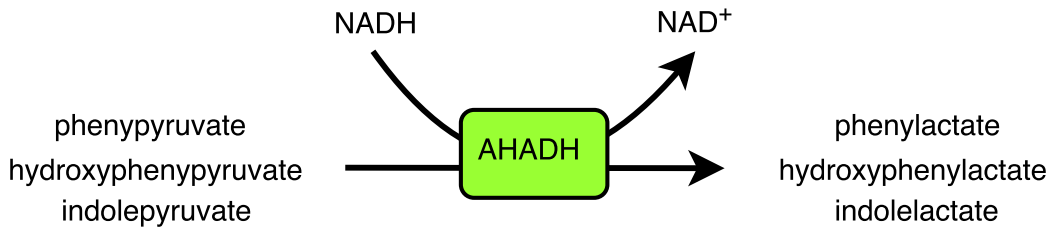

Figure 2.11. Simple representation of the conversion of aromatic ketoacids to aromatic hydroxyacids by AHADH.

For the aromatic amino acid assays the assay reaction mix was as follows; 0.25 mM NADH, 10 μl 0.0456 mg.ml^{-1} *T. brucei* cASAT or 2.5 μl 0.2162 mg.ml^{-1} *T. cruzi* cASAT, 20 μl AHADH (850 U.ml^{-1}), 25 mM α-ketoglutarate, X μl ddH_2O, Y μl 50 mM L-tryptophan, 50 mM L-phenylalanine, or 50 mM L-aspartate, in a total volume of 1 ml. For Michaelis-Menten kinetics the concentrations of the substrates, 50 mM tryptophan, 50 mM phenylalanine, or 50 mM aspartate, were varied in the reaction in ranges between 0.05 – 25 mM, with each assay measurement performed in triplicate. The reaction assay was performed by first adding all the necessary components in a 1 cm path length plastic cuvette, bar the NADH and cASAT enzyme, and blanking the solution at 340 nm. NADH was then added, and a steady blank rate was measured at 340 nm for 1 min. cASAT was then added to start the reaction, following careful stirring, and the resultant decreasing absorbance rate was monitored ($\Delta Abs_{340nm/min}$). Rates were plotted against their corresponding substrate concentrations to generate the graphical data.

2.6.2 ASAT/AAT ratio activity assay.

To measure reduction of ASAT and AAT activity in cASAT RNAi cells compared to wild type cells, LDH/MDH assays were employed as outlined previously [140]. 1×10^8 cells were centrifuged at 1,500g for 10 min at 4 ^{o}C, washed twice in 1 X PSG, and centrifuged again. The pellet was re-suspended in chilled 2X cell lysis buffer (TES, 2% CHAPS, protease inhibitors) and 1X PSG to have a final equivalent concentration of 5×10^6 cells/100 μl, at 4 ^{o}C. The ASAT assay contained 250 mM ASAT buffer, X ddH_2O, 100 μl cells sample, 10 U malic dehydrogenase (MDH), 0.25 mM NADH and 25 mM α-ketoglutarate in a 1 ml volume of path length 1 cm. Absorbance is read using

a 340 nm wavelength. The AAT assay contained 250 mM AAT buffer, ddH_2O, 50 μl cells sample, 10 U lactic acid dehydrogenase (LDH), 0.18 mM NADH and 25 mM α ketoglutarate in a 1 ml volume of path length 1 cm. Absorbance is read at wavelength 340 nm. ASAT/AAT activity levels were normalised to cell counts.

2.7 Quantification of aromatic ketoacid production.

AHADH was subsequently used to detect both real time production of ketoacids *in vitro* by bloodstream form and procyclic form *T. brucei* cells and to quantify detectable ketoacids in Rat sera and media used for macrophage & glial cell treatments. Each assay was performed with the same components, with the sample volume varying depending on the experiment being performed. The basic component list is as follows; 0.25 mM NADH, 10 μl AHADH (850 $U.ml^{-1}$), 500 μl 100 mM NaCl/25 mM Tris buffer (pH 7.4), X μl ddH_2O, Y μl Sample – to a total volume of 1 ml. Sample volumes used – 100 μl Media for *in vitro* quantification of ketoacids produced by procyclic form and bloodstream form *T. brucei*, and 100/200 μl rat sera. The reaction assay was performed by first adding all the necessary components in a 1 cm path length plastic cuvette, bar the NADH, and blanking the solution at 340 nm. NADH was then added, and a steady rate was measured at 340 nm for 1 min. Finally, the specified quantity of media/sera or control media was added and the subsequent decrease in absorbance recorded, corresponding to the ketoacid concentration.

2.8 NMR experiments.

A combination of H-NMR and ^{13}C-NMR were employed to investigate several different aspects of the project;

1. To clarify whether the cASAT was responsible for the production of ketoacids from aromatic amino acids, and simultaneously ascertain if tryptophan was the precursor for the production of indolepyruvate.

2. To investigate the dynamics and stability of indolepyruvate, and to clarify conflicting reports on the matter.

3. To investigate whether indolepyruvate was a possible substrate for macrophage migration inhibitory factor (MIF).

2.8.1 ^{13}C-NMR monitored production of indolepyruvate from tryptophan by cASAT RNAi bloodstream form *T. brucei*.

It was unclear from the literature available as to whether cASAT was actively metabolising tryptophan *in vitro*, and if so what the resultant product was – kynurine, kynurenic acid, indole-3-acetate, indolepyruvate, etc. ^{13}C labelled (Indole-2-^{13}C) tryptophan was used to increase detection sensitivity and to avoid interference from the CH/CH_2 on the pyruvyl moiety responsible for the keto-enol tautomerism.

Bloodstream form wild type and cASAT RNAi cells were cultured in HMI-9 media for 24 hours in the presence or absence of 1 μg.ml^{-1} tetracycline. Cells were collected by centrifugation at 1,500 g for 10 min, washed twice in 1X PSG (pH 7.4), centrifuged, and re-suspended at 5×10^7 cells.ml^{-1} in HMI-9 media supplemented with 150 μM single labelled (indole-2-^{13}C)-tryptophan for a five-hour incubation at 37 ^{o}C in a 5% CO_2 incubator. Cell viability was actively monitored via microscopic examination during incubation, and media samples were collected at 1 hour intervals by removing cells by centrifugation at 14,000 g for 5 min. Media samples were snap frozen in liquid nitrogen and stored at -80 ^{o}C until use for NMR. 600 μl samples, consisting of 540 μl media and 60 μl D_2O (lock), were run on an 800 MHz Agilent DD2/4.2 K premiumCOMPACT spectrometer. All ^{13}C-NMR spectra were recorded at 25 ^{o}C, and samples were referenced to internal glucose at 98.64 ppm. Data was acquired with active proton decoupling and NOE, 7.35 μs 90^o pulse width, 1 s relaxation delay, spectral width -15.0 ppm to 235.2 ppm, with 3200 scans performed. Post-acquisition Line Broadening was 1 Hz exponential.

2.8.2 ^{1}H-NMR – pH kinetic experiments of indolepyruvate.

It had been observed via the AHADH ketoacid detection assays that indolepyruvate was not detectable in cell culture media (HMI-9 or DMEM) after a 24 hour period, whereas

4-hydroxyphenylpyruvate and phenylpyruvate were, albeit at lower concentrations than the initial levels. This was likely due to one of two effects; the AHADH assay only detects the keto tautomeric form of the ketoacids, and the ketoacids may have been present in the enolic form, or the ketoacids may have been breaking down into another compound which is not quantifiable using the AHADH assay.

Indolepyruvate was obtained as the enol tautomer in powdered form. 1 mM solutions of indolepyruvate were prepared by dissolving the powder in 100 mM potassium phosphate buffers of pH 6.8, 7.4, 7.8, 8, and 9, each of which had been supplemented with 10% D_2O and 1mM TSP. 600 μl volume samples were then immediately placed in the AV III 400 MHz NMR spectrometer and run as follows; with water suppression using pre-saturation pulse (f1), pulse with 0.3 times ph1 (ph1=0 2 2 0 1 3 3 1), pre-saturation equal to ph1, 90^o high power pulse, relaxation delay 1- 5*T1, number of scans = TD0*NS (where TD0 $\leqslant$30 min). This allowed a spectra of indolepyruvate to be generated approx. every 30 min. All scans were obtained at 20 ^{o}C. The data was then arrayed using Mnova 9.0 software, and integral points for each peak in the spectra were recorded and referenced to the TSP peak at 0 ppm. Graphical and statistical analysis was performed using Graphpad 6.0, unless otherwise stated.

2.8.3 Identification of indolepyruvate breakdown products.

A set of experiments was performed to assess whether or not breakdown products of indolepyruvate could be extracted and identified. Two 8 mg.ml^{-1} solutions of indolepyruvate at pH 6.8 and 8 were prepared, and incubated for 24 h at 37 ^{o}C. The lids on the 50 ml tubes used were loose, to allow air access to the solutions. Any organic breakdown products that would have formed were extracted as follows; 15 mls of dichloromethane (CH_2Cl_2) were added to a separating funnel with 15 ml of one of the indolepyruvate solutions. The mixture was shaken well for 2 min, then the aqueous and organic layers were allowed to separate. The upper aqueous layer was discarded and the lower dichloromethane (DCM) layer was decanted off into a conical flask containing excess $MgSO_4$. Constant swirling was applied until the $MgSO_4$ had absorbed any remaining H_2O. The DCM was transferred to a rotavap with the pressure reduced to 990 psi and a set temperature of 50 ^{o}C, until the DCM had evaporated entirely. A residue was deposited which was redissolved in DCM or DMSO for NMR studies.

This procedure was then repeated, with the same starting indolepyruvate sample. The sample was first acidified with 0.3 M HCl to a pH of ≈ 1, then transferred to the separating funnel, before proceeding to extract any compounds. Again, this was repeated with the starting indolepyruvate sample, but the sample was basified with 1 M NaOH to a pH of ≈ 14. The extraction then proceeded as before. A small sample of each fraction dissolved in dichloromethane was applied to a TLC plate, and run in a solution of ethyl acetate. Once the plate had run it was stained with potassium permanganate and visualised under UV light (Fig. 2.12). This verified that each sample contained different compounds. ^{1}H-NMR and ^{13}C-NMR spectra of the fractions were obtained to aid compound identification.

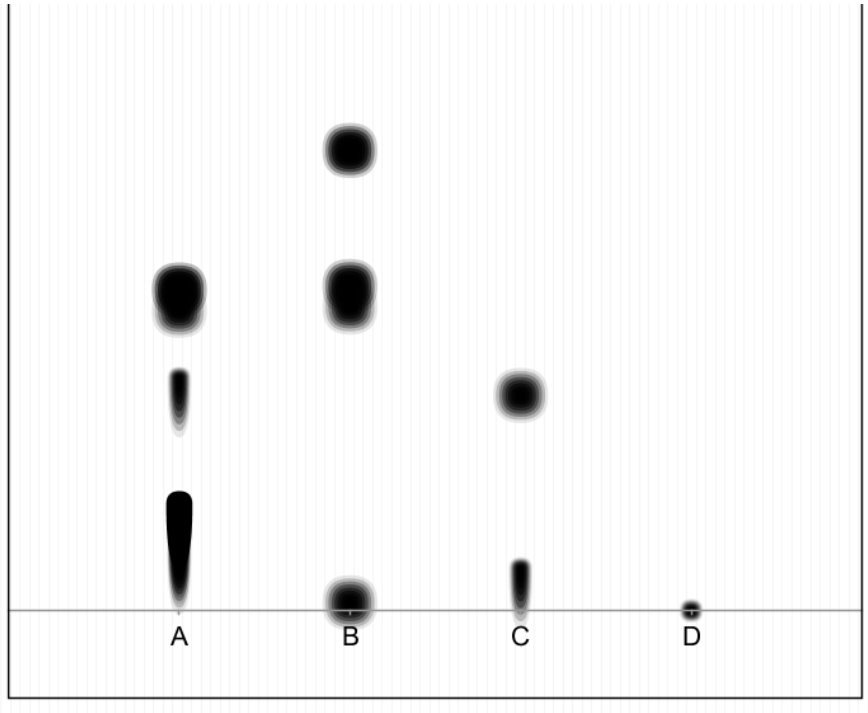

Figure 2.12. Simulated TLC plate of the extracted products of indolepyruvate. Lane A is fresh indolepyruvate dissolved in ethyl acetate. Lane B is the fraction isolated at pH 8. Lane C is the fraction isolated following acidification. D is the fraction isolated following basification.

2.8.4 MIF tautomerase NMR and other experiments.

To assess the ability of MIF to catalyse the tautomeric interconversion of indolepyruvate, ^{1}H-NMR experiments were performed as outlined by Rosengren et al. [141]. 1 mM of either hydroxyphenylpyruvate (the control) or indolepyruvate was dissolved

in a 50 mM acetate/D_2O buffer (pH 6.2) and immediately run (0 min sample) on a 800 MHz Agilent DD2/4.2 K premiumCOMPACT spectrometer, maintained at 22 ^oC. Scans were then recorded every 15 min over a 90 min period. The same procedure was carried out when the samples were prepared with the addition of 1 μg recombinant human MIF (obtained from the Dr. Seamus Donnelly). Samples were all referenced to 1 mM 4,4-dimethyl-4-silapentane-1-sulfonic acid (DSS) at 0 ppm. The disappearance of the enol singlet at 6.32 ppm and appearance of a keto singlet at 3.98 ppm was monitored for hydroxyphenylpyruvate, whilst the disappearance of the enol singlet at 6.8 ppm and appearance of a keto singlet at 4.24 ppm was monitored for indolepyruvate. Spectral acquisition conditions; number of scans 128, 2 s relaxation delay, D_2O solvent selected, 90^o pulse angle, with a 2.85 pulsewidth.

D-dopachrome tautomerase assay.

A modified 96 well plate form of the standard D-dopachome (D-dopa) MIF tautomerase assay was performed. MIF catalyses the conversion of D-dopa to 5,6-dihydroxyindole-2-carboxylic acid (DHICA), a reaction that can be monitored spectrophotometrically by the disappearance of D-dopachrome absorbance at 475 nm. triplicate reactions for each condition were prepared. Five conditions were used; Inhibitor + D-dopa, IPA (indolepyruvate) + D-dopa, MIF + D-dopa, MIF + IPA + D-dopa, and MIF + Inhibitor + D-dopa. 1 μg MIF was added to each well as required, as was 100 1 μM indolepyruvate prepared in 1X PBS, and the inhibitor (Ebelson) was added to a final concentration of 10 μM. The reaction was started by quickly dissolving D-dopachrome in sterile 1X PBS and aliquoting into each well. The rates of reaction were recorded as $\Delta\text{Absorbance}_{475nm}.\text{s}^{-1}$.

MIF indolepyruvate AHADH assay.

Hydroxyphenylpyruvate or indolepyruvate were prepared in 1X PBS (controls) and immediately assayed, as per the previously described AHADH assay. These aromatic ketoacid solutions were incubated at 20 ^oC and assayed every 20 min for a 60 min period. The assays were repeated but with the addition of 1 μg MIF to both hydroxyphenylpyruvate and indolepyruvate solutions. Similarly, the experiment was repeated

and monitored at the start (0 h) and end (12 h) of a 12 hour period.

2.9 ^{15}N-labelled Tryptophan Metabolomics.

To assess the metabolic role of the amino group abstracted from tryptophan in *T. brucei*, mass spectrum analysis of ^{15}N-amino tryptophan was performed. Bloodstream form MITat 1.2 cells were seeded at 2×10^5 cells.ml^{-1} in CMM in the absence or presence of 100 μM ^{15}N-tryptophan, supplemented with 10% FBS and 100 μM each of methionine, tyrosine, phenylalanine, leucine, arginine, and hypoxanthine (to simulated the use of FCS GOLD serum used in [77]). Cells were cultured for 36 hours in an incubator at 37 ^{o}C with 5% CO_2. Cells were removed from culture flasks, transferred to 50 ml tubes and rapidly chilled to 4 ^{o}C by submerging the tubes in a dry-ice/ethanol bath, with constant swirling to prevent freezing. Cells were centrifuged at 1,000 g for 10 min at 4 ^{o}C, then the supernatant was removed (5 μl was kept for spent media analysis), the pellet (5×10^7 cells.ml^{-1}) was re-suspended and transferred to a 1.5 ml chilled eppendorf. The cells were then centrifuged at 2,500 g for 5 min at 4 ^{o}C, and the supernatant was carefully removed. The pellet was then re-suspended in 200 μl of a 1:3:1 ratio chloroform:methanol:H_2O (extraction solvent), and mixed vigorously in a shaker incubator at 4 ^{o}C for 1 hour. Samples were then centrifuged at 14,000 g for 3 min at 4 ^{o}C. The supernatant was removed, transferred to a new 1.5 ml chilled eppendorf, and stored under N_2 gas at -80 ^{o}C until shipped on dry ice to the Glasgow polyomics facility for mass spectrometry analysis. Furthermore, samples of the extraction solvent, a pooled sample of each replicate, including samples with or without ^{15}N-labelled Tryptophan, were prepared for quality control purposes. Three replicates of each condition were prepared. The final shipped samples were; control pellet extract (CP), ^{15}N-tryptophan (NP), control spent media (CSM), ^{15}N-tryptophan spent media, non-labelled tryptophan fresh media control (FMN), ^{15}N-tryptophan fresh media control (FMC), extraction solvent control (MatrixBlank), and pooled sample of all samples (Pooled). For metabolite separation, samples were run on a Dionex ultiMate 3000 RSLC system (Thermo Fisher Scientific) with a ZIC-pHILIC column (Merck Sequant). For mass spectrum analysis, samples were run on a Thermo Orbitrap QExactive system (Thermo Fisher Scientific). Additional technical information is provided in the appendices.

Chapter 3

Characterisation of recombinant cytoplasmic aspartate aminotransferase, from *T. brucei* and *T. cruzi*.

3.1 Cytoplasmic aspartate aminotransferases.

Aminotransferases constitute one of the most extensively studied families of enzymes to date, in terms of amino acid sequencing, enzymatic functions, and availability of crystal structures [142]. Aspartate aminotransferases (EC 2.6.1.1) are part of family I and subgroup α of the aminotransferases, which also contains phenylalanine and tyrosine aminotransferases, amongst others (Table 3.1) [142, 143]. Typically, aspartate aminotransferases function to catalyse the conversion of aspartate to glutamate, with the concurrent transamination of an α-ketoacid, principally α-ketoglutarate. However, as members of subgroup I, aspartate aminotransferases are also noted for their ability to use aromatic amino acids for transamination, in addition to their typical aspartate/glutamate substrates [142, 144]. In most organisms the aspartate aminotransferase plays a crucial role in the glutamate-malate shuttle in the mitochondria, where the inter-conversion of amino acids and α-ketoacid are used to balance the transport of these substrates in and out of the mitochondrial matrix, which has the overall function of transferring glycolytically produced reducing equivalents to the Krebs cycle (via NADH-NAD^+). While this is a specific function for ASAT, many broad specificity aspartate aminotransferases that can transaminate other amino acid substrates have been characterised, particularly in Trypanosomatida and certain bacteria [143, 145–147]. Both the cytosolic and mitochondrial ASATs of higher organisms are generally considered more specific to the typical aspartate reaction described above [143]. However, some ASATs have also been discovered in these organisms that are able to transaminate a broad variety of substrates. For example, mouse mASAT can also utilise aromatic amino acids and aromatic ketoacids in addition to aspartate [148]. A comprehensive database of characterised ASATs is available at BRENDA [149]. In bloodstream form *T. brucei*, a role for ASAT in a glutamate-malate shuttle does not appear to exist given the lack of a Krebs cycle and electron transport chain in this organism [84]. Despite this, Marciano et al. have partially characterised a broad specificity *T. brucei* cytosolic aspartate aminotransferase (TbcASAT) [98, 150].

In an effort to further characterise the possible functional roles of TbcASAT in *T. brucei*, independent studies on the recombinant protein were carried out. These studies were comprised of bioinformatic analysis, recombinant enzyme production, kinetic characterisation of recombinant enzymes, and crystallographic studies. *T. cruzi* aspar-

Table 3.1. Subgroups of aminotransferases.

An overview of the four subgroups of aminotransferases, including enzyme commission number and substrate preferences. TbcASAT is a member of Subgroup I, where the aspartate aminotransferases (AspAT) are located. Table modified from [142].

Sub-group	Enzyme	EC no.	Primary substrates	
			Amino acid	Oxoacid
I	AspAT	2.6.1.1	L-aspartate	α-ketoglutarate
	AlaAT	2.6.1.2	L-alanine	α-ketoglutarate
	TyrAT	2.6.1.5	L-tyrosine	α-ketoglutarate
	His$P$AT	2.6.1.9	L-histidinol-P	α-ketoglutarate
	PheAT	2.6.1.58	L-phenylalanine	pyruvate
II	AcornAT	2.6.1.11	N-acetyl-L-ornithine	α-ketoglutarate
	OrnAT	2.6.1.13	L-ornithine	α-ketoglutarate
	ω-AaAT	2.6.1.18	β-alanine	pyruvate
	GaBaAT	2.6.1.19	4-aminobutyrate	α-ketoglutarate
	DapaAT	2.6.1.62	7,8-diaminopelargonate	methylthio-2-oxobutanoate
III	D-AlaAT	2.6.1.21	D-alanine	α-ketoglutarate
	BcaaAT	2.6.1.42	L-leucine	α-ketoglutarate
IV	SerAT	2.6.1.51	L-serine	pyruvate
	PSerAT	2.6.1.52	3-phospho-L-serine	α-ketoglutarate

tate aminotransferase (TccASAT) was also expressed recombinantly and characterised for comparative purposes.

3.1.1 Bioinformatic analysis of Trypanosomatid cASAT.

A search for aspartate aminotransferases in the TriTrypDB genomic database [151] yields two results for *T. brucei*; a cytosolic (TbcASAT) and mitochondrial (TbmASAT) ASAT. A single entry for a putative cytosolic ASAT (TcCLB.503841.70) in *T. cruzi* also exists, as does an entry for a mitochondrial ASAT (TcCLB.510945.70). An overview of this information:

- TbcASAT is a cytosolic aspartate aminotransferase (Tb927.10.3660) located on chromosome 10, position 950373 - 954227. Its translated sequence is 1212 bp,

yielding a 403 amino acid protein with a predicted molecular weight of 44.79 kDa.

- TbmASAT is a mitochondrial aspartate aminotransferase (Tb927.11.5090) located on chromosome 11, position 1454038 - 1457608. Its translated sequence is 1254 bp, yielding a 417 amino acid protein with a predicted molecular weight of 46 kDa.

- TccASAT is a cytosolic aspartate aminotransferase (TcCLB.503841.70) located on chromosome 38, position 212037 - 213251. Its translated sequence is 1215 bp, yielding a 404 amino acid protein with a predicted molecular weight of 44.89 kDa.

Clustal omega alignment of TbcASAT against a selection of cytosolic ASAT sequences from other Trypanosomatidae revealed that cASAT is broadly conserved within the Trypanosomatida order (Fig. 3.1, Table. 3.2)(sequence IDs are contained in the appendices). Both sequences from *T. brucei* and *T. gambiense* were identical, which is not unexpected given that *T. gambiense* is clonally related to *T. brucei* [2]. It was slightly surprising that both *T. evansi* and *T. equiperdum* shared the same sequence identity with TbcASAT, though both are believed to be evolved from a post-*T. brucei* common ancestor [152]. Other trypanosomes displayed high identity and similarity with TbcASAT, as did the trypanosomatidae *C. fasiculata* and *L. mexicana* to a lesser extent. The sequence of *T. cruzi* shared 61% identity and 77.3% similarity to that of TbcASAT, in agreement with previous reports [98]. Interestingly, when the sequences were used to generate a simple phylogeny, it was found to display very similar relationships amongst the Trypanosomatidae to those that had been established previously (Fig. 3.4) [11, 12]. It is possible then that cASAT could be used to delineate evolutionary relationships within Trypanosomatidae. Higher organism cASAT were well conserved with respect to TbcASAT, having between 44-47% identity (Table. 3.2). Most importantly, and in all cases, the 4 invariant residues associated with subgroup Iα aminotransferases, Gly(314AT), Asp(340AT), Lys(385AT), and Arg(562AT), were fully conserved [142]. The regions flanking 3-4 amino acids either side of the Lys258 and Asp222, which bind the pyridoxal-5-phosphate (PLP) cofactor, also appear to be highly conserved amongst all ASAT examined (Fig. 3.1 & 3.2). The mitochondrial ASAT from *T. brucei* (TbmASAT) shares little sequence identity with TbcASAT, at

40 % (Table. 3.2). This is not unusual between the two ASAT isoforms, as in humans both cytosolic and mitochondrial isoforms share only 49 % sequence identity [153]. Again, the invariant residues are are conserved within mASAT, despite its low overall identity and similarity with either TbcASAT or TccASAT (Fig. 3.3). It is interesting that while both *T. brucei* ASATs share the four invariant residues, TbmASAT has been shown to be highly specific for aspartate and α-ketoglutarate whereas TbcASAT has a broader substrate specificity [98]. The most notable result of the sequence alignments was the observation that the N-terminal sequences (from position 1 - 19 in Fig. 3.1) of the trypanosomatids are divergent amongst each other, and the N-terminal of TbcASAT is highly divergent from the N-terminal of higher organism cASATs (1 - 29 in Fig. 3.2). This N-terminal variation may affect the substrate specificities of trypanosomatid cASATs through alteration of the structure of these enzymes [154, 155].

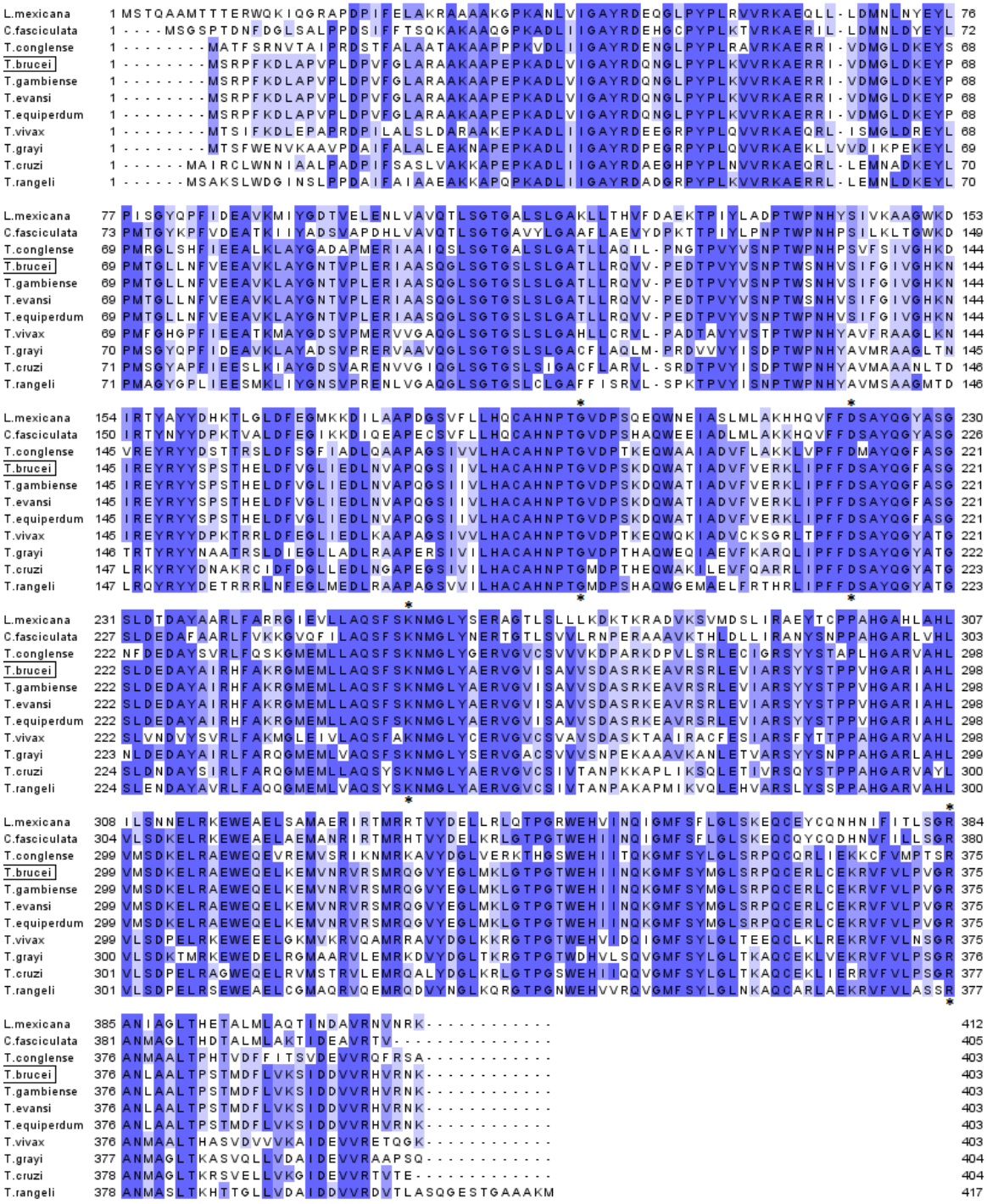

Figure 3.1. Multiple sequence alignment of TbcASAT with cASATs of other Trypanosomatidae.

The Trypanosomatidae subjected to analysis were *T. grayi*, *L. mexicana*, *C. fasciculata*, *T. congolense*, *T. brucei*, *T. gambiense*, *T. evansi*, *T. cruzi*, and *T. rangeli*. ■ indicates $\leqslant 90\%$ identical residues, ■ indicates $\leqslant 65\%$ semi-conserved residues, and ■ indicates $\leqslant 45\%$ partially conserved residues. Key invariant residues are denoted with $*$ [142]. Protein sequences were obtained from TriTrypDB (http://tritrypdb.org/tritrypdb/), and were analysed with Clustal Omega (https://www.ebi.ac.uk/Tools/msa/clustalo/).

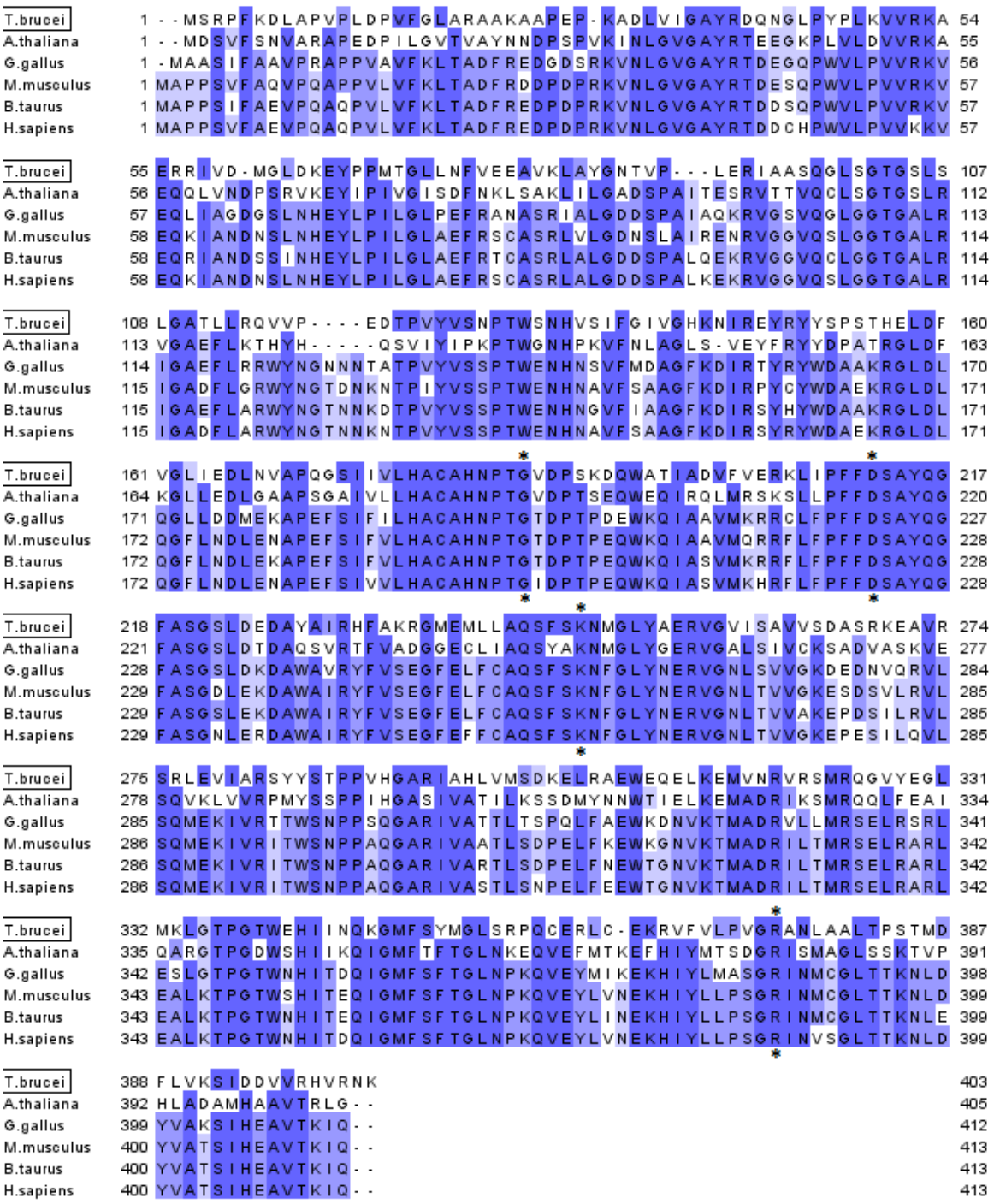

Figure 3.2. Multiple sequence alignment of TbcASAT with cASATs of higher organisms.

The organisms subjected to analysis were *Homo sapiens*, *Mus musculus*, *Arabidopsis thaliana*, *Gallus gallus*, *Bos taurus*, and *T. brucei*. ■ indicates ⩽ 90% identical residues, ■ indicates ⩽ 65% semi-conserved residues, and ■ indicates ⩽ 45% partially-conserved residues. Key invariant residues are denoted with ∗ [142]. Protein sequences were obtained from UniProt (http://www.uniprot.org/) and TriTrypDB (http://tritrypdb.org/tritrypdb/), and were analysed with Clustal Omega (https://www.ebi.ac.uk/Tools/msa/clustalo/).

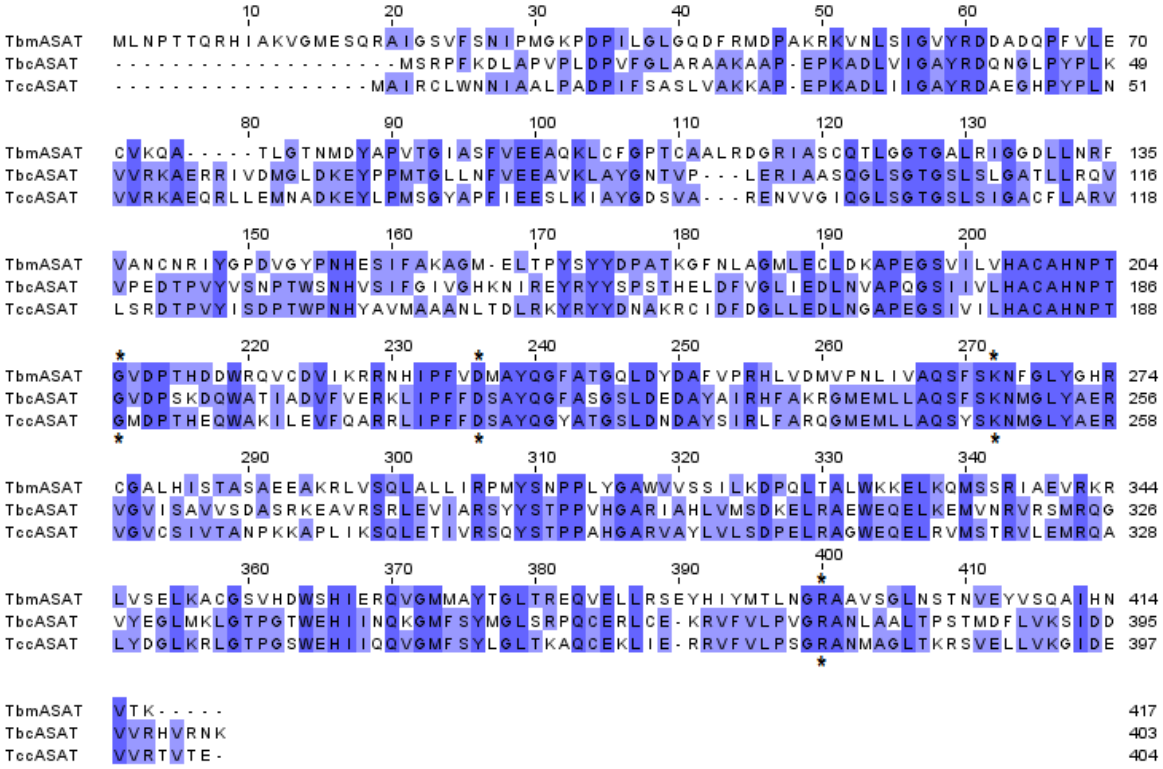

Figure 3.3. Multiple sequence alignment of TbmASAT, TbcASAT, and TccASAT. The aligned sequences of the mitochondrial and cytosolic ASAT from *T. brucei*, and the cytosolic ASAT from *T. cruzi*. ■ indicates $\leqslant$ 90% identical residues, ■ indicates $\leqslant$ 65% semi-conserved residues, and ■ indicates $\leqslant$ 45% partially-conserved residues. Key invariant residues are denoted with $*$ [142]. Protein sequences were obtained from TriTrypDB (http://tritrypdb.org/tritrypdb/), and were analysed with Clustal Omega (https://www.ebi.ac.uk/Tools/msa/clustalo/).

Table 3.2. Sequence identities between TbcASAT and cASATs from other organisms.

BLAST analysis performed for TbcASAT against both Trypansomatidae (including TbmASAT) and higher organism cASAT. As expected, the African trypanosomes typically shared the highest identities and similarities with TbcASAT. All higher organisms cASAT displayed < 50% identity with TbcASAT. Analysis performed with protein-protein BLAST (https://blast.ncbi.nlm.nih.gov/Blast.cgi) and EMBOSS Needle (https://www.ebi.ac.uk/Tools/psa/emboss_needle/).

Organism	Identity (%)	Positives (%)	E-value	Similarity (%)
T. evansi	100	100	0	100
T. gambiense	100	100	0	100
T. equiperdum	99	99	0	99.8
T. congolense	70	83	0	82.6
T. vivax	65	79	0	79.9
T. grayi	63	78	0	77.8
T. cruzi	61	78	0	77.3
T. rangeli	60	76	0	72.7
C. fasciculata	57	72	$6e^{-171}$	70.8
L. mexicana	55	73	$1e^{-165}$	50.6
G. gallus	47	63	$1e^{-123}$	60.6
A. thaliana	44	62	$4e^{-122}$	61.4
B. taurus	46	60	$6e^{-120}$	58.7
H. sapiens	45	61	$8e^{-120}$	59.4
M. musculus	45	59	$1e^{-117}$	58.7
T. brucei mASAT	40	59	$5e^{-99}$	53.8

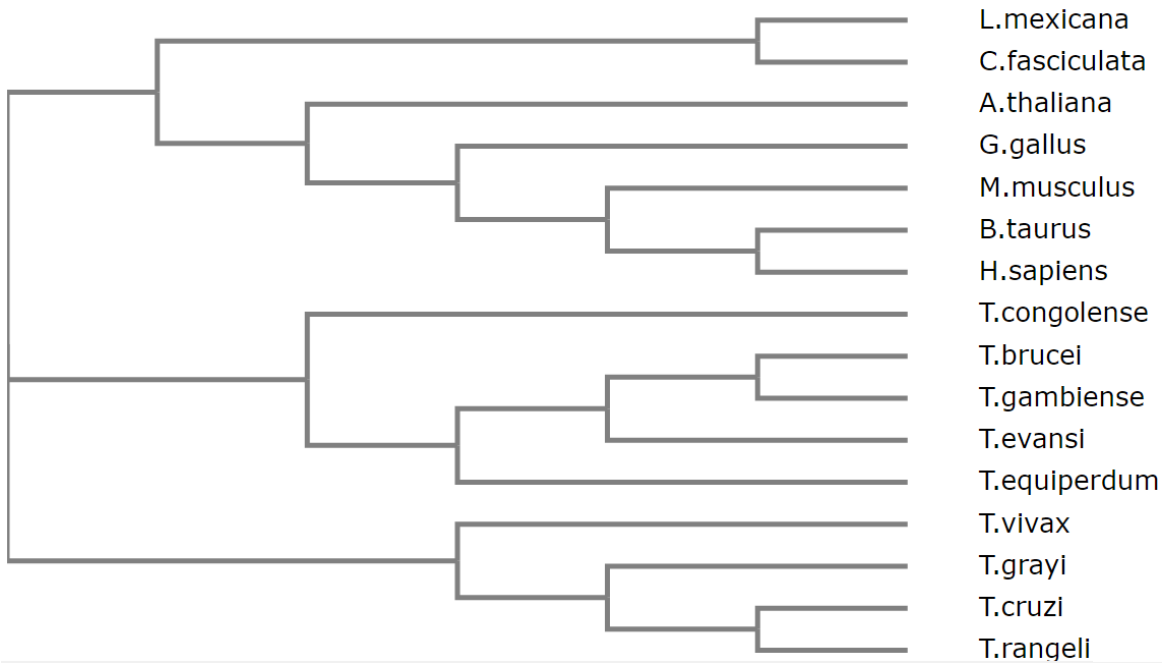

Figure 3.4. Simple phylogenetic cladogram constructed from cASAT protein sequences.

The basic relationships of each of the cASAT enzymes from both Trypanosomatidae and higher organisms. It is a simple representation only, as distance correction (which corrects for multiple substitutions at a single site amongst divergent sequences) was not applied. Calculated and drawn using the EMBL-EBI Simple Phylogeny tool (https://www.ebi.ac.uk/Tools/phylogeny/simple_phylogeny), which utilises PHYLIP tree and neighbour-joining to construct the cladogram.

3.1.2 Expression and purification of recombinant cASAT.

The full open reading frames of both TbcASAT (Tb927.10.3660) and TccASAT (TcCLB.503841.-70) were successfully amplified by PCR from genomic DNA using specialised primers designed to facilitate the insertion of the amplification products into the pNIC28-Bsa4 expression vector via ligation independent cloning (LIC). The pNIC28-Bsa4 vector was digested with BsaI to remove the stuffer insert and prepare the vector for the LIC step. The purified BsaI-digested pNIC28-Bsa4 vector migrated as a single band with the expected size of 5,353 bp (Fig. 3.5). The genomic *cASAT* amplification products obtained were of the correct size, ≈ 1,200 bp, and no non-specific amplification bands were present. The pNIC28-Bsa4 - *cASAT* ligation products were then transfected into BL21-DE3 *E. coli*. Colonies were screened selectively by growth on kanamycin + sucrose LB agar plates, with successful clones sequenced to confirm that the cASAT ORFs were correctly inserted into the pNIC28-Bsa4, contained no site mutations, and were in-frame. Suitable clones were found for both *T. brucei* and *T. cruzi* that had high sequence identity with their predicted cASAT sequences, ≈ 85% and ≈ 92%, respectively (Fig. 3.6 and 3.7). The sequence identity is likely 100% for both clones when terminal read errors from sequencing are taken into account, given that the inner sequences of both enzymes match identically. Clones that contained suitable expression vectors were then screened by small scale expression, to assess whether or not soluble, recombinant protein could be produced. IPTG-induced expression yielded large quantities of soluble cASAT, though small quantities of insoluble cASAT were present in both *T. brucei* and *T. cruzi* (Fig. 3.8). TbcASAT and TccASAT of the predicted correct size (44 kDa monomer in each case, excluding the hexahistidine tag) were both expressed. Having obtained pure cASAT protein from the small scale expression, clones were then brought forward for large scale protein expression, to be used in enzymatic assays and for crystallisation trials. Protein expression was shown to be tightly regulated, with little recombinant protein detected prior to IPTG addition (Fig. 3.9). The IPTG induction lead to the production of large quantities of recombinant protein, which could be successfully isolated through Ni^{2+} chromatography, and purified to homogeneity by multiple washes with extraction buffer. In addition, it was noted that both TbcASAT and TccASAT appeared to migrate slightly below their expected molecular weight, to ≈ 40 kDa (Fig. 3.9). Whilst the migration of protein to points above or below their expected molecular weight in SDS-PAGE is unusual, it is known to occasionally occur.

This phenomenon, termed "gel shift" is not well defined, but may be due to variations in SDS-protein binding, protein secondary structure, intrinsic protein charge, or post-translational modifications of protein [156]. Accurate masses could be confirmed with mass spectrophotometry.

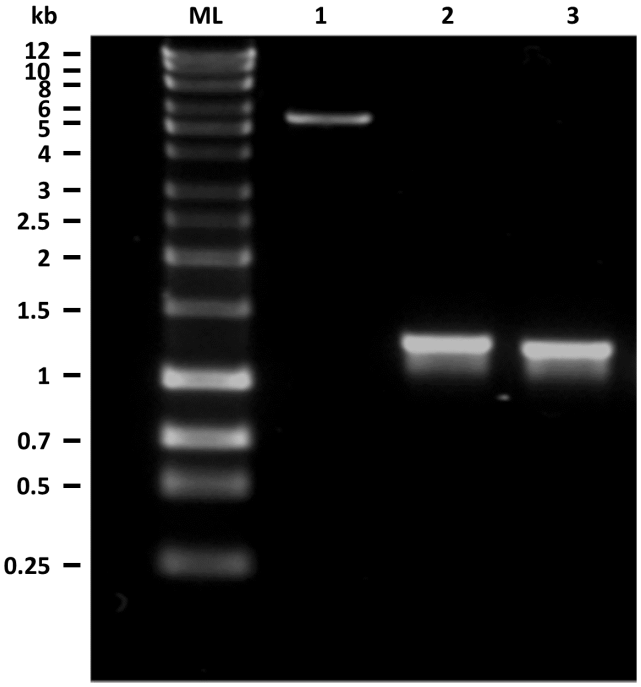

Figure 3.5. DNA Gel of amplified *T. brucei cASAT* DNA, *T. cruzi cASAT* DNA, and linearised pNIC28-Bsa4 vector.

EtBr stained DNA gel showing the linearised pNIC28-Bsa4 vector, post-stuffer removal via gel extraction (lane 1, ≈ 5300 bp), the amplification of *cASAT* DNA from *T. brucei* (lane 2, $\approx 1,200$ bp), and the amplification of *cASAT* DNA from *T. cruzi* (lane 3, $\approx 1,200$ bp). ML = Molecular ladder.

Blast Result

Aspartate aminotransferase [**Trypanosoma brucei brucei** strain 927/4 GUTat10.1] Sequence ID: ref|XP_822615.1|**Length: 403** Number of Matches: 1

Identical Proteins - **Proteins identical to the subject Range 1: 1 to 344**

Score	Expect	Method	Identities	Positives	Gaps
700 bits(1806)	0.0	Compositional matrix adjust.	341/344(99%)	341/344(99%)	0/344(0%)

```
Query  23   MSRPFKDLAPVPLDPVFGLARAAKAAPEPKADLVIGAYRDQNGLPYPLKVVRKAERRIVD  82
            MSRPFKDLAPVPLDPVFGLARAAKAAPEPKADLVIGAYRDQNGLPYPLKVVRKAERRIVD
Sbjct  1    MSRPFKDLAPVPLDPVFGLARAAKAAPEPKADLVIGAYRDQNGLPYPLKVVRKAERRIVD  60

Query  83   MGLDKEYPPMTGLLNFVEEAVKLAYGNTVPLERIAASQGLSGTGSLSLGATLLRQVVPED  142
            MGLDKEYPPMTGLLNFVEEAVKLAYGNTVPLERIAASQGLSGTGSLSLGATLLRQVVPED
Sbjct  61   MGLDKEYPPMTGLLNFVEEAVKLAYGNTVPLERIAASQGLSGTGSLSLGATLLRQVVPED  120

Query  143  TPVYVSNPTWSNHVSIFGIVGHKNIREYRYYSPSTHELDFVGLIEDLNVAPQGSIIVLHA  202
            TPVYVSNPTWSNHVSIFGIVGHKNIREYRYYSPSTHELDFVGLIEDLNVAPQGSIIVLHA
Sbjct  121  TPVYVSNPTWSNHVSIFGIVGHKNIREYRYYSPSTHELDFVGLIEDLNVAPQGSIIVLHA  180

Query  203  CAHNPTGVDPSKDQWATIADVFVERKLIPFFDSAYQGFASGSLDEDAYAIRHFAKRGMEM  262
            CAHNPTGVDPSKDQWATIADVFVERKLIPFFDSAYQGFASGSLDEDAYAIRHFAKRGMEM
Sbjct  181  CAHNPTGVDPSKDQWATIADVFVERKLIPFFDSAYQGFASGSLDEDAYAIRHFAKRGMEM  240

Query  263  LLAQSFSKNMGLYAERVGVISAVVSDASRKEAVRSRLEVIARSYYSTPPVHGARIAXLVM  322
            LLAQSFSKNMGLYAERVGVISAVVSDASRKEAVRSRLEVIARSYYSTPPVHGARIA LVM
Sbjct  241  LLAQSFSKNMGLYAERVGVISAVVSDASRKEAVRSRLEVIARSYYSTPPVHGARIAHLVM  300

Query  323  SDKELRAEWEQELKEMVNRVRSMRQGVYEGLMKLGTPXXWEHII  366
            SDKELRAEWEQELKEMVNRVRSMRQGVYEGLMKLGTP  WEHII
Sbjct  301  SDKELRAEWEQELKEMVNRVRSMRQGVYEGLMKLGTPGTWEHII  344
```

Figure 3.6. BLAST alignment of the *T. brucei* cASAT sequence in pNIC-Bsa4 against the genomic sequence.

The query sequence of the *T. brucei* cASAT inserted into pNIC-Bsa4 analysed via BLAST against the genomic sequence of *T. brucei*. The constructed plasmid was sequenced from the T7 promoter (5' - TAATACGACTCACTATAGGG - 3').

Blast Result

Aspartate aminotransferase [**Trypanosoma cruzi** Dm28c]
Sequence ID: gb|ESS67588.1|Length: 404 Number of Matches: 1 Range 1: 1 to 372

Alignment statistics for match #1

Score	Method	Identities	Positives	Gaps
661 bits(1705)	0.0	Compositional matrix adjust.	331/373(89%)	335/373(89%)	2/373(0%)

```
Query  24   MAIRCLWNNVAALPADPIFSASLVAKNAPEPKVDLIIGAYRDAEGHPYPLRAVRKAEQRL  83
            MAIRCLWNNVAALPADPIFSASLVAKNAPEPKVDLIIGAYRDAEGHPYPLRAVRKAEQRL
Sbjct  1    MAIRCLWNNVAALPADPIFSASLVAKNAPEPKVDLIIGAYRDAEGHPYPLRAVRKAEQRL  60

Query  84   LEMNVDKEYLPMSGYAPFIEESLKIAYGDSVARENLVGVQGLSGTGSLSIGACFLARVLS  143
            LEMNVDKEYLPMSGYAPFIEESLKIAYGDSVARENLVGVQGLSGTGSLSIGACFLARVLS
Sbjct  61   LEMNVDKEYLPMSGYAPFIEESLKIAYGDSVARENLVGVQGLSGTGSLSIGACFLARVLS  120

Query  144  PKTPVYISDPTWPNHYAVMAAANLTDLRKYRYYDSAKRCIDFDGLLEDLNLAPEGSIVIL  203
            PKTPVYISDPTWPNHYAVMAAANLTDLRKYRYYDSAKRCIDFDGLLEDLNLAPEGSIVIL
Sbjct  121  PKTPVYISDPTWPNHYAVMAAANLTDLRKYRYYDSAKRCIDFDGLLEDLNLAPEGSIVIL  180

Query  204  HACAHNPTGMDPTHEQWNKILEVFQARRLIPFFDSAYQGYATGSLDNDAYSIRLFARQGM  263
            HACAHNPTGMDPTHEQWNKILEVFQARRLIPFFDSAYQGYATGSLDNDAYSIRLFARQGM
Sbjct  181  HACAHNPTGMDPTHEQWNKILEVFQARRLIPFFDSAYQGYATGSLDNDAYSIRLFARQGM  240

Query  264  EMLLAQSYSKNMGLYAERVGVCSVVTAXPKKAPLIKSQLETIVRSQYSTPPAHGARVAYL  323
            EMLLAQSYSKNMGLYAERVGVCSVVTA PKKAPLIKSQLETIVRSQYSTPPAHGARVAYL
Sbjct  241  EMLLAQSYSKNMGLYAERVGVCSVVTADPKKAPLIKSQLETIVRSQYSTPPAHGARVAYL  300

Query  324  VLSDSELRAGGSRSCK-*CRRVCSKCAKLCTXXLRDSVPXAXGXHIIQQVXMXSYLXXXX  382
            VLSDSELRAG  +  +    RV      L     R   P +   HIIQQV M SYL
Sbjct  301  VLSDSELRAGWEQELQVMSTRVLEMRQALYDGLKRLGTPGSW-EHIIQQVGMFSYLGLTK  359

Query  383  SPXXKLXERXVFV  395
            +   KL ER VFV
Sbjct  360  AQCEKLIERRVFV  372
```

Figure 3.7. BLAST alignment of the *T. cruzi* cASAT sequence in pNIC-Bsa4 against the genomic sequence.

The query sequence of the *T. cruzi* cASAT inserted into pNIC-Bsa4 analysed via BLAST against the genomic sequence of *T. cruzi*. The constructed plasmid was sequenced from the T7 promoter (5' - TAATACGACTCACTATAGGG - 3').

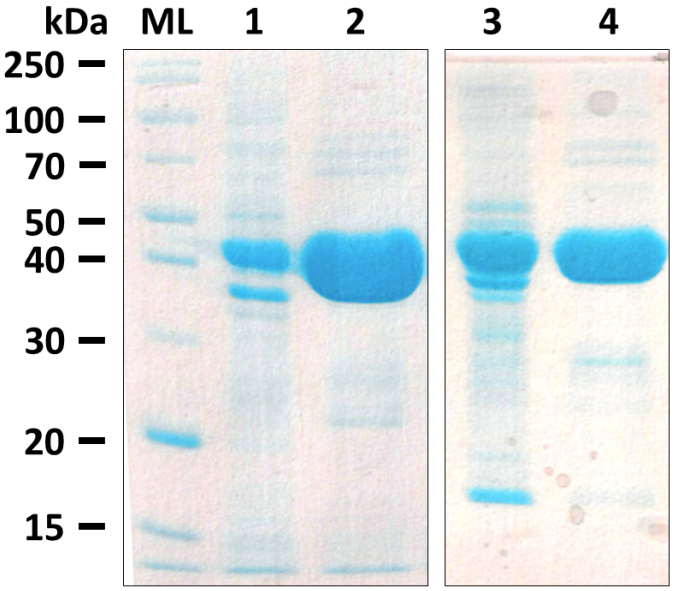

Figure 3.8. Small scale purification SDS-PAGE of *T. brucei* and *T. cruzi* cASAT. Coomassie stained 12% SDS-PAGE of the small scale expression of *T. brucei* (lanes 1 - 2) and *T. cruzi* (lanes 3 - 4) cASAT. The post-lysis cell pellets are shown in lanes 1 and 3, and the supernatant fractions are shown in lanes 2 and 4. ML = Molecular ladder.

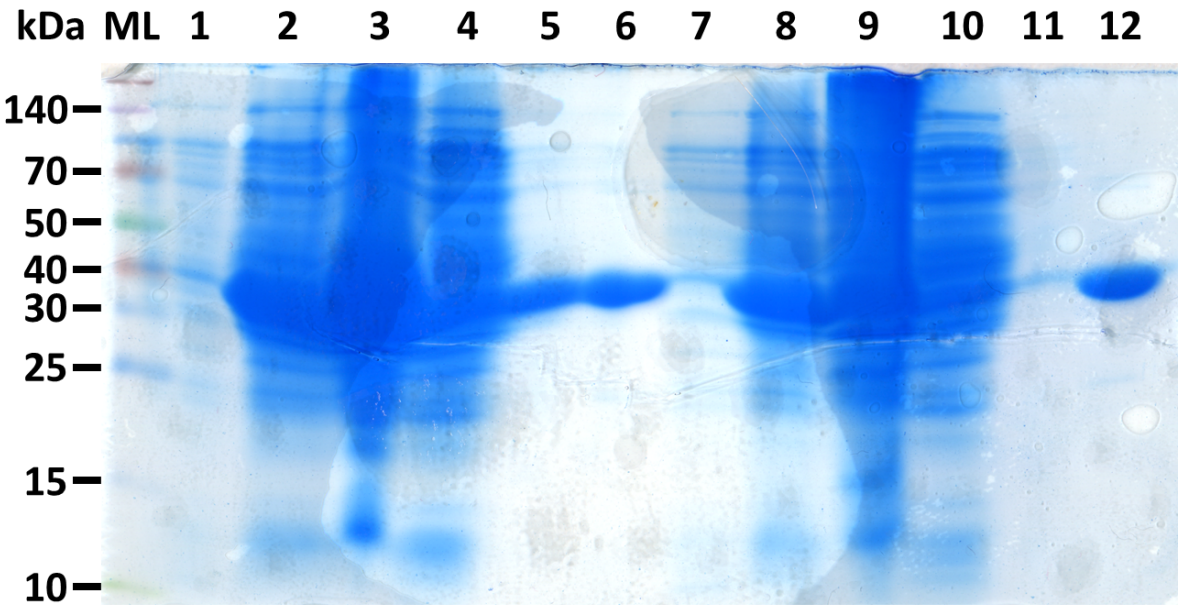

Figure 3.9. Large scale purification SDS-PAGE of *T. brucei* and *T. cruzi* cASAT. Coomassie stained 12% SDS-PAGE of the large scale expression of *T. brucei* and *T. cruzi* cASAT. Lanes 1 - 6 are *T. brucei* cASAT, lanes 7 - 12 are *T. cruzi* cASAT. Purification scheme as follows; lane 1, non-induced *E. coli*; lane 2, IPTG induced *E. coli*; lane 3, *E. coli* post-homogenisation sample; lane 4, supernatant applied to Ni^{2+} column; lane 5, eluted TbcASAT following 3X wash with buffer; lane 6, final eluted, purified TbcASAT after multiple washes. This scheme is repeated in the same order for lanes 7 - 12 to produce purified TccASAT. ML = Molecular ladder.

3.1.3 Kinetic properties of *T. brucei* and *T. cruzi* cASAT.

Having generated pure and homogeneous recombinant cASAT, enzymatic assays were conducted to establish the kinetic parameters of both enzymes. Assays were conducted by measuring the rate of production of ketoacid or aromatic ketoacid from the amino acids, which was coupled it to the observable NADH-dependent conversion of these ketoacids to hydroxyacid derivatives, using MDH or AHADH. Further details are provided in the materials and methods.

Unlike the alanine aminotranferases (AAT) in *T. brucei* and *T. cruzi*, which have narrow substrate specificity [150], the cASAT enzymes are much broader in accepting both 2-oxoacids to be transaminated and amino acid amino group donors. Firstly, both enzymes can effectively use the aspartate-α-ketoglutarate substrate pair, although *T. cruzi* had a 4.5-fold greater affinity for aspartate, as well as a 8.5-fold higher catalytic efficiency when α-ketoglutarate was the amino group acceptor (Fig. 3.10). Both enzymes could utilise pyruvate as the amino group acceptor with phenylalanine or tryptophan, although they did so poorly (Fig. 3.11). Both cASAT enzymes could utilise aromatic amino acids effectively for transamination of α-ketoglutarate (Fig. 3.12). Interestingly, while both enzymes displayed a preference for aromatic amino acid donors, *T. brucei* displayed a much higher affinity (K_m) for phenylalanine and tryptophan, relative to aspartate (8-fold and 125-fold, respectively) with α-ketoglutarate as the amino acceptor (Table 3.3). *T. cruzi* had a less pronounced preference for phenylalanine and tryptophan, relative to aspartate (5.4-fold and 1.7-fold, respectively) with α-ketoglutarate as the amino acceptor (Table 3.3). Comparatively, *T. brucei* cASAT had 16 times greater affinity for tryptophan than *T. cruzi* cASAT. The effectiveness of the 2-oxoacids as amino group acceptors was also investigated, with tryptophan and phenylalanine as the amino donors. Strikingly, both cASAT enzymes preferred oxaloacetate as the amino group acceptor with $\geqslant 3$ times greater affinity than that shown for the corresponding α-ketoglutarate-tryptophan pair (Fig. 3.13 and Fig. 3.14). In a similar manner, this oxaloacetate preference was found when phenylalanine was used as an amino donor (Fig. 3.16 and Fig. 3.15). Unexpectedly, it was discovered that the oxaloacetate and phenylalanine pairing was more optimal than that of oxaloacetate and tryptophan, given the initial data with α-ketoglutarate as the amino group acceptor; the V_{max} was higher, K_m was lower, and V_{max}/K_m was higher than the α-ketoglutarate

and tryptophan equivalents. These data indicate both *T. brucei* and *T. cruzi* cASAT can utilise aspartate effectively, but have a preference for aromatic amino acids - *T. brucei* markedly so for tryptophan with α-ketoglutarate as the amino acceptor - and that both preferentially utilise oxaloacetate as the amino group acceptor. Unfortunately the assay was limited to the use of α-ketoglutarate here, as both oxaloacetate and KMTB were found to be substrates for the AHADH coupling enzyme (in contrast to reported specificities [98, 157]) and the kinetic parameters of the aromatic amino acids with either α-ketoacid as the amino group acceptor could not be obtained, though with 2 mM oxaloacetate in the assay phenylalanine was the preferred amino group donor by both enzymes. All calculated kinetic parameters, including V_{max}, K_m, and V_{max}/K_m are included in Table 3.3.

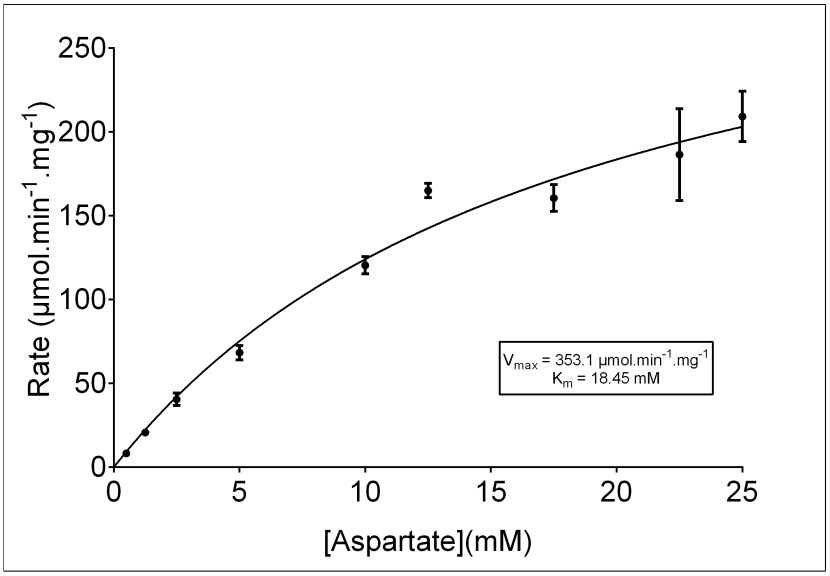

(a) TccASAT

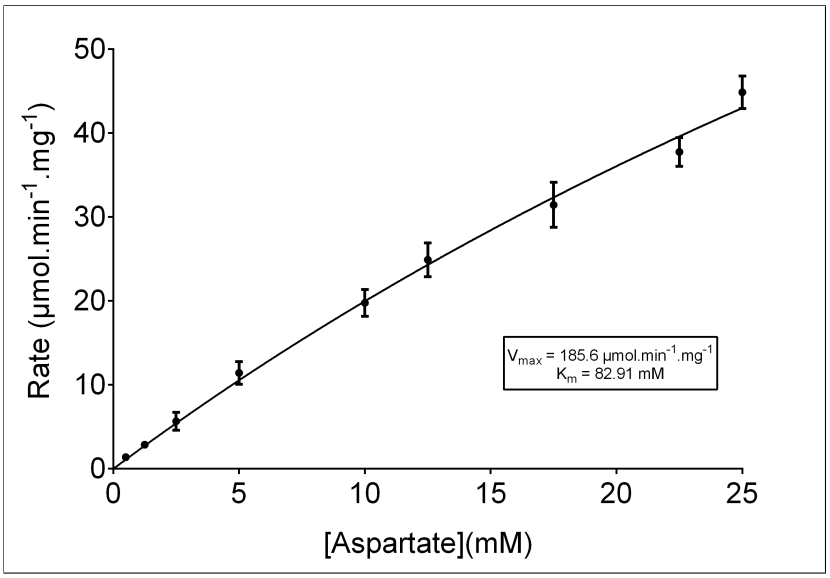

(b) TbcASAT

Figure 3.10. Michaelis–Menten kinetics of *T. brucei* and *T. cruzi* cASAT for aspartate with α-ketoglutarate as the amino group acceptor.

(a) Michaelis–Menten kinetic curves of *T. cruzi* cASAT with varying concentrations of aspartate in the presence of 25 mM α-ketoglutarate. **(b)** Michaelis–Menten kinetic curves of *T. brucei* cASAT with varying concentrations of aspartate in the presence of 25 mM α-ketoglutarate. The reaction buffer used was 100 mM Tris–HCl (pH 7.5), 25 mM NaCl, 0.25 mM NADH, 20 U of MDH (coupling enzyme), at 25 °C. The reaction was started by the addition of cASAT, and the decrease in absorbance at 340 nm was monitored as a reflection of the rate of activity of the enzyme. Error bars indicate SD, triplicate measurements.

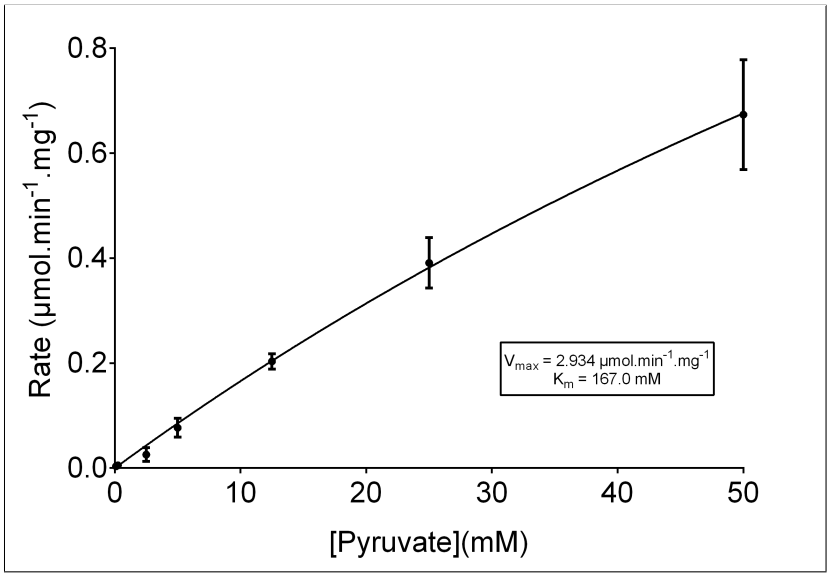

(a) TccASAT

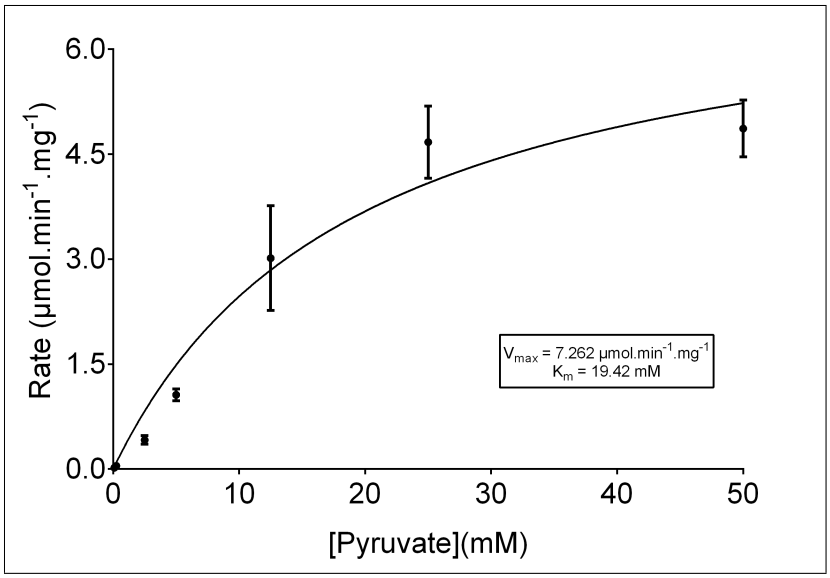

(b) TbcASAT

Figure 3.11. Michaelis–Menten kinetics of *T. brucei* and *T. cruzi* cASAT for pyruvate with phenylalanine as the amino group donor.

(a) Michaelis–Menten kinetic curves of *T. cruzi* cASAT with varying concentrations of pyruvate in the presence of 25 mM phenylalanine. **(b)** Michaelis–Menten kinetic curves of *T. brucei* cASAT with varying concentrations of pyruvate in the presence of 25 mM phenylalanine. The reaction buffer used was 100 mM Tris–HCl (pH 7.5), 25 mM NaCl, 0.25 mM NADH, 20 U.ml^{-1} of AHADH (coupling enzyme), at 25 °C. The reaction was started by the addition of cASAT, and the decrease in absorbance at 340 nm was monitored as a reflection of the rate of activity of the enzyme. Error bars indicate SD, triplicate measurements.

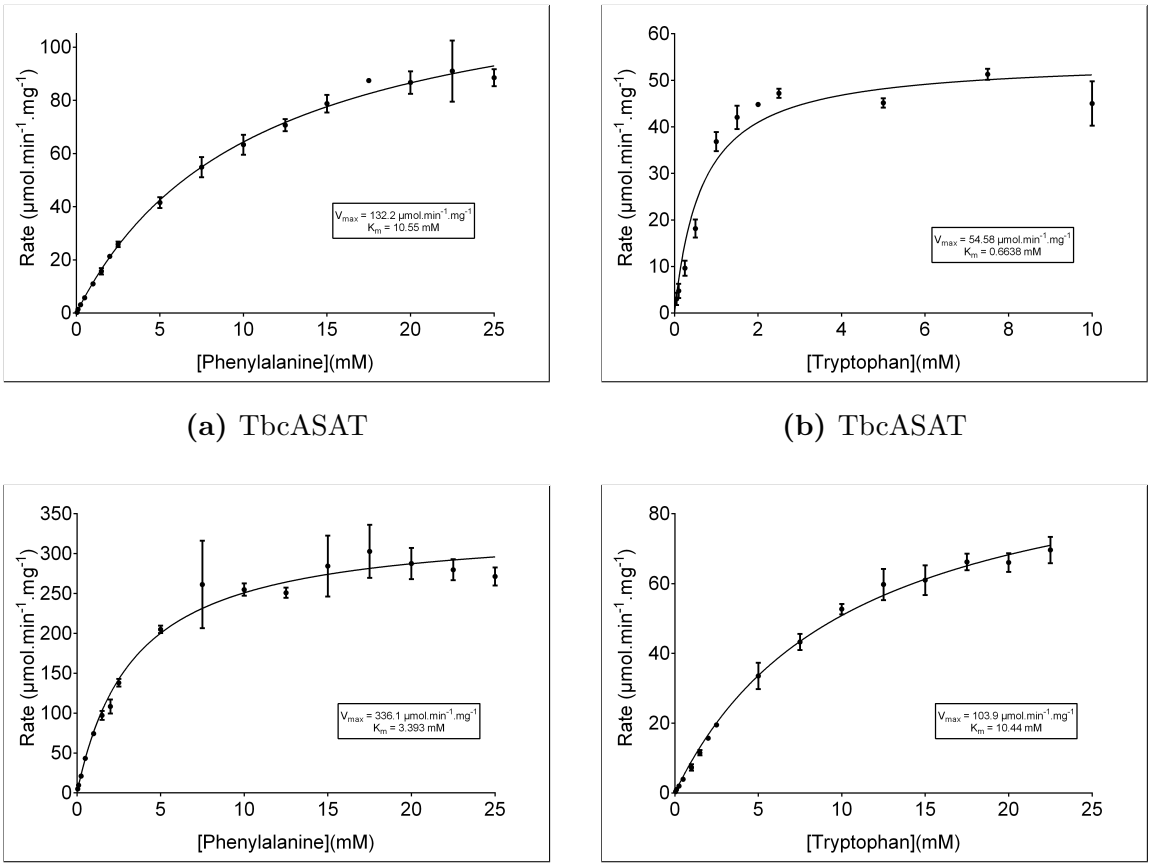

(a) TbcASAT **(b)** TbcASAT

(c) TccASAT **(d)** TccASAT

Figure 3.12. Michaelis–Menten kinetics of *T. brucei* and *T. cruzi* cASAT for tryptophan and phenylalanine, with α-ketoglutarate as the amino group acceptor. **(a)** Michaelis–Menten kinetic curves of *T. brucei* cASAT with varying concentrations of phenylalanine in the presence of 25 mM α-ketoglutarate. **(b)** Michaelis–Menten kinetic curves of *T. brucei* cASAT with varying concentrations of tryptophan in the presence of 25 mM α-ketoglutarate. **(c)** Michaelis–Menten kinetic curves of *T.cruzi* cASAT with varying concentrations of phenylalanine in the presence of 25 mM α-ketoglutarate. **(d)** Michaelis–Menten kinetic curves of *T.cruzi* cASAT with varying concentrations of tryptophan in the presence of 25 mM α-ketoglutarate. The reaction buffer used was 100 mM Tris–HCl (pH 7.5), 25 mM NaCl, 0.25 mM NADH, 20 U.ml^{-1} of AHADH (coupling enzyme), at 25 °C. The reaction was started by the addition of cASAT, and the decrease in absorbance at 340 nm was monitored as a reflection of the rate of activity of the enzyme. Error bars indicate SD, triplicate measurements.

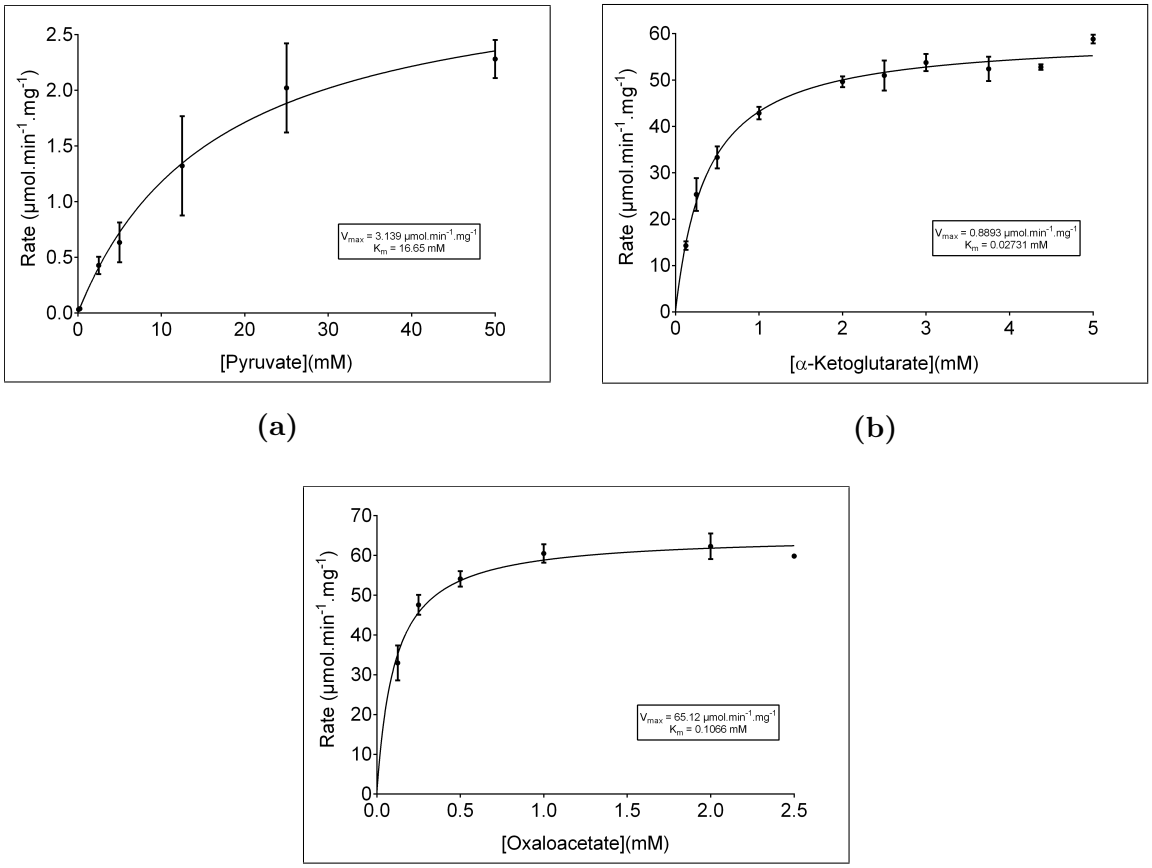

Figure 3.13. Michaelis–Menten kinetics of *T. brucei* cASAT for pyruvate, α-ketoglutarate, and oxaloacetate with tryptophan as the amino group donor.
(a) Michaelis–Menten kinetic curves of *T. brucei* cASAT with varying concentrations of pyruvate in the presence of 25 mM tryptophan. **(b)** Michaelis–Menten kinetic curves of *T. brucei* cASAT with varying concentrations of α-ketoglutarate in the presence of 25 mM tryptophan. **(c)** Michaelis–Menten kinetic curves of *T.brucei* cASAT with varying concentrations of oxaloacetate in the presence of 25 mM tryptophan. The reaction buffer used was 100 mM Tris–HCl (pH 7.5), 25 mM NaCl, 0.25 mM NADH, 20 U.ml^{-1} of AHADH (coupling enzyme), at 25 °C. The reaction was started by the addition of cASAT, and the decrease in absorbance at 340 nm was monitored as a reflection of the rate of activity of the enzyme. Error bars indicate SD, triplicate measurements.

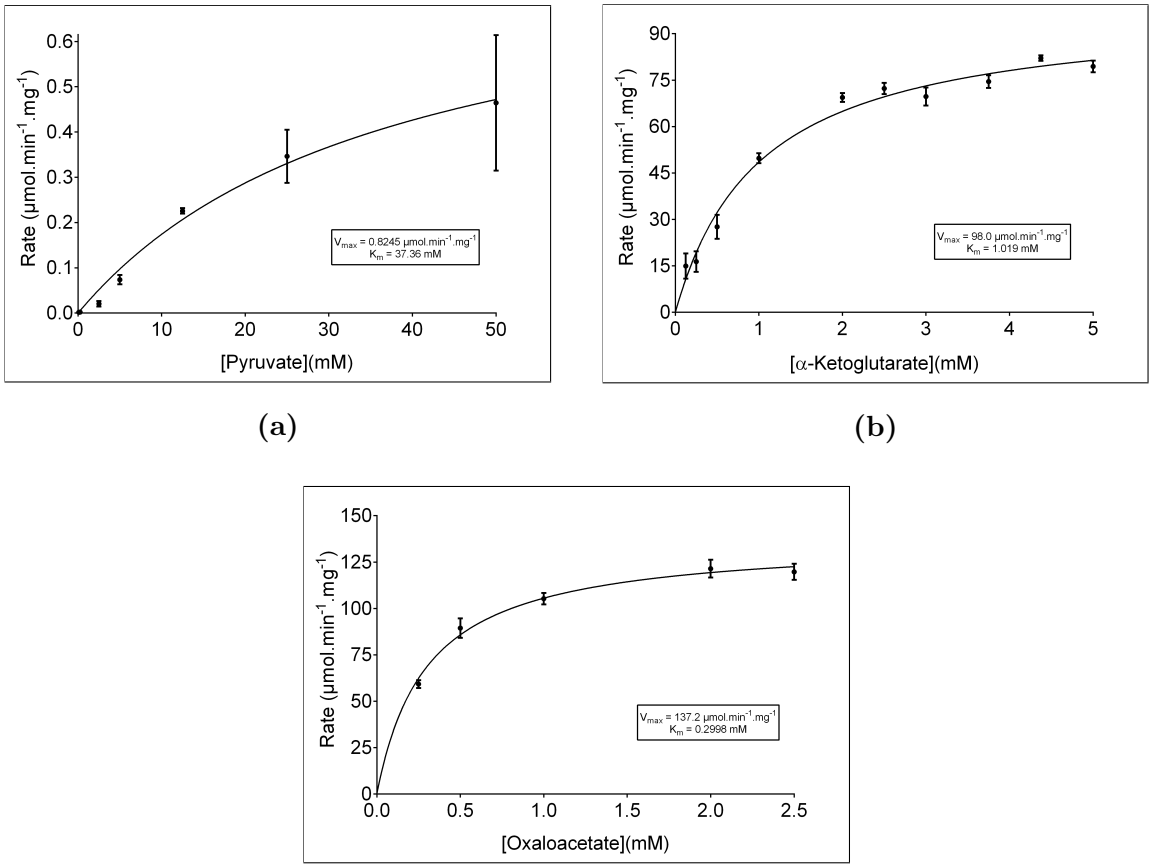

Figure 3.14. Michaelis–Menten kinetics of *T. cruzi* cASAT for pyruvate, α-ketoglutarate, and oxaloacetate with tryptophan as the amino group donor.
(a) Michaelis–Menten kinetic curves of *T. cruzi* cASAT with varying concentrations of pyruvate in the presence of 25 mM tryptophan. **(b)** Michaelis–Menten kinetic curves of *T. cruzi* cASAT with varying concentrations of α-ketoglutarate in the presence of 25 mM tryptophan. **(c)** Michaelis–Menten kinetic curves of *T. cruzi* cASAT with varying concentrations of oxaloacetate in the presence of 25 mM tryptophan. The reaction buffer used was 100 mM Tris–HCl (pH 7.5), 25 mM NaCl, 0.25 mM NADH, 20 U.ml^{-1} of AHADH (coupling enzyme), at 25 °C. The reaction was started by the addition of cASAT, and the decrease in absorbance at 340 nm was monitored as a reflection of the rate of activity of the enzyme. Error bars indicate SD, triplicate measurements.

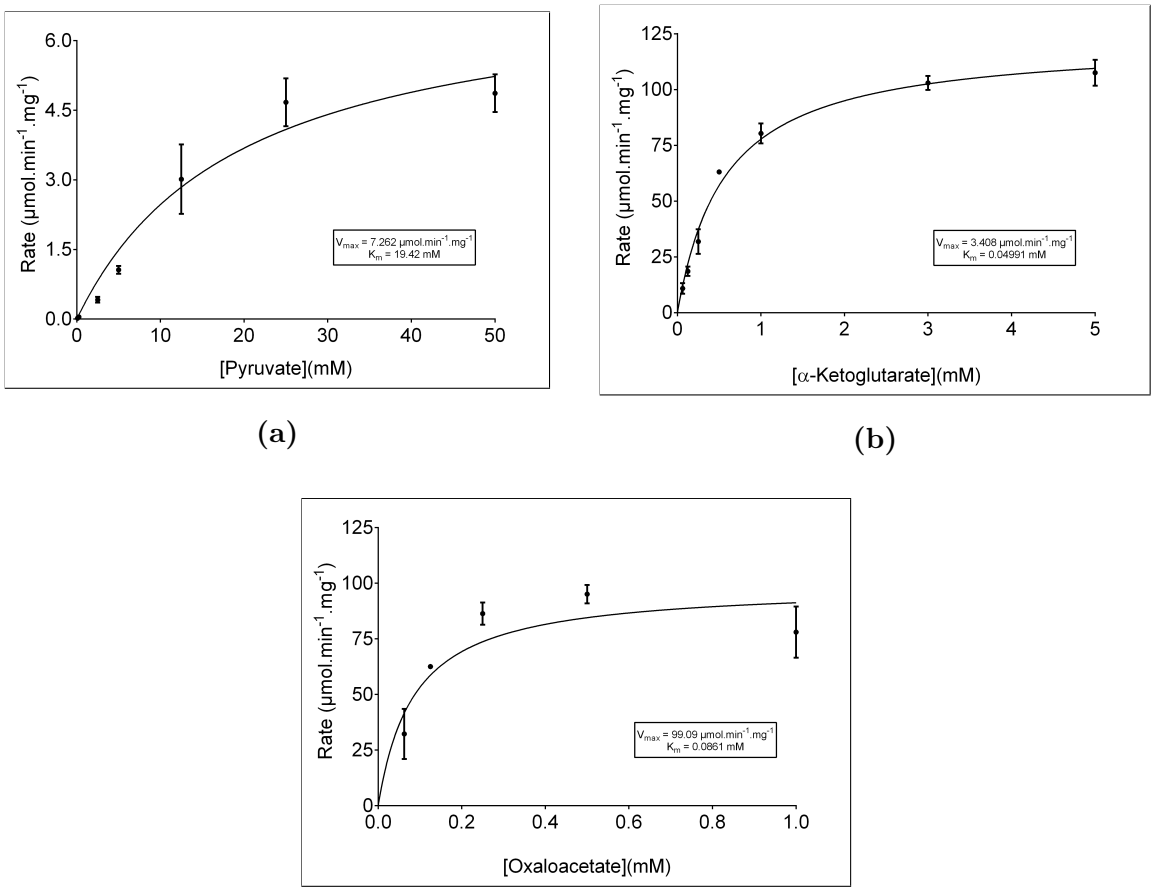

Figure 3.15. Michaelis–Menten kinetics of *T. brucei* cASAT for pyruvate, α-ketoglutarate, and oxaloacetate, with phenylalanine as the amino group donor. **(a)** Michaelis–Menten kinetic curves of *T. brucei* cASAT with varying concentrations of pyruvate in the presence of 25 mM phenylalanine. **(b)** Michaelis–Menten kinetic curves of *T. brucei* cASAT with varying concentrations of α-ketoglutarate in the presence of 25 mM phenylalanine. **(c)** Michaelis–Menten kinetic curves of *T. brucei* cASAT with varying concentrations of oxaloacetate in the presence of 25 mM phenylalanine. The reaction buffer used was 100 mM Tris–HCl (pH 7.5), 25 mM NaCl, 0.25 mM NADH, 20 U.ml^{-1} of AHADH (coupling enzyme), at 25 °C. The reaction was started by the addition of cASAT, and the decrease in absorbance at 340 nm was monitored as a reflection of the rate of activity of the enzyme. Error bars indicate SD, triplicate measurements.

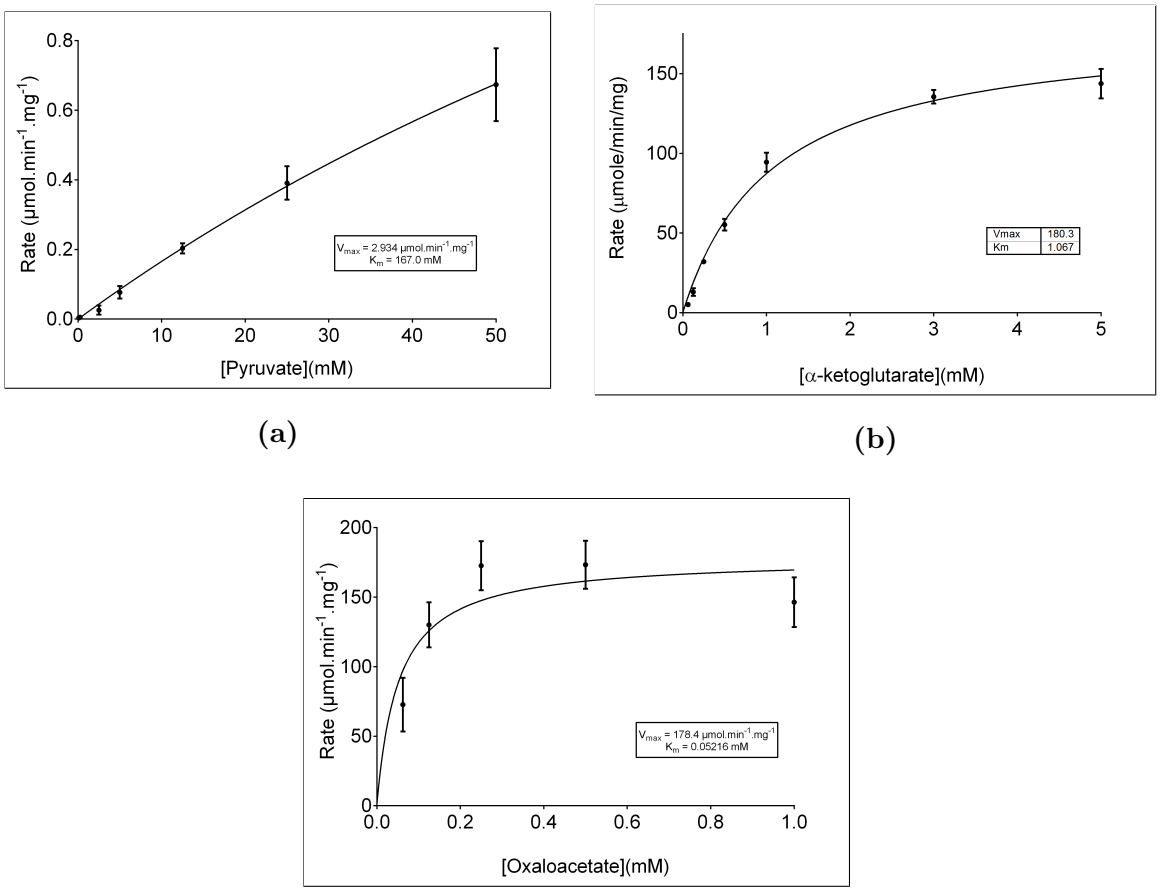

Figure 3.16. Michaelis–Menten kinetics of *T. cruzi* cASAT for pyruvate, α-ketoglutarate, and oxaloacetate, with phenylalanine as the amino group donor. **(a)** Michaelis–Menten kinetic curves of *T. cruzi* cASAT with varying concentrations of pyruvate in the presence of 25 mM phenylalanine. **(b)** Michaelis–Menten kinetic curves of *T. cruzi* cASAT with varying concentrations of α-ketoglutarate in the presence of 25 mM phenylalanine. **(c)** Michaelis–Menten kinetic curves of *T. cruzi* cASAT with varying concentrations of oxaloacetate in the presence of 25 mM phenylalanine. The reaction buffer used was 100 mM Tris–HCl (pH 7.5), 25 mM NaCl, 0.25 mM NADH, 20 U.ml^{-1} of AHADH (coupling enzyme), at 25 °C. The reaction was started by the addition of cASAT, and the decrease in absorbance at 340 nm was monitored as a reflection of the rate of activity of the enzyme. Error bars indicate SD, triplicate measurements.

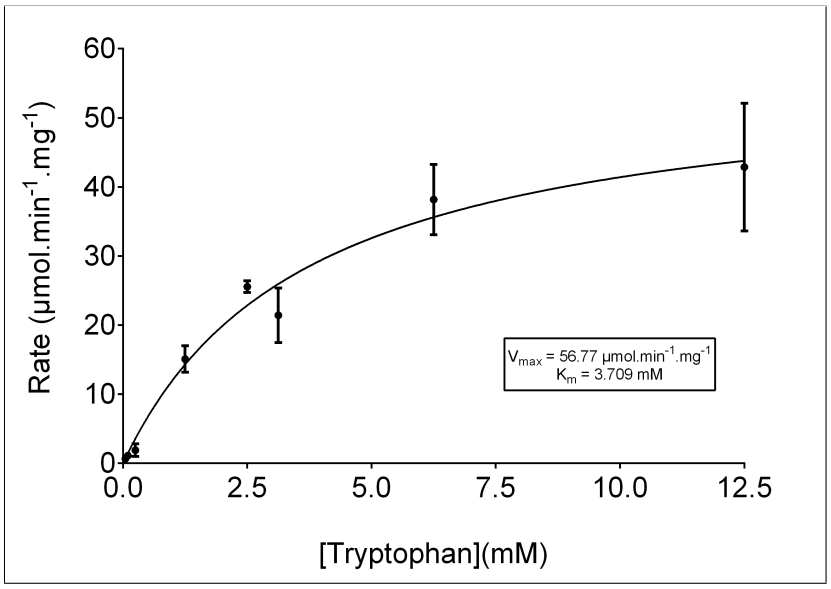

(a) TccASAT

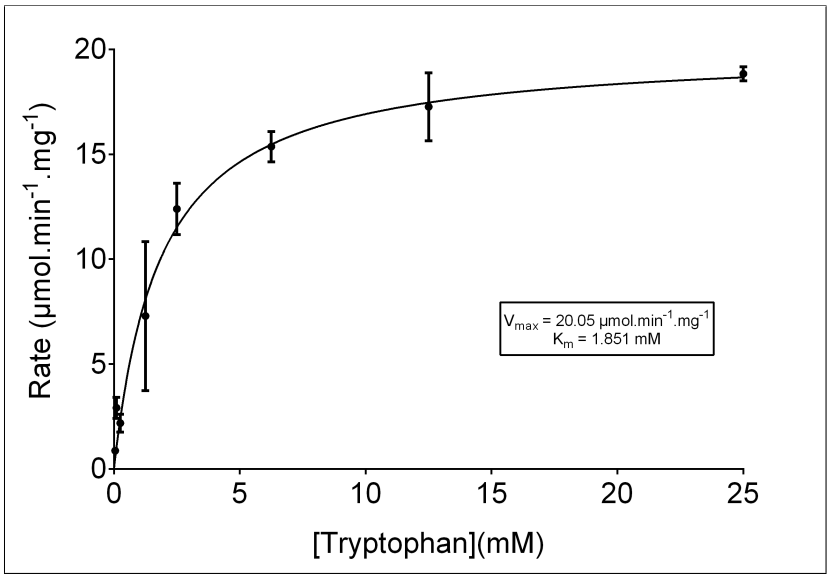

(b) TbcASAT

Figure 3.17. Michaelis–Menten kinetics of *T. brucei* and *T. cruzi* cASAT for tryptophan with oxaloacetate as the amino group acceptor.

(a) Michaelis–Menten kinetic curves of *T. cruzi* cASAT with varying concentrations of tryptophan in the presence of 2 mM oxaloacetate. **(b)** Michaelis–Menten kinetic curves of *T. brucei* cASAT with varying concentrations of tryptophan in the presence of 2 mM oxaloacetate. The reaction buffer used was 100 mM Tris–HCl (pH 7.5), 25 mM NaCl, 0.25 mM NADH, 20 U.ml^{-1} of AHADH (coupling enzyme), at 25 °C. The reaction was started by the addition of cASAT, and the decrease in absorbance at 340 nm was monitored as a reflection of the rate of activity of the enzyme. Error bars indicate SD , triplicate measurements.

Table 3.3. Kinetic parameters of *T. brucei* and *T. cruzi* cASAT. (Top) Kinetic parameters of cASAT for varying amino acids utilising α-ketoglutarate as the amino group acceptor. **(Middle)** Kinetic parameters of cASAT for α-ketoacids utilising tryptophan as the amino group donor. **(Bottom)** Kinetic parameters of cASAT for α-ketoacids utilising phenylalanine as the amino group donor. The kinetic parameters are a mean of triplicate measurements ± SD, were calculated with GraphPad Prism ver. 6.01, and were obtained experimentally as described in the materials and methods.

Amino acids	*T. brucei* cASAT			*T. cruzi* cASAT		
	V_{max} (μmol.min^{-1}.mg^{-1})	K_m (mM)	V_{max}/K_m (μmol.min^{-1}.mg^{-1}.mM^{-1})	V_{max} (μmol.min^{-1}.mg^{-1})	K_m (mM)	V_{max}/K_m (μmol.min^{-1}.mg^{-1}.mM^{-1})
Aspartate	185.6 ± 43.02	82.91 ± 23.73	2.23	353.1 ± 35.64	18.45 ± 3.54	19.13
Phenylalanine	132.2 ± 3.98	10.55 ± 0.74	12.53	336.1 ± 9.13	3.39 ± 0.33	99.05
Tryptophan	54.58 ± 1.94	0.66 ± 0.09	82.22	103.9 ± 3.16	10.44 ± 0.71	9.95

α-Keto acid	*T. brucei* cASAT			*T. cruzi* cASAT		
	V_{max} (μmol.min^{-1}.mg^{-1})	K_m (mM)	V_{max}/K_m (μmol.min^{-1}.mg^{-1}.mM^{-1})	V_{max} (μmol.min^{-1}.mg^{-1})	K_m (mM)	V_{max}/K_m (μmol.min^{-1}.mg^{-1}.mM^{-1})
Oxaloacetate	65.12 ± 1.29	0.10 ± 0.01	610.88	137.2 ± 3.02	0.29 ± 0.02	457.63
α-Ketoglutarate	59.43 ± 0.88	0.37 ± 0.02	158.14	98.00 ± 2.83	1.01 ± 0.09	88.36
Pyruvate	3.13 ± 0.34	16.65 ± 4.41	0.18	0.82 ± 0.20	37.36 ± 17.01	0.02

α-Keto acid	*T. brucei* cASAT			*T. cruzi* cASAT		
	V_{max} (μmol.min^{-1}.mg^{-1})	K_m (mM)	V_{max}/K_m (μmol.min^{-1}.mg^{-1}.mM^{-1})	V_{max} (μmol.min^{-1}.mg^{-1})	K_m (mM)	V_{max}/K_m (μmol.min^{-1}.mg^{-1}.mM^{-1})
Oxaloacetate	99.09 ± 9.07	0.08 ± 0.03	1238.62	178.4 ± 15.00	0.05 ± 0.02	3568
α-Ketoglutarate	122.0 ± 3.40	0.56 ± 0.049	215.62	180.3 ± 6.45	1.06 ± 0.09	170.09
Pyruvate	7.26 ± 0.80	16.65 ± 4.99	0.43	2.93 ± 1.27	167.0 ± 90.06	0.01

3.2 Crystallisation of trypanosomal cASAT.

Most recently, the mitochondrial aspartate aminotransferase from *T. brucei* (TbmASAT), which is highly specific for aspartate, was crystallised. This revealed interesting insights into the proteins structure, such as the lack of requirement of a normally crucial Lys237. This lysine is usually required to bind the pyridoxal-5-phosphate (PLP) co-factor in the active site of the protein, via a schiff-base bond. When this lysine was mutated to an alanine residue in TbmASAT the PLP remained bound in the enzymes active site [153]. Though mASAT is different in its amino acid sequence and substrate specificity when compared to cASAT, both are aminotransferases of the same sub-group [142]. It is possible that the 3D conformation of each enzyme plays an important role in the difference in their substrate specifities.

In an effort to further understand the nature of *T. brucei* and *T. cruzi* cASAT preference for aromatic amino acid substrates, and having generated both purified recombinant *T. brucei* and *T. cruzi* cASAT, attempts were made to produce 3D x-ray crystallography structures. This was undertaken in collaboration with the X-Ray Crystallography Group (Dr. Amir Khan). This is the first time that a crystal structure for either enzyme has been proposed.

3.2.1 Crystal structure of *T. cruzi* cASAT.

Purification of *T. cruzi* and *T. brucei* cASAT.

Both *T. cruzi* and *T. brucei* recombinant proteins were expressed as described in the materials and methods. Additional purification steps were undertaken to aid crystallisation of the proteins, that were not performed for the biochemical studies. The large scale protein expression previously described (page 103) for biochemical studies was also used to generate protein for the crystallisation studies. The N-terminal hexahistidine tag was removed with rTEV cleavage, to reduce any possible structural disruptions that would prevent successful crystallisation (Fig. 3.18). Though N-terminal His tags have been shown to rarely interfere in the ordering of crystallised proteins [158], the possibility that the N-terminal segments of both cASATs would be involved in the structural integrity of these proteins influenced the decision to remove the His-tags.

High molecular weight (≈ 90 kDa) contaminating protein bands were observed in the rTEV cleaved TbcASAT SDS-PAGE gel (Fig. 3.18a). To obtain protein pure enough to crystallise, both TccASAT and TbcASAT rTEV cleaved samples were run through a Superdex 200(16/600) gel filtration column. Samples of high homogeneity were separated and eluted off the column, and in agreement with the SDS-PAGE analysis, *T. brucei* cASAT appeared to contain more contaminating proteins than that of *T. cruzi* cASAT prior to filtration (Fig. 3.19). In both cases the elution profiles migrated as a single peak, representative of a single complex, and both enzymes eluted at a similar elution volume. The pure protein fractions were concentrated to 8 $mg.ml^{-1}$ and were initially screened on Midas, Morpheus, Wizard JB screen and JB screen classic matrices. These screens were selected for differing reasons, for example, the Midas screen uses combinations of salts and pH close to physiologically relevant values, whereas the Morpheus screen uses a more broad range of buffers and precipitants such as HEPES and PEG. A total of 480 random screens were conducted, yielding multiple 'needle' like crystal sets and 3 structured dipyramidal crystal sets (two for *T. brucei*, one for *T. cruzi*). Two of these crystal sets were deemed suitable for x-ray diffraction, one each from both species (Fig. 3.20). The procedures outlined here are discussed in-depth in the materials and methods chapter.

X-Ray diffraction and crystal structure of *T. cruzi* cASAT.

Harvested crystals of both species were subjected to synchrotron single beam x-ray diffraction, the data from which was gathered and processed by Dr. Amir Khan. Using a molecular replacement approach with previously obtained ASAT structures, it was possible to construct a model of the crystal structure of *T. cruzi* cASAT (Fig. 3.21a). The TccASAT model is of medium resolution at 2.1 angstroms. The structure is comprised of a dimer of identical subunits, each containing a PLP binding domain at the active sites. The model suggests that TccASAT is a globular, α/β protein [159]. Overall, each subunit is composed of 12 α-helices and 9 parallel and anti-parallel β-sheets. The N-terminal arm (residues 1 - 19) is clearly extended from each subunit across into the opposite subunit (Fig. 3.21b). Unfortunately, *T. brucei* cASAT crystals did not produce useful diffraction data.

To confirm that the crystal structure obtained for *T. cruzi* was representative of

the active enzyme, enzymatic assays were conducted on the recombinant protein at varying pH, and with the buffer that achieved ordered crystal growth. The enzyme has a broad pH activity range, with the highest activity observed at a mid to high pH range (pH 7 - 10, Fig. 3.22). Crucially, the enzyme was also active in the crystallisation buffer. Moreover, the enzyme appeared to have a higher activity in the crystallisation buffer, than in the universal buffer at the same pH. Taken together, this data suggests that the crystallised *T. cruzi* protein was probably in its native state.

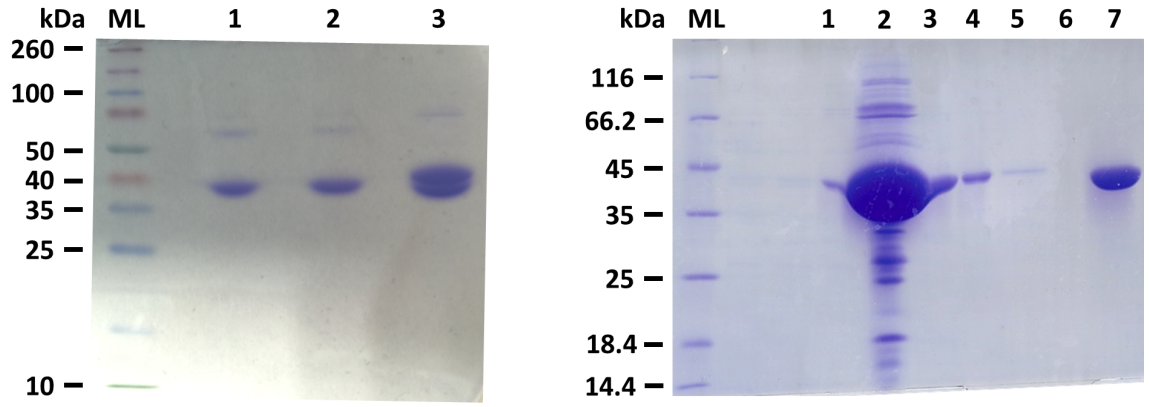

(a) **(b)**

Figure 3.18. Analysis of *T. brucei* and *T. cruzi* cASAT following elution from Ni^{2+} column.

Coomassie stained 12% SDS-PAGE gels of rTEV cleaved, purified cASAT. **(a)** *T. brucei* cASAT. Lanes 1, 2, and 3 each contain rTEV cleaved cASAT at ≈ 40 kDa from three different purified samples. **(b)** *T. cruzi* cASAT. Lanes 1 to 5 are of column bound and eluted cASAT, with lane 2 containing the largest amount of eluted protein. Lanes 3 and 4 contain buffer-washed fractions of protein. The rTEV cleaved and purified cASAT is present in lane 7.

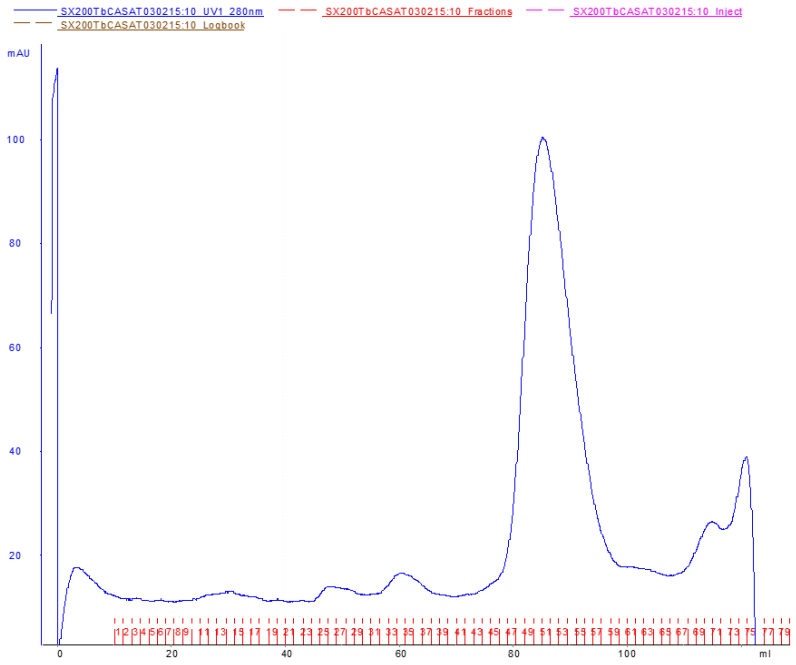

(a)

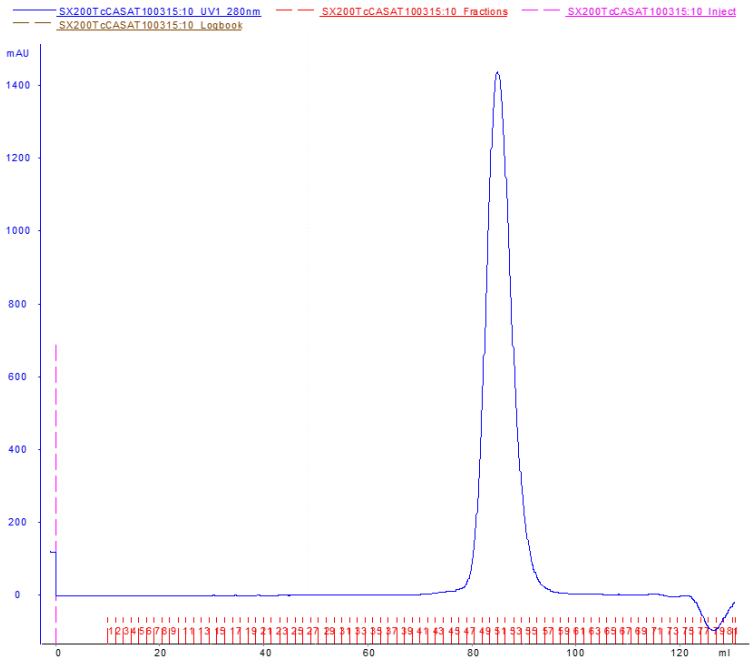

(b)

Figure 3.19. Chromatographs of purified *T. brucei* and *T. cruzi* cASAT.
The cASAT elution profiles on a Superdex 200(16/600) gel filtration column. Peaks eluted at lower volumes indicate a higher molecular weight protein contaminant. **(a)** *T. brucei* cASAT eluted between fractions 49 - 59. **(b)** *T. cruzi* cASAT eluted between fractions 45 - 57. Protein concentration in a given fraction is determined by absorbance readings at 280 nm (mAU, y-axis) against the fraction number (volume in ml, x-axis). Bed volume of 120 ml.

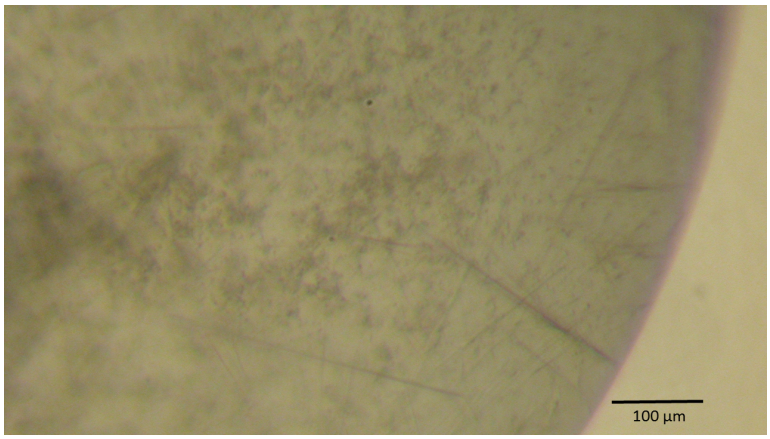

(a)

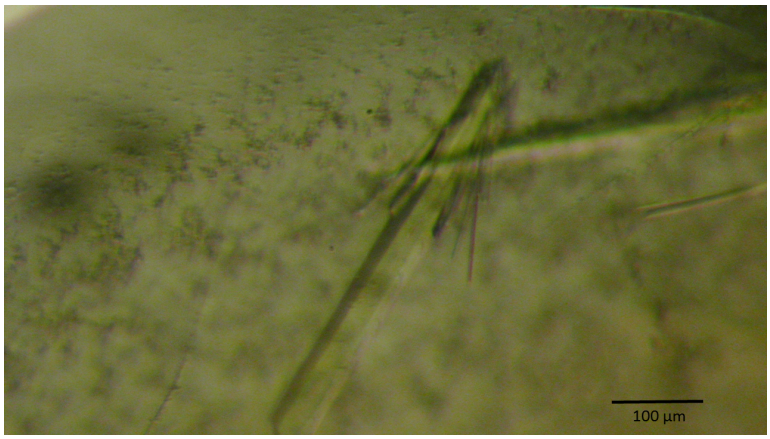

(b)

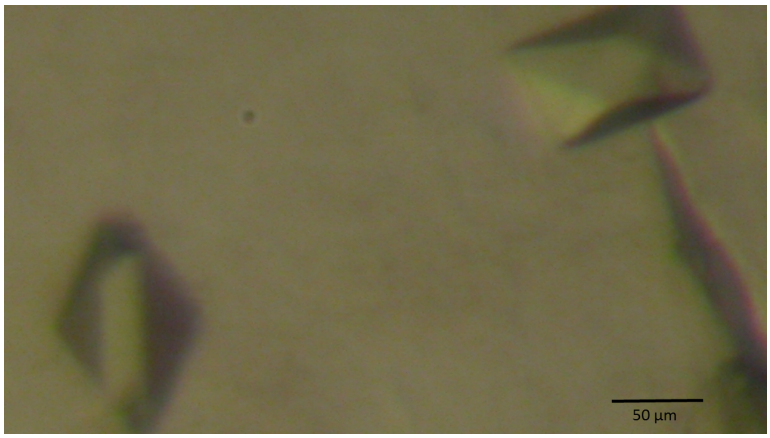

(c)

Figure 3.20. cASAT crystals obtained from matrix screens.

(a) Representative image of the 'needle' structures that formed in multiple screens, which are not suitable for x-ray examination. **(b)** An ordered crystal of *T. cruzi* cASAT, amongst some 'needle' like structures. **(c)** Several ordered crystals of *T. brucei* cASAT. Crystallisation conditions for (b) and (c) are outlined in the materials and methods. Images acquired at 14 days post crystallisation trial setup with a Nikon DSLR camera attached to a Nikon bifocal microscope.

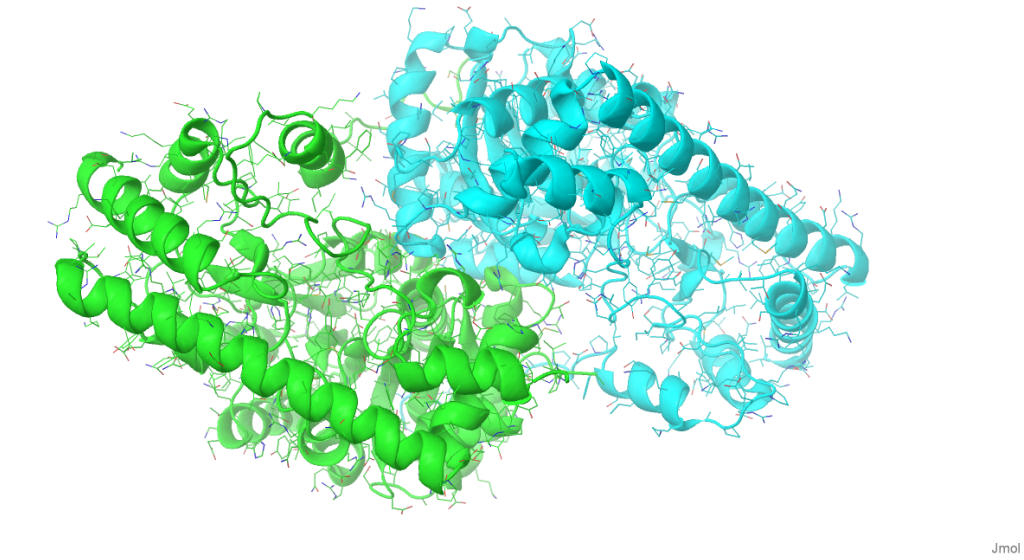

(a)

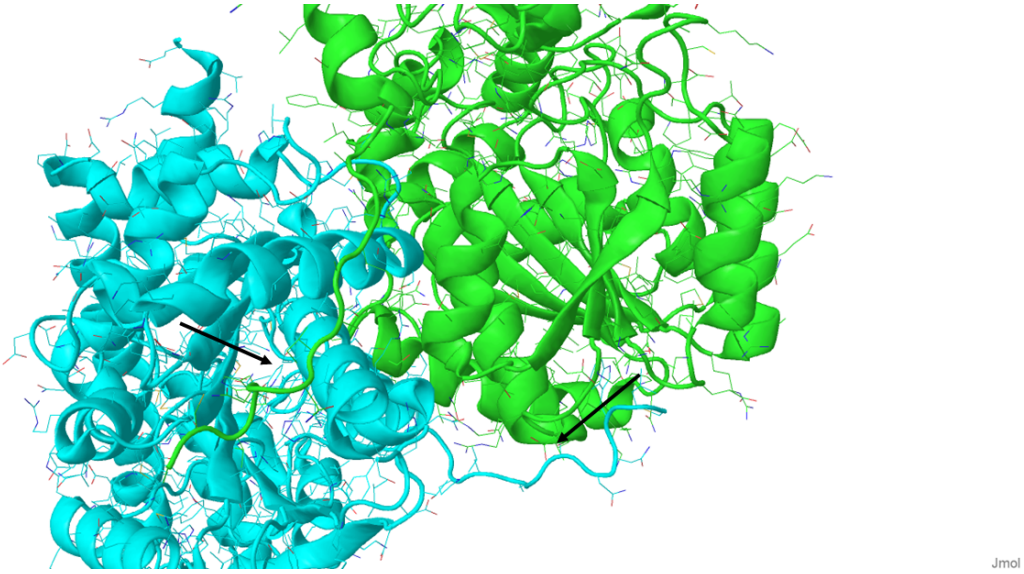

(b)

Figure 3.21. Proposed crystal structure of *T. cruzi* cytosolic aspartate aminotransferase.

(a) *T. cruzi* cASAT crystallises as a homodimer comprised of identical subunits, with each subunit comprised of one catalytic site and one PLP binding domain. **(b)** The N-terminal arms of each subunit appear to interact with the opposite subunit (highlighted with black arrows). The structure was refined by a molecular replacement approach, performed by Dr. Amir Khan. Resolution is 2.1 angstroms, modelled in Jmol (http://www.jmol.org/). The structure has yet to be published.

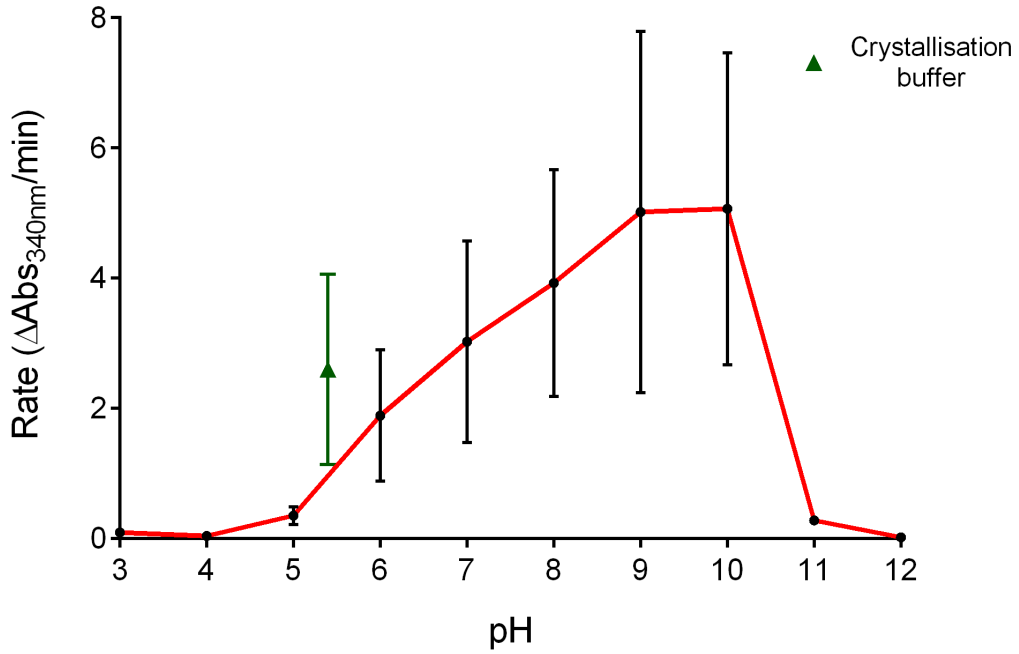

Figure 3.22. The activity of *T. cruzi* cASAT at different pH ranges.

T. cruzi cASAT was found to be active at a broad pH range, with peak activity being observed between pH 9 and 10. The protein was also active in crystallisation buffer, more so than in the universal buffer at the same pH. Recombinant *T. cruzi* cASAT was incubated in universal buffer at different pH (3 - 12) or crystallisation buffer, at 37 ^{o}C for 30 min and 60 min. The enzyme was then assayed with 25 mM phenylalanine in an AHADH assay, as previously described. Small volumes (50 μl) of the incubated samples were used in the assay, to ensure that the pH of the assay buffer was not altered. the high margin of error is due to the sequential measurement of samples, i.e. assaying samples 3,4,5,...12 after 30 min incubation, then 3,4,5,...12 again after 60 min. The crystallisation buffer was a 50:50 solution of 10 mM Tris pH 7.5 & 50 mM Acetate pH 4.6, the final pH of this solution was 5.4. Error bars indicate SD, duplicate measurements.

3.3 Discussion.

3.3.1 Bioinformatic analysis of TbcASAT and Trypanosomatid cASAT.

A broad search for aspartate aminotransferases in TriTrypDB genomic database for both *T. brucei* and *T. cruzi* yielded four putative aminotransferases. Firstly, the ORF of each of these cASATs were predicted to produce proteins of a similar size, $\approx$ 40 kDa, to other cASATs [153]. Secondly, all four of these enzymes have been confirmed as possessing aminotransferase activity [98, 99, 150], which was consistent with the presence of four conserved residues - Gly(314AT), Asp(340AT), Lys(385AT), and Arg(562AT) - primarily associated with aminotransferase activity in all four candidates (Table 3.4) [142]. Each alignment of these residues is shifted with respect to other aligned sequences, yet in each case the internal spacing of the invariant residues is the same. In addition, the regions flanking these key residues were also highly conserved, suggesting that in all cases these regions must play important roles, either functionally or structurally, for the protein. However, there is at least one feature that appears to be unique to the trypanosomatidae cASATs examined here; the regions spanning the N-terminal portions of the proteins were notably varied. Amongst the trypanosomatidae both *C. fasiculata* and *L. mexicana* have 4 and 9 amino acids, respectively, added to the beginning of their N-termini. Furthermore, the trypanosomal protozoa, *T. cruzi*, *T. grayi*, and *T. rangeli* have N-terminal regions (positions 1 - 12, page 77) that are distinctly different to the corresponding regions in the *T. brucei* related African trypanosomes. The cASAT from *T. cruzi* has been characterised as a broad specificity aminotransferase, as has the *L. mexicana* ASAT, for which a crystal structure has been obtained [155, 160]. Some studies have suggested that the N-terminal tail may play a role in the broad substrate selectivity of these enzymes [143, 154, 155]. Jensen et al. highlights that site-directed mutagenesis of residues proximal to the N-terminal segment of an *E. coli* ASAT could be used to broaden its substrate specificity [143]. Truncation of the divergent N-terminal region of *P. falciparum* ASAT, which could also utilise aromatic amino acids as substrates, lead to loss of activity of the enzyme [154]. Comparison of TbcASAT with cASAT from higher organisms further highlights the variation in the N-terminal tail, which appears to be more conserved amongst higher organisms. Given the stricter

substrate specificities of ASATs from higher organisms, this variation may represent a mechanism by which TbcASAT, and other trypanosomal cASATs, have developed broader specificities. It has also been alternatively suggested that aminotransferases originally displayed broad substrate specificities, and that they have evolved over time to become more substrate specific [143]. Analysis of the phylogenetic relationships of the trypanosomatidae cASAT sequences obtained from TriTrypDB produced a broadly accurate representation of the trypanosomatidae evolutionary relationships. The relationships produced were found to be similar to those determined by more dedicated phylogenetic studies which used 18S rRNA or HSP70 genes [11, 12]. This bioinformatic data highlights the common conservation of key residues amongst the aspartate aminotransferases, and further highlights the variability of the N-terminal which appears to be a feature of the broad substrate specificity cASATs. It is possible that this N-terminal segment is involved in regulating cASAT substrate specificity.

Table 3.4. The positions of the four key invariant residues in selected trypanosomal ASATs.

The four invariant residues identified in *T. brucei* cASAT and mASAT, and in *T. cruzi* cASAT, as defined by Mehta et al. [142].

Mehta et al. residue identification [142]	TccASAT	TbcASAT	TbmASAT
Gly(314AT)	Gly189	Gly187	Gly205
Asp(340AT)	Asp214	Asp212	Asp230
Lys(385AT)	Lys250	Lys248	Lys266
Arg(562AT)	Arg377	Arg375	Arg394

3.3.2 Kinetic data for *T. brucei* and *T. cruzi* cASAT.

It was initially demonstrated by Berger et al. that TbcASAT has a particularly broad substrate specificity. Though TbcASAT possesses aspartate aminotransferase activity, it is capable of performing transaminations with aspartate, aromatic amino acids, glutamine, and alanine with similar efficiency, in the presence of α-ketomethiobutyrate (KMTB) as the amino acceptor [99]. For example, with KMTB the K_m obtained for tyrosine, phenylalanine, tryptophan, glutamine, leucine, and histidine are all between 6 - 18 mM. Similar K_m data are reported for aspartate with α-ketoglutarate (10.38 mM). It should be noted that these kinetic parameters were obtained using non-standard

methods. In lieu of enzymatic assays, a HPLC method was employed. While HPLC based assays have the advantage over continuous enzymatic assays of application to a wider range of substrate determinations, they also have limitations. As reported by Berger et al., the rate determinations were not based on initial rate data, as is the case for most classical determinations of enzymatic kinetic constants. In a more limiting manner, the rates were determined in a non-continuous fashion; values were obtained at a single 15 minute time point, and utilised a low substrate concentration range of between 0.1 - 10 mM [99]. Nonetheless, this ability to transaminate KMTB supported a suggested role for TbcASAT in the final step of a proposed methionine regeneration cycle in *T. brucei*, where the final step in methionine regeneration would be the TbcASAT catalysed transamination of KMTB with an amino group abstracted from other amino acids [161]. Studies on methionine regeneration are notably incomplete [99, 161–163]. Only one study could be identified where a complete methionine recycling pathway was proposed to function, conducted in *Saccharomyces cerevisiae* [163]. Even within this study, the involvement of aminotransferases appeared to be non-specific, with nine possible aminotransferases identified in crude cell extracts as potential catalysts for the conversion of KMTB to methionine. Furthermore, the authors also suggested non-enzymatic deamination was a source of excessive consumption of amino acids (242 % in excess of methionine production in one case). Creation of a knockout mutant of four of the aminotransferases suggested to be responsible for converting KMTB to methionine was not possible. Therefore, it was not clear how well the proposed methionine recycling pathway functioned in this study. In other work performed by Heilbronn et al., a tyrosine aminotransferase was identified as being able to preferentially utilise KMTB for transamination reactions with aromatic amino acids [162]. However, this study was again performed using non-traditional methods, in a similar manner to those used previously [99]. KMTB does not appear to have been well characterised as a substrate for other enzymes [149].

Subsequent work by Marciano et al. provided further analysis of the kinetic properties of several aminotransferases from trypanosomatids, including the cASATs of *T. brucei* and *T. cruzi* [98, 150]. In these studies a more typical enzymatically based method for determining the kinetic parameters of *T. brucei* and *T. cruzi* ASATs was employed, using AHADH and MDH in NADH-dependent coupled assays. They noted similar findings to those of Berger et al. with respect to the trypanosomal cASATs

broad specificity and KMTB utilisation, but also found that α-ketoglutarate was the preferred amino acceptor with all amino acid donors used. Taking aspartate as an example, Marciano et al. report a V_{max} of ≈ 400 μmol.min^{-1}.mg^{-1} with α-ketoglutarate, whilst Berger at al. reports a specific activity almost 100 times lower for the same reaction (4.59 μmol.min^{-1}.mg^{-1}) [98, 99]. This suggested that KMTB transamination may not be the primary α-ketoacid substrate for these enzymes or that they are poor catalysts of KMTB. Successful expression and purification of both TccASAT and TbcASAT described here allowed for additional kinetic characterisation of both enzymes. In agreement with Marciano et al., it was found that the amino acids tryptophan and phenylalanine can be utilised effectively by both *T. brucei* and *T. cruzi* cASAT with α-ketoglutarate as amino group acceptor, in addition to aspartate (pages 91 - 93) [98]. Interestingly, both this study and the work by Marciano et al. indicate that *T. brucei* cASAT has a much greater preference for tryptophan as a substrate in conjunction with α-ketoglutarate, as well as a higher preference for aromatic amino acids overall (page 99) [98].

It was demonstrated by Berger et al. that KMTB was the preferred amino group acceptor for TbcASAT, and further demonstrated by Marciano et al. that α-ketoglutarate was a better amino group acceptor that KMTB. Clearly a discrepancy exists between both studies as to what is the primary 2-oxoacid co-substrate for TbcASAT. Unfortunately, attempts to conduct similar investigations into KMTB as a substrate for both cASATs were prevented in this study as, contrary to previous reports, KMTB was found to be a potent substrate for AHADH [98, 139]. As an alternative, two other 2-oxoacids - oxaloacetate and pyruvate - were assayed here with tryptophan and phenylalanine. Kinetic parameters were obtained that were of the same proportional relationship to one another as those obtained by Marciano et al. when α-ketoglutarate was used as the co-substrate, though both the V_{max} and K_m values reported here are lower and higher respectively than those reported by Marciano et al. (page 99) [98]. This can be explained, at least partially, by simple recombinant protein batch variation and alternative assay buffers used, etc., in conjunction with a lower 25 ^{o}C assay temperature that was employed here.

Both enzymes could utilise pyruvate as an amino acceptor from tryptophan, although much more poorly than α-ketoglutarate. As the K_m is high and the V_{max} is

low for pyruvate for both cASAT enzymes, it is unlikely to be an important substrate for cASAT in either parasite. It was found, however, that oxaloacetate was the most preferred amino acceptor when either tryptophan or phenylalanine acted as the amino donor, based on the enzymatically determined V_{max}, K_m, and V_{max}/K_m parameters (page 99). It is possible that oxaloacetate could be the preferred amino acceptor *in vivo*. A preference for oxaloacetate would seem to make more sense metabolically than the postulated role for α-ketoglutarate with AAT [96]. It has been suggested that AAT may be involved in the shuffling of amino groups from aromatic amino acids to α-ketoglutarate to regenerate glutamate for transamination of pyruvate to alanine. This role for AAT would seem functionally redundant, as both alanine and pyruvate are ultimately excreted end products of glycolytic metabolism and are not known to be metabolised further. However, it is possible that AAT could function with cASAT in a coupled manner. In this case, it is speculated that transamination of aromatic amino acids would not be used to supply aspartate for biosynthesis, but rather to supply aromatic ketoacids for other undetermined purposes. Linking AAT and cASAT through α-ketoglutarate and glutamate could provide directional drive to the formation of aromatic ketoacids as a consequence of pyruvate to alanine conversion. Alternatively, transamination of oxaloacetate to aspartate could prove important for purine salvage and adenine nucleotide synthesis in bloodstream form *T. brucei*. Recent reports indicate that *T. brucei* does not appear to have an active aspartate uptake mechanism [94], and no aspartate uptake was observed from culture media [93]. Glucose derived oxaloacetate could feed into aspartate synthesis through TbcASAT, where aromatic amino acids are used to transaminate oxaloacetate and produce aspartate. This process could supply all the aspartate required by *T. brucei*.

While many ASAT have broad substrate specificities, both TbcASAT and TcASAT have significantly lower K_m values for tryptophan and phenylalanine compared to most other substrates such as aspartate, which have been published elsewhere (excluding an *E. coli* ASAT [149, 164]). This functional purpose of these perceived preferences needs to be examined, to clarify why this broad substrate specificity may have developed in these enzymes.

3.3.3 The crystal structure of *T. cruzi* cASAT.

Instances of aromatic amino acid transaminases have been demonstrated as early as the 1960s [165]. Notably, the ability of aspartate aminotransferases to accept a broad range of substrates varies greatly; mammalian ASATs tend to be specific for an aspartate - α-ketoglutarate [143]. This is also true of mitochondrial ASATs (mASAT) from protozoa [98]. In contrast, many broad specificity ASATs have been characterised, mostly from plant, parasitic, and bacterial sources [99, 143, 145]. Crystallographic studies have been previously applied to ASATs in attempts to explain the possible structural mechanisms for these substrate preferences [146, 147]. Both *T. cruzi* and *T. brucei* cASAT have a broad substrate specificity, with each enzyme displaying a preference for aromatic amino acids as substrates. In an effort to understand the basis for this preference, crystallographic studies were undertaken here. These studies have lead to advances towards a *T. brucei* cASAT structure, and yielded a well resolved structure for *T. cruzi* cASAT.

Here, the crystal structure of *T. cruzi* cASAT has been obtained for the first time. TccASAT crystallised as an asymmetric dimer, a common occurrence for aminotransferases [153], with each subunit comprised of a 404 amino acid, 44.8 kDa monomer. The aminotransferases of subgroup I contain four invariant amino acids; in *T. cruzi* cASAT all four of these residues have been found to be conserved, including the important Lys(385AT) and Asp(340AT) residues [142]. These residues are responsible for binding the PLP co-factor, primarily through forming a schiff base with Lys(385AT). Bujacz et al. have identified a broad-specificity aminotransferase from a *Psychrobacter* species of bacterium, which is capable of deamination of phenylalanine, tyrosine, and tryptophan [146]. They suggest that two arginine residues on opposite monomers of the dimer, Arg280 and Arg374, may alter the active site to accept a broad range of substrates depending on their conformation. It could be possible that a similar mechanism could be present in *T. cruzi*, as these residues are also present (Arg284, Arg377). Interestingly, the N-terminal section of *T. cruzi* cASAT was found to be more disordered than those from related aminotransferases (Dr. Amir Khan, personal communication), which would seem to match the data obtained during the comparative sequence alignments. The presence of the disordered N-terminal arm in TccASAT was confirmed by the crystallographic studies performed here. It was demonstrated

recently that the N-terminal residues of ASAT from *P. falciparum* were required for some of the catalytic activity of the enzyme, as truncation of 13 amino acids from the N-terminal reduced catalytic efficiency by 50% [154]. The authors suggested that though the arm (13 residues, 1 - 15) is attached to the small domain of ASAT and is far from the active site, it may act to stabilise the conformations of the 'open' and 'closed' states. Another study has suggested that both the N-terminal tail and the flexibility of an arginine residue, Arg291, play a role allowing a range of substrates to be used by the aminotransferase, in this case from *L. mexicana* [155]. The first 20 amino acid residues of the N-terminal of *L. mexicana* BSAT inserts into a cleft in the co-factor binding domain of the opposite monomer. It is possible that the N-terminal may then regulate the function of the PLP co-substrate. Arg291 is involved in the binding of the side chains of the substrates. The Arg291 residue in the broad substrate specificity *L. mexicana* and *L. major* ASATs appears to be able to undergo extended rotation that was not observed in the more aspartate specific ASATs [153, 155]. Such mechanisms could be applicable to *T. cruzi* cASAT. However, the sequence alignment data previously provided indicates that the the Arg291 appears to be conserved between TccASAT and the sequences of higher organism cASATs, which tend to be more substrate specific.

The key to substrate specificity could lie in the differences between the N-terminal tails, given that the N-termini of the Kinetoplastida are markedly different to those of higher organisms. Speculating on this basis and from examination of the cASAT alignment sequences, it is possible that the substrate specificities of *T. cruzi*, *T. grayi*, and *T. rangeli* could be similar to one another, as could those of the *T. brucei* related cASATs. A study by Jäger et al. demonstrated that a V39L mutation in the N-terminus of an ASAT in *E. coli* could improve the overall catalytic ability of ASAT, while not appearing to affect substrate specificity [166]. In the African trypanosomes and higher organisms this valine is conserved, but is switched to an isoleucine in *T. cruzi* (page 77). It is possible that this allows TccASAT to be more catalytically efficient than TbcASAT (page 99). TccASAT has a lower V_{max}/K_m for oxaloacetate with tryptophan as the amino donor than TbcASAT, whereas TccASAT has a higher V_{max}/K_m for oxaloacetate with phenylalanine as the amino donor than TbcASAT. It is possible that the differences between the amino acid residues of the TccASAT and TbcASAT N-terminal arms influences the differences in the phenylalanine/tryptophan

utilisation by the two enzymes. Additional work needs to be carried out, including obtaining the crystal structure for *T. brucei*, which would further aid this research and allow for a better comparison of the N-terminal arm contributions to the substrate specificities of each enzyme. Attempts to generate truncated N-terminal cASATs and determinations of their kinetic abilities should also be pursued.

3.3.4 Conclusions.

Further to the studies of Berger et al. and Marciano et al., it has been demonstrated that both *T. brucei* and *T. cruzi* cASAT have a broad substrate specificity. In agreement with Marciano et al., it has been shown that TbcASAT has a preference for tryptophan when α-ketoglutarate acts as the amino acceptor [98]. Additionally, it has been demonstrated for the first time that oxaloacetate is the preferred amino group acceptor in the transamination reactions with tryptophan and phenylalanine based on all the kinetic parameters obtained (V_{max}, K_m, and V_{max}/K_m). Given the low K_m and the high V_m for the reactions, this could be the preferred reaction set *in vivo*, though this remains to be established. The crystal structure of TccASAT has been obtained, and early analysis has highlighted the unusual structure of its N-terminal arm, which may play a role in determining the catalytic efficiency and substrate specificity of the enzyme [143, 154]. If that is the case, the sequence similarities of the broad specificity TccASAT and TbcASAT to other trypanosomatids suggests that many trypanosomatids may have a broad specificity cASAT. The variation in the N-terminal arm of each enzyme may also explain the small differences in the kinetic abilities reported here.

Chapter 4

Functional characterisation of the role of TbcASAT in *T. brucei*.

Having demonstrated that TbcASAT was a broad-substrate specificity aminotransferase, with a preference for aromatic amino acids in the presence of an α-ketoacid amino acceptor, the possible functions this enzyme might play in the growth and metabolism of *T. brucei* were examined.

4.1 RNAi of *cASAT* in bloodstream form and procyclic form *T. brucei*.

4.1.1 Creation of cASAT RNAi cell lines.

In order to establish whether cASAT played a key functional role in bloodstream and/or procyclic form *T. brucei*, conditional RNAi was performed. To generate a TbcASAT conditional RNAi cell line, a 446 bp fragment of the TbcASAT open reading frame (Tb927.10.3660, nucleotides 556 - 1002) was amplified from *T. brucei* gDNA and sub cloned into the p2T7-177 vector. The p2T7-177 vector contains both tetracycline promoter and operator elements that allow conditional RNAi induction in the presence of tetracycline. A BLAST analysis of the selected 446 bp nucleotide sequence against the *T. brucei* genome revealed no significant off-target hits, with the maximum shared identity with other genes being just 8%. The vector was then linearised with NotI and transfected into Lister 427 MITat 1.2 cells for bloodstream RNAi, while Lister 427 cells were also used for procyclic RNAi. Both cell lines had been modified to express the T7 RNA polymerase and Tet repressor protein, and selective pressure was maintained by the addition of G418 and hygromycin to the cultures [123]. Positive clones were selected with the addition of phleomycin. The dsRNA was produced by the addition of tetracycline to cultured cells, generating dsRNA corresponding to the fragment of *cASAT* and leading to knockdown of the *cASAT* gene product.

4.1.2 The effects of *cASAT* RNAi knockdown on bloodstream and procyclic form *T. brucei*.

Induction of RNAi of *cASAT* in the cells was found to have a dramatic and deleterious effect on the growth of bloodstream cells, when compared to the parental cell line (wild type) not containing the RNAi vector (Fig. 4.8). In these cells, growth was arrested after 24 hours of dsRNA induction when compared to both non-induced cASAT RNAi and wild type cells (containing no RNAi vector). Growth remained arrested at 48 hours, with cell numbers decreasing at later stages, indicative of cell death (Fig. 4.1). Interestingly, a growth phenotype was also observed in the non-induced cells. Growth of the non-induced cells was slower, with a doubling time of ≈ 10.6 hours, when compared to the ≈ 7.3 hour doubling time of wild type cells. The discrepancy between the growth of the wild type cells and the non-induced cASAT RNAi cells is likely due to minor production of dsRNA in the absence of tetracycline in these cells, though it has the effect of a significant increase ($\approx 50\%$) in the doubling times of the cells. Overall, this data was consistent with the view that bloodstream *T. brucei* complete one cycle of cell division then enter growth arrest before dying 72 hours post RNAi induction.

Quantitative reverse transcriptase PCR (qRT-PCR) analysis was performed to confirm that the knockdown of *cASAT* was specific, and that the effect of knockdown on the cell growth was a true reflection of the decrease in *cASAT* RNA expression. The qRT-PCR analysis was performed using a combination of the Brilliant® SYBR Green qRT-PCR 1-step Master Mix kit (Stratagene) and MxPro 3000 instrument (Stratagene) as described in the materials and methods chapter. It was found that there was ≈ 66 % decrease in the transcript level of *cASAT* expressed in induced cells, relative to the non-induced cells (Fig. 4.2). The specificity of the knockdown of *cASAT* was confirmed by assessing the RNA transcript levels of *mASAT*, which were not significantly altered between induced and non-induced cASAT RNAi cells (Fig. 4.3).

Having established that the knockdown of the *cASAT* mRNA was successful, enzyme assays of ASAT and alanine amino transferase (AAT) activity were conducted to assess if the there was a reduction in cASAT activity as a result of the decrease in *cASAT* mRNA. It was found that activity of cASAT in the cASAT RNAi cell line was significantly reduced to between $30 - 50\%$ of wild type cell activity (Fig. 4.4a). This

reduction in activity is similar to the reduction in the *cASAT* mRNA level. Again, a minor reduction in the ASAT activity in non-induced cells was noted, due to minor production of dsRNA in the absence of tetracycline in these cells. In conjunction with this result, the activity levels of AAT appeared to be relatively unaffected, with no decrease or increase in activity noted in either induced or non-induced cells, when compared to wild type cells (Fig. 4.4b)

The bloodstream form cASAT RNAi cells were examined qualitatively using phase contrast microscopy. Non-induced cells appeared to grow normally, with no aberrant morphological changes noted at either 24 (Fig. 4.6a) or 48 (Fig. 4.6b) hour time points, but maintained the same morphology as that of wild type bloodstream form *T. brucei* (Fig. 4.5). In contrast, severe disruption to cell morphology occurred in induced knockdown cells, including detached flagella and disrupted cell shape at 24 hours (Fig. 4.7a) and inability to detect phase dense cells or DAPI stained DNA after 48 hours (Fig. 4.7b). The absence of multinucleated cells here suggests that cASAT RNAi lethality may be due to a failure in cytokinesis in these cells, which would support the growth curve data. While some induced cASAT RNAi cells appeared motile at 48 hours in culture media, the lack of structured cells in the phase contrast images could be due to compromised structural integrity of these cells, which are subsequently lysed during processing for microscopy.

Procyclic cells transfected with the TbcASAT RNAi vector showed no decrease in growth rates or cell viability when TbcASAT RNAi was induced, compared to non-induced RNAi and wild type cells (Fig. 4.8). The qRT-PCR data revealed that the levels of *cASAT* mRNA were reduced by $\approx$ 58 % in the induced TbcASAT RNAi procyclic cells, compared to non-induced TbcASAT RNAi procyclic cells (Fig. 4.9), similar to knockdown levels seen in the bloodstream form cells. It was also shown the induction of RNAi in these cells did not reduce the expression of *mASAT* RNA in the procyclic cells, indicative of specific *cASAT* knockdown occurring only, as shown previously for bloodstream form *T. brucei* (Fig. 4.10).

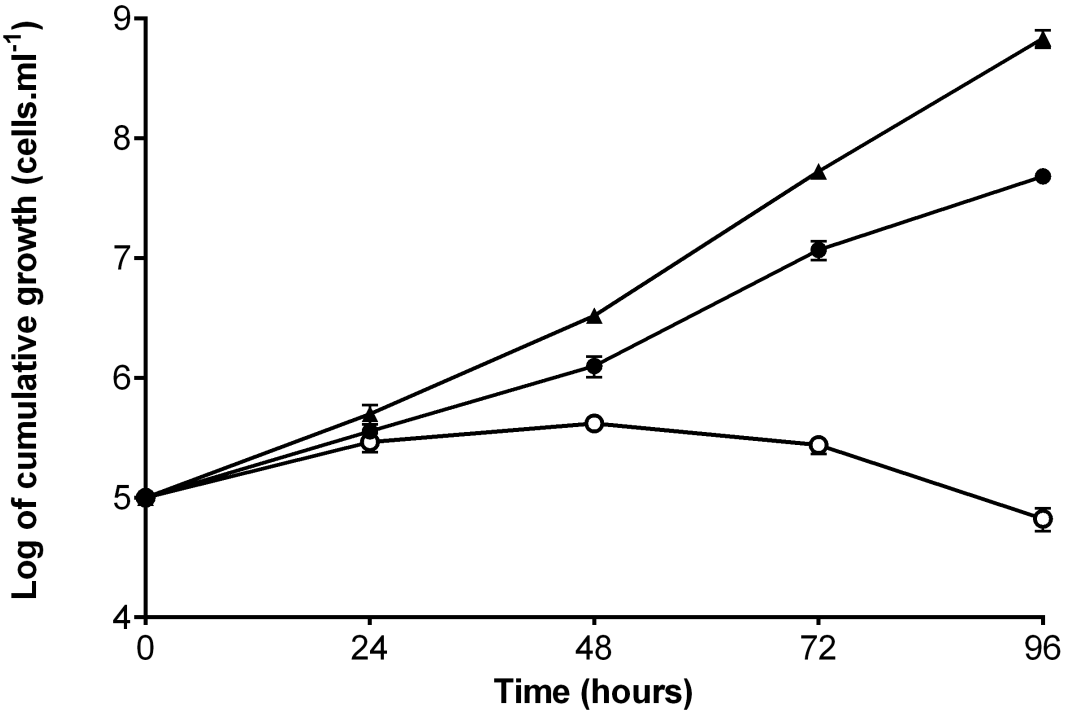

Figure 4.1. Cumulative growth curve of cASAT RNAi bloodstream form cells. Growth of bloodstream form wild type cells (▲) and cASAT RNAi cells in the presence (○) or absence (●) of tetracycline was monitored for 96 hours and expressed as the log cumulative no. of cells.ml^{-1} (Error bars represent SD).

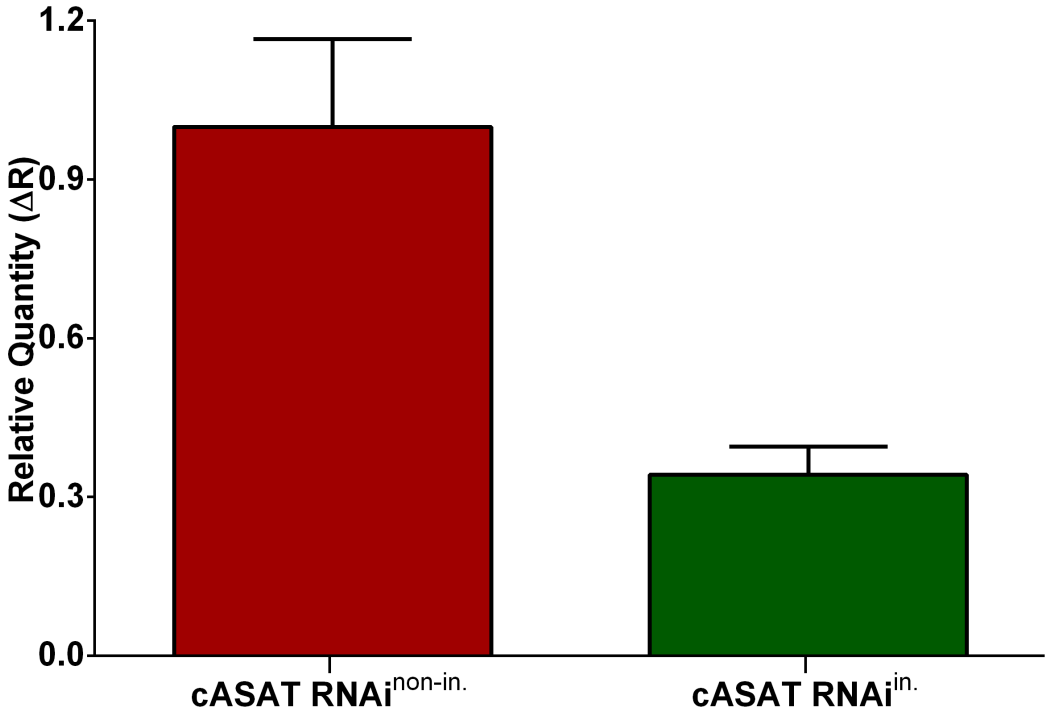

Figure 4.2. A qRT-PCR analysis of the *cASAT* mRNA levels in bloodstream form cASAT RNAi cells.

Bars express the quantity of *cASAT* mRNA from induced cells (cASAT RNAi$^{in.}$) relative to that of non-induced cells (cASAT RNAi$^{non\text{-}in.}$), for RNAi knockdown following 24 hours in culture. The *cASAT* RNA levels were normalised against actin mRNA. Relative quantification was calculated using the ΔΔCt method [125] and is shown as the ratio of induced RNA to non-induced RNA (Error bars represent SD, triplicate samples).

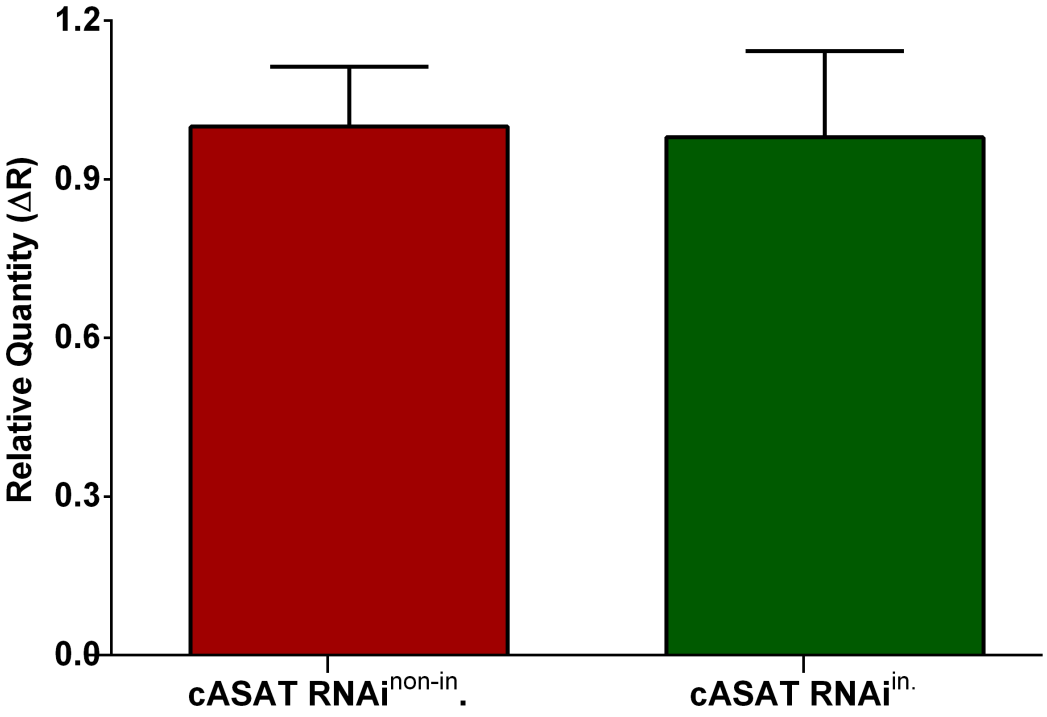

Figure 4.3. A qRT-PCR analysis of the *mASAT* mRNA levels in bloodstream form cASAT RNAi cells.

Bars express the quantity of *mASAT* mRNA from induced cells (cASAT RNAi$^{\text{in.}}$) relative to that of non-induced cells (cASAT RNAi$^{\text{non-in.}}$), for RNAi knockdown following 24 hours in culture. The *cASAT* RNA levels were normalised against actin mRNA. Relative quantification was calculated using the ΔΔCt method [125] and is shown as the ratio of induced RNA to non-induced RNA (Error bars represent SD, triplicate samples).

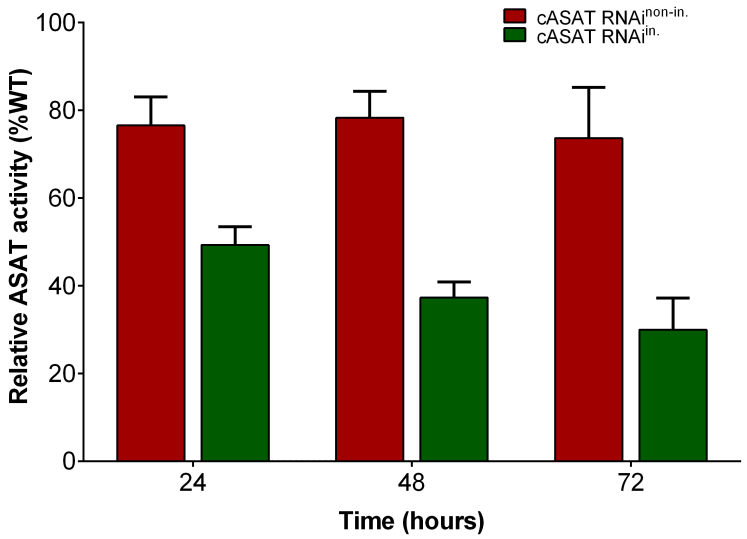

(a)

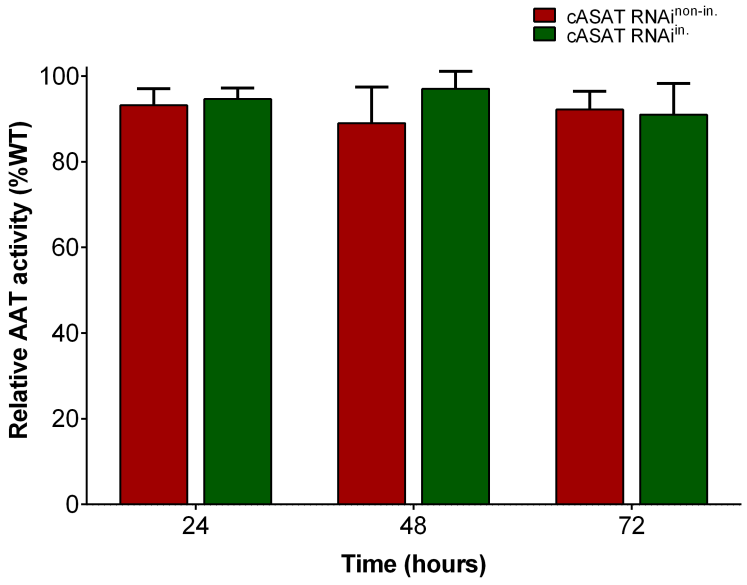

(b)

Figure 4.4. The relative activity of ASAT and AAT from bloodstream form cASAT RNAi cells post-knockdown.

(a) The activity of the ASAT enzyme in bloodstream form cASAT RNAi cells following induction of RNAi by tetracycline addition to cell cultures. Ablation of cASAT mRNA leads to significant reduction in detectable ASAT activity, when compared to WT and non-induced cASAT RNAi cells. **(b)** The activity of the alanine aminotransferase (AAT) in bloodstream form cASAT RNAi cells following induction of RNAi by tetracycline addition to cell cultures. AAT levels remain constant, indicating no reduction in AAT activity when ASAT activity is reduced, and no compensatory increase in AAT activity. Protein was extracted from whole cell lysates at 24 hour intervals and assayed as specified in the materials & methods. Each assay contained the equivalent of 10^8 cells.ml^{-1} per sample. Error bars indicate SD, triplicate measurements.

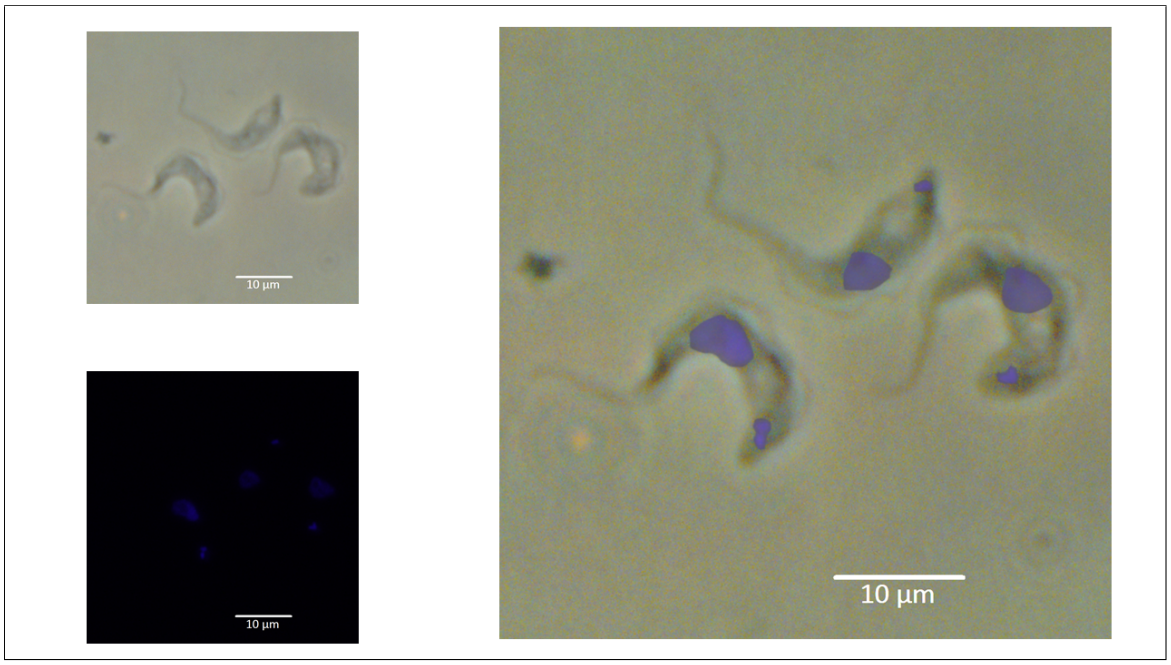

Figure 4.5. Phase contrast image of wild type bloodstream form *T. brucei*.

Representative image of wild type bloodstream form cells after 48 hours of culture.

All images are comprised of phase contrast (top left), DAPI staining (bottom left), and phase + DAPI merge (right). Scale bar indicates 10 μ m.

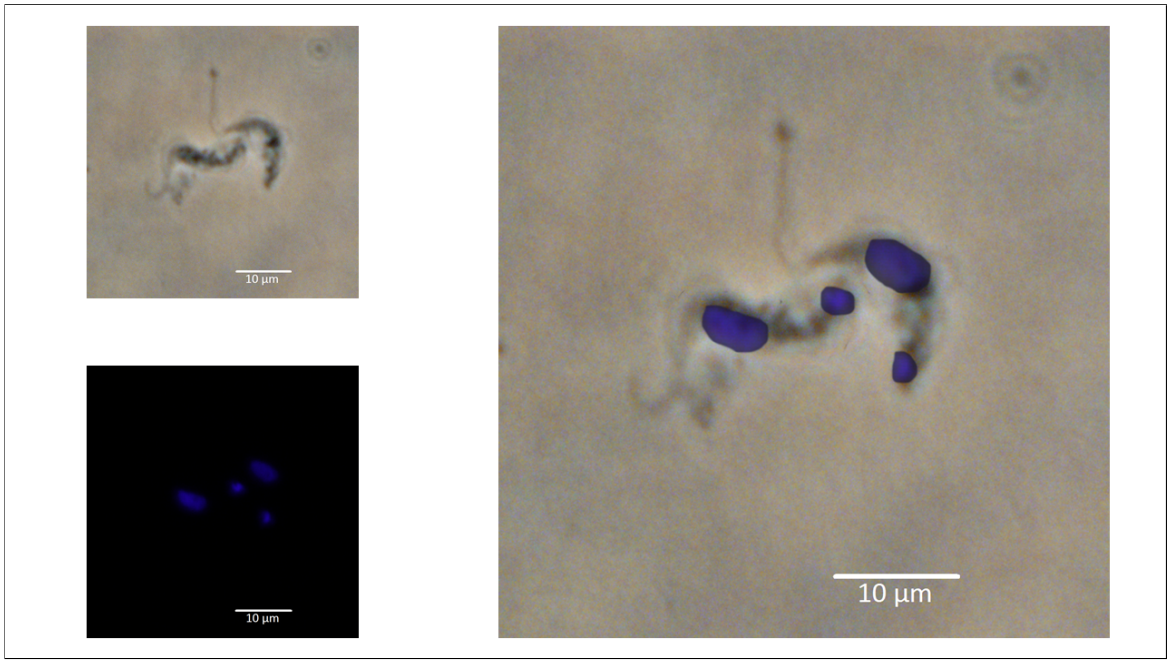

(a) cASAT RNAi$^{non-in.}$ - 24 hr

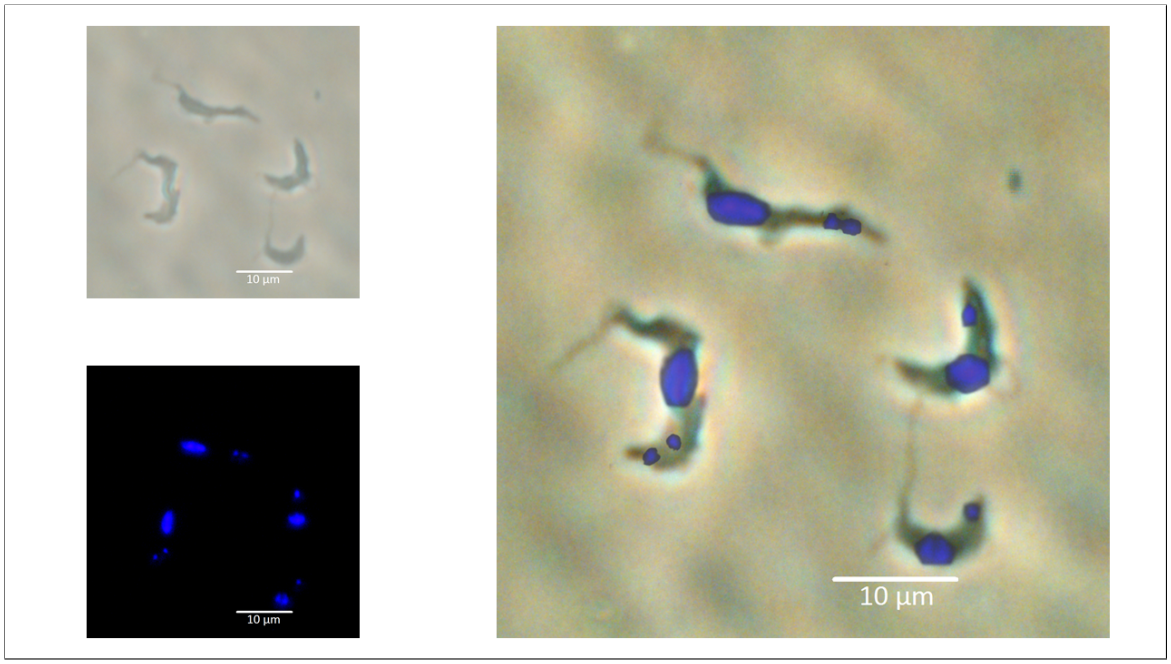

(b) cASAT RNAi$^{non-in.}$ - 48 hr

Figure 4.6. Morphological analysis of bloodstream form non-induced cASAT RNAi cells.

Phase contrast images of non-induced cASAT RNAi bloodstream form *T. brucei*. Images of cASAT RNAi cells cultured without tetracycline, for 24 (a) and 48 (b) hour periods.

All images are comprised of phase contrast (top left), DAPI staining (bottom left), and phase + DAPI merge (right). Scale bar indicates 10 μm.

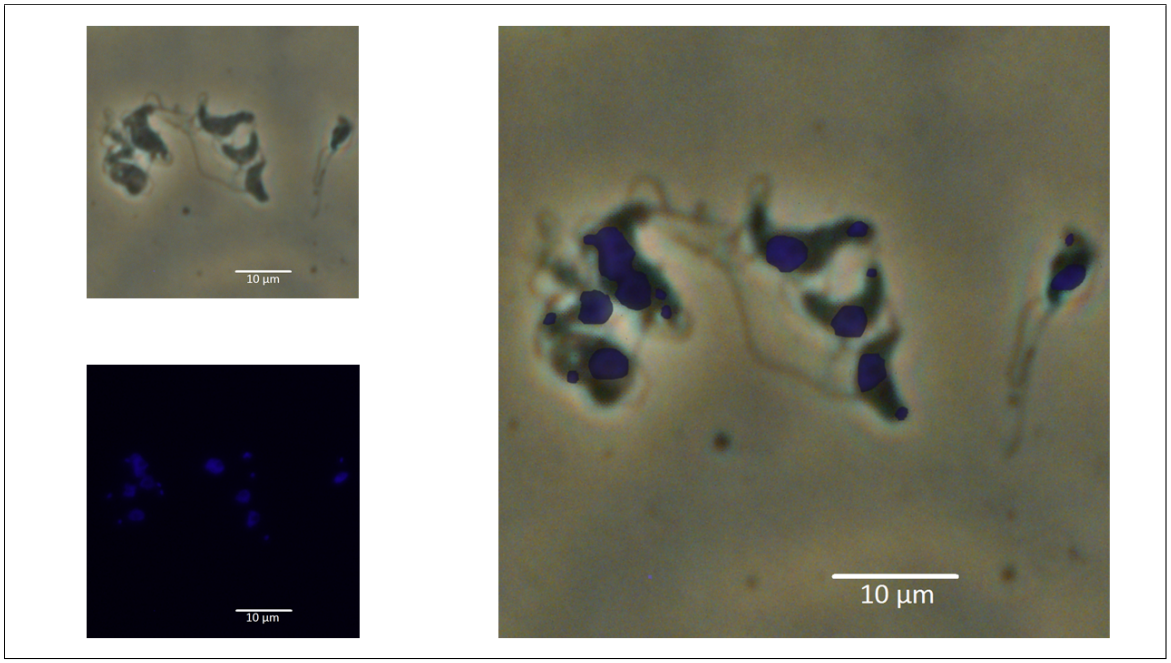

(a) cASAT RNAi$^{in.}$ - 24 hr

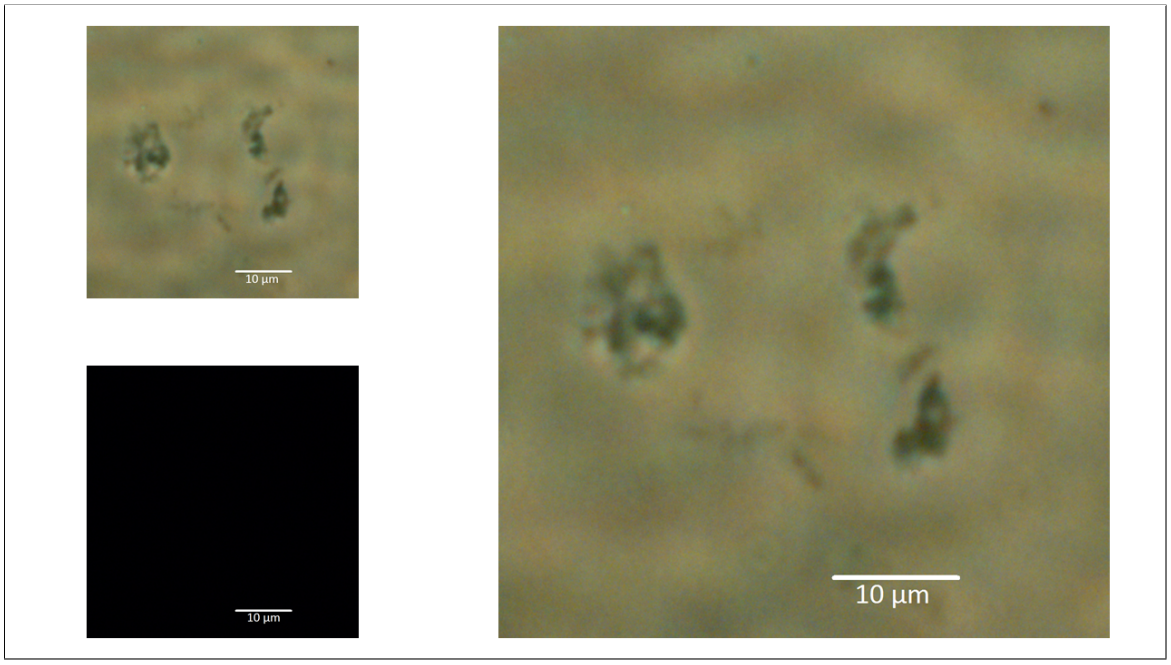

(b) cASAT RNAi$^{in.}$ - 48 hr

Figure 4.7. Morphological analysis of bloodstream form induced cASAT RNAi cells.

Phase contrast images of induced cASAT RNAi bloodstream form *T. brucei*. Images of cASAT RNAi cells cultured with tetracycline, for 24 (a) and 48 (b) hour periods.

All images are comprised of phase contrast (top left), DAPI staining (bottom left), and phase + DAPI merge (right). Scale bar indicates 10 μm.

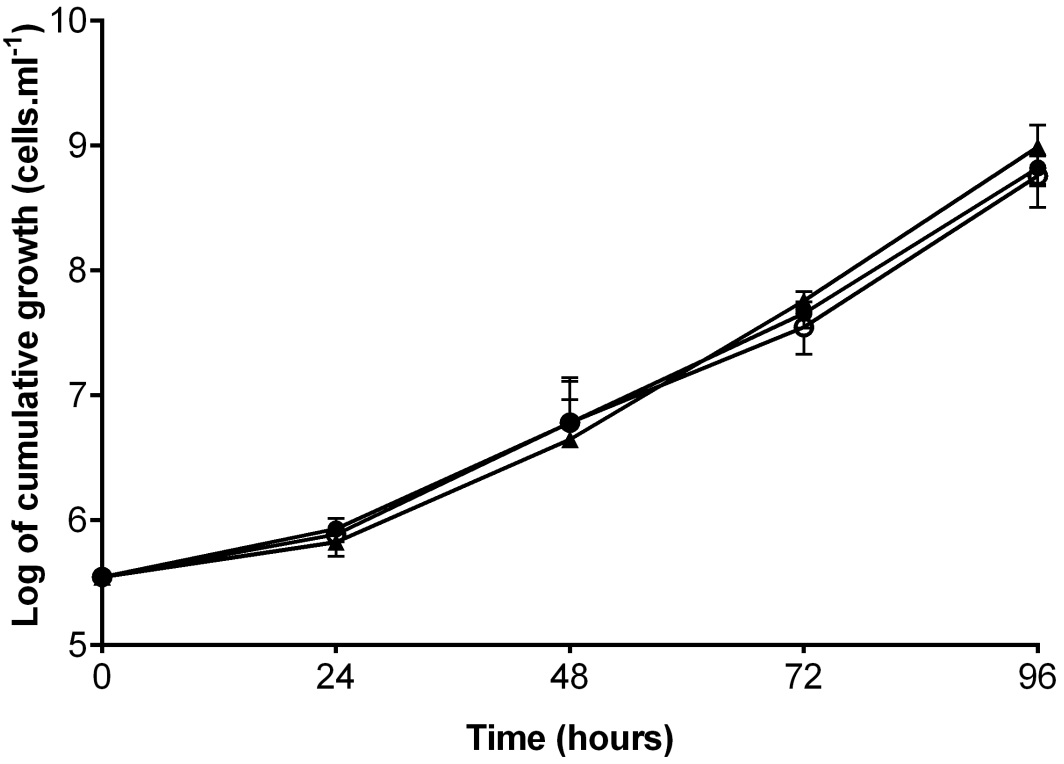

Figure 4.8. Cumulative growth curve of cASAT RNAi procyclic form cells. Growth of procyclic form wild type cells (●) and cASAT RNAi cells in the presence (○) or absence (▲) of tetracycline was monitored for 96 hours and expressed as the log cumulative no. of cells.ml^{-1} (Error bars represent SD, triplicate measurements).

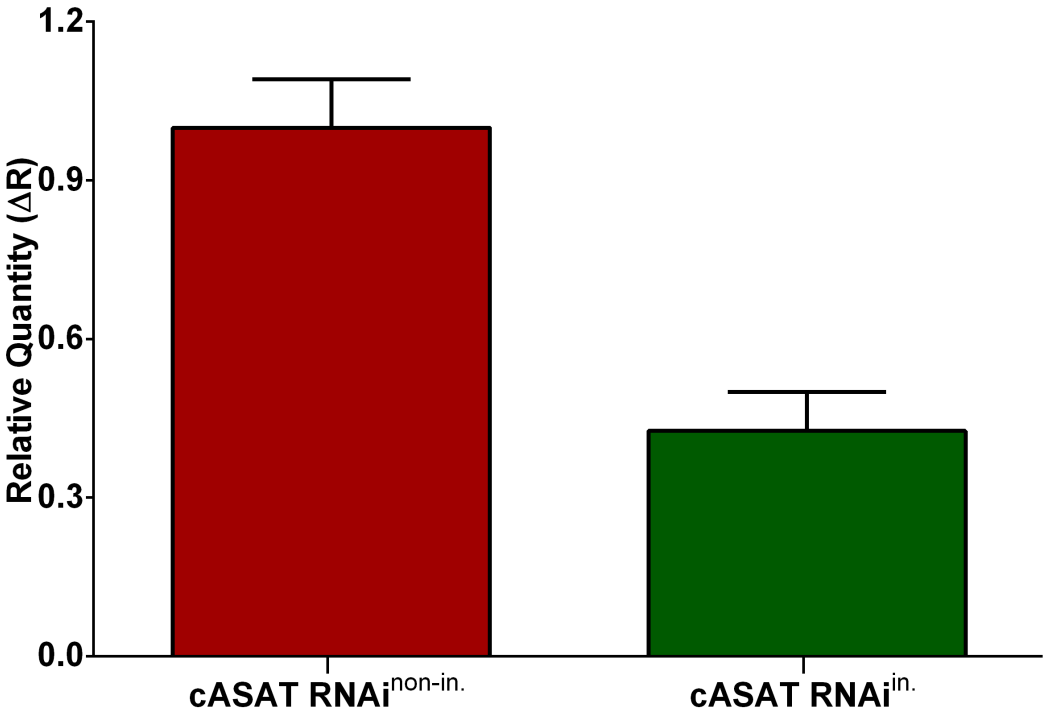

Figure 4.9. A qRT-PCR analysis of the *cASAT* mRNA levels in procyclic form cASAT RNAi cells.

Bars express the quantity of *cASAT* mRNA from induced cells (cASAT RNAi$^{in.}$) relative to that of non-induced cells (cASAT RNAi$^{non\text{-}in.}$), for RNAi knockdown following 24 hours in culture. The *cASAT* RNA levels were normalised against actin mRNA. Relative quantification was calculated using the ΔΔCt method [125] and is shown as the ratio of induced RNA to non-induced RNA (Error bars represent SD, triplicate samples).

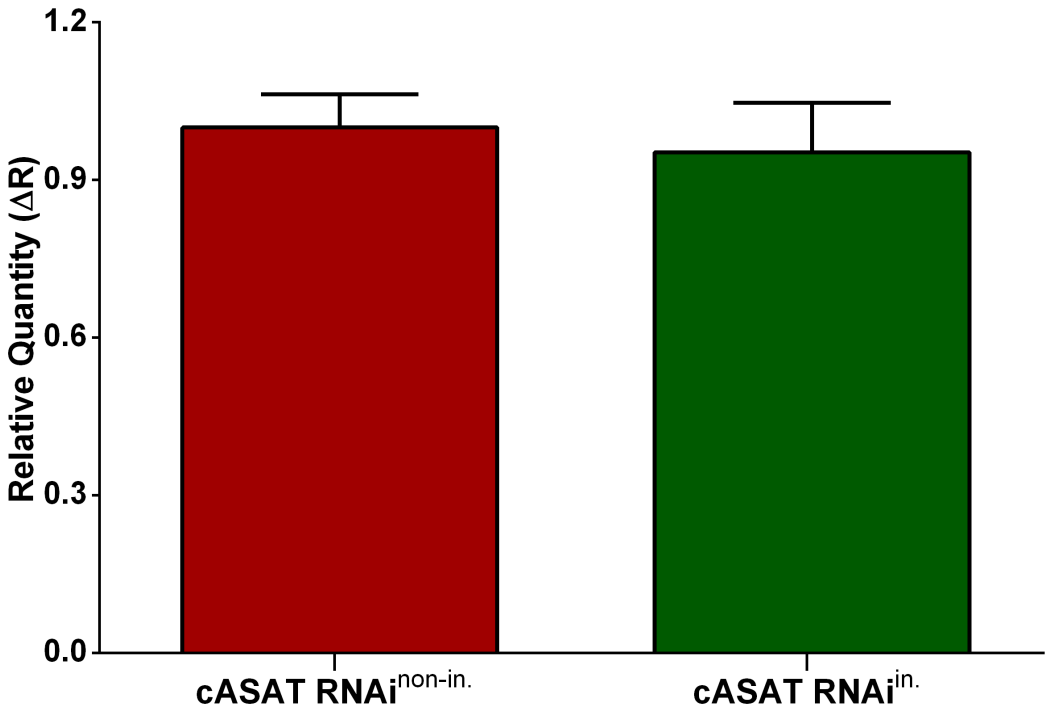

Figure 4.10. A qRT-PCR analysis of the *mASAT* mRNA levels in procyclic form cASAT RNAi cells.

Bars express the quantity of *mASAT* mRNA from induced cells (cASAT RNAi$^{in.}$) relative to that of non-induced cells (cASAT RNAi$^{non\text{-}in.}$), for RNAi knockdown following 24 hours in culture. The *cASAT* RNA levels were normalised against actin mRNA. Relative quantification was calculated using the $\Delta\Delta$Ct method [125] and is shown as the ratio of induced RNA to non-induced RNA (Error bars represent SD, triplicate samples).

4.1.3 Culture media metabolite supplementation and its effects on cASAT RNAi cell growth.

Berger et al. had proposed that a methionine recycling pathway could exist in *T. brucei* [101] based on the production of ^{15}N-methionine from ^{15}N-tyrosine by the related *C. fasciculata* trypanosomatid, and that TbcASAT was likely the enzyme involved in converting KMTB to methionine via deamination of aromatic amino acids [99]. To investigate whether the reduction in the ability to generate methionine due to TbcASAT knockdown was lethal to bloodstream form cells, attempts were made to rescue the growth arrest and cell death knockdown effects by supplementing culture media with methionine, which should rescue some or all of the knockdown if loss of TbcASAT prevents regeneration of methionine. In addition, attempts were made to rescue the growth defect with adenosine supplementation, considering the possibility that TbcASAT may play a role a purine salvage pathway in *T. brucei* (page 149).

cASAT RNAi cells were cultured in HMI-9 media containing 10% FCS supplemented with either methionine or adenosine. It was found that methionine supplementation did not rescue the growth phenotype of the cASAT RNAi cells, however, it did delay the decrease in cell numbers from cell death, although no difference in the ability to delay cell death was observed between the different methionine concentrations (Fig. 4.11). This data seems to suggest that cells are not growing/dividing but are still viable. The addition of adenosine to the media also had little effect on rescuing the growth of the induced cASAT RNAi cells, as only a minor increase in cell growth in the induced RNAi cell with adenosine was observed compared to the induced cells lacking adenosine (Fig. 4.12). The adenosine experiment was performed with a single concentration however (1 mM), so perhaps increasing this concentration may rescue growth in future experiments.

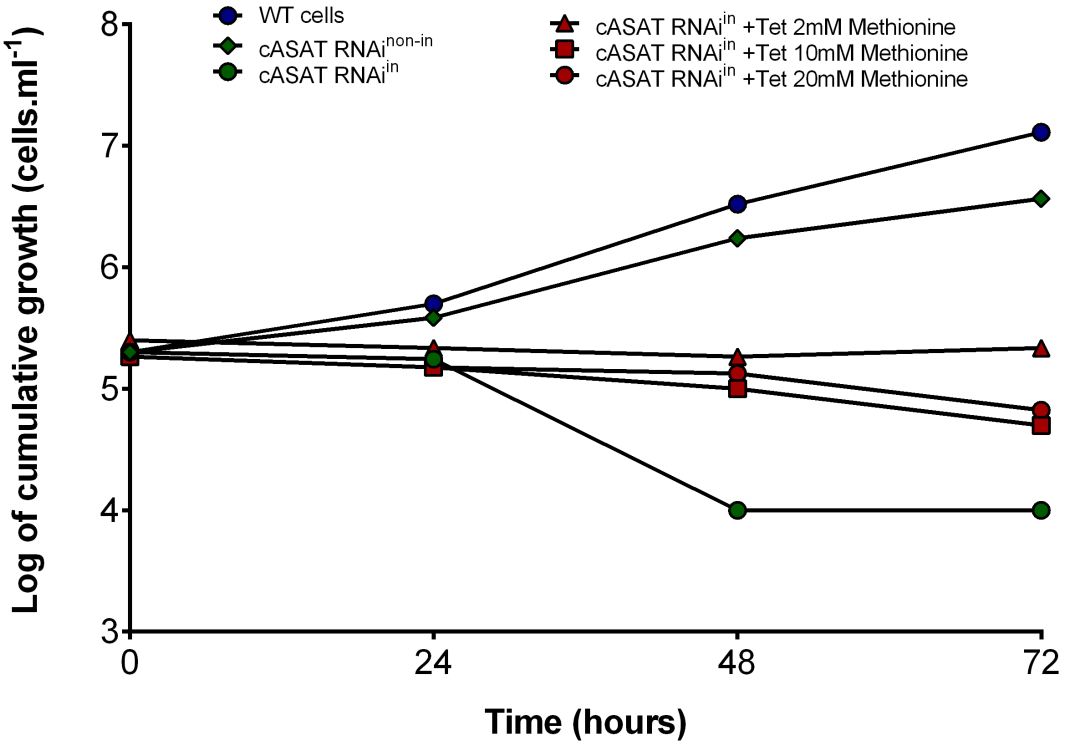

Figure 4.11. Growth curve of bloodstream form cASAT RNAi cells in media supplemented with methionine.

Growth of bloodstream form wild type cells and both non-induced (cASAT RNAi^{non-in}) and induced (cASAT RNAi^{in}) cASAT RNAi cells in the presence or absence of varying concentrations of methionine (2 mM - 20 mM). Cells were monitored for 72 hours and cell numbers expressed as the log cumulative no. of cells.ml^{-1}.

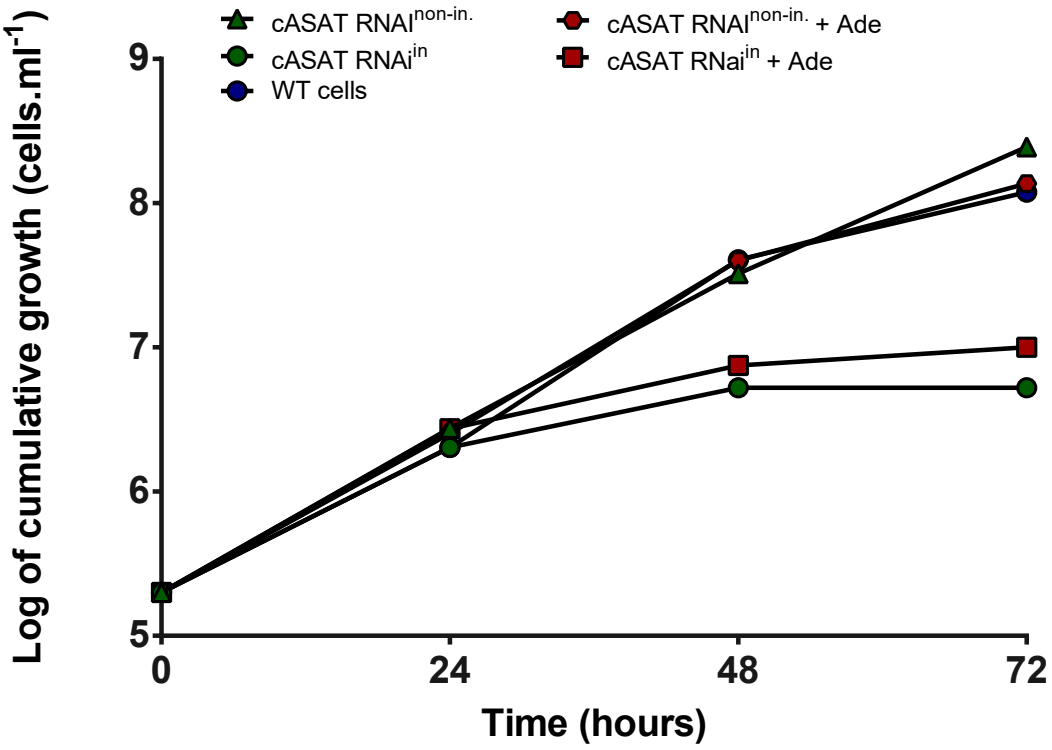

Figure 4.12. Cumulative growth curve of bloodstream form cASAT RNAi cells in media supplemented with adenosine.

Growth of bloodstream form wild type and both non-induced (cASAT RNAi^{non-in}) and induced (cASAT RNAi^{in}) cASAT RNAi cells in the presence or absence of 1 mM supplemented adenosine (Ade). Cells were monitored for 72 hours and expressed as the log cumulative no. of cells.ml^{-1}.

4.1.4 RNAi of TbcASAT and total ketoacid production.

Infection with *T. brucei* has been demonstrated to lead to an increase in aromatic ketoacids in the excreted urine of the infected hosts [107, 111]. It has been suggested that these aromatic ketoacids could be a byproduct of aromatic amino acid deamination by TbcASAT [99]. Therefore, it was important to also determine if cASAT was indeed responsible or partially responsible for the production of ketoacids in bloodstream form *T. brucei*, or if there were other contributors to the observed aforementioned increase in host urinary aromatic ketoacids. To investigate this issue, the recombinant AHADH enzyme was used to assay media that bloodstream form wild type and cASAT RNAi cells (induced and non-induced) were cultured in, with 1 mM each of tryptophan, phenylalanine, and tyrosine (further outlined in the materials and methods). AHADH is specific in its ability to convert aromatic ketoacids to their hydroxy-acid derivatives, a reaction with uses the spectrophotometrically-monitorable oxidation of NADH to NAD^+ [157].

The results indicated that transamination by TbcASAT is the predominant, and perhaps the only source, of secreted aromatic ketoacids from *T. brucei*. Under these conditions, ketoacid levels were $\approx$ 0.5 mM in the supernatant of wild type cells. Crucially, both the non-induced and induced cASAT RNAi cells secreted lower total amounts of ketoacids (Fig. 4.14). Furthermore, the decrease in detectable secreted aromatic ketoacids was similar to the decrease in the ASAT activity previously shown when cASAT was knocked down (page 123). It was also found that the subtraction of the 10% FBS in the culture media led to a lower level of detected aromatic ketoacids. Given the high density at which these cells were cultured (5×10^7 cells.ml^{-1}), it is possible that removal of FBS could have been unfavourable for cell growth and could have lead to less metabolically active cells. The contribution of free amino acids in the FBS to the secreted aromatic ketoacids in this case would be almost negligible.

Secretion of aromatic ketoacids is not essential for *T. brucei* survival.

Knockdown of TbcASAT was lethal to bloodstream form *T. brucei*, and also lead to a significant reduction of detectable aromatic ketoacids in culture media of these cells. It is possible that these cells needed to secrete aromatic ketoacids for other purposes,

perhaps to generate other metabolic substrates, or through aromatic ketoacid meditated transport uptake of other metabolites. To investigate whether bloodstream form *T. brucei* was dependent on the secretion of these aromatic ketoacids, a tetracycline-inducible conditional AHADH expression vector was introduced into MITat 1.2 cells. The resultant excretion of aromatic ketoacids into the culture media, and the growth of this strain was monitored (Fig. 4.13). Interestingly, when AHADH expression was induced, these cells (AHADH^{in}) grew at almost identical rates to both non-induced and wild type cells, with doubling times of 7.3 hours (wild type, AHADH^{non-in}) and 7.7 hours (AHADH^{in}) (Fig. 4.16a). This was also surprising, as it was thought that the NADH required to sustain the reduction of the aromatic ketoacids by AHADH would deplete NADH availability for other cellular functions. Additionally, the AHADH^{in} cells secreted $\approx$ 60 - 70 % lower concentrations of aromatic ketoacids in both induced and non-induced cell culture media, compared to the wild type parental cells (Fig. 4.16b). Both non-induced and induced AHADH^{in} cells were found to have similar decreased levels of aromatic ketoacids in their culture media, which could be due to leaky expression of the AHADH^{in} vector in the absence of tetracycline. This, and the growth curve data, indicate that the expressed AHADH must have a much lower activity than that of TbcASAT. In any case, this data demonstrates that the inability to secrete aromatic ketoacids is not likely to be detrimental to the parasite.

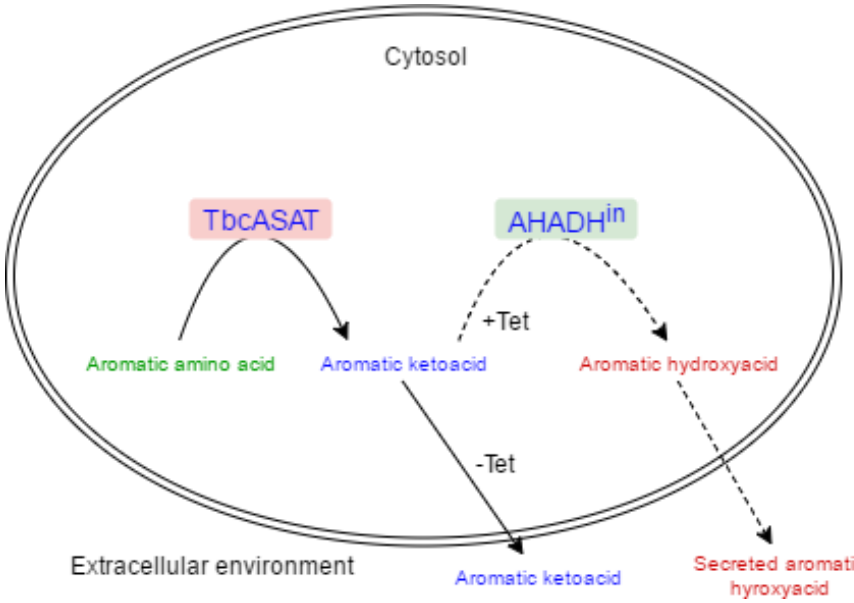

Figure 4.13. Simple diagram of the function of *T.brucei* AHADH^{in} cells.
The alternation between production of either aromatic ketoacids or aromatic hydroxyacids in bloodstream form *T. brucei* AHADH^{in} cells was enabled with the addition or subtraction of tetracycline. When tetracycline is present, the cells produce recombinant AHADH which converts the aromatic ketoacids to their hydroxy derivatives. Co-substrate representations were removed for simplicity.

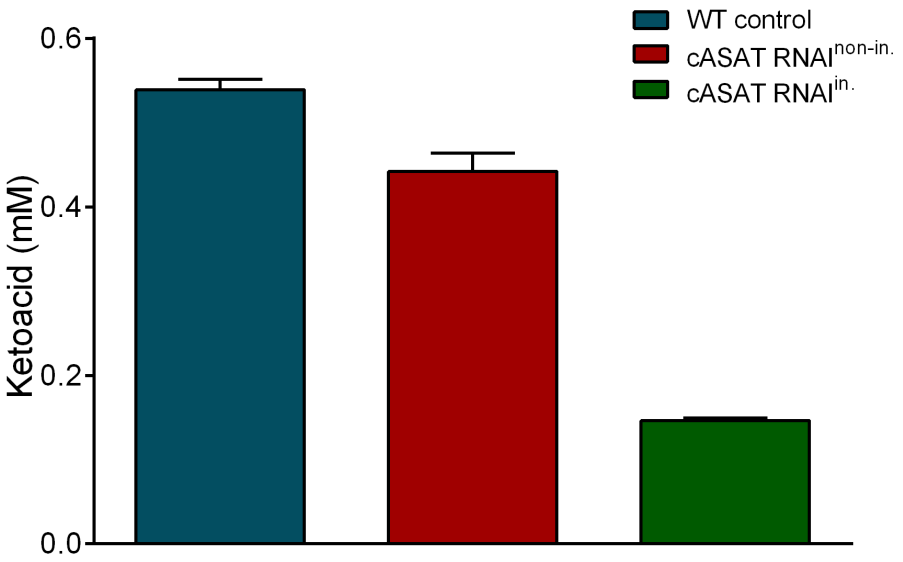

Figure 4.14. TbcASAT is responsible for the majority of ketoacid production by bloodstream form *T. brucei*.

Graph of total ketoacids (mM) detected in the media after 4 hours culture of wild type (WT), non-induced RNAi (cASAT RNAi$^{non-in.}$), and induced RNAi (cASAT RNAi$^{in.}$) cells. Cells were cultured at high density (5×10^7 cells.ml^{-1}) in CMM with 10% FBS, supplemented with 1 mM each of tryptophan, phenylalanine, and tyrosine. The AHADH assay was performed as indicated in the materials and methods chapter. Triplicate measurements, error bars indicate SD.

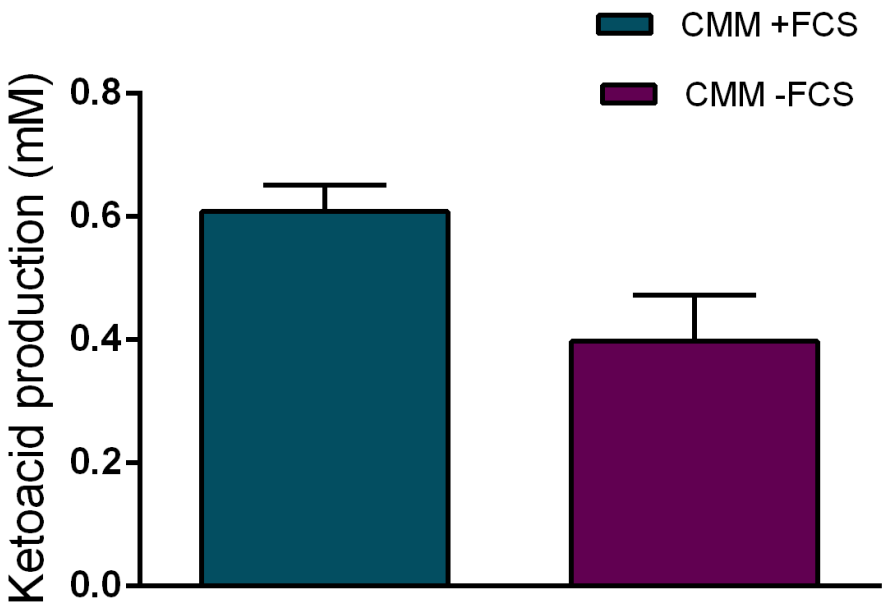

Figure 4.15. Removal of 10% FCS supplement leads to lower secreted ketoacid levels.

Ketoacid production was optimal in the presence of FCS (CMM +FCS), and decreased by ≈ 35% when FBS was absent from the culture media (CMM -FCS). Graph of total ketoacids (mM) detected in the media after 5 hours. Wild type cells were cultured at high density (5×10^7 cells.ml^{-1}) in CMM with or without 10% FBS, supplemented with 1 mM each of tryptophan, phenylalanine, and tyrosine. AHADH assay was performed as indicated in the materials and methods. Triplicate measurements, error bars indicate SD.

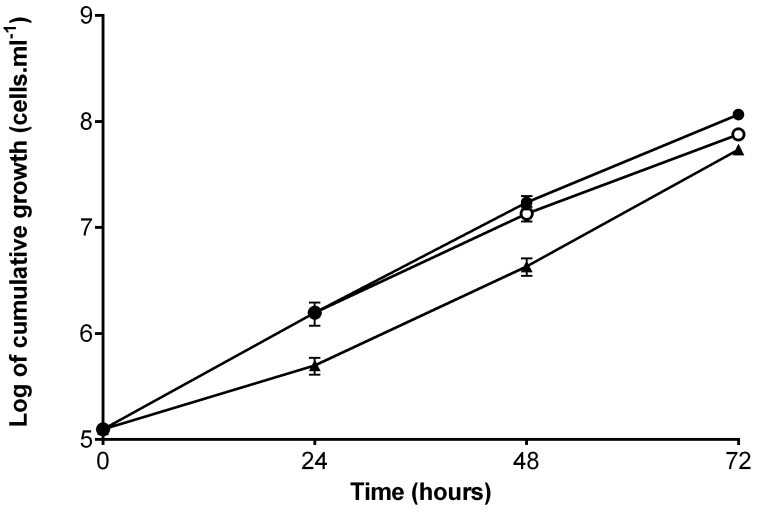

(a)

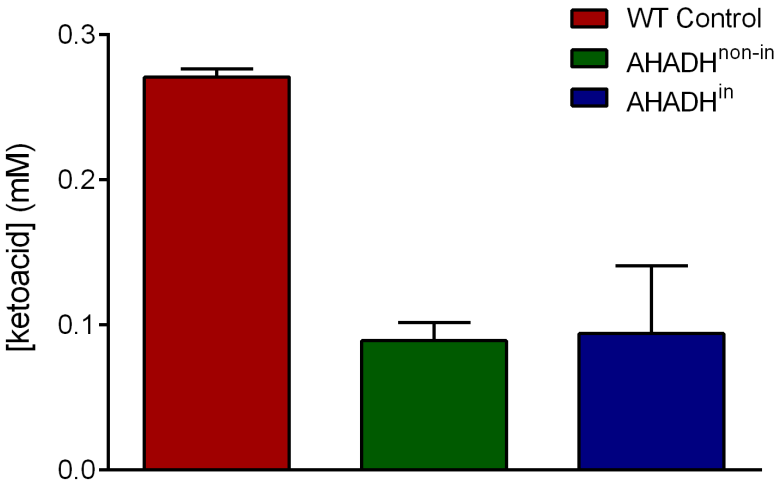

(b)

Figure 4.16. Newly generated bloodstream form AHADH^{in} cells grow normally and secrete lower amounts of aromatic ketoacids.

(a) Bloodstream form AHADH^{in} cells were found to grow at similar rates to wild type MITat 1.2 *T. brucei* (▲), whether induced (○) or non-induced (●). **(b)** Secreted aromatic ketoacid concentrations in HMI-9 culture media, as measured via AHADH assay after 48 hours. AHADH cells were either non-induced or induced with 2 mg.ml^{-1} tetracycline. Error bars indicate SD, triplicate measurements.

4.2 The production of aromatic ketoacids from aromatic amino acids.

4.2.1 Rates of production of aromatic ketoacids by bloodstream form *T. brucei*.

The source of the aromatic ketoacids that are detected in the *T. brucei* infected host has not been demonstrated unequivocally in the literature. Whether the aromatic ketoacids are produced as a host metabolic response to infection by the parasite, or whether the parasite directly produced these ketoacids itself had not been directly determined. It has been shown here that aromatic ketoacids can be detected in the culture media of *T. brucei*, and TbcASAT plays a role in producing these ketoacids. The direct contribution of each of the aromatic amino acids to the detected aromatic ketoacids was characterised in the following experiments, given that the recombinant enzyme kinetic data suggested they may be metabolised to different extents and so may have differing functions for the parasite.

The recombinant AHADH enzyme was used to assay media that cells had been cultured in. Wild type cells were cultured at high density (5×10^7 cells.ml^{-1}) in CMM with 10% dialysed FBS, to remove any exogenous aromatic amino acids. 2 mM of either tryptophan, phenylalanine, tyrosine, or a combination of the three, were added to the media prior to incubation of the cells. Cells were then cultured for 4 - 6 hours, with media samples being taken at hourly intervals, and cell viability being monitored via microscopy. Cells were removed from the samples by centrifugation at 14,000 g for 5 min and the supernatant (media) was assayed for ketoacid content, as described in the materials and methods chapter.

The observed rates for ketoacid production were linear over time, and so rate constants for ketoacid production could be estimated (Fig. 4.17). Both the observed rates for aromatic ketoacid production from phenylalanine (101.2 ± 13.32 nmol/h/5×10^7 cells) and tyrosine (94.67 ± 11.18 nmol/h/5×10^7 cells) were more than double that observed for tryptophan (45.74 ± 2.391 nmol/h/5×10^7 cells). This would be in agreement with the enzyme kinetic data outlined previously which demonstrated that cASAT had a higher V_{max} for phenylalanine (page 99). Kinetic parameters of *T. brucei* TbcASAT

for tyrosine were not obtained for technical reasons, and so the same rationale between the relationship of the enzymatically obtained V_{max} and secretion rates here cannot be inferred. However, Marciano et al. obtained similar ratios of kinetic parameters repeated here [98], and they observed no difference in the V_{max} for tyrosine and tryptophan, so the different rates observed for tyrosine and tryptophan aromatic ketoacid secretion rates demonstrated here is not obvious. This suggests that the recombinant enzyme V_{max} and *in vitro* cell secretion rate for hydroxyphenylpyruvate may be a coincidence. It was also observed that in the absence of aromatic amino acids in the media, the production of aromatic ketoacids was rapidly halted (Fig. 4.18). This confirms that the entire source of the aromatic ketoacids is from individual extracellular aromatic amino acids, and not from those generated by catabolism of protein (as FBS was present). The initial rate observed for ketoacid production is likely due to the metabolism of any remaining internal aromatic amino acid pools.

Interestingly, when all 3 amino acids were added to culture at 2 mM each, that rate of production of aromatic ketoacids increased to 148.8 ± 12.18 nmol/h/5×10^7 cells (Fig. 4.19). Given the higher K_m of cASAT for tryptophan and the lower indolepyruvate production rate, it could have been expected that the ketoacid production rate would decrease slightly, or at least remain at the highest observed production rate observed, as for phenylalanine. This data suggests that the increased concentration of external aromatic amino acids caused a corresponding increase in aromatic ketoacid secretion, and that cASAT is possibly unsaturated and operating below its maximal capacity.

To test this hypothesis, a similar experiment was conducted to measure ketoacid secretion in response to increasing aromatic amino acid concentration in the culture media. Wild type cells were cultured at 5×10^7 cells.ml^{-1} in CMM with 10% dialysed FBS, supplemented with various concentrations of tryptophan, phenylalanine, or tyrosine as indicated. After 4 hours, samples of the extracellular medium were prepared by centrifugation at 14,000 g to remove cells and the supernatant assayed for aromatic ketoacid content using AHADH, as described in the methods. The data indicates that the rate of secretion of aromatic ketoacids was limited by the availability of aromatic amino acids in the media over the concentration range of aromatic amino acids examined (up to 1 mM), and that production of aromatic ketoacids can vary with the extracellular concentration of aromatic amino acids. Also, in agreement with

previously obtained data (Fig. 4.17), the rate of accumulation of indolepyruvate in the media is approximately half that of the other two aromatic ketoacids.

The increased secretion of aromatic ketoacids in response to increasing aromatic amino concentrations suggest that TbcASAT is operating well below its V_{max} and that perhaps the rate of uptake of aromatic amino acids limits the rate of aromatic ketoacid secretion. Hasne has measured the amino acid transport rates in bloodstream form *T. brucei*, including the aromatic amino acids [94]. The V_{max} data obtained by Hasne are reported in Table 4.1. The combined maximum uptake rate of aromatic amino acids is 173 pmol/s/1 $\times 10^8$, whilst the maximum secretion rate of aromatic ketoacids for bloodstream form cells of 148.8 ± 12.18 nmol/h/5 $\times 10^7$ from the data obtained here can be calculated to be $\approx$ 83 pmol/s/1 $\times 10^8$ cells. Importantly, Hasne notes that tyrosine uptake is strongly inhibited in the presence of tryptophan (50% inhibition) and phenylalanine (80% inhibition), whilst the uptake of phenylalanine is inhibited by tyrosine (40% inhibition) and tryptophan (70% inhibition) [94]. It seems reasonable to suggest that upon accounting for possible cross-inhibition of these transporters, the secretion of aromatic ketoacids is in close correspondence with the uptake of extracellular aromatic amino acids observed by Hasne. This view is further supported by our recombinant enzyme data, of which the V_{max} are an order of magnitude higher (page 99). If it were the case that the uptake of aromatic amino acids was not limited, a massive increase in the rates of aromatic ketoacid excretion would be expected to those observed here. Therefore, the uptake of aromatic amino acids appears to be the rate limiting factor in aromatic ketoacid secretion.

Table 4.1. V_{max} for aromatic amino acid transport by bloodstream form *T. brucei*.

Data obtained from a report by Hasne [106].

Amino acid	No. of transporters	Maximum rate of transport
tyrosine	one	37 pmol/s/1 $\times 10^8$ cells
tryptophan	two[a]	3.2 pmol/s/1 $\times 10^8$ cells
		22 pmol/s/1 $\times 10^8$ cells
phenylalanine	two	16.8 pmol/s/1 $\times 10^8$ cells
		94 pmol/s/1 $\times 10^8$ cells

[a] excluding one very low affinity transporter.

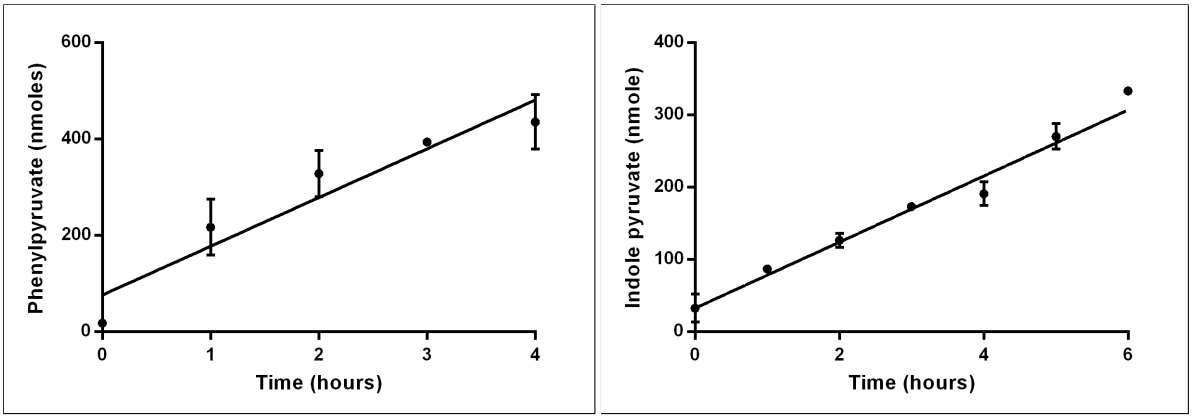

(a) **(b)**

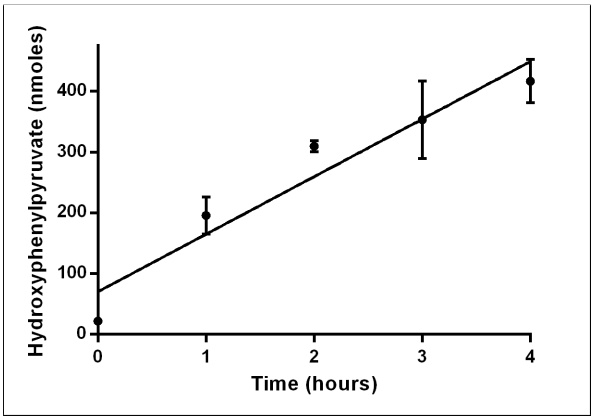

(c)

Figure 4.17. Rates of production of phenylpyruvate, indolepyruvate, and hydroxyphenylpyruvate by bloodstream form *T. brucei*.

(a) The rate of production of phenylpyruvate from phenyalanine by bloodstream form *T. brucei* is approximately 101.2 ± 13.32 nmol/h/5×10^7 cells. **(b)** The rate of production of indolepyruvate from tryptophan by bloodstream form *T. brucei* is approximately 45.74 ± 2.391 nmol/h/5×10^7 cells. **(c)** The rate of production of hydroxyphenylpyruvate from tyrosine by bloodstream form *T. brucei* is approximately 94.67 ± 11.18 nmol/h/5×10^7 cells. Data was fitted with linear regression. Error bars indicate SD, triplicate measurements.

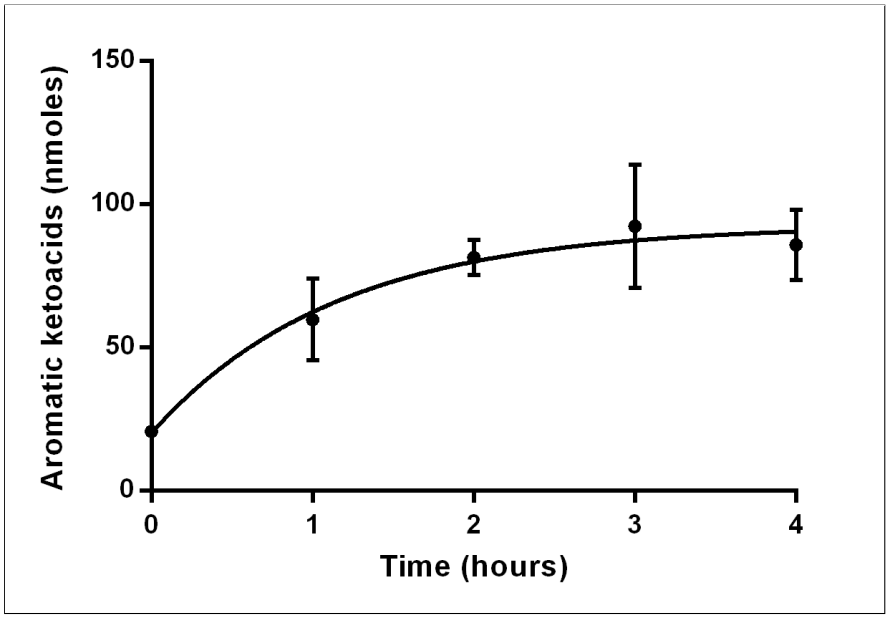

Figure 4.18. Rates of production of aromatic ketoacids by *T. brucei* in the absence of an external aromatic amino acids source.

In the absence of any aromatic amino acids in the external media, the production of aromatic ketoacids decreases rapidly, with a half-time of 47.56 min. 5×10^7 cell.ml^{-1} were cultured in CMM + 10% dialysed FBS containing no endogenously supplied tryptophan, phenylalanine, or tyrosine. Data was fitted with a polynomial curve. Error bars indicate SD, triplicate measurements.

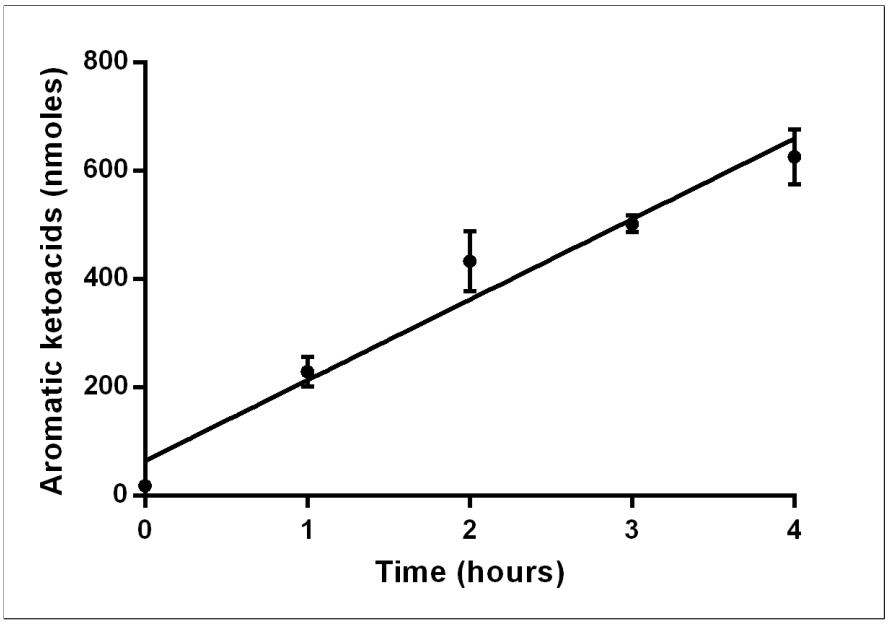

Figure 4.19. Rates of production of aromatic ketoacids by *T. brucei* in the presence of externally supplied aromatic amino acids.

The rate of production of the combined aromatic ketoacids from the aromatic amino acids by bloodstream form *T. brucei* is approximately 148.8 ± 12.18 nmol/h/5×10^7 cells. 5×10^7 cell.ml^{-1} were cultured in CMM supplemented with 2 mM each of tryptophan, phenylalanine, or tyrosine. Data was fitted with linear regression. Error bars indicate SD, triplicate measurements.

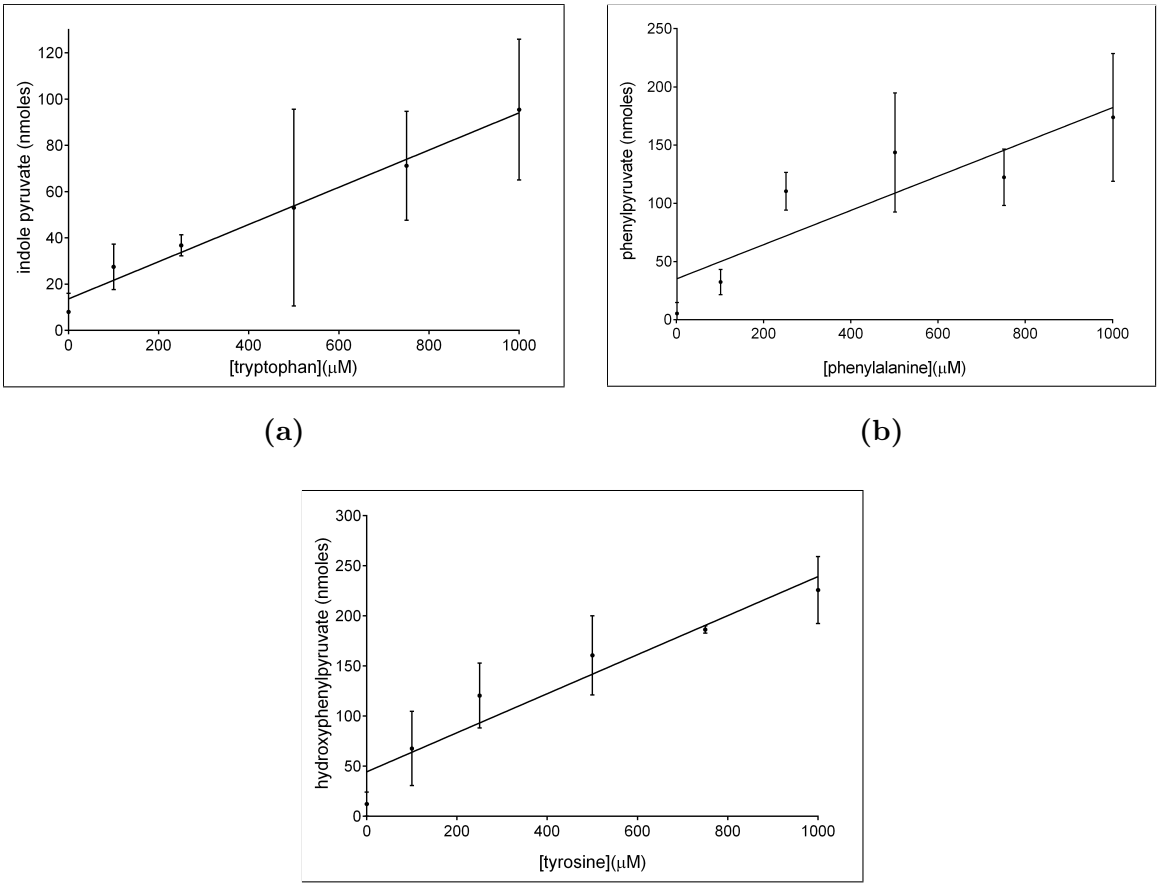

(a) **(b)**

(c)

Figure 4.20. Ketoacid production by *T. brucei* in response to increasing aromatic amino acid concentration.

(a) The amount of indolepyruvate detected in culture media increases with increasing concentrations of tryptophan, as was found with **(b)** the increase of phenylpyruvate excretion with increasing concentrations of phenylalanine, and **(c)** the increase of hydroxyphenylpyruvate excretion with increasing concentrations of tyrosine. Data was fitted with linear regression. Error bars indicate SD, triplicate measurements.

4.2.2 ^{13}C-NMR of tryptophan metabolites produced by bloodstream form *T. brucei*.

Reduction of TbcASAT activity in *T. brucei* had been demonstrated to lead to a subsequent reduction in concentrations of detectable aromatic ketoacids in cell culture media, though it had not been determined if TbcASAT was the sole producer of these aromatic ketoacids. The cASAT RNAi cell line generated previously was used in conjunction with ^{13}C-NMR, in order to establish if cASAT was primarily responsible for the conversion of aromatic amino acids to ketoacids, and if so, what the identities of the ketoacid products were. This analysis was performed by incubating wild type, non-induced cASAT RNAi, and induced cASAT RNAi cells (RNAi induced with tetracycline 48 hours prior to incubation) in HMI-9 media supplemented with 150 μM labelled ^{13}C-L-(indole-2-C)-tryptophan, at 5×10^7 cells.ml^{-1}. The viability of cells was monitored periodically via microscopy, and media samples were taken every hour for 5 hours. Cells were removed by centrifugation at 14,000 g for 5 min, and the supernatant was examined by ^{13}C-NMR, as outlined in the materials and methods.

Indolepyruvate ($\approx$ 127.97 ppm) could be clearly distinguished from tryptophan ($\approx$ 127.86 ppm) on the ^{13}C spectra (Fig. 4.21). While indolepyruvate was present in the media of both wild type and non-induced cASAT RNAi cells, it was almost completely absent in that of the induced cASAT RNAi cells. Moreover, the production of indolepyruvate was constant and consistent over time (Fig. 4.22). The use of ^{13}C-labelled tryptophan further supports tryptophan as the indolepyruvate precursor, as prior attempts to detect non-labelled metabolites in spectra were unsuccessful. In addition, no other tryptophan deamination products (e.g. tryptophol, indole lactate) were detected in the ^{13}C spectra based on comparisons with spectral data deposited in the Biological Magnetic Resonance Data Bank (BMRB, http://www.bmrb.wisc.edu/). Altogether the ^{13}C-NMR data has revealed that TbcASAT is responsible for the conversion of tryptophan to the aromatic ketoacid indolepyruvate.

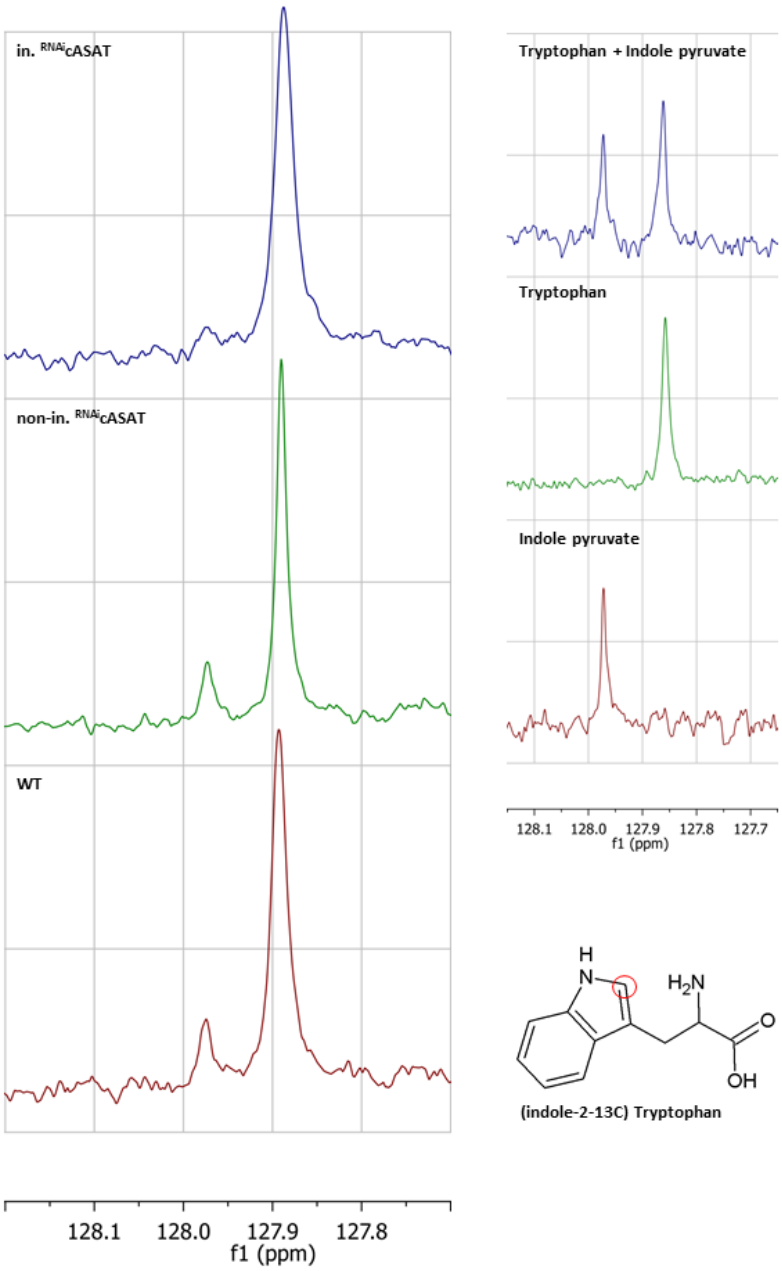

Figure 4.21. The cASAT dependent production of indolepyruvate by bloodstream form *T. brucei* monitored by ^{13}C-NMR.

The production of indolepyruvate from tryptophan by *T. brucei* is clearly distinguishable after 5 hours of culture. **Left**; the production of indolepyruvate by wildtype (WT), non-induced cASAT RNAi (non-in. ^{RNAi}cASAT), and induced cASAT RNAi (in. ^{RNAi}cASAT). **Top right**; the chemical shift of indolepyruvate ($\approx$ 127.97 ppm) and L-tryptophan ($\approx$ 127.86 ppm) can clearly be distinguished from each other. **Bottom right**; L-(indole-2-C)-tryptophan. The red circle indicates the location of the ^{13}C nuclei.

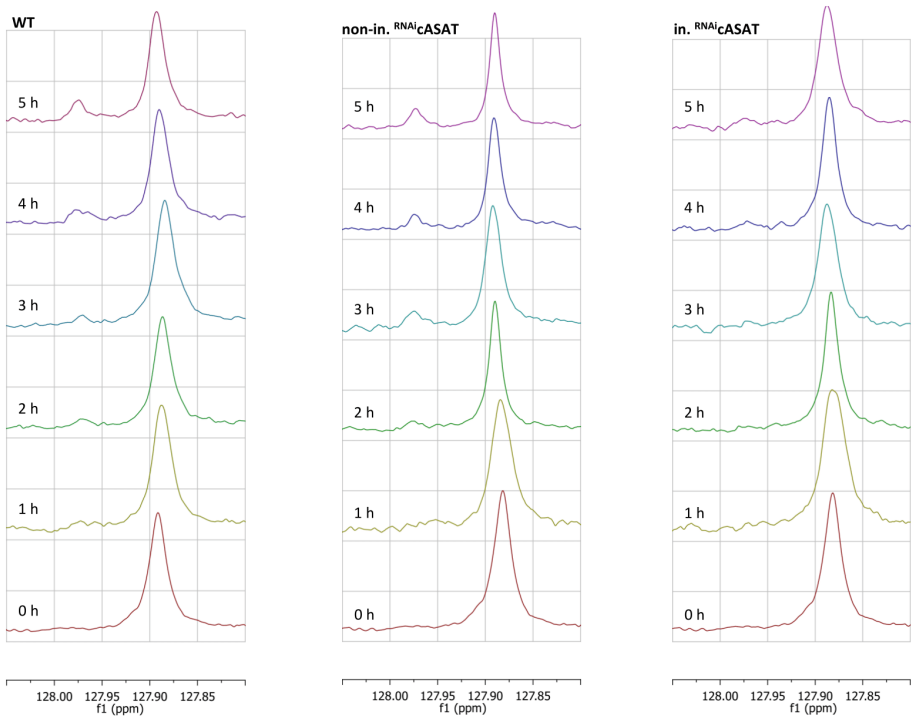

Figure 4.22. Time-course of the production of indolepyruvate by bloodstream form *T. brucei* cASAT from L-tryptophan.

The production of indolepyruvate from tryptophan by *T. brucei* as monitored at hourly intervals for a 5 hour period. The rate of production of indolepyruvate by wildtype (WT) and non-induced cASAT RNAi (non-in. ^{RNAi}cASAT) appears to be consistent. In contrast, the induced cASAT RNAi (in. ^{RNAi}cASAT) cells appear to produce little indolepyruvate. The chemical shift of indolepyruvate is ($\approx$ 127.97 ppm) and of L-tryptophan is ($\approx$ 127.86 ppm).

4.3 Preliminary metabolomic analysis of the role of cASAT in transamination of 2-oxoacids via Mass-spectrometry.

It was determined that *T. brucei* TbcASAT activity was essential in bloodstream form cells. It was determined kinetically that the enzyme favoured the use of aromatic amino acids as amino group donors in the transamination reactions of 2-oxoacids, and that secretion of aromatic ketoacids was not an essential function for the survival of *T. brucei in vitro*. To further examine why loss of TbcASAT function would be detrimental to the parasite, mass spectrum analysis was employed to investigate the metabolic fate of the amino group donated from tryptophan.

4.3.1 Mass spectrum analysis of intracellular metabolite levels.

Bloodstream form MITat1.2 cells were incubated in CMM Media containing 10% FCS, supplemented with 100 μM ^{15}N-amino labelled tryptophan, for 36 hours at 37 °C. Following cell quenching and metabolite extraction, samples were stored under N_2 gas in a -80 °C freezer, until shipped on dry ice for analysis by Glasgow Polyomics Institute (analysis method can be found in the appendix, cell processing and metabolite extraction procedure are outlined in the materials and methods chapter).

The quality of the samples subjected to mass spectrum analysis was consistent, bar a couple of outliers (Fig. 4.23a). The percentage of ^{15}N-tryptophan was lower than expected in the fresh media, likely due to a combination of the contribution of unlabelled tryptophan supplied by the FCS and the addition of less ^{15}N labelled tryptophan to the media than calculated through a procedural error, although enough ^{15}N-tryptophan was still present at high enough levels to allow for the detection of ^{15}N in other metabolites at low levels (Fig. 4.23b). As expected, the most prominently labelled metabolite was tryptophan, at $\approx$ 25 % (Fig. 4.24a). The small discrepancy between the 30 % labelling in the fresh medium and the 25 % labelling that was detected intracellularly is difficult to account for, though the reverse conversion of

indolepyruvate to tryptophan by cASAT may account for this variation. Subsequent labelling of other metabolites was found to be much lower, as outlined above. Alanine was labelled consistently at ≈ 4.5 % (Fig. 4.24b), with the relevant contribution of ^{15}N from tryptophan being ≈ 18 % . Alanine is supplied almost entirely from the transamination of pyruvate, likely by glutamate, as demonstrated by Creek et al [77]. Asparagine was found to be significantly labelled, between ≈ 2.5 - 4.25 %, with the contribution from ^{15}N-tryptophan being reasonably high at ≈ 10 - 17 %. Asparagine is predominantly synthesised from the precursor aspartate [77]. Other amino acids were labelled at lower levels; leucine/isoleucine at ≈ 2 - 2.5 %, methionine at ≈ 0.9 - 1.4 %, and valine at ≈ 0.75 - 1.15 %.

In addition to the labelling detected in intracellular amino acids, both uracil and adenosine were found to be well labelled. Uracil was labelled at ≈ 3.2 - 3.4 %, with the contribution from ^{15}N-tryptophan ≈ 12.8 - 13.6 %. Adenosine was labelled similarly, ≈ 1.5 - 3.5 %, with the contribution from ^{15}N-tryptophan ≈ 6 - 14 %, though the exact quantification could not be obtained. The full table of labelled metabolites can be found in Table 4.2.

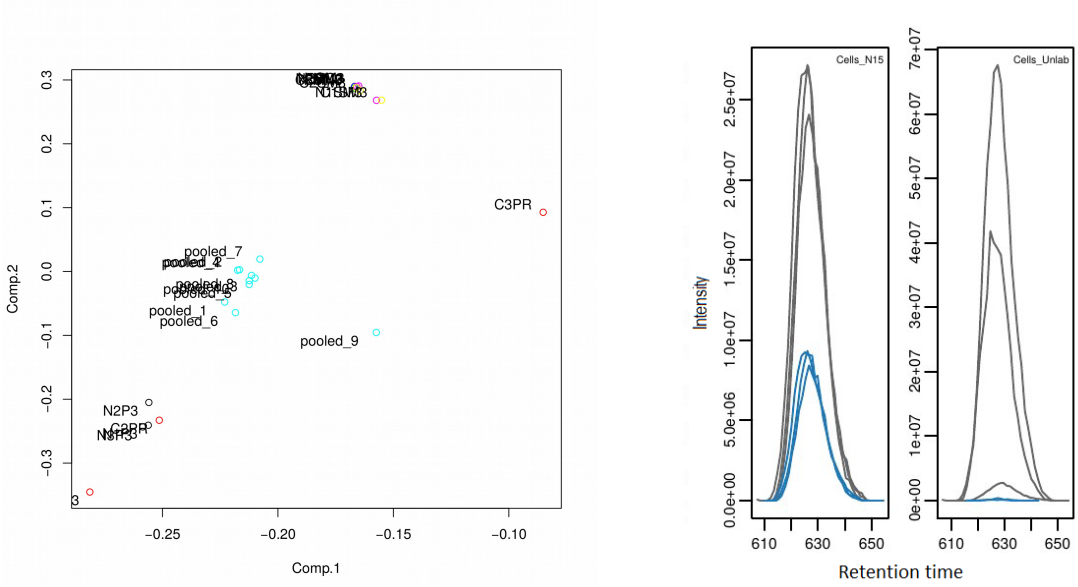

(a) PCA of samples **(b)** Tryptophan detection

Figure 4.23. Principle component analysis and ^{15}N-labelled tryptophan detection in labelled and unlabelled samples.

(a) Principle component analysis (PCA) of the samples for mass spectrum analysis. Samples are separated by compound abundance, to remove outliers (such as C3PR). **(b)** Relative abundance of intracellular tryptophan in both unlabelled (Cells_Unlab) and ^{15}N-labelled (Cells_N15) samples. Blue line indicates labelled tryptophan, grey line indicates unlabelled tryptophan.

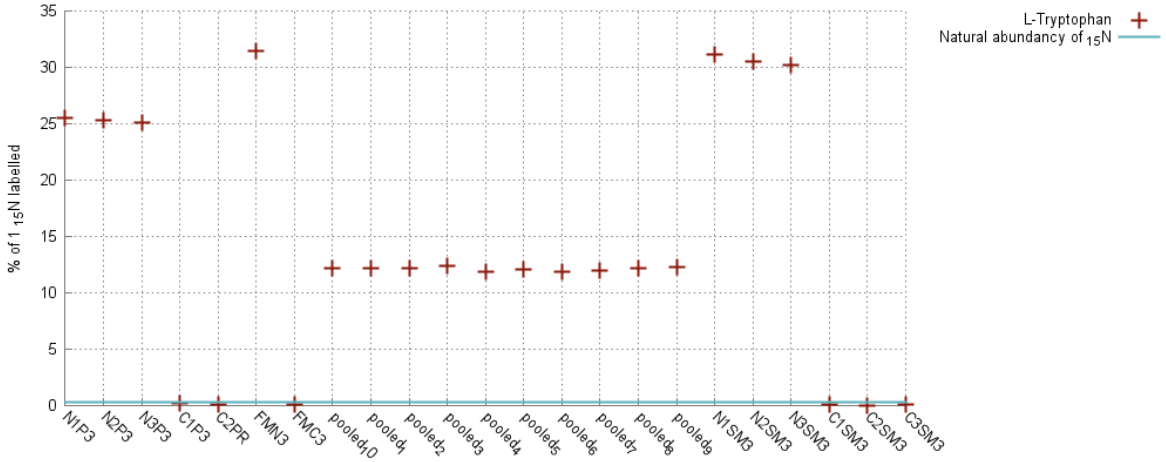

(a) Tryptophan

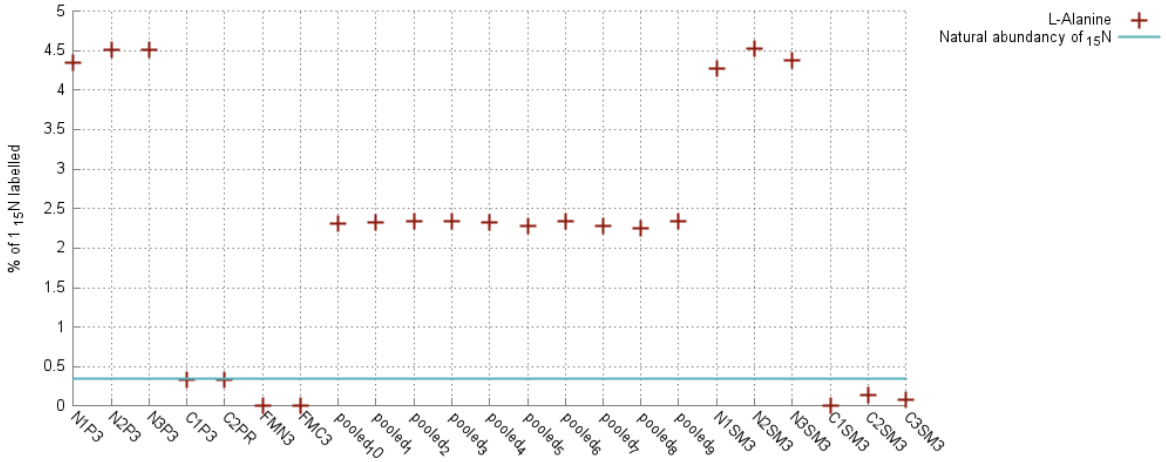

(b) Alanine

Figure 4.24. ^{15}N-labelling of tryptophan and alanine intracellularly in blood-stream form *T. brucei.*

(a) Percentage of intracellular labelling of tryptophan. **(b)** Percentage of intracellular labelling of alanine. NP samples contain intracellular metabolites extracted from cells that were cultured in the presence of ^{15}N-tryptophan

N = ^{15}N labelled samples, C = unlabelled control samples, P = pellet (intracellular), SM = spent media, FM = fresh media.

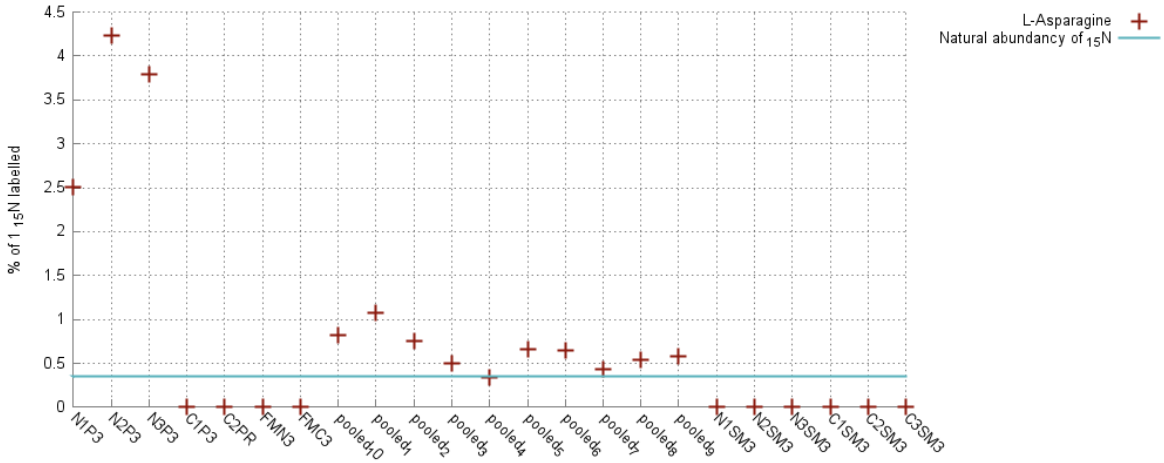

(a) Asparagine

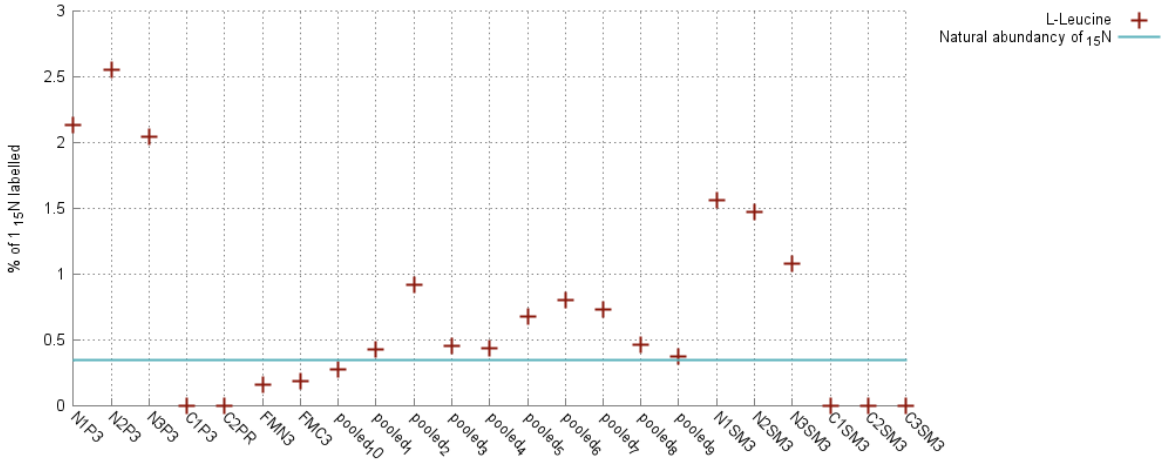

(b) Leucine

Figure 4.25. **^{15}N-labelling of asparagine and leucine/isoleucine intracellularly in bloodstream form *T. brucei*.**

(a) Percentage of intracellular labelling of asparagine. **(b)** Percentage of intracellular labelling of leucine/isoleucine. NP samples contain intracellular metabolites extracted from cells that were cultured in the presence of ^{15}N-tryptophan

N = ^{15}N labelled samples, C = unlabelled control samples, P = pellet (intracellular), SM = spent media, FM = fresh media.

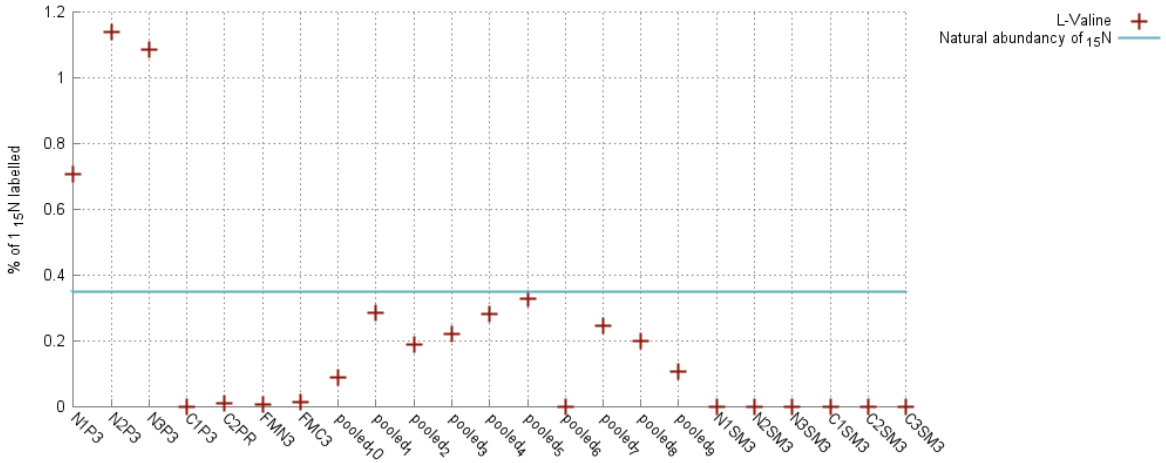

(a) Valine

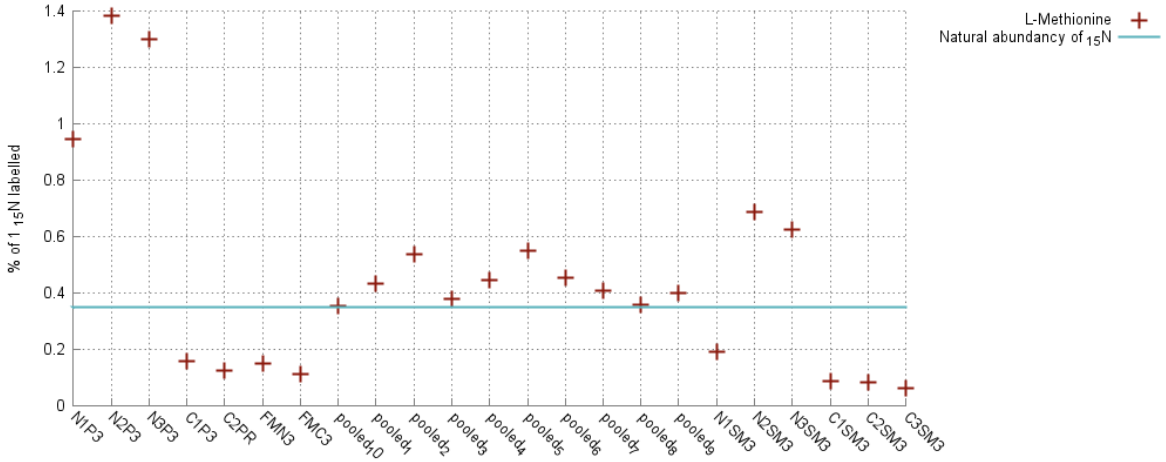

(b) Methionine

Figure 4.26. **^{15}N-labelling of valine and methionine intracellularly in bloodstream form *T. brucei*.**

(a) Percentage of intracellular labelling of valine. **(b)** Percentage of intracellular labelling of methionine. NP samples contain intracellular metabolites extracted from cells that were cultured in the presence of ^{15}N-tryptophan

N = ^{15}N labelled samples, C = unlabelled control samples, P = pellet (intracellular), SM = spent media, FM = fresh media.

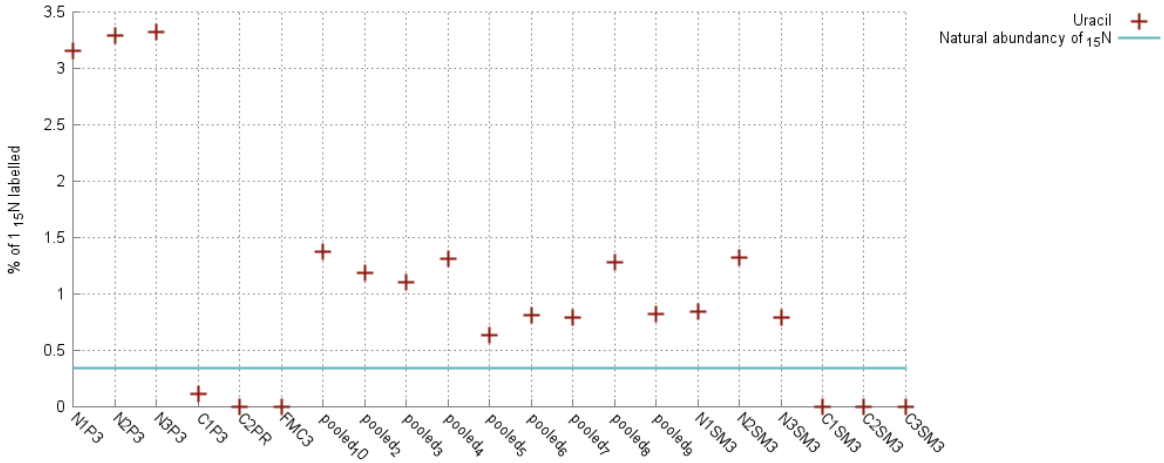

(a) Uracil

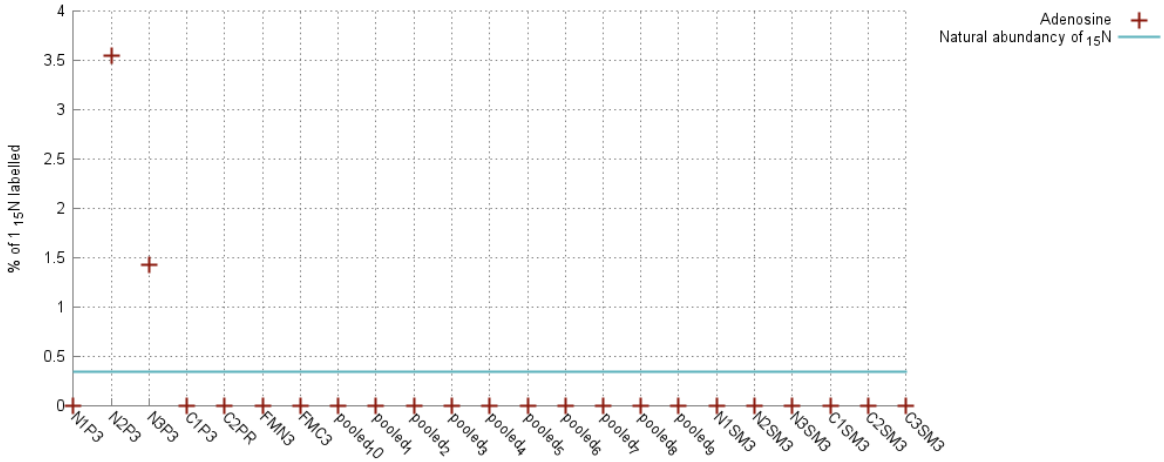

(b) Adenosine

Figure 4.27. ^{15}**N-labelling of uracil and adenosine intracellularly in bloodstream form *T. brucei*.**

(a) Percentage of intracellular labelling of uracil. **(b)** Percentage of intracellular labelling of adenosine. NP samples contain intracellular metabolites extracted from cells that were cultured in the presence of ^{15}N-tryptophan

N = ^{15}N labelled samples, C = unlabelled control samples, P = pellet (intracellular), SM = spent media, FM = fresh media.

Table 4.2. Percentage of ^{15}N-labelling of internal metabolites from ^{15}N-tryptophan source.

The proportional percentage of ^{15}N-labelling detected in internal *T. brucei* metabolites when ^{15}N-tryptophan is used as the amino group donor (* = indicates lower quality of quantification).

Metabolite	**% ^{15}N labelled**	**% labelling contributed by ^{15}N-Tryptophan**
adenosine	$1.5 - 3.5$	$6 - 14$*
alanine	4.5	18
asparagine	$2.5 - 4.25$	$10 - 17$
leucine/isoleucine	$2 - 2.5$	$8 - 10$
methionine	$0.9 - 1.4$	$3.6 - 5.6$
uracil	$3.2 - 3.4$	$12.8 - 13.6$
valine	$0.75 - 1.15$	$3 - 4.6$
tryptophan	25	-

4.4 Discussion.

4.4.1 The effects of the knockdown of *cASAT*.

Previous work on aminotransferases within trypanosomes, related species, and other organisms, has shown that these enzymes can have broad substrate specificity and varied metabolic functions within an organism [142, 145, 146, 167]. The role of AAT in *T. brucei* has recently been studied by Spitznagel et al., who established a clear metabolic role for AAT in procyclic form cells in the metabolism of proline [96]. AAT's role is to provide the entry route for proline-derived carbon into the modified Krebs cycle in these cells, where it links the glutamate and pyruvate producing steps of proline metabolism. As might be expected, the requirement for AAT function was not essential in normal SDM-79 media containing high levels of glucose, but was revealed when glucose levels were decreased from 10 mM to 0.15 mM. Under these conditions the cells become more dependent on proline oxidation as an energy source. The possible function of AAT in bloodstream form cells remains unresolved, but it was suggested that AAT catalysed transamination might provide directionality to the cASAT transamination reactions [96]. This could occur through linking cASAT transamination to the transamination of pyruvate, the sole end point of glycolysis in these cells. Ultimately, this scheme proposed that cASAT/AAT could function together to transfer amino groups from aromatic amino acids onto pyruvate to secrete alanine (Fig. 4.28). However, it was not obvious why generation of alanine or the corresponding ketoacids would be essential to bloodstream form cells. Ketoacids do not appear to be further metabolised in bloodstream form cells. It is also notable that both cASAT and AAT reside in the cytoplasmic compartment, indicating that this coupling mechanism is a possibility. Furthermore, if such a link between the the two aminotransferases were to function, it would require α-ketoglutarate generated in the mitochondria to be exported into the cytoplasm, where it would be converted to glutamate by ASAT and then re-imported into the mitochondria for further use. The metabolic role for cASAT within *T. brucei* warranted investigation.

RNAi of cASAT in bloodstream form *T. brucei* was deleterious to cell growth and viability (Fig. 4.1). The specificity of this knockdown was confirmed by qRT-PCR (Fig. 4.2), which ensured the cell viability defects were due to a loss of cASAT.

When the ASAT activity of induced and non-induced cells was measured, it was found that cASAT activity had decreased significantly in bloodstream form cells (up to 70% compared to wild type). The total activity of ASAT in bloodstream form cells is reportedly 50 nmol.min^{-1}.mg^{-1} [96]. It is interesting that a 70% loss in this activity in bloodstream cells - reduced to $\approx$ 15 nmol.min^{-1}.mg^{-1} - has such a dramatic effect on growth when coupled with the measured excretion rate of aromatic ketoacids. The maximum secretion rate of aromatic ketoacids was 148 nmoles/h/5 $\times$ 10^7 cells (or 8.8 nmol.min^{-1}.mg^{-1}, where 1×10^8 cells = 0.56 mg protein [168]). Even with the reduction of the ASAT activity observed here, there still appears to be sufficient capacity for amino acid transamination to account for this aromatic ketoacid secretion. In addition, there appears to be a threshold where loss of cASAT activity leads to unrecoverable loss of cell viability, as 80% activity in non-induced cells was sufficient to sustain cell growth, albeit at a lower rate than wild type cells (7.3 hour vs 10.6 hour doubling time). However, 50% activity and below leads to cell growth cycle arrest and eventually cell death (Fig. 4.4a). Perhaps the loss of activity below a certain threshold disrupts other linked metabolic processes irrecoverably in these cells. Qualitatively, cells can be seen to develop aberrant morphology, even after 24 hours of knockdown (Fig. 4.7). The arrest in growth of these cells and absence of multinucleated cells suggest that cell division itself is halted, before the cells eventually die. This further highlights the need for fully active cASAT at wild type levels, as morphological changes are rapidly onset in when activity is reduced by more than 50%.

The absence of any decline in cell viability or growth in procyclic cASAT RNAi cells is striking (Fig. 4.8). Knockdown of cASAT mRNA in these cells was of similar levels to that observed in bloodstream cells at $\approx$ 55% (Fig. 4.9), and was specific for cASAT (Fig. 4.10). There are several possibilities to explain this result. Procyclic form cells have much higher total ASAT activity (200 nmol.min^{-1}.mg^{-1}) than bloodstream form cells (50 nmol.min^{-1}.mg^{-1}) [96]. This is due to the combined expression of mASAT and the continuously expressed cASAT in procyclic cells. The mASAT is only well expressed in the procyclic stage cells, and is highly specific for aspartate [150]. It is possible that mASAT plays a role equivalent to the glutamate-malate shuttle in procyclic form cells, for transfer of intermediates into the partial Krebs cycle in conjunction with cASAT. However, loss of cASAT, which would be expected to function as part of this shuttle, did not affect the cells. Only cASAT is expressed in bloodstream form cells, perhaps

because a glutamate-malate shuttle is not required given the lack of a Krebs cycle or electron transport chain. The functional differences between the two isoforms remains unclear.

Berger et al. suggested that TbcASAT could have a role in the generation of aromatic ketoacids that had been detected in the urine of infected host animals [99, 111]. It was demonstrated here that RNAi of TbcASAT did lead to a reduction in the concentration of detected aromatic ketoacids in cell culture media. Whether this reduction is entirely due to the activity of TbcASAT remains to be established. It is also notable that the excretion of aromatic ketoacids is not required for cell viability; growth rates were unaffected when cells alternately excreted the aromatic hydroxyacid derivative generated by the inducible AHADH^{in}. Experiments performed, where a "rescue copy" of *T. cruzi* cASAT was constitutively expressed in the cASAT RNAi cell line, rescued the lethal RNAi phenotype in bloodstream form cells. Interestingly, this modified cell line also produced lower total amounts of aromatic ketoacids of the same order that was observed with the induced cASAT RNAi cells [136].

Why is knockdown of TbcASAT lethal, if there is not a requirement to secrete aromatic ketoacids? Given the preference of the aromatic amino acid - oxaloacetate pairing by TbcASAT, the generation of aspartate from oxaloacetate could be metabolically important. In *T. brucei* there is a requirement for NH_2 to synthesise adenine nucleotides from hypoxanthine - the main purine source in culture - which is likely primarily provided by aspartate generated from oxaloacetate [77]. Creek et al. note that knockdown of PEPCK is lethal to cells, in a similar manner to TbcASAT knockdown [77]. Since PEPCK is responsible for the generation of oxaloacetate from phosphoenolpyruvate, which would then be utilised by TbcASAT to generate aspartate, reduction in the activity of either enzyme would be expected to be lethal. The requirement for aspartate in purine salvage has been further highlighted by the need for adenylosuccinate synthase (ADSS) and adenylosuccinate lyase (ADSL) in bloodstream from cells, which are both involved in the generation of AMP [169]. While probing the quorum sensing ability of *T. brucei* with genome wide RNAi, Mony et al. found that RNAi of either ADSS or ADSL drastically reduced the growth rates of these cells. Supplementation with cAMP could restore the loss of ADSS activity, possibly through restoration of the purine balance [169]. In addition, aspartate is also required for the synthesis of uridine

monophosphate (UMP), despite the presence of a pyrimidine synthesis pathway [77].

It has been demonstrated here that reduction of the activity of TbcASAT is lethal to bloodstream form cells, most likely due to the subsequent decrease in available aspartate. The effect is made more evident by the lack of any uptake of aspartate from the extracellular media [93, 94]. In this case the synthesis of aspartate from oxaloacetate by TbcASAT would be the primary source of aspartate in these cells. Aromatic amino acids are the preferred amino donors by cASAT, tryptophan in particular, and a consequence of this preference is the production of aromatic keto acids. It has been suggested previously that secreted ketoacids may be have roles in immune regulation of the host, but that remains to be established [107, 108].

4.4.2 Secretion of aromatic ketoacids by *T. brucei*.

When bloodstream form *T. brucei* were cultured in the presence of aromatic amino acids, secreted aromatic ketoacids were detected in spent culture media. Secreted aromatic ketoacids were not detected in procyclic form cell spent culture media (not shown). Additionally, RNAi of TbcASAT was linked to a decrease in the detectable levels of these secreted aromatic ketoacids. Numerous reports have highlighted the link between *T. brucei* infection and a subsequent decrease in host aromatic amino acid pools, with a corresponding increase in the levels of excreted aromatic amino acid catabolites [109, 110, 170, 171]. None of these studies report on the *in vitro* secretion rates of the individual aromatic ketoacids, which have been examined here for the first time. The secretion of aromatic ketoacids by bloodstream form *T. brucei* was linear with respect to time. As noted by McGettrick et al. [172], the calculated rate of oxaloacetate production by PEPCK would be ≈ 56 nmoles/h/5×10^7 cells, which would meet the requirements for indolepyruvate production (47.74 nmoles/h/5×10^7 cells) from tryptophan with oxaloacetate as the amino group acceptor. Importantly, this rate of production of indolepyruvate was obtained with high exogenous concentrations of tryptophan (2 mM) in culture media. With lower concentrations of free tryptophan in the host, the rate of excretion of indolepyruvate would be expected to be lower *in vivo*. Supplementation with either tyrosine or phenylalanine resulted in higher corresponding aromatic ketoacid secretion rates than that displayed for tryptophan. In addition, it was surprising that the rate of production of aromatic ketoacids seemed to be lim-

ited by the availability of the aromatic amino acid substrate. Thisn suggests that the transamination reaction may not be the rate limiting step in aromatic ketoacid production, but rather that the production of aromatic ketoacids could be limited by the rates of aromatic amino acid uptake. Indeed, the rates of aromatic amino acid transport reported by Hasne are very similar to the aromatic secretion rates reported here (section 4.2.1) [94]. When 2 mM of each aromatic amino acid was added exogenously, the rate of aromatic ketoacid production reached almost 150 nmoles/h/5×10^7 cells. In this case the calculated rate of oxaloacetate production would not be sufficient to meet the demands of aromatic amino acid deamination. It could be possible under these conditions that α-ketoglutarate could act as the amino group acceptor, allowing for high rates of aromatic ketoacid secretion to persist. This could be tested experimentally, by monitoring the production of alanine while varying the concentration of exogenous aromatic amino acids. If α-ketoglutarate was accepting 'excess' amino groups, then a corresponding increase in alanine excretion would be expected, since pyruvate production is already high enough that glycolytic flux is unlikely to be affected. Whether this would occur in an *in vivo* infection is unclear, as aromatic amino acids are unlikely to present at concentrations exceeding 220 μM in the blood of humans [93]. It could be possible that *T. brucei* infection may increase the synthesis and release of aromatic amino acids by the host; indolepyruvate is an inhibitor of tryptophan-2,3-dioxygenase (TPO), an enzyme involved in regulation of circulating tryptophan. Inhibition of TPO has been shown to lead to a corresponding decrease in circulating tryptophan levels in the blood [173].

It was found that procyclic form cells did not secrete aromatic amino acids, at least not *in vitro* (data not shown). Unlike the bloodstream form, procyclic cells can catabolise amino acids, such as proline and threonine [138, 174]. It is possible that procyclic cells utilise aromatic amino acids for other processes, such as protein synthesis. On the other hand, these cells do express a mitochondrial MDH (in addition to a glycosomal and cytosolic MDH) that possesses the ability to reduce hydroxyphenylpyruvate and phenylpyruvate [175]. Perhaps any aromatic ketoacids that are produced by procyclic *T. brucei* are subsequently reduced and are undetectable by the assays employed here. In contrast, bloodstream form cells expressed only a cytosolic MDH, which is specific for oxaloacetate and does not reduce aromatic ketoacids [176].

Both *in vivo* and *in vitro* studies report on a dramatic time-dependent decrease in free aromatic amino acids due to the presence of bloodstream form *T. brucei* [93, 109]. It was noted in one of these studies that free tryptophan concentrations in the sera of mice were lowered to below detectable levels during *T. brucei* infection [109]. This indicated, in conjunction with our enzymatic data, that tryptophan may be the preferred aromatic amino acid substrate for TbcASAT *in vivo*. Using ^{13}C-NMR and conditional RNAi, it is shown here that TbcASAT is directly responsible for aromatic ketoacid production from aromatic amino acids in *T. brucei*. Firstly, with ^{13}C-labelled tryptophan as the only aromatic amino acid source, the sole product detected in the carbon spectra was indolepyruvate. Indolepyruvate had been implicated as a possible precursor to tryptophol by Stibbs and Seed [107], though they could not explain how the required decarboxylation reaction could occur to allow this. The corresponding ^{13}C chemical shifts of tryptophol and indole lactate were not detected in the spectra. It is clear from this ^{13}C-NMR data that indolepyruvate is, in fact, the sole excreted end product of tryptophan metabolism by the parasite. However, the subsequent modification of indolepyruvate to other compounds once excreted cannot be ruled out (to be discussed). Coupling ^{13}C-NMR with RNAi of cASAT in bloodstream from *T. brucei* was also crucial in demonstrating that the cASAT enzyme is responsible for the conversion of tryptophan to indolepyruvate, and so implies that it functions in the same manner with phenylalanine and tyrosine, although similar experiments should be conducted to establish if this is the case. Unfortunately, the quantity of tryptophan that was converted to indolepyruvate could not be established accurately, due to the technical limits of ^{13}C-NMR.

4.4.3 ^{15}N-tryptophan metabolic data.

The preliminary metabolomic data gathered on the metabolism of ^{15}N-labelled tryptophan tentatively supports the role of TbcASAT in generating aspartate for purine salvage and UMP synthesis.

Although aspartate itself could not be monitored due to low labelling of the metabolite - perhaps due to high turnover rates - the relatively high labelling of asparagine (page 153) can be taken as a direct indicator of the presence of ^{15}N-labelled aspartate. Asparagine is synthesised from aspartate and glutamate or ammonia, and

is important for nitrogen homoeostasis. In *T. brucei* glutamate and aspartate were the preferred substrates for asparagine synthase A (ASA) [177]. The particularly high level of labelled asparagine detected here may be explained by the growth of the MITat1.2 cells in media containing low levels of asparagine [93]. Although RNAi of the ASA was not lethal in cells grown in HMI-9 media, which contains high levels ($\approx$ 190 μM) of asparagine, when asparagine was removed from the media the cells grew at significantly slower rates [177]. It is possible that in the low asparagine environment used here, the production of asparagine from aspartate is favoured, given that it can no longer be acquired through uptake from the media.

The labelling of uracil and adenosine further supports a role for ^{15}N-tryptophan derived aspartate in purine and pyrimidine synthesis (page 155). Uracil is synthesised from aspartate via orotate in *T. brucei*, while adenosine (in the form of AMP) is synthesised by the action of adenylosuccinate lyase. Adenylosuccinate, synthesised directly from aspartate, is cleaved by adenylosuccinate lyase into fumarate and AMP. Taken together, both uracil and adenosine show a combined labelling of $4.7 - 6.9\%$, indicating the importance of ^{15}N derived from tryptophan in both pyrimidine and purine salvage. Interestingly, uracil can be taken up by *T. brucei* from the media as well as synthesised *de novo*. It is likely that the synthesis of UMP from orotate may be more important than the generation of uracil [77], and should be examined in the same manner via mass spec, though uracil can still be used to infer aspartate derived pyrimidine synthesis here.

Alanine was found to be the most labelled metabolite, at 4.5% (page 152). Given that α-ketoglutarate is a good substrate for cASAT, it is possible that it may be used to regenerate glutamate which then further transfers its amino group to pyruvate via AAT, producing alanine. This cycle was previously suggested by Spitznagel et al., whereby AAT would provide directional drive to cASAT through the high throughput of pyruvate from glycolysis [96]. The purpose of the pathway, if it exists, remains a mystery. Surprisingly, some degree of labelling was found in valine and leucine/isoleucine. While no obvious reason can be determined as to why these amino acids incorporated ^{15}N from tryptophan, it is possible that the promiscuity of the transaminase allows for the exchange of the amino group to α-ketoisocaproate [99]. It may also be possible that once the amino group is incorporated into glutamate (as suggested above) it is

then used to synthesise both valine and leucine/isoleucine, as glutamate can act as an amino donor and regenerate α-ketoglutarate in the process.

It had been proposed that cASAT may be involved in a methionine recycling pathway [101, 161]. However, growing evidence suggest that such a pathway does not exist in *Trypanosomes*. Recently, Creek et al. demonstrated that no carbon labelling from ^{13}C-glucose could be detected in intracellular methionine [77]. It had also been previously shown that *T. brucei* could uptake methionine from culture media, essentially satisfying its methionine requirements [93, 106]. Further evidence that this pathway is unlikely to function is provided here, as methionine supplementation of culture media did not rescue the growth defect of induced *cASAT* RNAi cells (page 131). In addition, the ^{15}N labelling of methionine intracellularly from tryptophan was low, contrary to what would be expected by Berger et al. [101]. It is possible that the initial proposal for methionine salvage from aromatic amino acids by cASAT was based on a misguided interpretation - it was shown that cASAT can indeed utilise α-ketomethiobutyrate (KMTB) and aromatic amino acids to generate methionine. However, the reported K_m and V_{max} are higher and lower, respectively, than those reported here for both α-ketoglutarate and oxaloacetate. In addition, methionine generation was reported for *C. fasiculata* via NMR, but not for *T. brucei*, where it was instead inferred from enzymatic data [101]. It is proposed here that the study by Berger et al. demonstrated enzymatically that cASAT could transaminate α-ketomethiobutyrate to methionine, but that such conversion does not occur in appreciable amounts *in vitro* in *T. brucei*.

Unfortunately, several peaks were of too poor quality to quantify correctly, and repeated mass spectrum analysis is essential, as it would be of great interest to re-examine aspartate labelling. Attempts should also be made to achieve a higher concentration of ^{15}N-tryptophan to detect lesser labelled metabolites. This could be achieved by removing the additional supplemented amino acids added to simulate the use of FCS Gold by Creek et al. [93]. More specifically, the removal of phenylalanine and tyrosine, which would dilute the contribution of tryptophan to aspartate generation through cASAT.

4.4.4 Conclusions.

This study has established that TbcASAT is an essential enzyme for bloodstream form *T. brucei*, but not in procyclic form cells. Though it has not been thoroughly investigated, this is likely due to a stage specific mASAT that is expressed by procyclic *T. brucei* which could compensate for loss of cASAT activity. Unlike the reported amino acid preferences of other ASATs [98, 99, 150], *T. brucei* cASAT has a strong preference for aromatic amino acids as substrates when coupled with α-ketoglutarate (compared here to *T. cruzi* cASAT), in particular for tryptophan. It was demonstrated for the first time, however, that oxaloacetate is the preferred amino acid acceptor by recombinant TbcASAT. The amino group donated by aromatic amino acids through TbcASAT is likely used to transaminate oxaloacetate to generate aspartate, which has multiple roles in purine salvage and pyrimidine synthesis, amongst others [77]. Fig 4.28 outlines the possible pathways that TbcASAT is involved in, as speculated here. The quantification of the secretion rates of the aromatic ketoacids from the corresponding aromatic amino acids has been carried out. The sole source of the aromatic ketoacids appears to be the circulating free aromatic amino acids, as secretion of aromatic ketoacids rapidly disappears in their absence. The aromatic ketoacid secretion rates are high, and suggest that there is sufficient capacity available to convert PEPCK-produced oxaloacetate to aspartate as proposed.

What remains to be understood is why a broad substrate specificity aminotransferase has developed a preference for aromatic amino acid substrates, which *T. brucei* consequently secretes aromatic ketoacids in large quantities, when many amino acids would be suitable amino group donors for aspartate generation. The possibility that aromatic ketoacids could play a role in the regulation of the host inflammatory response will be examined next.

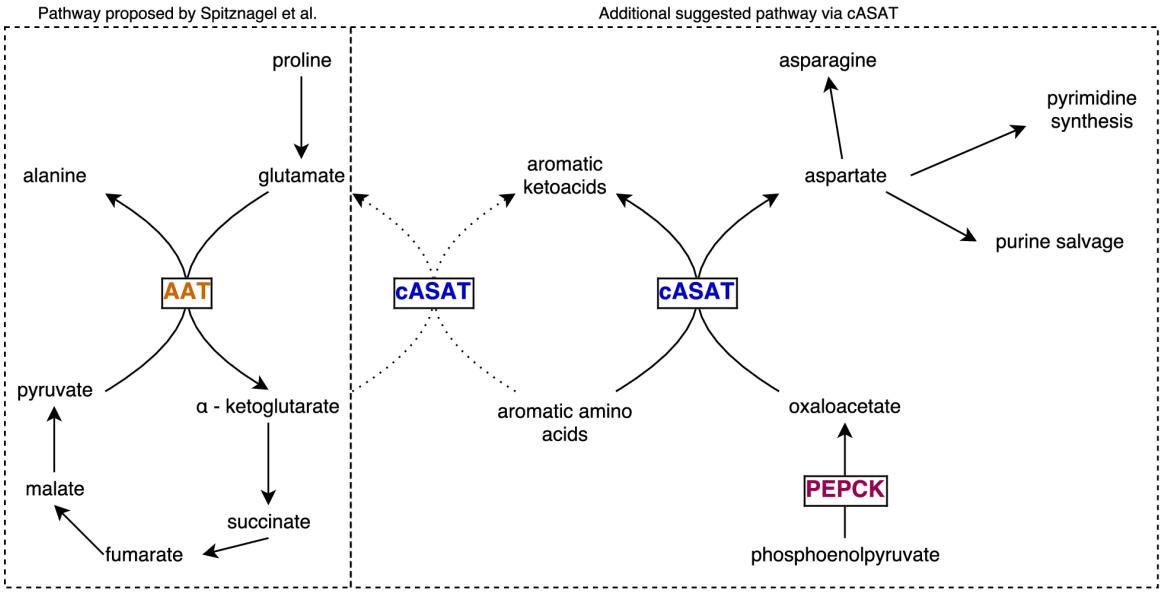

Figure 4.28. Proposed possible pathway for the metabolic role of cASAT in *T. brucei*.

Simplified scheme of aromatic amino acid metabolism by cASAT in *T. brucei*, in conjunction with the proline metabolic pathway as proposed by Spitznagel et al. [96]. cASAT generates aromatic ketoacids and aspartate from aromatic amino acids and oxaloacetate, derived from phosphoenolpyruvate by PEPCK. cASAT may also use aromatic amino acids and α-ketoglutarate to regenerate glutamate, which can then be used to convert pyruvate to alanine. Black arrows indicate enzymatic steps. Two cASAT boxes are represented for clarity.

Chapter 5

Multiple immunological roles for aromatic ketoacids produced by *T. brucei*.

Data previously outlined here (chapters 3 and 4) strongly suggests that the metabolism of aromatic amino acids and the consequent excretion of aromatic ketoacids by bloodstream, but not procyclic, form *T. brucei* is essential for the parasite. Several lines of evidence suggest a possible role for these aromatic ketoacids in host immune suppression. Circulating aromatic amino acid concentrations are drastically decreased in the presence of *T. brucei*. For example, voles infected with *T. gambiense* were shown to have significant decreases in free circulating phenylalanine and tyrosine, and a complete absence of circulating tryptophan was observed during *T. brucei* infection [109]. When bloodstream form *T. brucei* is cultured *in vitro*, a significant depletion of free aromatic amino acids occurs with time [93]. Aromatic ketoacids can be detected as secretory products of *T. brucei* metabolism; significant levels of aromatic ketoacids could be detected in the urine of infected mice [111], and aromatic ketoacid derivatives could be detected via radiochromatographic assays conducted on *T. gambiense* cultured *in vitro* [102]. Finally, aromatic amino acid metabolites have been implicated in immune suppression by trypanosomes, and other organisms. The reputed tryptophan metabolite, tryptophol, induces sleep like behaviour in mice [108]. Inability to generate AhR ligands from tryptophan catabolism has been linked to dysbiosis in IBD patients [178].

In collaboration with both the Inflammation Research group (Prof. Luke O'Neill) and Molecular Immunology group (Dr. Aisling Dunne) at Trinity College Dublin, several investigations were undertaken into the possible roles *T. brucei* derived aromatic ketoacids may have in inflammation regulation in their hosts.

5.1 Investigation of the role of *T. brucei* secreted aromatic ketoacids in the modulation of the host innate immune system.

5.1.1 Determination of the levels of aromatic ketoacids in the blood sera of Rats infected with *T. brucei*.

It was necessary to determine if aromatic ketoacids could be detected at physiologically relevant amounts *in vivo* in the host during an infection with *T. brucei*. El Sawalhy

et al. had provided evidence that aromatic ketoacids could be detected in the urine of mice infected with *T. evansi* at low levels that correlated with the level of parasitemia [111]. No study could be found, however, where the levels of aromatic ketoacids had been measured in the blood serum of infected mammals. It is possible that the levels of ketoacids would be higher than those detected in urine, for two reasons; urine has been processed by the kidneys and so a reduction of aromatic ketoacids could occur, and that *T. brucei* reside in the bloodstream of their infected mammalian host. Consequently, an AHADH assay was utilised to quantify circulating ketoacid levels in rats infected with *T. brucei*.

Ketoacid concentrations were significantly elevated in the sera of *T. brucei* infected rats, to between $0.25 - 0.55$ mM (Fig. 5.1), with low concentrations of ketoacid present in uninfected rats (below 100 μM). The cell count in the blood ranged from 0.63×10^8 cells.ml^{-1} to 7.38×10^8 cells.ml^{-1}. While no linear correlation was found between cell count and ketoacid concentration, the highest cell counts yielded the highest ketoacid concentrations, and the lowest cell counts yielded the lowest ketoacid concentrations. Importantly, not only were measurements of ketoacid concentration obtained here vastly increased to those detected in mice urine, but notably were obtained at much lower levels of parasitemia (El Sawalhy et al. reached 1.5×10^9 cells.ml^{-1}) [111]. The concentration of aromatic ketoacids recorded with the AHADH assay in the sera of *T. brucei* infected rats are twice as high as those reported by El Sawalhy et al. in the urine of *T. evansi* infected mice [111].

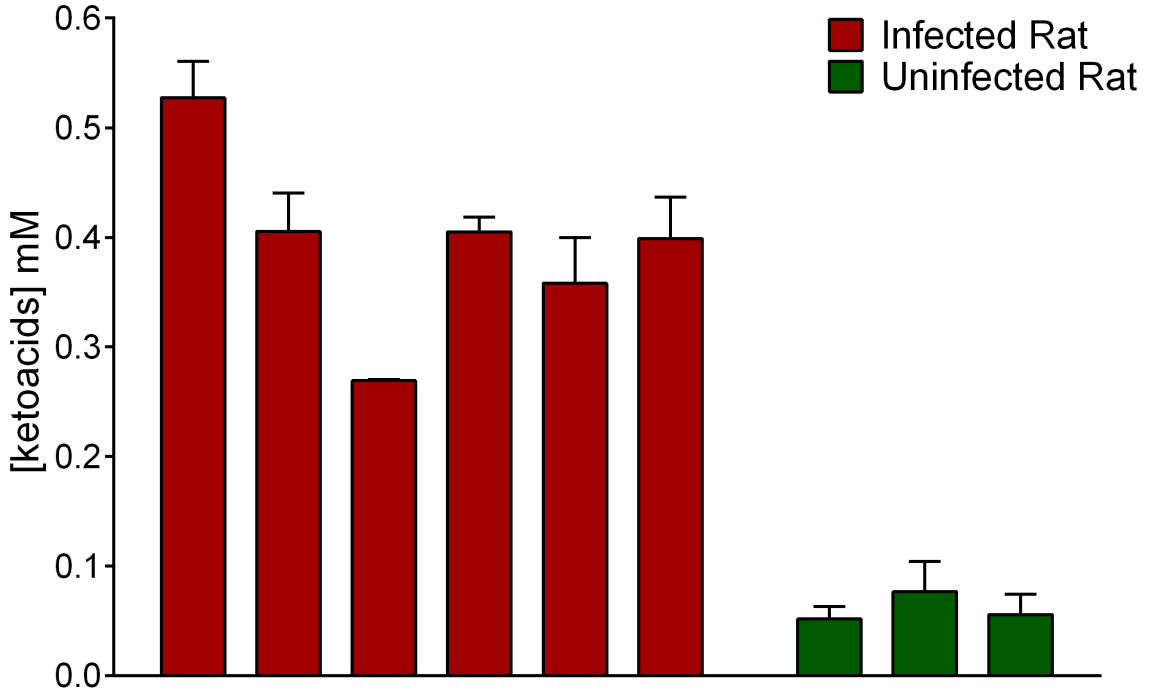

Figure 5.1. Ketoacid concentration in blood serum taken from rats infected with *T. brucei*.

The concentration range of ketoacids in the blood serum from infected rats fell between the $0.2 - 0.5$ mM, whereas the ketoacid concentration in uninfected rats never rose above 80 μM. Each bar represents one rat, ketoacid concentrations were a mean of three determinations per rat. Error bars represent SD.

5.1.2 Investigation of the effects of the *T. brucei* metabolite indolepyruvate on the macrophage inflammatory response.

A bacterial lipopolysaccharide (LPS) based model was used to drive the innate inflammatory response in macrophages for these experiments. LPS is known to bind to TL4 and induce production of inflammatory cytokines such as IL-1, TNF-α, and IL-6 [179]. The following experiments were conducted in collaboration with the Inflammation Research Group. A number of factors focused the research efforts carried out here on indolepyruvate as having a potentially important role in host modulating the host inflammatory response. Firstly, the reported complete disappearance of free circulating tryptophan in *T.b. gambiense* infected voles [109]. Secondly, the data gathered in this study on *T. brucei* cASAT having a preference for tryptophan as a substrate. Finally, previous research indicated that transport affinity of aromatic amino acids uptake by bloodstream form *T. brucei* was highest for tryptophan [94]. Moreover, indolepyruvate had already been characterised as a potent anti-oxidant in many systems [108, 173, 180].

Treatment of bone marrow derived macrophages (BMDMs) with spent culture media from wild type and cASAT RNAi *T. brucei*.

BMDM cells treated with spent culture media from bloodstream form *T. brucei* showed significantly lower expression of LPS-induced pro-IL-1β (Fig. 5.2). However, LPS-induced expression of pro-IL-1β was substantially restored when BMDMs were treated with spent media from bloodstream from *T. brucei* subjected to cASAT knockdown for 48 h. A partial suppressive effect on pro-IL-1β expression was also observed when the BMDMs were incubated with media from non-induced cASAT RNAi cells. The concentration of total aromatic ketoacids in the spent media of wild type, non-induced, and induced cASAT RNAi cells was found to be $\approx 0.55 \pm 0.04$ mM, 0.4 ± 0.06 mM, and 0.18 ± 0.07 mM, respectively (mean $\pm$ SD of 3 measurements). Taken together, these data demonstrated that suppression of cASAT activity leads to decreased secretion of aromatic ketoacids into the spent media. This suggests that the presence of aromatic ketoacids in the spent media was responsible for suppression of LPS-induced pro-IL-

1β expression by BMDMs. The results obtained with spent media from non-induced cASAT RNAi cells can be attributed to partial knockdown of cASAT, and consequently decreased secretion of aromatic ketoacids, due to leaky transcription of dsRNA in the absence of the tetracycline inducer.

In vitro treatment of BMDMs with indolepyruvate.

It appeared that *T. brucei* secreted aromatic ketoacids had a suppressive effect on the LPS-induced production of pro-IL-1β by BMDMs, but it was not clear if this effect was directly attributable to aromatic ketoacids, or whether some other *T. brucei*-derived secreted factor was causing this suppression. In order to establish unequivocally whether aromatic ketoacids alone were responsible for the inhibitory effect on LPS-induced pro-IL-1β expression, BMDMs were incubated with indolepyruvate.

A solution of indolepyruvate (1 mM) was prepared by in DMEM media. The BMDMs were pre-treated with this 1 mM solution for 30 min prior to a 24 hour period of LPS (100 ng.ml^{-1}) induced stimulation of these cells. It was shown that indolepyruvate alone could inhibit the LPS induced expression of pro-IL-1β by BMDMs (Fig. 5.3a). The suppression of LPS-induced pro-IL-1β by BMDMs was also shown to be dose dependent. Lower concentrations of indolepyruvate (0.2 - 1 mM) were capable or suppressing LPS-induced pro-IL-1β expression (Fig. 5.3b). Crucially, these levels of indolepyruvate are closer to the levels of aromatic ketoacids detected in the sera of *T. brucei* infected rats, and so are more physiologically relevant. Furthermore, indolepyruvate could still suppress LPS-induced pro-IL-1β expression when the concentration of LPS used to stimulate BMDMs was increased tenfold from 10 ng.ml^{-1} to 100 ng.ml^{-1} (Fig. 5.3b). This data suggests that indolepyruvate is capable of suppressing LPS-induced pro-IL-1β expression by BMDMs in a manner that is physiologically relevant to the levels of aromatic ketoacids detectable in the blood of a *T. brucei* infected host.

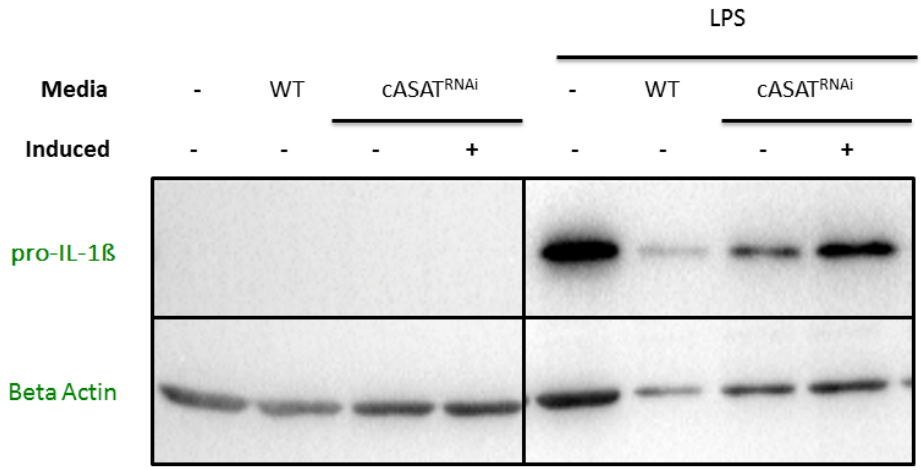

Figure 5.2. The effect of spent media from wild type and cASAT RNAi bloodstream form *T. brucei* on LPS-induced pro-IL-1β production in BMDMs.
BMDMs were treated with modified DMEM supernatants taken from wild type MITat1.2 (WT) or cASAT RNAi cells (cASAT^{RNAi}) which were non-induced (−) or induced (+) for 48 hours with 2 mg.ml^{-1} tetracycline. Supernatants were diluted 1:1 in plain DMEM + 10% FBS for BMDM treatment. The western blot shows protein extracted from the treated BMDMs. β-actin was used as a loading control.
Sample from one mouse, representative of three repeated experiments.

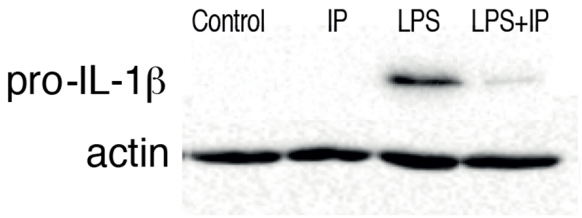

(a)

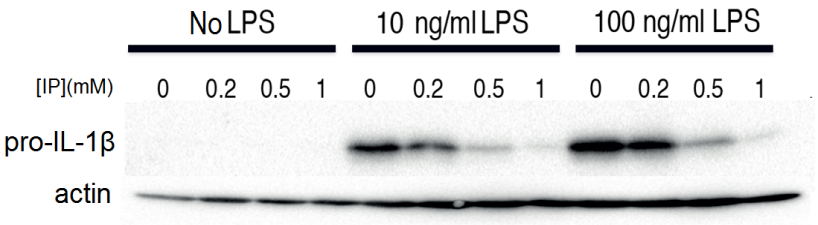

(b)

Figure 5.3. Indolepyruvate inhibits LPS-induced expression of pro-IL-1β by BMDMs.

(a) Indolepyruvate (IP) suppresses LPS induced pro-IL-1β production in BMDMs when applied at a 1 mM concentration. **(b)** Various concentrations of indolepyruvate (0.2 - 1 mM) prepared in DMEM can suppress LPS-induced pro-IL-1β production in a dose dependent manner in BMDMs, at both high and low [LPS] treatments.

Sample from one mouse, representative of three repeated experiments.

5.1.3 Investigation of the effects of the *T. brucei* secreted aromatic ketoacids on the inflammatory response of mixed glial cells.

It is well established that in the late stage of trypanosomiasis, the parasite invades the CNS of the host, leading to numerous complications including meningoencephalitis [181]. It has also been suggested that tryptophan metabolites excreted by *T. brucei* or possibly produced by the host in response to *T. brucei* infection could have a role in late stage symptoms, such as increased daytime sleepiness [102]. Research on the treatment of rats with moderate to high doses of indolepyruvate demonstrated that the compound could cause a decrease in REM sleep and food intake in treated rats [182]. Indeed, clinical trials conducted by Politi et al. have shown that treatment of insomniacs with indolepyruvate could improve both length and quality of sleep [180]. It was speculated that perhaps the aromatic ketoacids secreted by *T. brucei* may be relevant in the late stage of the disease, particularly given the immune privileged nature of the brain. The following experiments were performed in collaboration with Glyn Williams of the Molecular Immunology Group.

Indolepyruvate suppresses LPS-induced pro-IL-1β production in mixed glial cell populations.

The ability of indolepyruvate to suppress LPS-induced pro-IL-1β production by an activated mixed glial cell population (80% astrocytes, 20% microglia [183]) was assessed by pre-treating glial cells for 30 min with different concentrations of indolepyruvate (0.25 - 1 mM) prepared in DMEM media, prior to stimulation with LPS (100 ng.ml^{-1}) and subsequent incubation for 24 h.

As was observed with BMDMs, indolepyruvate was capable of suppressing the expression of LPS-induced pro-IL-1β by mixed glial cells (Fig. 5.4a). As the concentration of indolepyruvate used to treat the mixed glial cells was increased, the ability of indolepyruvate to suppress LPS-induced pro-IL-1β expression became more effective, indicating that indolepyruvate could act in a dose-dependent manner. Additionally, both hydroxyphenylpyruvate and phenylpyruvate (Fig. 5.4b and 5.4c) exhibited

a much weaker ability to suppress LPS-induced pro-IL-1β expression by mixed glial cells, in comparison to indolepyruvate. These results are similar to those reported by McGettrick et al. [172].

Aromatic ketoacids induce significant expression of HO-1.

In the absence of an obvious role for hydroxyphenylpyruvate and phenylpyruvate secreted by *T. brucei* in the modulation of the host inflammatory response, screens were conducted with aromatic ketoacids and other inflammatory regulators. It was discovered that all three aromatic ketoacids secreted by *T. brucei* were potent inducers of heme oxygenase 1 (HO-1) expression. HO-1 is an inducible isoform of the heme oxygenases (HO-2 is constitutively expressed, while HO-3 remains uncharacterised), and is known to have a key role in the regulation of cell anti-inflammatory and pro-inflammatory mechanisms [184]. HO-1 primarily acts through the generation of three byproducts of heme catabolism; biliverdin, carbon monoxide gas, and the release of Fe^{2+} from heme. Biliverdin, and the subsequently produced bilirubin, are potent anti-oxidants. Carbon monoxide gas can promote an anti-inflammatory response while suppressing a pro-inflammatory response in macrophages [184].

While probing for other cytokines in response to aromatic ketoacid treatment, HO-1 expression was discovered to have been up-regulated by indolepyruvate. As a result, the dose response of HO-1 to each aromatic ketoacid was measured. Cells were pre-treated for 30 min with different concentrations of each aromatic ketoacid (0.25-1 mM) prepared in DMEM media, prior to stimulation with LPS (100 ng.ml^{-1}) and subsequent incubation for 24 h. Strikingly, while only indolepyruvate was found to suppress LPS-induced pro-IL-1β production, indolepyruvate, hydroxyphenylpyruvate, and phenylpyruvate were all found to be potent inducers of HO-1 expression (Fig. 5.5).

When spent DMEM media that bloodstream form *T. brucei* (2.5×10^7 cells.ml^{-1}) had been cultured in was applied to mixed glial cells, HO-1 expression by the mixed glial cells was potently induced, in a dose-dependent manner (Fig. 5.6a). This strongly suggested that the aromatic ketoacids secreted by *T. brucei* were responsible for the induction of HO-1, that had been observed by the treatment of mixed glial cells with the individual aromatic ketoacids.

To confirm this, the AHADH^{in} *T. brucei* cell line was used to test whether this HO-1 induction was due to aromatic ketoacid secretion or due to other secreted factors from *T. brucei*. Previous experiments relied on lower excretion of aromatic ketoacids, whereas this cell line alternatively excretes aromatic hydroxyacids. Wild type *T. brucei* and induced AHADH^{in} were cultured in DMEM culture media containing 1 mM each of tryptophan, phenylalanine, and tyrosine for four hours at 3×10^7 cells.ml^{-1}. Cells were removed by centrifugation at 14,000 g for 10 min, and the media supernatants were used to treat the mixed glial cells. Initial results indicate that the aromatic ketoacids secreted by *T. brucei* are responsible for HO-1 induction in a dose dependent manner, as the relative absence of aromatic ketoacids does not lead to HO- induction (Fig. 5.6b), though an increase in sample size is necessary. These results suggest that aromatic ketoacid secretion by *T. brucei* may play an important role in dampening the inflammatory response of the host CNS during late stage infection with *T. brucei*.

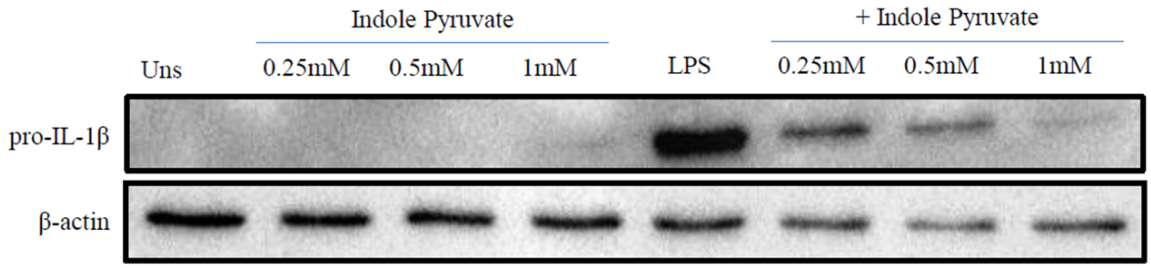

(a) Indolepyruvate treatment.

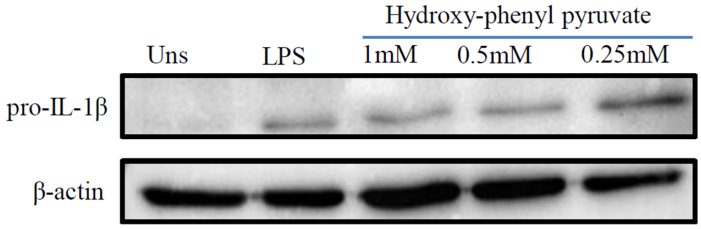

(b) Hydroxyphenylpyruvate treatment.

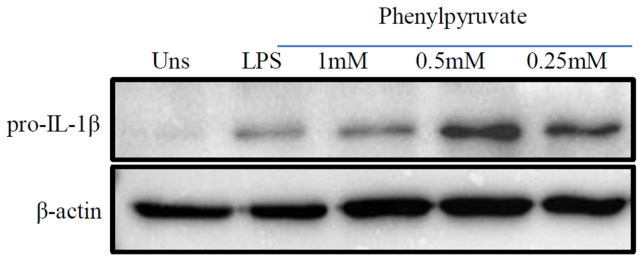

(c) Phenylpyruvate treatment.

Figure 5.4. Indolepyruvate can prevent the LPS-induced expression of pro-IL-1β by mixed glial populations.

(a) Varying concentrations of indolepyruvate (0.25 - 1 mM) could suppress pro-IL-1β production in a dose dependent manner in mixed glial cell populations. **(b)** Varying concentrations of hydroxyphenylpyruvate (0.25 - 1 mM) did not suppress pro-IL-1β production to a significant extent, as was also observed with **(c)** phenylpyruvate treatments.

The western blot shows protein extracted from the treated mixed glial cells. β-actin was used as a loading control. Sample from one mouse, representative of three repeated experiments.

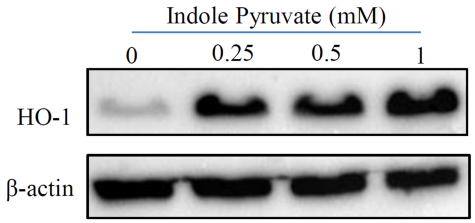

(a) Indolepyruvate treatment.

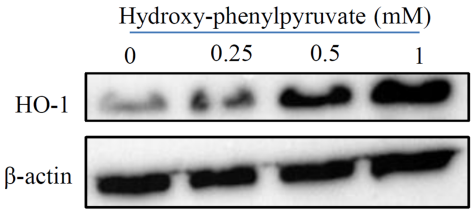

(b) Hydroxyphenylpyruvate treatment.

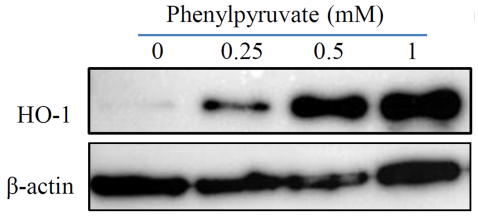

(c) Phenylpyrvate treatment.

Figure 5.5. HO-1 expression is induced in mixed glial cells by indolepyruvate, phenylpyruvate, and hydroxyphenylpyruvate.

(a) Varying concentrations of indolepyruvate (0.25 - 1 mM) induced HO-1 production in a dose dependent manner in mixed glial cell populations. HO-1 was also expressed in a dose dependent manner with **(b)** hydroxyphenylpyruvate (0.25 - 1 mM) treatment, and with **(c)** phenylpyruvate treatment (0.25 - 1 mM).

These western blots show protein extracted from the treated mixed glial cells. β-actin was used as a loading control. Sample from one mouse, representative of three repeated experiments.

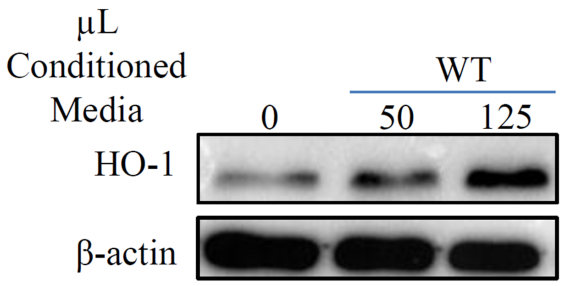

(a)

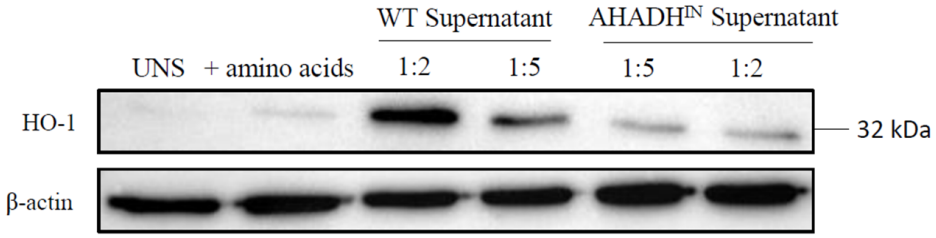

(b)

Figure 5.6. Spent culture media from *T. brucei* induces HO-1 expression in mixed glial cells.

(a) DMEM media that had been used to culture *T. brucei* was shown to increase the expression of HO-1, with increasing volumes added as a proportion of 500 μl normal DMEM + 10% FCS to mixed glial cells. **(b)** Mixed glial cells treated with either spent media supernatants from wild type *T. brucei* (WT supernatant) or spent media supernatants from 48 hour induced AHADH^{in} cells. Fractional dilutions in DMEM + 10% were used to assess if there was a threshold for HO-1 expression. Abbreviations; Control mixed glial cells (UNS), control mixed glial cells with DMEM media containing aromatic amino acids (+amino acids).
These western blots show protein extracted from the treated glial cells. β-actin was used as a loading control. Sample from one mouse.

5.2 The stability & degradation of indolepyruvate, and the possible function for MIF as an indolepyruvate tautomerase.

The stability of indolepyruvate and the possible biological functions it may have has been examined in several studies [173, 185–187]. Indolepyruvate is known to undergo tautomerisation, and there are notable differences in the stability of each of the tautomeric forms. It is recognised that the enol form of indolepyruvate readily reacts with ROS, and subsequent breakdown and chemical rearrangements can give rise to diverse indole structures that possess biological activity. For example, ASAT mediated transamination of L-tryptophan gives rise to indolepyruvate, which in turn spontaneously reacts in aqueous solution to form a large number of compounds that act as agonists of the aryl hydrocarbon receptor (AhR) [188]. Tyrosine and the serotonin-precursor 5-hydroxytryptophan also activate AhR signalling in combination with aspartate aminotransferase, suggesting that 4-hydroxyphenylpyruvate and 5-hydroxyindolepyruvate also act as pro-agonists of AhR. Herein are outlined two additional, and important, data sets gathered over the course of this work, which may further clarify some elements of the role of indolepyruvate in *T. brucei*-host dynamics during infection. This encompassed investigations of the nature of the stability of indolepyruvate, how enol-keto tautomerism plays a role in this stability, and how indolepyruvate breaks down into other indolic derivatives. It is also interesting to note that aromatic ketoacids, most typically phenylpyruvate, appear to be substrates for the mammalian host factor, macrophage migration inhibitory factor (MIF) [189]. Although MIF was the first described as a cytokine, the possibility that its tautomerase activity may be involved in regulating the enol-keto tautomerism of indolepyruvate has also been investigated.

5.2.1 The keto-enol tautomerism and degradation of indolepyruvate.

Enol-keto tautomerism of the pyruvyl moiety in aromatic ketoacids has been long documented [190, 191](Fig. 5.7), with early reports on the chemical properties of

indolepyruvate being fraught with disagreement, primarily if the compound was stable as an enol-keto tautomer, or if it 'broke down' into derivative chemicals via oxidation [192–194]. Surprisingly, almost 70 years on from these initial investigations into the stability of indolepyruvate, more modern scientific methods have not fully established if this degradation of indolepyruvate occurs, or to what extent it may occur [185, 186, 195]. It was important to examine the tautomerism of indolepyruvate and its possible breakdown, to clarify the chemical state of the compound used in the immune investigations outlined previously.

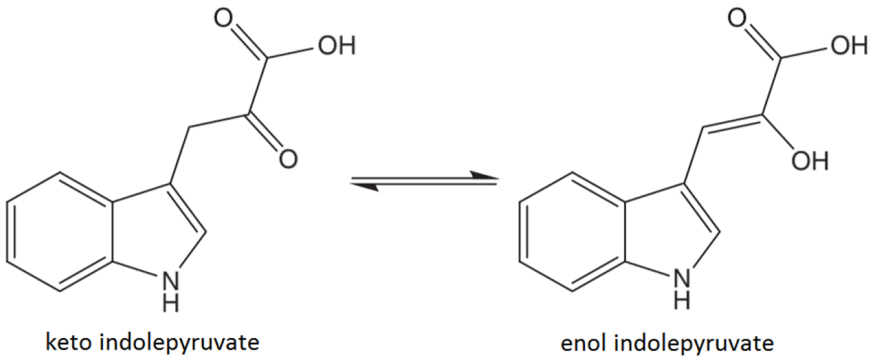

Figure 5.7. Chemical structures of keto and enol forms of indolepyruvate.
The two tautomeric structures on indolepyruvate. Interconversion of the tautomers occurs on the pyruvyl moiety attached to the indole ring.

5.2.2 Initial investigations of indolepyruvate, and other aromatic ketoacids.

AHADH assay of indolepyruvate and phenylpyruvate in culture media.

To test the viability of the AHADH assay for assaying aromatic ketoacids in culture media, fresh solutions of 2 mM indolepyruvate, 2 mM phenylpyruvate, and 2 mM hydroxyphenylpyruvate were prepared in HMI-9 culture media + 10% FCS, and the pH of each solution was adjusted to pH 7.5. The media was placed in a 37 ^{o}C incubator and was assayed after a 30 min period using the AHADH assay, as described in the materials and methods chapter. The solution was then returned to the incubator, and assayed again at a 24 hour time point.

The AHADH assay, which is specific for the aromatic ketoacid keto tautomers, revealed that after 24 hours incubation at 37 ^{o}C, the keto forms of both phenylpyruvate

and hydroxyphenylpyruvate were detectable at levels similar to those obtained after the 30 min assay (Fig. 5.8). Strikingly, the keto tautomer of indolepyruvate was almost undetectable after 24 hours. It is possible that the keto tautomer had reverted back to the enol tautomer. If this reversion to the enol tautomer does occur, then perhaps the enol tautomer is further degraded to other products that are undetectable by this assay. It is unusual that both ketonic hydroxyphenylpyruvate and phenylpyruvate are still present after 24 hours when indolepyruvate is not, though they have been previously noted to be relatively stable in their ketonic form aqueous solutions at similar time points to those outlined here [196, 197]. These phenylpyruvates do also undergo oxidative degradation, generating benzaldehyde and oxalate derivatives [198]. The AHADH assay used here is almost instantaneous, which reduces but does not eliminate the error produced by the gradual conversion of aromatic ketoacid to aromatic hydroxyacid when the aromatic ketoacid becomes limiting as a substrate (Fig. 5.9).

1D ^{1}H-NMR spectra of indolepyruvate keto and enol forms.

As the AHADH assay could not detect the enolic forms of the aromatic ketoacids, it could not be used to quantify the contribution of enol tautomers to the overall concentration of indolepyruvate. Attempts were made to develop a 1D ^{1}H-NMR technique that could be used to easily and reliable quantify indolepyruvate, regardless of its tautomeric state, in various solutions. This would encompass an ability to identify both keto and enol tautomers of indolepyruvate. The identification and quantification of indolepyruvate production by *T. brucei* in culture media using 1D ^{1}H-NMR proved too difficult, as was the identification and quantification of pure indolepyruvate that had been prepared in culture media. Amongst the complex spectra of the culture media it was almost impossible to separate and identify either tautomer of indolepyruvate. As a consequence, 1D ^{1}H-NMR could not be used to quantify the relative ratio of either keto or enol tautomer in culture media. Alternatively, to demonstrate the two different tautomeric forms of indolepyruvate, pure indolepyruvate (powdered, enolic [199]) was dissolved in acetonitrile and examined via 1D ^{1}H-NMR. This yielded the classical spectra of enolic indolepyruvate (Fig. 5.10), as has been described elsewhere [195]. The experiment was then repeated using a different solvent, in this case a phosphate buffer. Indolepyruvate was dissolved in 100 mM phosphate buffer with 10% D_2O and obtaining

a ^{1}H-NMR spectra immediately (Fig. 5.11a), then acquiring a second spectra after the sample had been allowed to sit at room temperature for 12 hours (Fig. 5.11b). In this instance, both enolic and ketonic forms of indolepyruvate were observed, though the keto spectra was difficult to obtain in as 'clean' a state as the enol spectra (Fig. 5.11). Interestingly, the conversion of enol to keto form would be expected to be reflected by the conversion of the enol singlet at 6.81 ppm to the keto singlet peak at 4.24 ppm, but this was not observed; instead, a vast decrease in the enol singlet is evident, but only a minor appearance of the keto singlet occurs. Further experiments that were performed to investigate this disparity are outlined below. A full table of the spectral shifts of each tautomeric form obtained in these experiments are outlined in Fig. 5.12.

^{1}H-NMR was also employed to better understand the rates of interconversion from enol to keto forms in solution, at various pH. It had been noted that when indolepyruvate was prepared in either slightly acidic or basic buffers (pH 6.9 and pH 8) as opposed to pH 7.5, the development of the orange/red colour associated with keto tautomer appeared to form at a faster rate at a more basic pH (Fig. 5.13). The ability of basic buffers to accelerate the formation of the keto tautomer of hydroxyphenylpyruvate has been observed previously, and so this was predicted to be the same for indolepyruvate [190]. To investigate this further, samples of indolepyruvate were prepared in 100 mM phosphate buffer with 10% D_2O ranging from pH 6.8 - 9, and spectra were recorded every 30 min for 16 hours at 20 ^{o}C. Sample data was then arrayed and processed with Mestronova^{TM} software, including peak integrations. The change from enol to keto was apparent, with the multiple peaks in the aromatic region (7 - 8 ppm) changing (Fig. 5.14). Analysis of the data obtained was of mixed practicality, as elements of the data did not match the expected transition from enol to keto indolepyruvate. The disappearance of the peaks at 6.81, 7.87, and 7.94 ppm seemed to indicate that the enol form was being converted to the keto form of indolepyruvate (Fig. 5.15a, 5.15e, 5.15f). Calculating the half-lives of these curves confirmed that increasing the pH reduced the time taken to shift from the enol to keto indolepyruvate (Table 5.1), however, the rates were not consistent amongst the different shifts. In addition, many of the shifts in the aromatic region did not appear to change significantly (Fig. 5.15b, 5.15c, 5.15d), although this region is crowded and peaks were difficult to integrate separately. It could also be possible that the aromatic region would not alter significantly, as the benzene portion of the indole ring is far removed from the active pyruvyl moiety. Focusing on

the keto indolepyruvate shifts, the appearance of peaks at 4.24, 7.17, and 7.27 ppm indicate keto indolepyruvate formation. Unusually, the prime identifying singlet at 4.24 ppm was rapidly formed then seemed to disappear (Fig. 5.16a). By contrast, two other keto associated peaks form rapidly and are maintained with time (Fig. 5.16b, 5.16e). Again, the shifts associated with the aromatic benzene element of the indole ring maintain their peak intensities, likely for the reasons explained previously (Fig. 5.16c, 5.16d, 5.16f). When the enol and keto singlets (6.81 and 4.24 ppm, respectively) were plotted side by side (Fig. 5.17), it appeared to indicate that the enol form was being converted to the keto form, and subsequently the keto from was disappearing. It was predicted that the disappearance of the enol singlet would instead lead to a proportional increase in the keto singlet (Fig. 5.18). This further conflicts with the apparent stability of the shifts of the benzene ring. Overall, it seemed to indicate that the enol form was being converted to the keto form of indolepyruvate, which was subsequently being rapidly converted to some other unknown compound.

To clarify whether or not the keto form of indolepyruvate was being formed then degraded in this manner, the AHADH assay was employed. Indolepyruvate was prepared in 100 mM phosphate buffer at pH 6.8 and 8, and assayed every 20 min for 12 hours, during which time the two samples were incubated at 37 ^{o}C. Again, it was evident that the more basic pH produced a faster rate of enol to keto conversion (pH 6.8 $V_o \approx 1.9 \times 10^{-3}$ ΔAbs.min^{-1}, pH 8 $V_o \approx 4.2 \times 10^{-3}$ ΔAbs.min^{-1}). As with the ^{1}H-NMR, the keto tautomer was formed then tapered off gradually (Fig. 5.19). However, the keto tautomer did so at a slower rate than that which was indicated by the ^{1}H-NMR data. The faster rate of the keto decrease monitored by ^{1}H-NMR can be interpreted as an artifact of the hydrogen-deuterium exchange of the labile protons of the pyruvyl moiety, which seems to occur at a faster rate for the keto form of indolepyruvate. This is a consequence of the use of a buffer containing D_2O, which provided the exchangeable deuterium. When the proton is swapped for deuterium on the C1 carbon (Fig. 5.12), the signal at this position disappears, as deuterium is 'invisible' in a ^{1}H-NMR spectra. The increase in absorbance at the start of the AHADH assay, reflected by the negative portion of the graph, can be attributed to moderate absorbance by the indolic ring of enol indolepyruvate at the 340 nm wavelength used [197, 200]. Combining the two data sets suggested that indolepyruvate could be degrading to new compound(s) with similar aromatic ring structure.

Table 5.1. Half-lives (hours) of select enolic indolepyruvate peaks.

	pH			
ppm	6.8	7.4	8	9
6.8	5.06	2.65	2.53	1.88
7.87	3.78	2.31	2.21	2.36
7.94	3.51	2.04	1.92	2.36
Avg. half-life	4.11	2.33	2.22	2.2

5.2.3 NMR identification of indolepyruvate breakdown products.

Finally, attempts to identify any possible indolepyruvate breakdown products were undertaken, in collaboration with Dr. Paul Evans (Centre for Synthesis and Chemical Biology, UCD). Solutions of indolepyruvate (2 mM) were prepared in 100 mM phosphate buffers at pH 6.8 and 8, then incubated for 24 hours at 37 ^{o}C. Following incubation, the samples were extracted at their initial pH, and additionally at highly acidic and highly basic pH using dichloromethane (DCM), an organic solvent, as described in the materials and methods. The rotatory evaporator dried samples were then dissolved in $CDCl_3$ and analysed via NMR. The ^{1}H-NMR revealed that each fraction appeared to primarily contain only one distinct compound, and therefore three prospective compounds were isolated (Fig. 5.20). Taking these samples and examining their carbon spectra confirmed this distinctness for two of the compounds, and suggests that the same would be found for the third compound (Fig. 5.21). Sample bio_pb_2a could be the most relevant compound to indolepyruvate breakdown, as it occurred at physiological pH and temperature conditions. Early examination of this spectra indicate the compound contains an aldehyde group, evident by singlets at 10.1 ppm in the ^{1}H spectra and 185 ppm in the ^{13}C spectra, and an indole ring (Fig. 5.20b and 5.21). Compound bio_pb_2b was generated by rapidly acidifying the remaining fraction 2a and extracting the compound in DCM. It can be positively identified as indoleacetic acid, most prominently by its characteristic singlet at 3.8 ppm (3.65 ppm in D_2O and DMSO [201]), corresponding to position 1 in Fig. 5.12. The carbon spectra of bio_pb_2b is almost identical to that available in the HMDB database (HMDB00197), which further supports the identification of this compound as indoleacetic acid (Fig.

5.21) [201]. Finally, when a ^{1}H spectra of compound bio_pb_2b was 'spiked' with pure indoleacetic acid (powder, Sigma Aldrich), an increase in the peak integrals is observed when the spectra is re-run (Fig. 5.22). It is not clear how indoleacetic acid could be generated directly from indolepyruvate, as its production is normally catalysed enzymatically [202, 203]. The third compound, bio_pb_2c, remains unidentified as it was obtained in lower amounts than either the neutral or acidic indolepyruvate extractions. Further work is needed to fully characterise and conclusively identify these compounds.

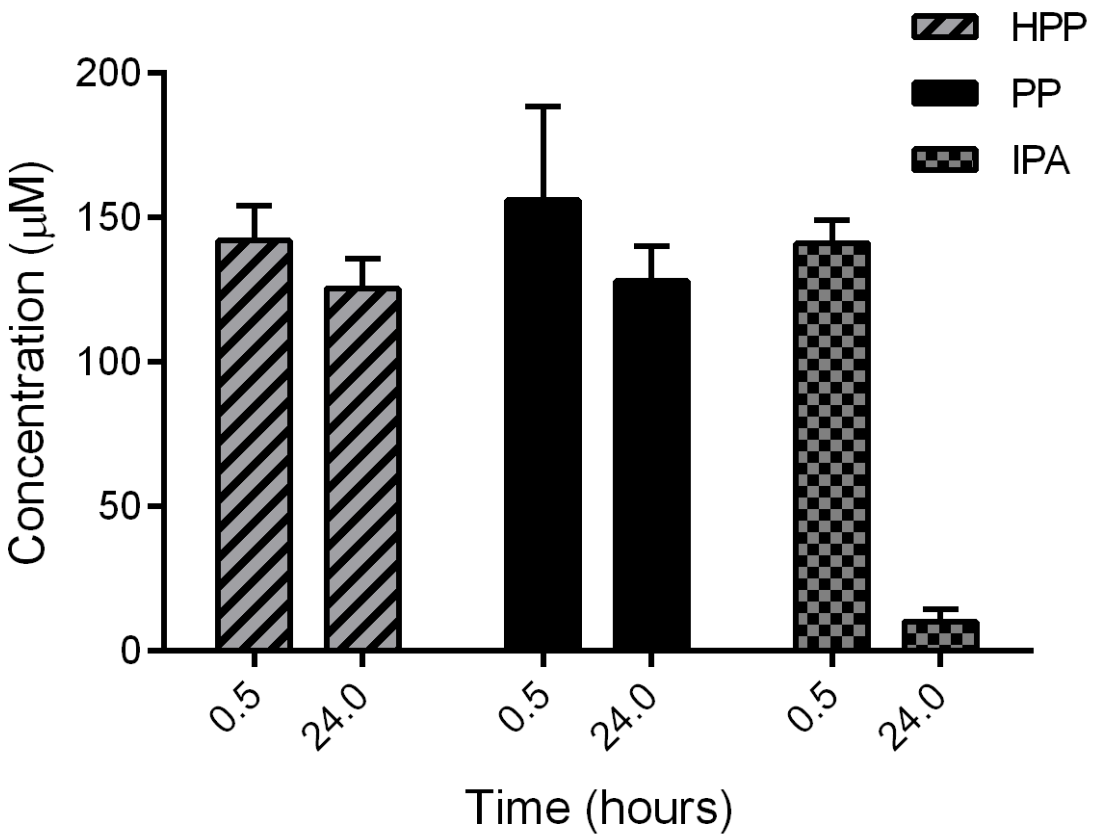

Figure 5.8. Concentrations of indolepyruvate, hydroxyphenylpyruvate, and phenylypyruvate in culture media at different time points.

(a) The detectable concentrations of the keto forms of hydroxyphenylpyruvate (HPP), phenylpyruvate (PP), and indolepyruvate (IPA), after incubation for 30 min and 24 h at 37 ^{o}C, as measured by AHADH assay. Solutions were prepared in HMI-9 culture media. Samples were assayed as 1:10 dilutions of an original 2 mM concentration in each case. Error bars indicate SD, triplicate measurements.

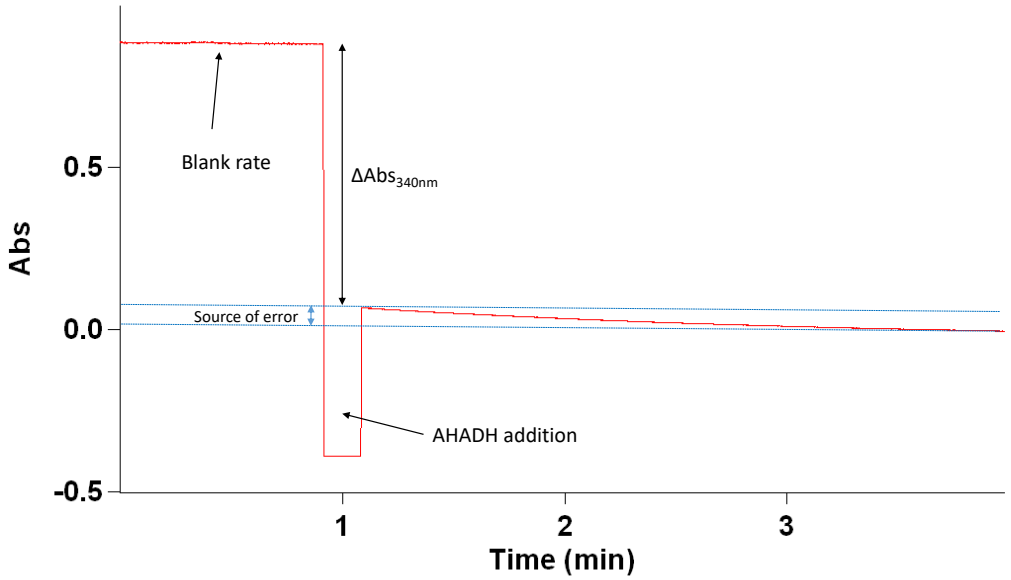

Figure 5.9. Representative example of the AHADH assay used to quantify the keto tautomers of the aromatic ketoacids.

This trace shows the detection of keto indolepyruvate after 30 min incubation at 37 ^{o}C using the AHADH assay. A blank rate is obtained, in the presence of the assay buffer, NADH, and indolepyruvate in solution. The AHADH enzyme is then added promptly, and the change in absorbance (ΔAbs_{340nm}) can be used to quantify the concentration of the keto tautomer of the aromatic ketoacid. The source of error in these measurements is highlighted.

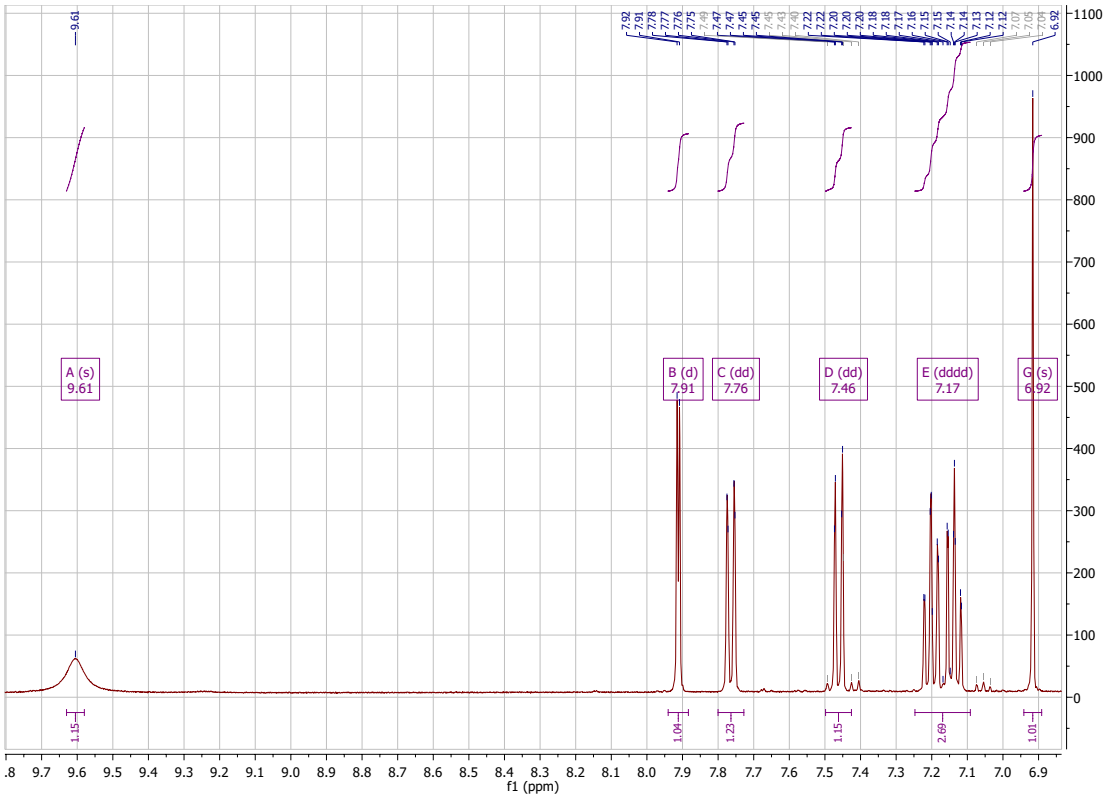

Figure 5.10. ^{1}H-NMR spectra of enolic indolepyruvate in deuterated acetonitrile. This spectra shows that indolepyruvate is in its enolic form when supplied as a pure powder (Sigma Aldrich), under these conditions. The spectra is identical to that obtained previously [195]. Spectra acquired in Spectra acquired in a 400 MHz strength field.

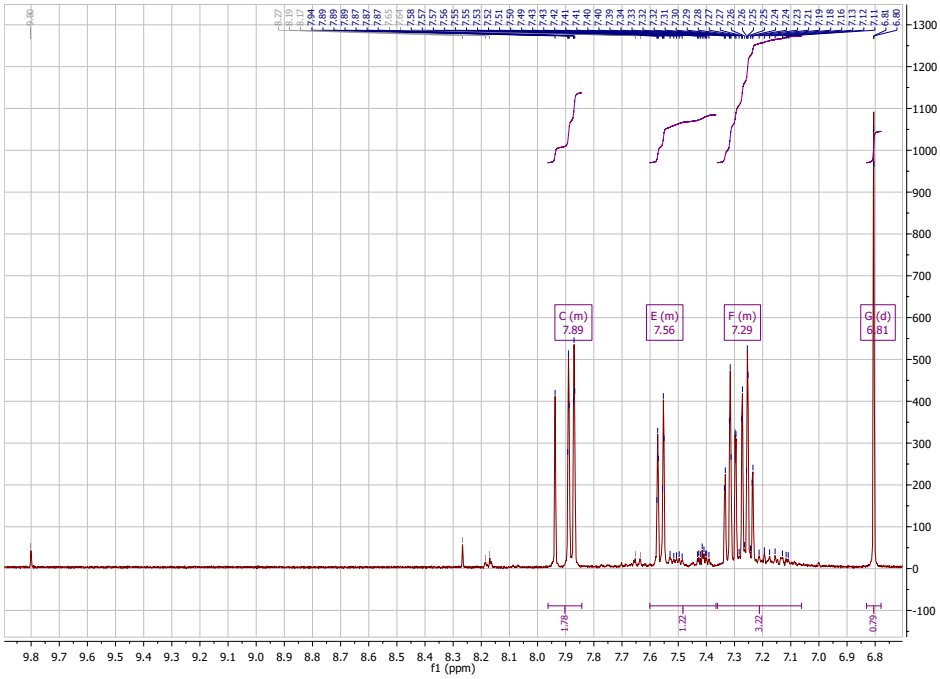

(a) Enol tautomer of indolepyruvate.

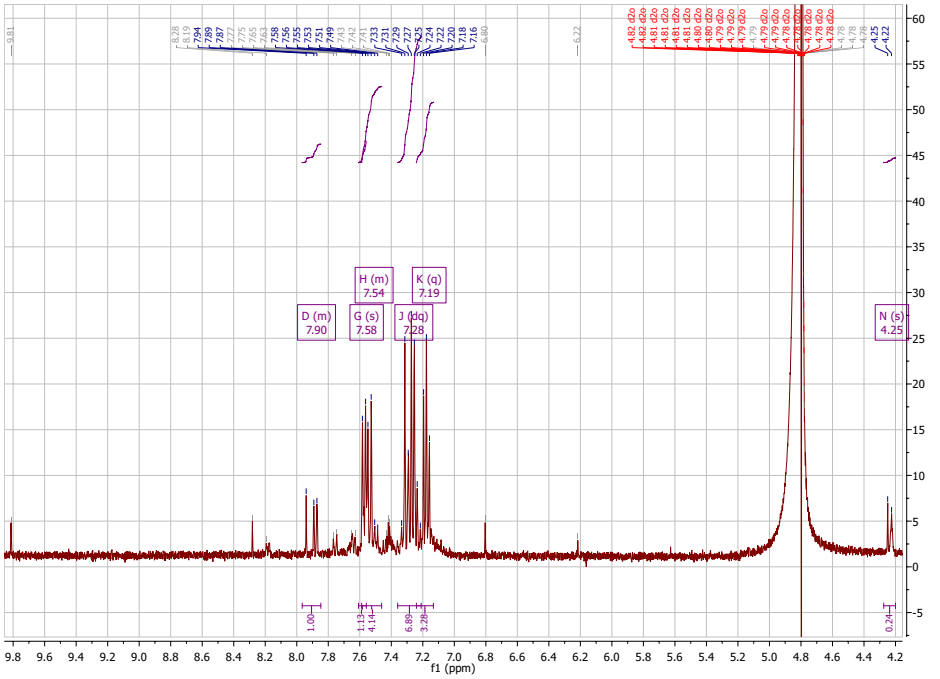

(b) Keto tautomer of indolepyruvate.

Figure 5.11. ^{1}H-NMR spectra of enolic and ketonic indolepyruvate.
(a) ^{1}H-NMR spectra of enol form indolepyruvate. The key identifier of the enol form is the singlet at 6.81 ppm. **(b)** ^{1}H-NMR spectra of the keto form of indolepyruvate. The keto form is primarily identified by the singlet at 4.24 ppm (some contaminating enol form can still be seen in this spectra). Spectra obtained in a 400 MHz strength field. Indolepyruvate was prepared in a 100 mM phosphate buffer with 10% D_2O.

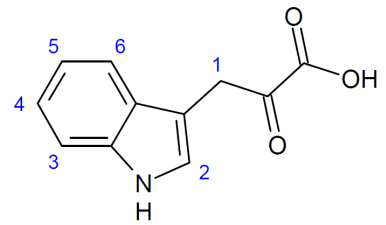

Keto form

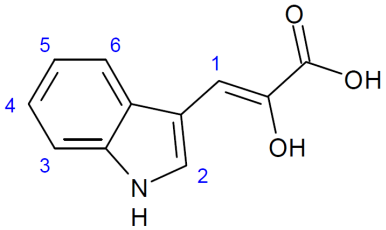

Enol form

	Indolepyruvate assignments		
	Position	Shift (ppm)	Multiplicity
keto	1	4.24*	singlet
	2	7.31	singlet
	3	7.56	doublet
	4	7.27	triplet
	5	7.17	triplet
	6	7.52	doublet
enol	1	6.81*	singlet
	2	7.94	singlet
	3	7.55	doublet
	4	7.31	triplet
	5	7.25	triplet
	6	7.87	doublet

Figure 5.12. ^{1}H-NMR shift and multiplicity assignments for keto and enol tautomers of indolepyruvate.

Summary figure and table of the ^{1}H-NMR chemical shifts of both indolepyruvate tautomers, in 100 mM phosphate buffer with 10% D_2O. The numbered positions on the indolepyruvate structures are mapped to the chemical shift table. (* indicates that trace signals can be detected in both spectra due to tautomerism).

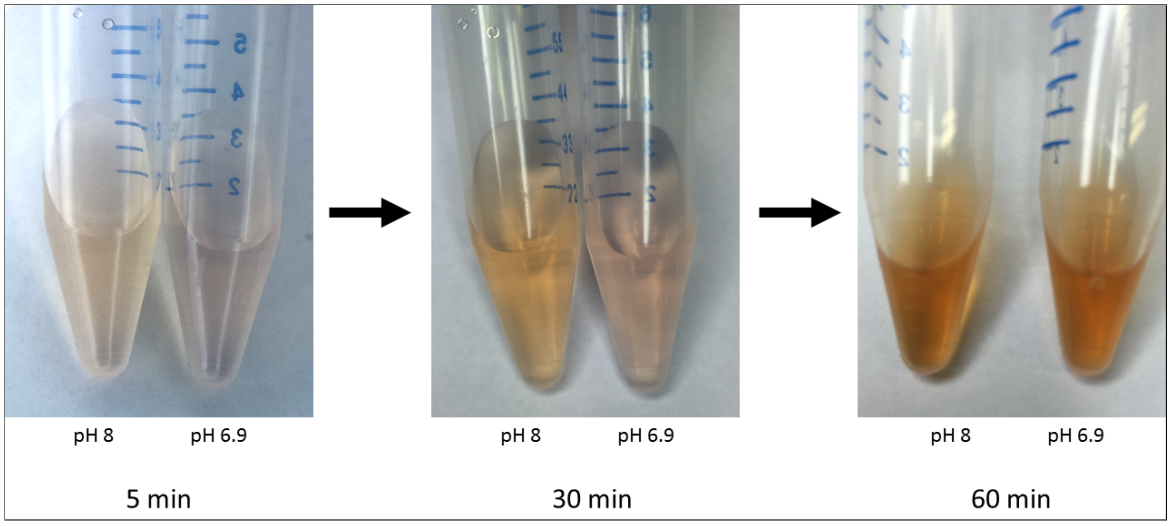

Figure 5.13. Colour changes of indolepyruvate in buffers of differing pH.
The characteristic orange/red colour associated with the keto tautomer of indolepyruvate was observed to develop at a faster rate under slightly alkaline conditions. This has similarly been observed for 4-hydroxyphenylpyruvate [190]. The samples here are of 2 mM indolepyruvate in 100 mM phosphate buffer at 37 ^{o}C, at pH 6.9 and 8, recorded at 5, 30, and 60 min time points.

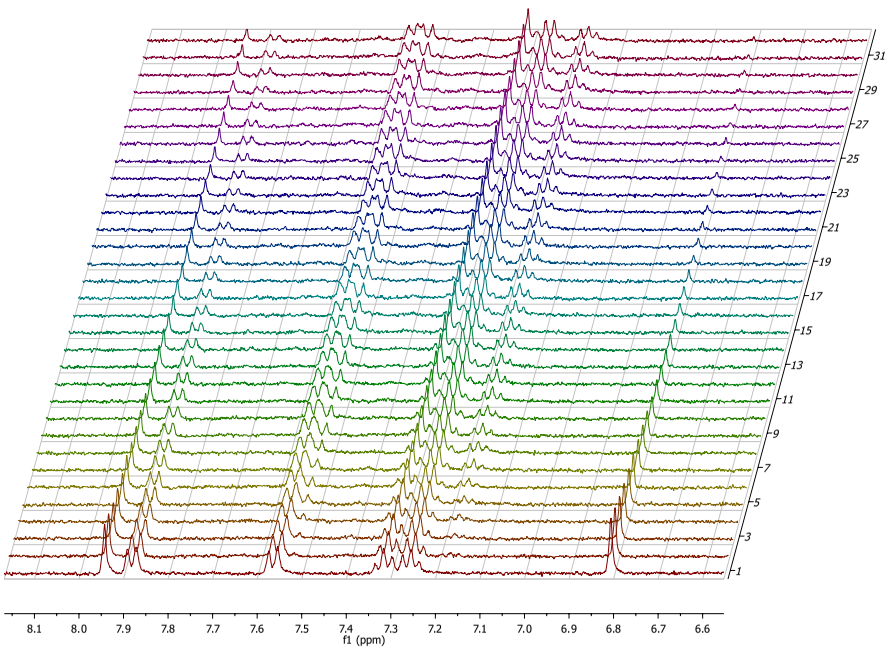

(a) 6.6 - 8.2 ppm

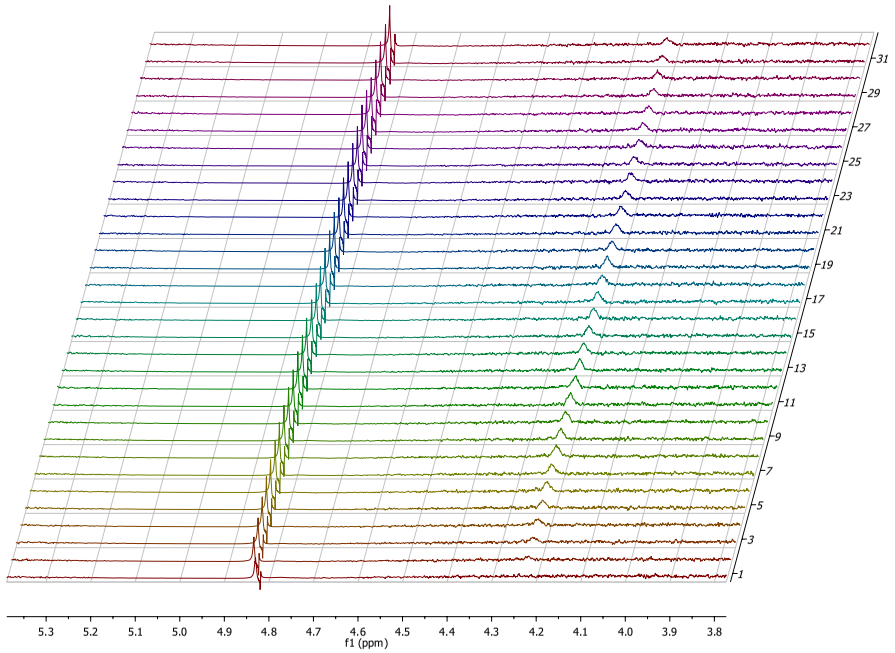

(b) 3.8 - 5.4 ppm

Figure 5.14. ^{1}H-NMR time course array of indolepyruvate.

(a) The disappearance of the enol singlets at 6.81 ppm and 7.94 ppm, and the doublet at 7.87 ppm can be clearly observed. The subsequent appearance of the keto triplet at 7.17 ppm and singlet at 7.31 ppm is also clear. **(b)** Unexpectedly, the keto singlet at 4.24 ppm is observed but is weak and does not appear in a manner that is proportional to disappearance of the 6.81 ppm enol singlet. This is most likely a result of the exchange of labile protons with deuterium from D_2O in the buffer.

Representative time course conducted at pH 7.4, each increment on the y-plane indicates 30 min. The peak at $\approx$ 4.8 can be attributed to HOD (semi-deuterated H_2O).

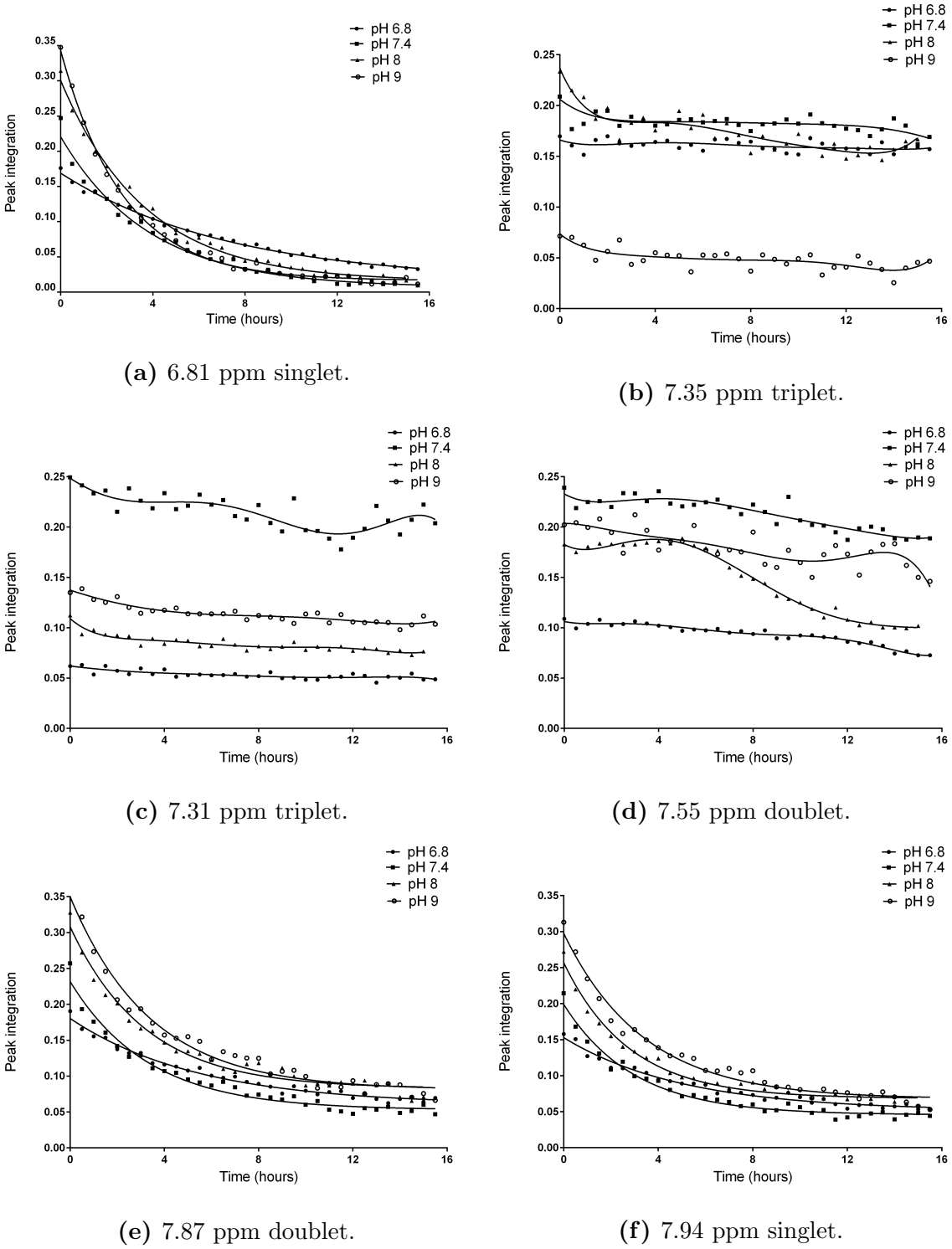

(a) 6.81 ppm singlet.

(b) 7.35 ppm triplet.

(c) 7.31 ppm triplet.

(d) 7.55 ppm doublet.

(e) 7.87 ppm doublet.

(f) 7.94 ppm singlet.

Figure 5.15. Peak integrations for enolic indolepyruvate.

Full set of integrations for the chemical shifts assigned to enolic indolepyruvate, at varying pH, over a 16 hour period.

All shifts referenced internally to 50 μM tetramethylsilane (TMS) at 0 ppm. Further conditions for spectra acquisition are outlined in the materials and methods.

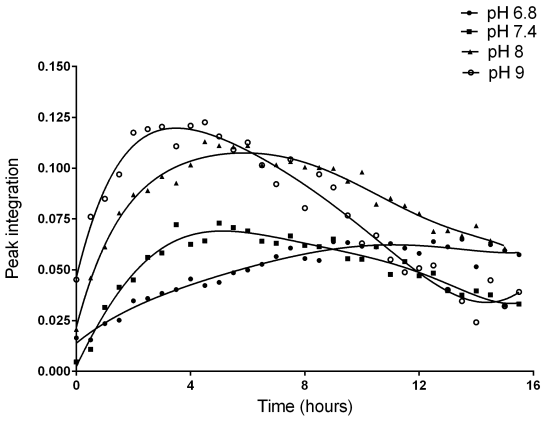

(a) 4.24 ppm singlet.

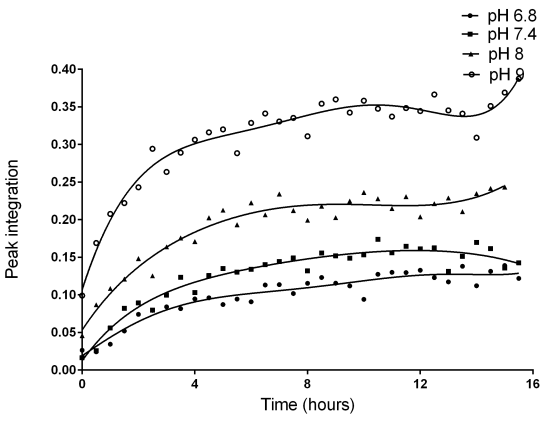

(b) 7.17 ppm triplet.

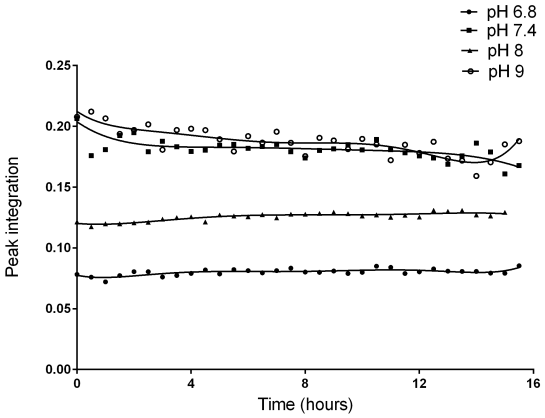

(c) 7.27 ppm triplet.

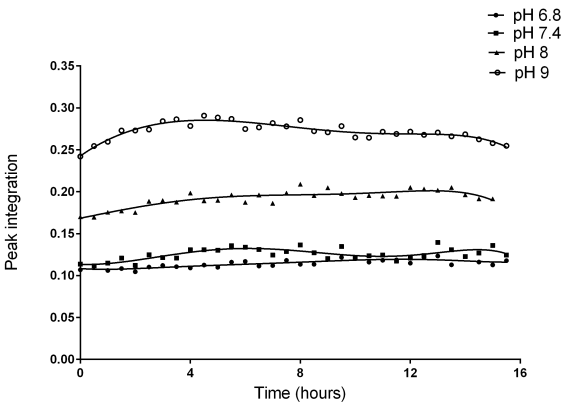

(d) 7.31 ppm singlet.

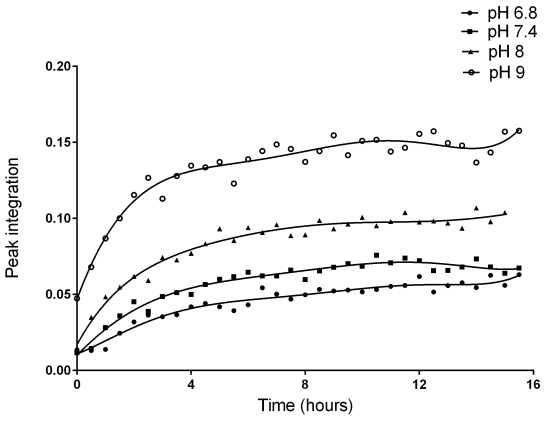

(e) 7.52 ppm doublet.

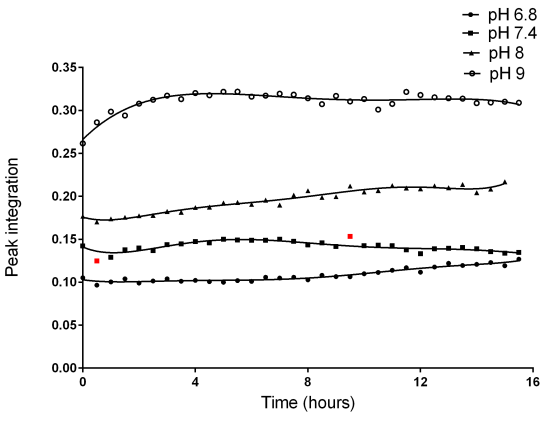

(f) 7.56 ppm doublet.

Figure 5.16. Peak integrations for ketonic indolepyruvate.

Full set of integrations for the chemical shifts assigned to ketonic indolepyruvate, at varying pH, over a 16 hour period.

All shifts referenced internally to 50 μM tetramethylsilane (TMS) at 0 ppm. Further conditions for spectra acquisition are outlined in the materials and methods.

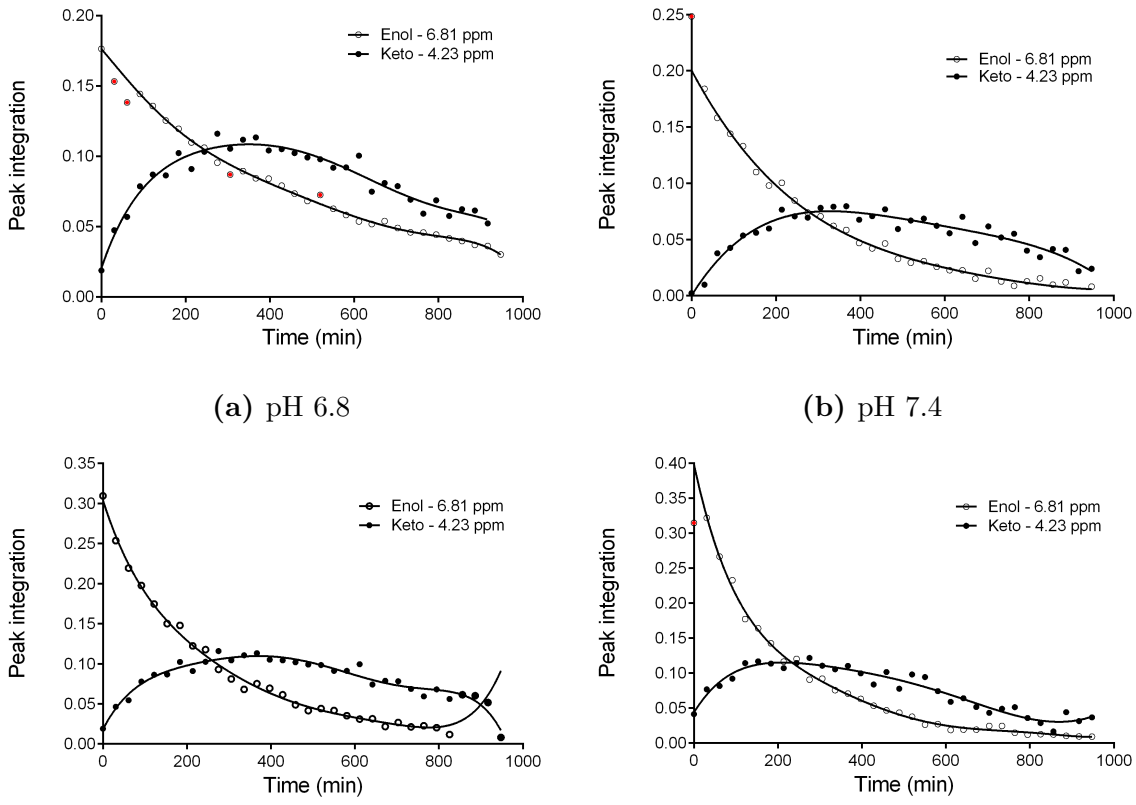

(a) pH 6.8 **(b)** pH 7.4

(c) pH 8 **(d)** pH 9

Figure 5.17. Comparative peak integrations of enol (6.81 ppm) and keto (4.24 ppm) singlets at varius pH.

Set of integrations for the chemical shifts assigned to the enol and keto singlets of indolepyruvate, at various different pH, over a 16 hour period.

All shifts referenced internally to 50 μM tetramethylsilane (TMS) at 0 ppm. Further conditions for spectra acquisition are outlined in the materials and methods.

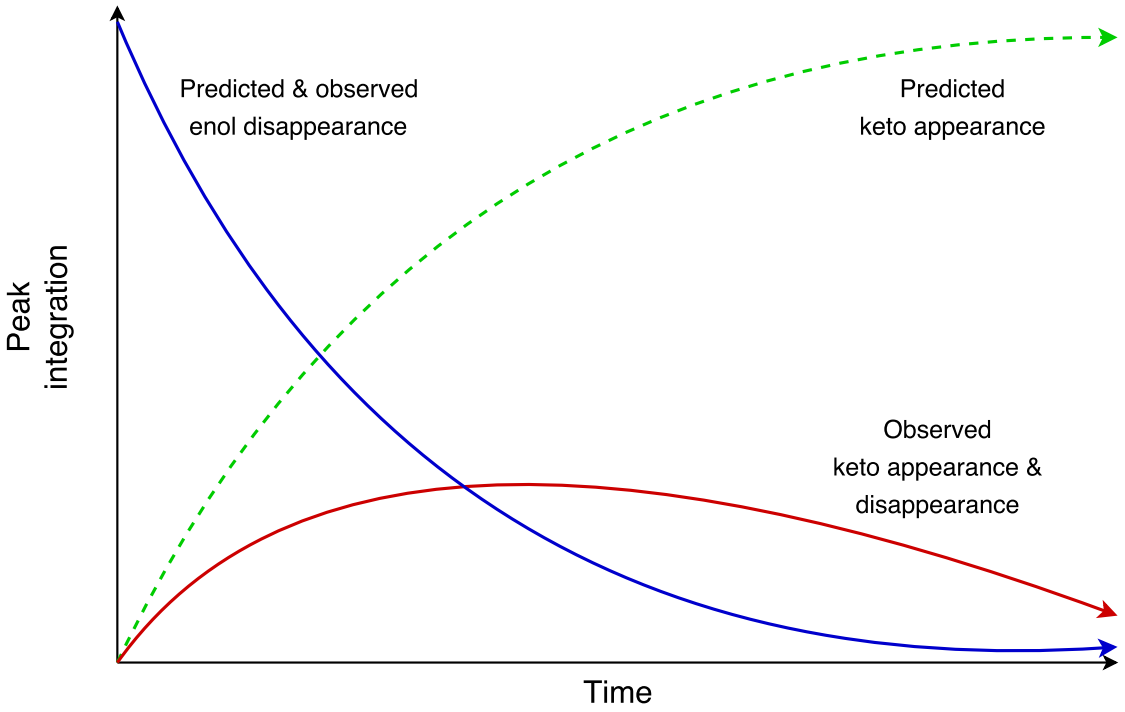

Figure 5.18. The predicted peak integrations for the enol (6.81 ppm) and keto (4.24 ppm) singlets of indolepyruvate.

This diagram represents the predicted integration curve of enol to keto conversions of indolepyruvate, when monitored at the enol (6.81 ppm) and keto (4.24 ppm) singlets. As the enol tautomer is converted to the keto tautomer, a proportional increase in the keto singlet was expected. Instead, a small increase and disappearance of the keto peak was observed as the enol peak disappeared.

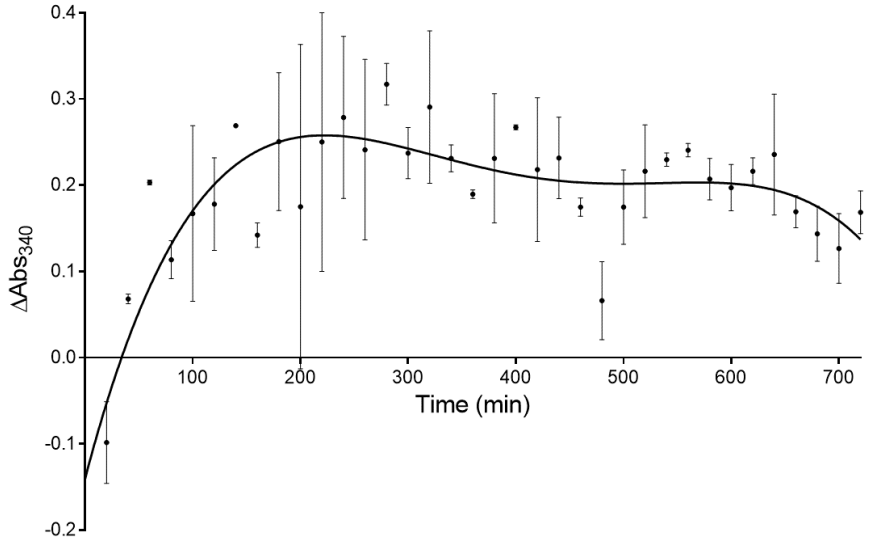

(a) pH 6.8

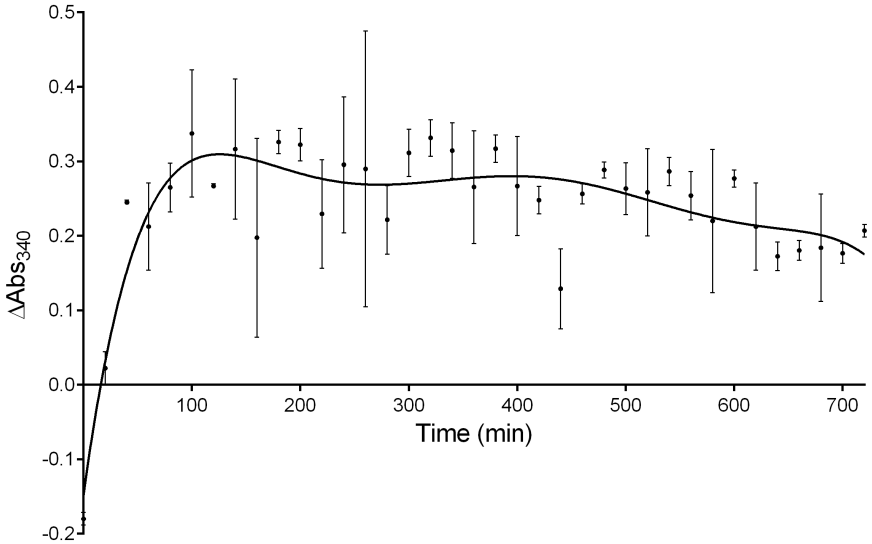

(b) pH 8

Figure 5.19. The conversion of enol to keto indolepyruvate at pH 6.8 and pH 8 as measured via AHADH assay.

The conversion of enolic indolepyruvate to ketonic indolepyruvate at mildly acidic and mildly basic pH over a 12 h period, as assessed via AHADH assay.

Error bars indicate SD, duplicate measurements.

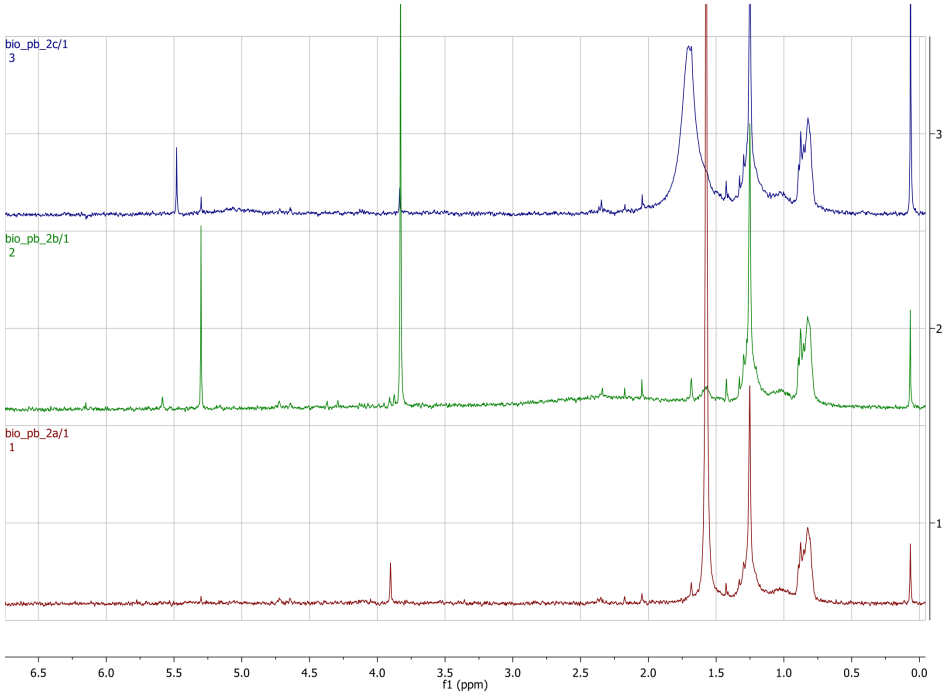

(a)

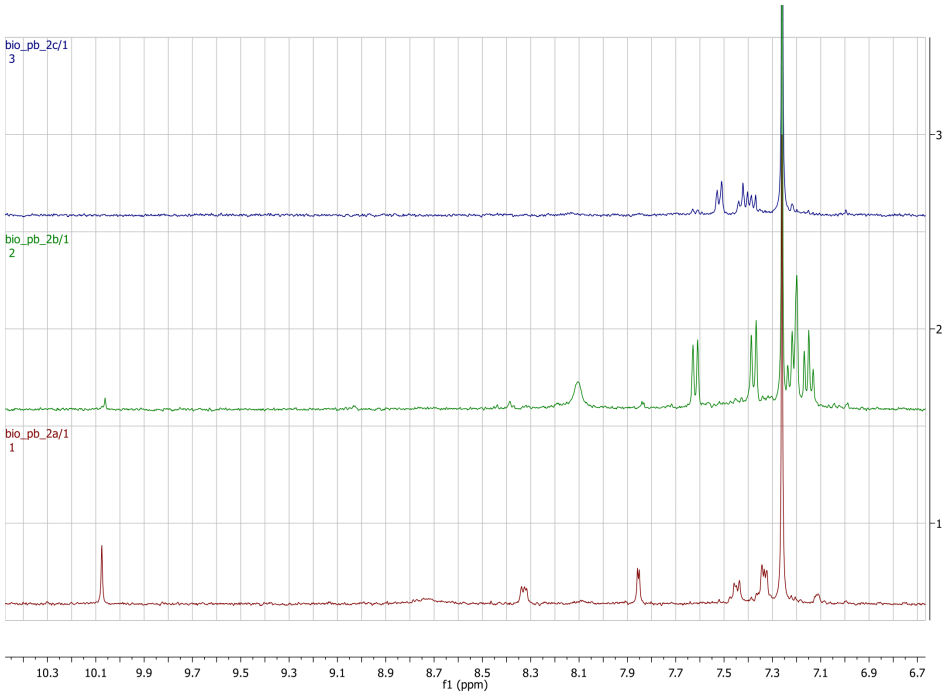

(b)

Figure 5.20. ^{1}H-NMR spectra of three isolated indolepyruvate breakdown products.

(a) $0 - 6.7$ ppm, **(b)** $6.7 - 10.4$ ppm. The three spectra obtained from the pH 8 extract (bio_pb_2a), the acidified fraction (bio_pb_2b), and the basic fraction (bio_pb_2c). Three different compounds are present, none of which appear to be indolepyruvate, with some small cross-contamination observed between the samples. Spectra obtained in a 400 MHz strength field.

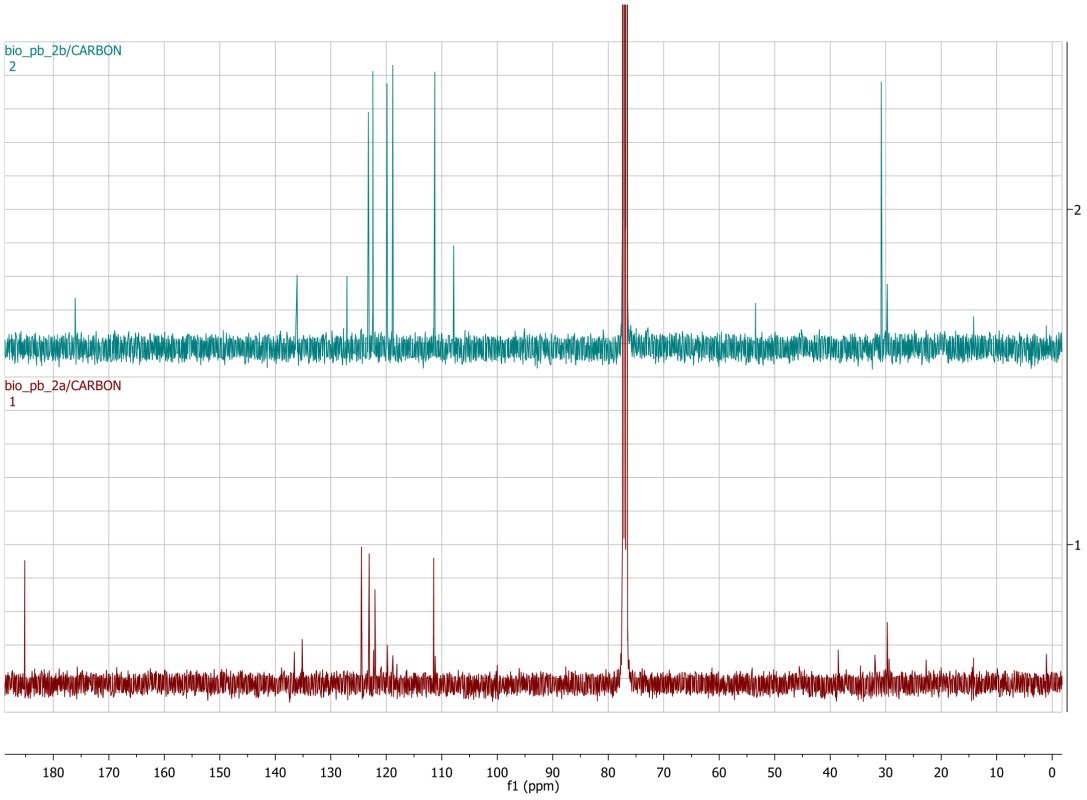

Figure 5.21. ^{13}C-NMR spectra of compounds bio_pb_2a and bio_pb_2b.
Carbon NMR spectra obtained of the normal (bio_pb_2a) and acidified (bio_pb_2b) fractions of indolepyruvate 'breakdown'. The spectra confirm the presence of two different compounds. Sample bio_pb_2a contains an aldehyde group, but remains unidentified. Sample bio_pb_2b is almost certainly indoleacetic acid. Not enough sample was available to obtain a spectra for the basic fraction (bio_pb_2c).

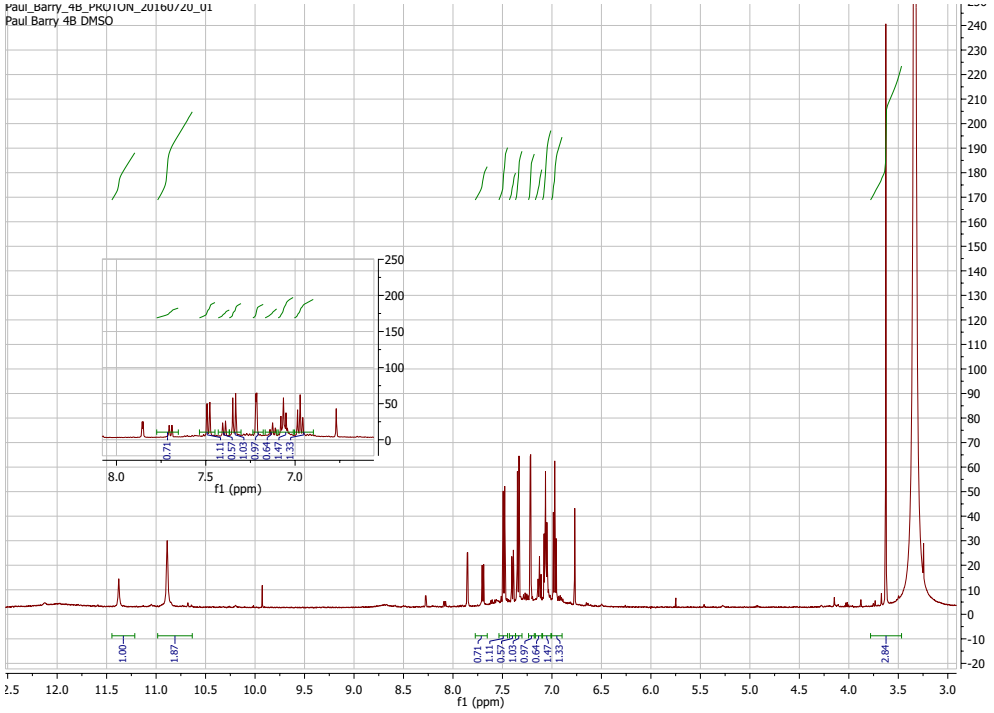

(a) pre-spiked sample.

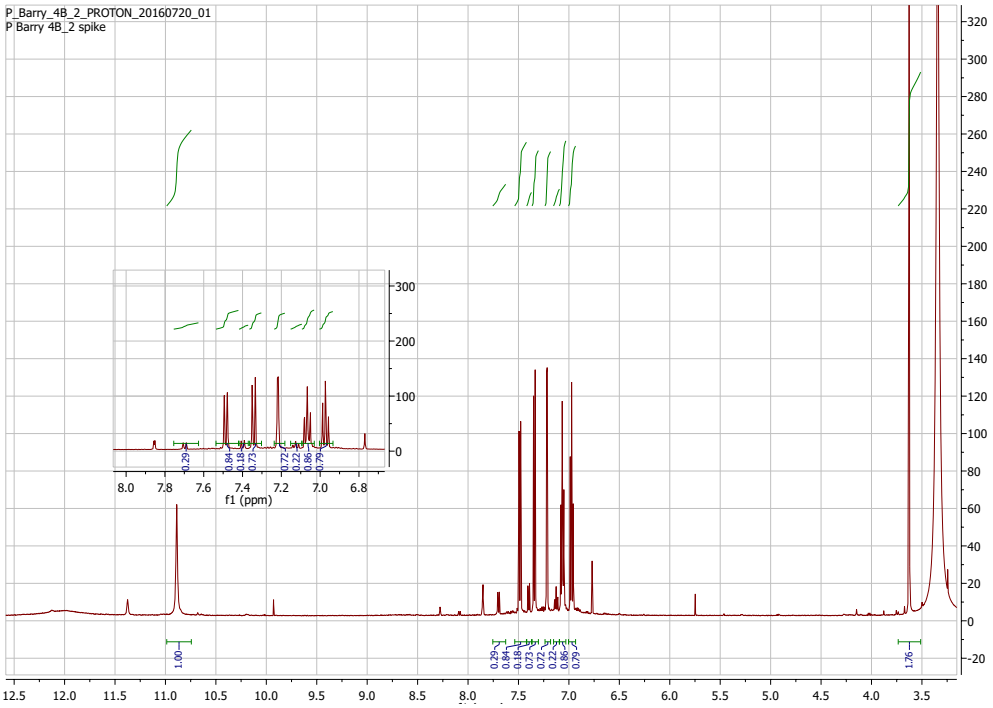

(b) spiked sample.

Figure 5.22. ^{1}H-NMR spectra of bio_pb_2b (indoleacetic acid). **(a)** bio_pb_2b observed by ^{1}H-NMR, prior to 'spiking' with indoleacetic acid. **(b)** The re-run spectra obtained after bio_pb_2b had been spiked with indoleacetic acid. The increase in the peak size at the exact positions of spectra (a) confirm that bio_pb_2b is indoleacetic acid.

5.2.4 The macrophage cytokine MIF is a minor indolepyruvate tautomerase.

MIF is a circulating pro-inflammatory cytokine released by multiple immune cells of both innate and adaptive immune systems, that seems to function primarily by reducing the anti-inflammatory effects of the glucocorticoids [204]. In 1996, Rosengren et al. discovered the MIF could function as an efficient tautomerase for D-dopachrome, but curiously not for its physiological L-dopachrome stereoisomer [189]. Shortly after, the same researchers demonstrated that MIF was a tautomerase for both hydroxyphenylpyruvate and phenylpyruvate [141]. Interestingly, no 'natural' substrate for the tautomeric functions of MIF has been described to date [205]. The finding that bloodstream forms of *T. brucei* secrete two of the few known substrates for the tautomerase activity of MIF, hydroxyphenylpyruvate and phenylpyruvate, raised the question of whether indolepyruvate might also undergo MIF catalysed tautomerisation. There were also implications for the possible role of MIF in host parasite interactions given the potential anti-inflammatory effects of indolepyruvate and the stability of this ketoacid within the host. It was speculated that MIF may catalyse the conversion of the enol form of indolepyruvate to its keto form, as had been observed with the other aromatic ketoacid substrates of MIF. Therefore an investigation of indolepyruvate as a potential substrate for MIF, and the possible role this may play in host-parasite interaction, was undertaken.

5.2.5 Indolepyruvate is a weak substrate of MIF.

Indolepyruvate can weakly inhibit MIF in a standard D-dopachrome assay.

To establish if indolepyruvate could inhibit the tautomerase activity of MIF, a variation of the D-dopachrome assay previously described [189] was performed as outlined in the materials an methods. MIF acts to catalyse the conversion of D-dopachrome to 5,6-dihydroxyindole-2-carboxylic acid (DHICA). 100 μM of indolepyruvate was found to partial inhibit the ability of MIF to convert D-dopachrome to DHICA (Fig. 5.23), though this inhibition was not as strong as that observed for ebelson, a typical inhibitor of MIF [206]. The $\approx$ 13.1% decrease in rate between the MIF + D-dopa and MIF +

IPA + D-dopa was small but significant ($P < 0.05$), whereas ebelson (MIF + Inhibitor + D-dopa) almosst completely inhibited MIF ($\approx$ 97%). The rate of D-dopachrome conversion to DHICA by MIF shown here is much lower than previously obtained [189], and it likely low due to degradation of MIF used (many months old, long term storage in -80 ^{o}C, etc.).

^{1}H-NMR of the indolepyruvate keto-enol tautomeric function of MIF.

The classic D-dopachrome tautomerase assay revealed the indolepyruvate could weakly inhibit the ability of MIF to convert D-dopachrome to DHICA, at the 100 μM concentration that was used. What could not be inferred however, is whether indolepyruvate simply acted by binding weakly at the tautomerase active site preventing D-dopachrome binding, or if MIF could act to convert the enol to keto form of indolepyruvate or vice-versa. To help resolve this, ^{1}H-NMR was utilised. The experiments were carried out as previously shown [141], and as outlined in the materials and methods.

In a replicate study of the one of the experiments conducted by Rosengren et al., it was first demonstrated MIF was a very effective tautomerase of hydroxyphenylpyruvate, with significant conversion from enol to keto occurring at both 0 min (from the point of addition of MIF) an 90 min (Fig. 5.25), compared to samples without the addition of MIF (Fig. 5.24). The 0 min timepoint cannot be measured instantaneously in the NMR experiment, and so MIF likely converts enol hydroxyphenylpyruvate to the keto tautomer rapidly over a 30 - 60 s time frame. In the time scale of this experiment, this was taken to be as close to 0 min as was possible. When the same experiment was performed with indolepyruvate, it was found that MIF had a low ability to convert the enol to keto form of the compound (Fig. 5.27) compared to samples lacking MIF (Fig. 5.26). A slight increase can be observed in the keto peaks, including the keto aromatic region (7 - 7.7 ppm), in the IPA + MIF sample (Fig. 5.27b) compared to the IPA samples (Fig. 5.26b). Unfortunately integration of the peaks proved tricky, due to the combined effects of hydrogen exchange with D_2O previously discussed and the broad water signal (4.8 ppm) that appears with the addition of MIF. As a consequence, the data provided here for both hydroxyphenylpyruvate and indolepyruvate remains qualitative.

AHADH assay of prepared ketoacid solutions and *T. brucei* derived ketoacids ± MIF in buffer, and culture media.

The NMR data obtained with hydroxyphenylpyruvate and indolepyruvate could only be used qualitatively, and so it remained unclear as to whether MIF could act as a tautomerase of indolepyruvate. To help investigate this further, the AHADH assay was employed. Firstly, a simplified AHADH assay where 1mM each of indolepyruvate and hydroxyphenylpyruvate were incubated in PBS ± 1 μg MIF and then assayed over a short time was performed. The assay revealed that MIF can convert enol indolepyruvate to keto pyruvate, though at an order of magnitude slower rate than that obtained for enol to keto hydroxyphenylpyruvate in the presence of MIF (Fig. 5.28a). Rates obtained over this time frame indicate that the rate of enol to keto conversion of indolepyruvate was more than doubled with addition of 1 μg MIF. On its own, the IPA enol-keto conversion rate was $\approx 0.95 \pm 0.2$ μM.min^{-1}, which was increased to $\approx 1.92 \pm 0.2$ μM.min^{-1} in the presence of MIF. Interestingly, the rate of conversion of enol to keto hydroxyphenylpyruvate in PBS was $\approx 2.47 \pm 0.4$ μM.min^{-1}, 2.6 times faster than that of indolepyruvate. Extension of the length of the assay to 12 hours indicated that MIF could also stabilise the presence of keto indolepyruvate to a small degree. The levels of keto indolepyruvate are ≈ 3.5 times higher in the presence of MIF, compared to the absence of MIF (Fig. 5.28b). Again, the apparent 'dip' in concentration associated with the enol tautomer of IPA can be attributed to moderate absorbance by the indolic ring of indolepyruvate at the 340 nm wavelength used for the assay (Fig. 5.28) [197, 200].

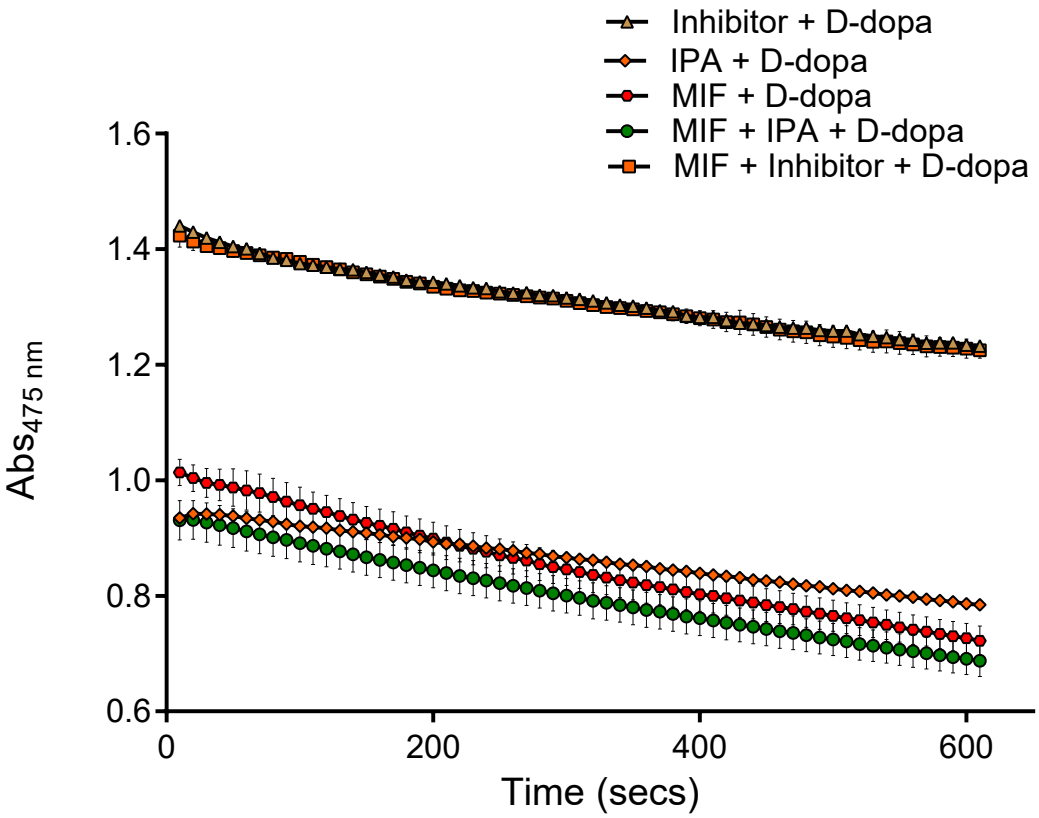

Figure 5.23. MIF D-dopachrome tautomerase assay with indolepyruvate (IPA). The rates of conversion of D-dopachrome (D-dopa) to 5,6-dihydroxyindole-2-carboxylic acid (DHICA) as measured by the decrease in absorbance of D-dopachrome at 475 nm. In the phosphate buffer used, D-dopachrome undergoes spontaneous breakdown (inhibitor + D-dopa, IPA + D-dopa). The rate of MIF + inhibitor + D-dopa was almost identical to the inhibitor + D-dopa rate ($313.9 \times 10^{-6} \pm 4.8 \times 10^{-6}$ and $306.5 \times 10^{-6} \pm 3 \times 10^{-6}$, respectively), indicating that MIF is almost completely inhibited in the presence of ebelson. Indolepyruvate (100 μM) did act to slow the rate of conversion of D-dopa to DHICA, though it did not strongly inhibit MIF; the MIF + IPA + D-dopa rate was $413.4 \times 10^{-6} \pm 10 \times 10^{-6}$, in comparison to the MIF + D-dopa rate of $476.2 \times 10^{-6} \pm 10 \times 10^{-6}$.

The MIF inhibitor used was ebeleson at a final concentration of 10 μM. Error bars indicate SD, triplicate measurements. Rates are reported as $\Delta\text{Absorbance}_{475nm}.\text{s}^{-1}$

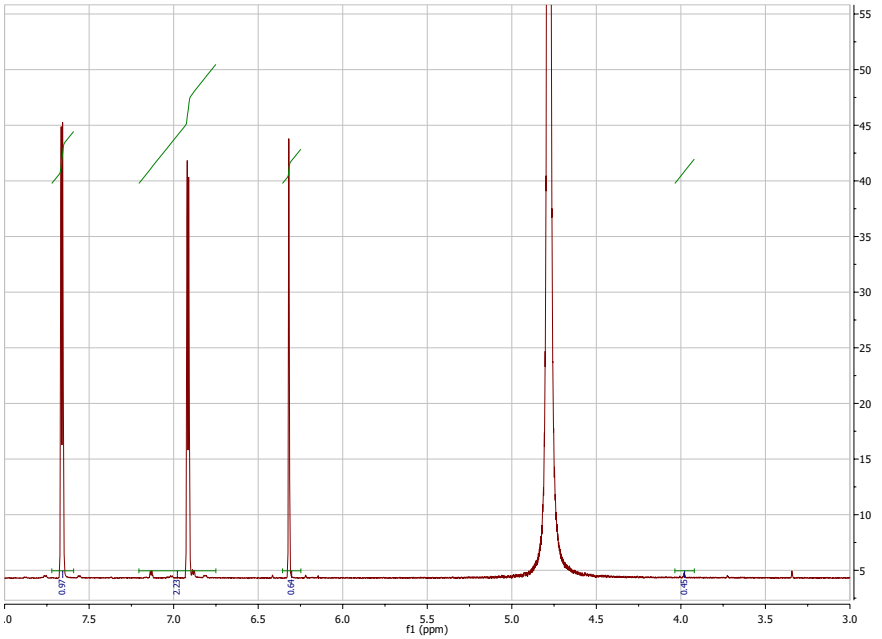

(a) HPP at 0 min

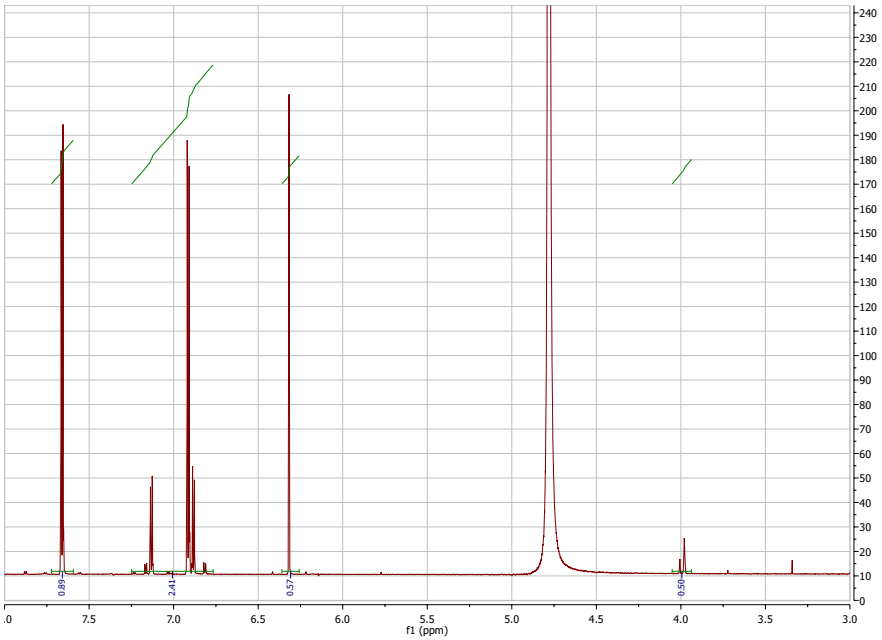

(b) HPP at 90 min

Figure 5.24. Time-dependent ^{1}H-NMR spectra of hydroxyphenylpyruvate (HPP) without MIF.

The spectra show the transition of enol to keto HPP after 90 min in the absence of MIF. The disappearance of the enol doublet and singlet at 7.66 ppm and 6.32 ppm, respectively, and the appearance of the keto singlet at 3.98 ppm can be used to monitor the tautomerism from one form to another. All shifts referenced internally to 1 mM 4,4-dimethyl-4-silapentane-1-sulfonic acid (DSS) at 0 ppm.

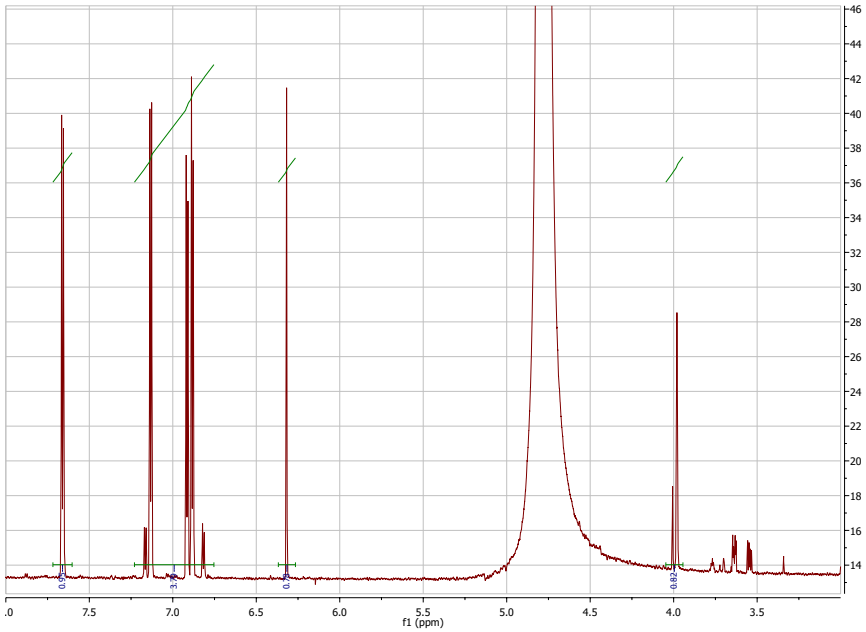

(a) HPP + MIF at 0 min

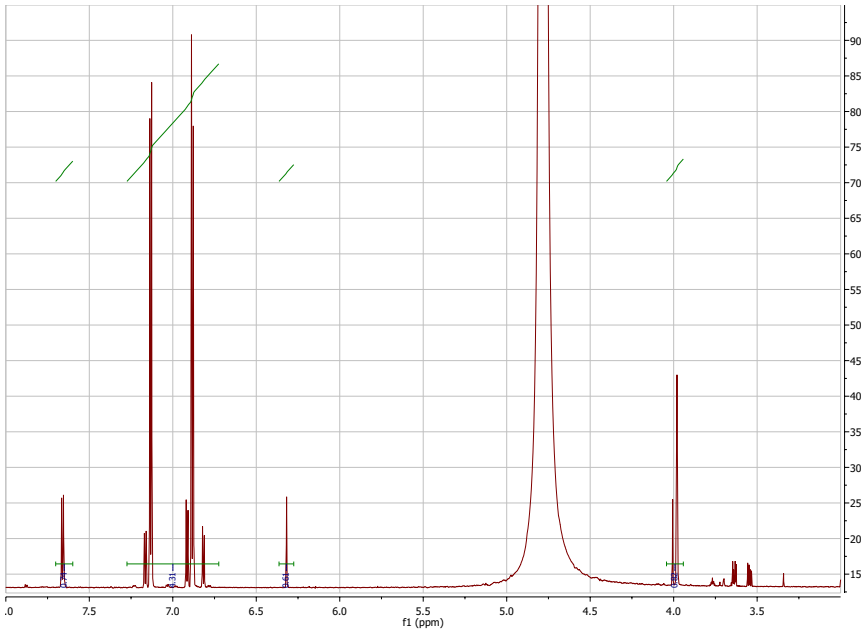

(b) HPP + MIF at 90 min

Figure 5.25. Time-dependent ^{1}H-NMR spectra of hydroxyphenylpyruvate (HPP) treated with MIF.

The spectra show the transition of enol to keto HPP after 90 min with 1 μg MIF (+ MIF). The disappearance of the enol doublet and singlet at 7.66 ppm and 6.32 ppm, respectively, and the appearance of the keto singlet at 3.98 ppm can be used to monitor the tautomerism from one form to another. It is clear that this tautomerism from enol to keto from occurs at a significantly faster rate in the presence of MIF than HPP on its own. All shifts referenced internally to DSS at 0 ppm.

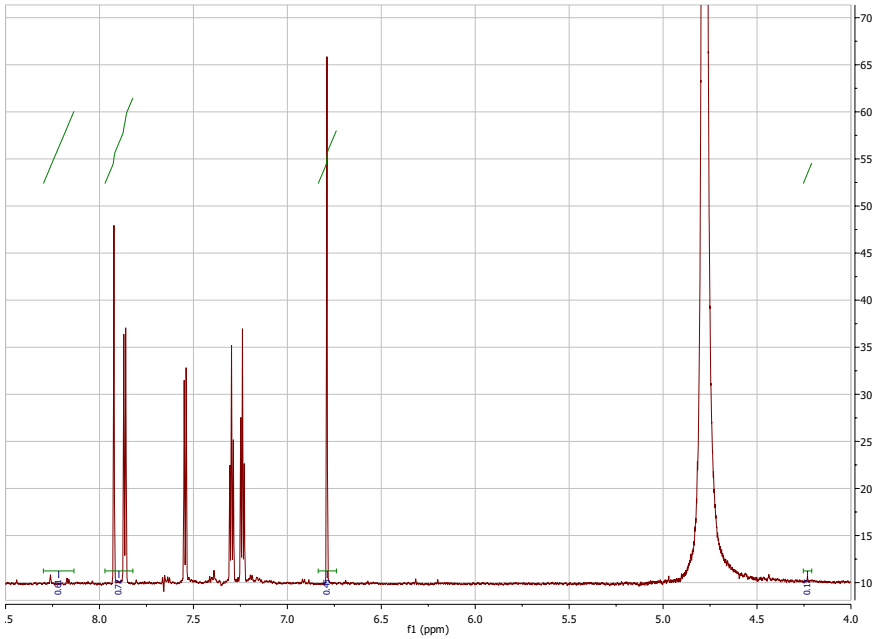

(a) IPA at 0 min

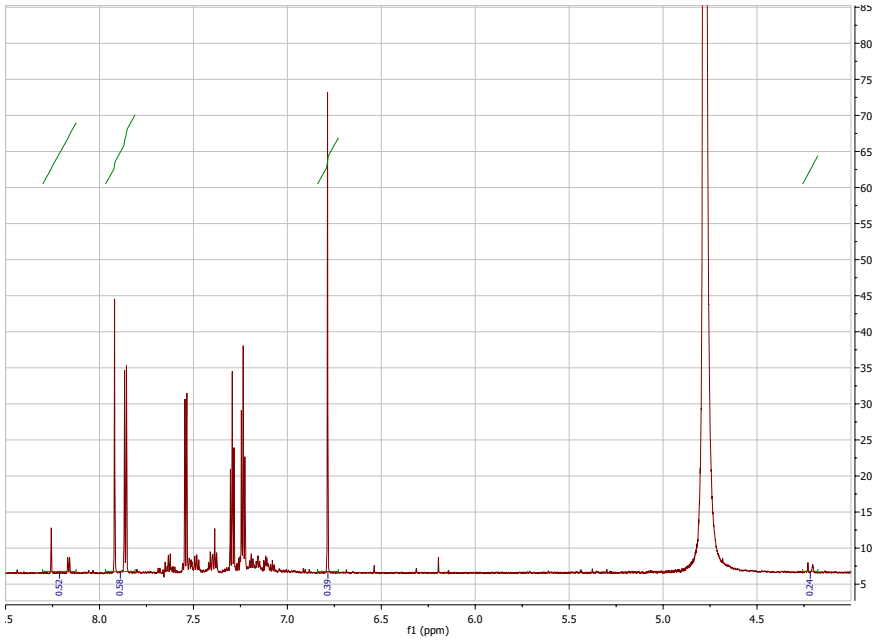

(b) IPA at 90 min

Figure 5.26. Time-dependent ^{1}H-NMR spectra of indolepyruvate (IPA) without MIF.

The spectra show the transition of enol to keto IPA after 90 min in the absence of MIF. The appearance of the keto singlet, doublet, and singlet at 8.26 ppm, 8.16 ppm, and 4.24 ppm, respectively, and the small decrease of the enol singlet at 6.81 ppm can be used to monitor the tautomerism from one form to another. All shifts referenced internally to DSS at 0 ppm.

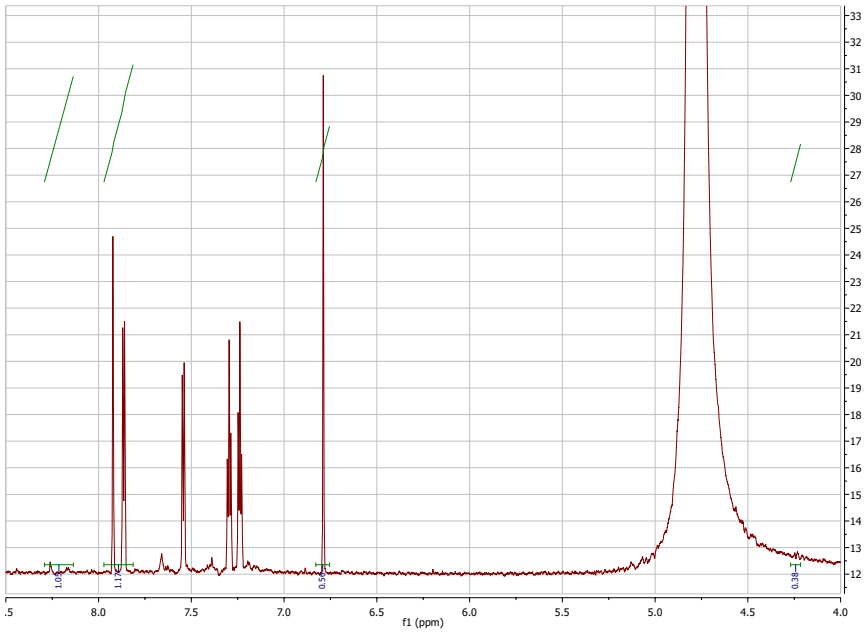

(a) IPA + MIF at 0 min

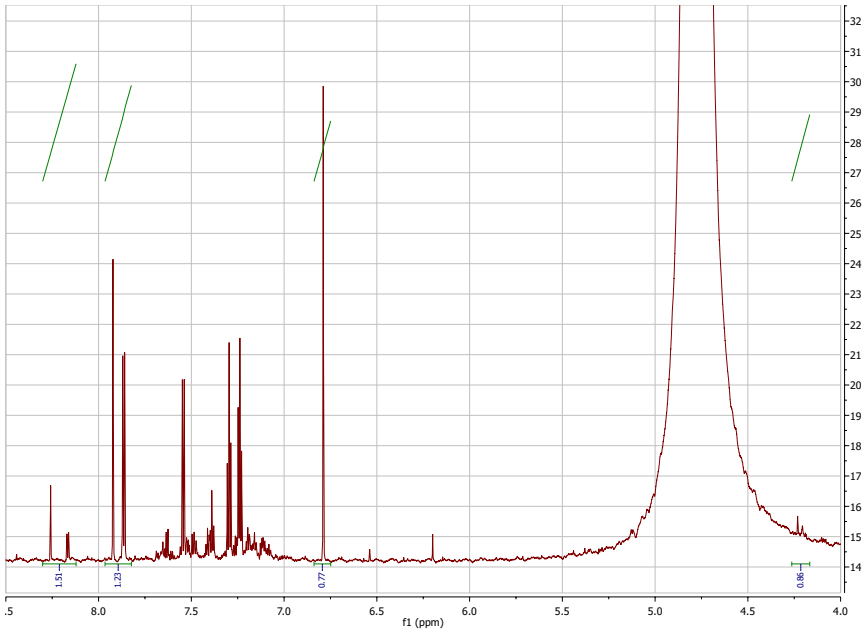

(b) IPA + MIF at 90 min

Figure 5.27. Time-dependent ^{1}H-NMR spectra of indolepyruvate (IPA) treated with MIF.

The spectra show the transition of enol to keto IPA after 90 min with 1 μg MIF (+ MIF). The appearance of the keto singlet, doublet, and singlet at 8.26 ppm, 8.16 ppm, and 4.24 ppm, respectively, and the small decrease of the enol singlet at 6.81 ppm can be used to monitor the tautomerism. The change in the rate of appearance of the keto form is minimal, although some increase in the rate in the presence of MIF appears to occur when comparing the 90 min time points. All shifts referenced internally to DSS at 0 ppm.

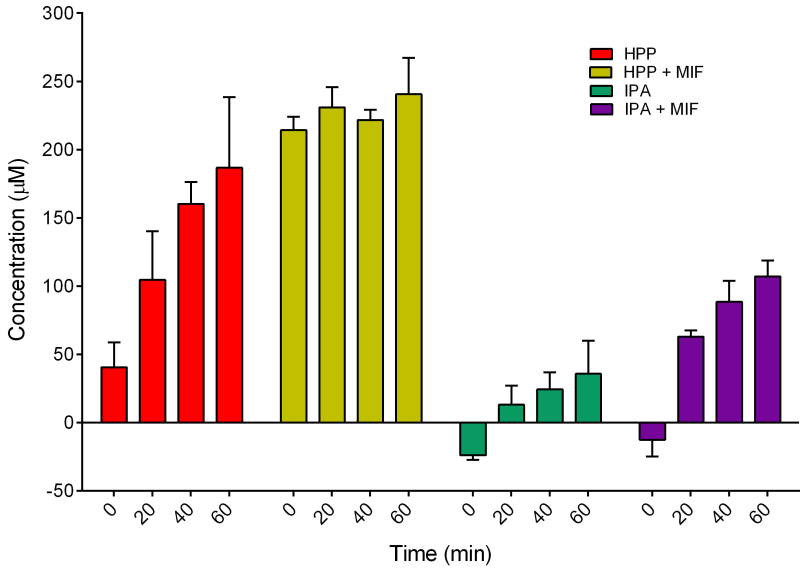

(a)

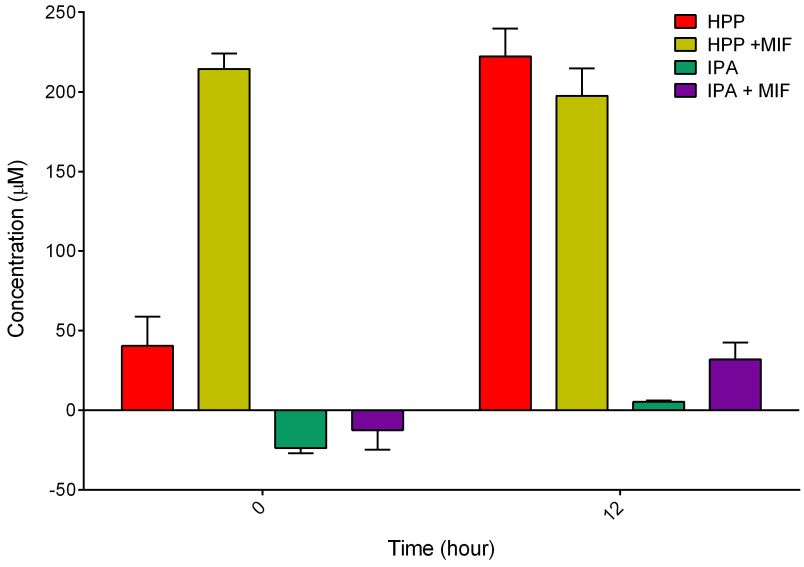

(b)

Figure 5.28. AHADH assay of the enol to keto conversion of indolepyruvate ± MIF.

The enol to keto conversion of indolepyruvate (IPA) and hydroxyphenylpyruvate (HPP) in the presence or absence of 1 μg MIF, measured by AHADH assay. **(a)** The rate of conversion of enol to keto conversion of HPP was almost instantaneous in the presence of MIF. MIF also increased the rate of enol to keto conversion of IPA. **(b)** The concentration of keto IPA is higher in the presence of MIF after a 12 hour incubation period.

Assays performed as outlined in the materials and methods. Solutions maintained at 20 ^{o}C. Concentrations represent a 1 in 4 dilution of a 1 mM solution of each ketoacid in the assay. Error bars indicate SD, triplicate measurements.

5.3 Discussion.

5.3.1 *T. brucei* cASAT also functions to convert aromatic amino acids to aromatic ketoacids.

Aromatic ketoacids are secreted by bloodstream form *T. brucei*. These aromatic ketoacids are produced as a consequence of aromatic amino acid deamination by TbcASAT. The amino groups from these deamination reactions are proposed to be used to generate aspartate and glutamate for metabolic purposes, a role which is supported by the enzymatic, functional, and metabolic data presented so far. Oxaloacetate appears to be the preferred amino group acceptor by TbcASAT when aromatic amino acids act as the amino group donors. Labelling of uracil and adenosine suggest the aspartate generated by oxaloacetate transamination is used for pyrimidine biosynthesis and purine salvage. It is proposed here that secretion of aromatic ketoacids produced from aromatic amino acid deamination could have a role in suppression of the host innate inflammatory response. Stibbs and Seed first reported the conversion of radiolabelled tryptophan into 'tryptophol' by *T.b. gambiense*, and suggested it could act as a possible sleep mediator in late stage CNS infections in the host [102]. Interestingly, they also suggest that tryptophan deamination could be used to generate glutamate to allow for converions of pyruvate to alanine, as a pyruvate detoxification function. However, they did not directly identify the enzyme that was responsible for this metabolism of tryptophan.

It was established that the concentrations of aromatic ketoacids in the blood sera of *T. brucei* infected rats (ranging in concentration from $0.2 - 0.5$ mM) were elevated significantly over baseline levels (below 100 μM). It is possible that during *T. brucei* infection, any newly produced tryptophan and phenylalanine (essential amino acids), or synthesised tyrosine (non-essential amino acid) would be almost immediately utilised by *T. brucei* for further aromatic ketoacid production. To reach the concentrations observed in the sera of rats reported here, the aromatic ketoacids likely persist in the blood and are constantly supplemented by the continuous production of new aromatic ketoacids by the parasite. El Sawalhy et al. also noted a significant increase of aromatic ketoacids (53.3 μM indolepyruvate, 117.3 μM hydroxyphenylpyruvate, 134.3 μM phenylpyruvate) in the urine of mice infected with *T. gambiense*, that increased linearly

with parasitemia [111]. The data on the concentration of aromatic ketoacids in rat sera obtained here was with a peak parasitemia ten times lower than that reported by El Sawalhy et al. ($\approx 1.5 \times 10^9$ cells.ml^{-1}), and so it is possible that circulating aromatic ketoacids could reach even higher concentrations in systemically infected animals. It is also possible that aromatic ketoacids have been filtered out by the hosts kidneys prior to urine excretion, which could explain the differences in concentration between the urine and sera. Importantly, this data was used to establish suitable concentration ranges of aromatic ketoacids to be used for subsequent immunological investigations.

5.3.2 Indolepyruvate secreted by *T. brucei* has a role in suppressing the host innate inflammatory response.

Aromatic ketoacids are significantly elevated in the bloodstream of the *T. brucei* infected host. Treatments of LPS stimulated murine BMDMs with varying concentrations of indolepyruvate (similar to concentrations likely to be experienced at or close to the peak of parasitemia) revealed that indolepyruvate could reduce the production of pro-IL-1β, a cytokine that is responsible for a pro-inflammatory response and is produced by macrophages. It was also demonstrated that the aromatic ketoacids secreted by *T. brucei* could similarly suppress pro-IL-1β production. Modulation of the host inflammatory response in this manner could be beneficial to the host in preventing a systemic inflammatory response at high parasitic loads, while also reducing the effectiveness of the immune response against the parasite, allowing it to proliferate and survive. Innate immune response modulation by the *T. gambiense* secretome has already been demonstrated [207]. The authors show that dendritic cells treated with the *T. gambiense* protein secretome are inhibited in their maturation, and production of IL-6, IL-10, and TNF-α are inhibited. The anti-inflammatory effects of indolepyruvate, hydroxyphenylpyruvate, and phenylpyruvate, have also been demonstrated to have a protective effect against UV-B induced damage on the skin of hairless mice [187]. Indolepyruvate was found to be more potent than hydroxyphenylpyruvate or phenylpyruvate in suppressing the production of IL-1β by UV-B irradiated keratinocytes, although in all cases high concentrations (5 - 25 mM) of the aromatic ketoacids were used. Inhibition of pro-IL-1β production by LPS-stimulate BMDMs has been achieved here with much lower concentrations (0.25 - 1 mM) of indolepyruvate. More generally, indolepyruvate

has been extensively studied for its anti-oxidant properties, playing roles in preventing free radical damage, serotonin regulation, and the prevention of mutagen damage [173]. Most research indicates an increase in inflammatory cytokines, including IL-1β, is observed in the host during infection with *T. brucei* [120, 208]. ELISA measurements of circulating cytokines in the blood of *T. brucei* infected rats revealed a significant elevation of TNF-α, IFN-γ, IL-6 and IL-1β [208]. Interestingly, Sileghem et al. observed a 20 - 30 fold increase in IL-1 secretion whilst only a two-fold increase in IL-1 production was observed from macrophages isolated from *T. brucei* infected mice [120]. Sileghen et al. do not provide a distinction between measurements of IL-1β and IL-1α, however, and does not provide extensive experimental methods. Given the elevated production of these cytokines during *T. brucei* infection, the effects of indolepyruvate on the host inflammatory system may be to suppress a 'hyper' inflammatory response and a lower the levels of expressed inflammatory cytokines.

The data outlined here was further developed with the Inflammation Research group [172]. In addition to the suppression of pro-IL-1β production, it was found that treatment of BMDMs with indolepyruvate prevented the LPS induced increase of glycolysis in these cells, an effect that was not observed with hydroxyphenylpyruvate and phenylpyruvate. Alteration of the glycolytic rate in these cells appeared to be HIF1-α dependent, and so this pathway was investigated further. Indeed, HIF1-α degradation was increased by indolepyruvate at higher indolepyruvate concentrations and in an AhR-independent manner. It was surmised that the crucial glycolytic shift required for macrophage activity in response to LPS stimulation was prevented by indolepyruvate, leading to the hydroxylation of HIF1-α and its targeting for proteosomal degradation. This degradation in turn prevents the production of pro-IL-1β by activated macrophages. The precise function of subsequent IL-1β reduction remains unknown. It is suggested here that this reduction may important at high levels of parasitemia, where indolepyruvate levels would also be high. The increased levels of indolepyruvate may act to suppress, but not eliminate, the inflammatory response of the host. This suppression would beneficial to the host and would allow the parasite to proliferate successfully.

5.3.3 Aromatic ketoacids secreted by *T. brucei* can suppress inflammatory cytokines and induce HO-1 expression in mixed glial cells.

T. brucei and its subspecies, *T. gambiense* and *T. rhodesiense*, have varying but potent effects on the host neural functions during the later stages of the disease, which is a consequence of invasion of the CNS by these parasites [16]. The mechanisms by which the parasite crosses the blood brain barrier (BBB) and the purpose of CNS invasion are not entirely understood [209]. Interestingly, it has been observed that increased secretion of IFN-γ by T cells promoted CNS invasion by *T. brucei* [210]. The same study also notes a significant increase in the levels of IL-1β, IL-6, IL-10, and TNF-α in the brains of infected mice. Clearly a robust innate immune response can be mounted within the CNS, but an over-active response could cause severe damage to the host. As noted by Bentivoglio et al., the parasite must carefully balance survival and proliferation in the host without damaging or killing the host [209]. It was established that indolepyruvate secreted by *T. brucei* may act to inhibit the host macrophage activation by inhibiting the LPS induced glycolytic increase in a HIF1-α dependent manner [172]. This in turn leads to a decrease in the expression of the inflammatory cytokine IL-1β demonstrated here.

Exploring a similar role for *T. brucei* and within the context of the CNS, it was found that pro-IL-1β production in LPS stimulated mixed glial cells could be suppressed by indolepyruvate secreted by *T. brucei*, but not by hydroxyphenylpyruvate or phenylpyruvate. This was similar to previous results in BMDMs, where indolepyruvate was the sole aromatic ketoacid found that could reduce pro-IL-1β production of LPS-activated macrophages [172]. However, both indolepyruvate and hydroxyphenylpyruvate suppressed LPS induced TNF-α production in mixed glia (unpublished data), and all three aromatic ketoacids suppressed IL-6 production (Table 5.2). TNF-α has been shown to be produced by macrophages when co-cultured with *T. gambiense*. Interestingly, the authors note that following an initial increase in TNF-α after 24 hours of co-culture, there is a subsequent decrease in TNF-α after a 48 hour period [211]. Perhaps at an increased parasite load the corresponding increase in indolepyruvate and hydroxyphenylpyruvate could reduce some of the expression of TNF-α. This could be important to the parasite, as TNF-α can lyse *T. brucei* [211]. Interestingly, this lytic

effect was only observed in bloodstream form cells isolated at the peaks of parasitemia [212]. Furthermore, TNF-α expression can be detected via PCR in brains isolated from *T. brucei* infected mice [213]. Taken together, it is possible that all three aromatic ketoacids may play roles in suppressing an inflammatory response withn the host CNS. The effects of the aromatic ketoacids on IL-10, an anti-inflammatory cytokine that is expressed by the host in response to *T. brucei* infection, are currently being investigated [114, 214].

It is interesting that LPS stimulated BMDMs treated with indolepyruvate displayed a reduction in pro-IL-1β alone, yet LPS stimulated mixed glial cells treated with indolepyruvate have a more extensive reduction of TNF-α, IL-6, and pro-IL-1β. Perhaps the different environments of these cells can explain these differences in cytokine suppression; it seems reasonable that suppression of an inflammatory response in the brain and CNS of the host would be more crucial to the host than the same response in the vascular system. There is some evidence to support this possibility. Infection of two different stains of mice with *T. brucei* yielded broadly different cytokine responses in each strain. The authors note that in both strains, however, a higher expression of IL-1β, TNF-α, IL-6, and IFN-γ in the brains of the infected mice compared to the spleens of these mice as measure by qPCR [210].

Table 5.2. Aromatic ketoacids can suppress different inflammatory cytokines in mixed glial cell populations.

LPS stimulated mixed glial cells were shown to have decreased levels of select cytokines with differing aromatic ketoacid treatments (ranging from 0.25 - 1 mM), as measured by ELISA. The response was dose dependent in each case.

Indolepyruvate	Hydroxyphenylpyruvate	Phenylpyruvate
IL-6	IL-6	IL-6
TNF-α	TNF-α	-
pro-IL-1β	-	-

It has also been demonstrated here that HO-1 is potently induced by all three aromatic ketoacids, and that spent media supernatants from cultured *T. brucei* also induces HO-1 expression. Furthermore, the use of the AHADH$^{in.}$ cells confirms that this is an effect of aromatic ketoacid secretion and not other secreted factors from the parasite. Research on the related *T. cruzi* parasite has shown that HO-1 is involved

in promoting parasite host invasion of cardiac tissue [215]. When HO-1 was inhibited, myocarditis was increased while parasitemia was decreased in mice. Conversely, expression of recombinant HO-1 or induction of wild type HO-1 lead to an increase in tissue parasitemia but lower overall levels of inflammatory cytokine expression. The authors speculate that HO-1 may be exploited by *T. cruzi* to promote a dampening of the innate immune response, thereby reducing the burden on the host while allowing for parasite survival and proliferation. Similar research on *Leishmania* and *Plasmodium* has demonstrated that HO-1 knockout mice had higher parasite loads and expressed greater levels of inflammatory cytokines than wild type infections [216, 217]. Notably, no study has proposed precisely what parasite factors are responsible for the induction of HO-1 during an infection. The data here suggests that HO-1 may be up-regulated by the aromatic ketoacids secreted by *T. brucei*, though the pathway by which they act is not yet clear. Early data has indicated that the IFNAR and JAK-STAT signalling pathways may play a role. Mixed glia cells from IFNAR knockout mice displayed a reduced ability to up-regulate HO-1 expression in response to indolepyruvate stimulation (personal communication, Glyn Williams). IFNAR is a component of the Type 1 interferon response pathway, and this pathway plays a crucial role in balancing the promotion of inflammatory mediators such as Natural killer cells, and limiting the expression the of pro-inflammatory cytokines in response to infection [218]. This is supported by recent findings showing that tryptophan derived gut metabolites such as indolepropionic acid and indolealdehyde have an anti-inflammatory role in astrocytes, and that these metabolites act through an IFNAR-AhR dependent pathway [219]. Furthermore, while HO-1 induction is likely most relevant post-CNS invasion, it has been noted that indolepyruvate and other tryptophan metabolites can cross the BBB [173, 219]; it is therefore tempting to speculate that during high parasitemia in the blood *T. brucei* derived aromatic ketoacids could enter the CNS and prepare it for parasite invasion by dampening the inflammatory response. Clearly further investigation is warranted.

5.3.4 Indolepyruvate degrades into other indolic compounds.

Kynurenic acid was one of the first metabolites to be purportedly produced from indolepyruvate, when rabbits were injected with indolepyruvate and the excreted urine

metabolites were analysed [220]. Since the publication of this report almost 100 years ago, indolepyruvate has been and continues to be studied intensively. As a ketoacid, indolepyruvate is subject to keto-enol tautomerism of its pyruvyl moiety [194], and in the enol form has been suggested to be less stable and undergo degradation, possibly through oxidative free-radical attack [221]. Early reports investigated the role of indolepyruvate as an auxin in maize development, where the authors suggest that indolepyruvate itself, in conjunction with indoleacetic acid, was a potent auxin [192]. The same authors also acknowledged indolepyruvate had not been detected in maize previously as maize extracts broke down under mild conditions, to yield some indoleacetic acid. A later report by different researchers further suggested that the auxin activity was entirely due to the breakdown products of indolepyruvate, rather than due to indolepyruvate itself as indolepyruvate appeared to breakdown in the isopropanol-hydrazoic acid solvent used previously [193]. More recently, a comprehensive study by Chowdhury et al. demonstrated that simple incubation of indolepyurvate in pH 7.4 phosphate buffer at 37 ^{o}C for 24 hours yielded diindole structures that were potent AhR agonists [185]. Importantly, the study notes that the supply of air is crucial to the development of these structures, acting as an oxidant. In contrast, similar studies by Tivendale et al. suggest that indolepyruvate undergoes keto-enol tautomerism, but is then relatively stable in buffered H_2O solutions. Conflicting reports such as these led to the independent investigations of indolepyruvate performed here, given the importance of the compound to the studies on the innate inflammatory response.

It had been noted during these studies that the detection of indolepyruvate in culture for the purpose of treating macrophages was anomalous; ketonic indolepyruvate was readily detectable in culture media immediately following application to cells, but the keto indolepyruvate was not detectable in the same culture media 24 hours later (via AHADH assay). This was confirmed by incubating indolepyruvate, hydroxyphenylpyruvate, and phenylpyruvate in culture media for a 24 hour period, which demonstrated that while both ketonic hydroxyphenylpyruvate and phenylpyruvate were still detectable at high levels, ketonic indolepyruvate was almost undetectable. The AHADH assay can only detect the keto form of α-ketoacids, and so it left open the possibility that the keto indolepyruvate produced by *T. brucei* that was used to treat cells was being converted to the AHADH undetectable enol form, or was breaking down. ^{1}H-NMR analysis revealed that in aqueous solution, indolepyruvate rapidly converts

from the enol to keto form. This was monitored by examining the characteristic peaks of each tautomer, following the disappearance of the enol peaks with the subsequent appearance of the keto peaks. However, the results obtained here were again unclear as the prominent disappearance of the enol signals over time did not correspond to an equatable appearance of keto peaks. Furthermore, the aromatic region of indolepyruvate remained relatively constant over time. Similar conclusions have been drawn by Tivendale et al., who also noted that the keto peak at 4.24 ppm would disappear as it formed [186]. Both data suggest that the disappearance of the keto peak may be due to exchange of hydrogen with deuterium supplied by the D_2O present in the buffer. Early attempts to conduct the same experiments in 100% H_2O were unsuccessful, as the broad water signal interfered with the keto singlet at 4.24 ppm. The relative stability of the aromatic regions of both tautomeric forms was also surprising, though it is likely due to the difficulty in separating the very similar signals for quantification purposes. Most concerningly, it was noted that from 0 - 16 hours the intensity of both the keto peaks did not decrease at a rate consistent with the complete disappearance of indolepyruvate that was observed in the culture media experiments. In the context of the studies by Tivendale et al. and Chowdhury et al., the data appears to be in agreement with Tivendale et al. that enolic indolepyruvate in converted to keto indolepyruvate. But contrary to Tivendale et al., it does not appear that the keto tautomer of indolepyruvate remains stable in aqueous solution, but may be converted to other substances. This would potentially agree with the data of Chowdhury et al., where indolepyruvate can be oxidised in solution to form other indolic compounds. However, neither proposal could be verified solely by ^{1}H-NMR, which may not be suitable to detect and quantify indolepyruvate under the conditions outlined here.

A similar experiment was conducted using the AHADH assay to measure the rate of development of the keto tautomer. Samples taken every 20 minutes from two solutions of indolepyruvate at different pH (acidic and basic) revealed the gradual formation of the keto tautomer. The formation of the keto tautomer occured at a faster rate in solution at a basic pH, which corroborated with the qualitative images demonstrating the faster appearance of the orange/red colour associated with keto indolepyruvate at higher pH. In both acidic and basic solutions the keto indolepyruvate concentration was found to decrease time. The disparity between the data provided here, and that provided elsewhere i.e. the research conducted by Tivendale et al. [186]

and Chowdhury et al. [185], can be rationalised by the availability of oxygen as an oxidant in each study. In the NMR experiments outlined here, the indolepyruvate solution was sealed in a narrow NMR sample tube (3 mm diameter), which would only expose a small surface area ($\approx$ 7 mm^2) at the surface of the solution. This would likely lead to minimal levels of oxygen exchange with the solution. It is tempting to suggest that Tivendale et al. inadvertently minimised oxygen exchange in their experiments also. They demonstrated that the enol tautomer of indolepyruvate is stable in $CDCl_3$, a solvent that would not be oxidising. It was also noted that bubbling N_2 gas through a solution of enol indolepyruvate was sufficient to obtain the keto tautomer and slow down its disappearance (not shown). The N_2 gas probably displaces dissolved oxygen, preventing the oxidation of enol indolepyruvate. Notably, Chowdhury et al. actively exposed their solutions of indolepyruvate to air, and other oxidising agents, and observed the formation of new diindole products [185]. Other researchers have noted that the enol tautomer is subject to free radical attack, and that it is an excellent anti-oxidant [173, 187, 221]. Indeed, Bartolini et al. demonstrated the rate of formation of each tautomer of indolepyruvate via HPLC over much shorter time frames than those performed here [221]. In summary, it appears that enol indolepyruvate is gradually tautomerised to keto indolepyruvate in aqueous solution, the rate of which is partially dependent on pH. Indolepyruvate, likely the enol form, then breaks down due to the presence of an oxidative substance (which was oxygen in the data provided here). It seems that the enol form of indolepyruvate is more susceptible to oxidation, at least from a structural standpoint [222], though the susceptibility of the keto tautomer to oxidation has not been determined. It could be the case that enol indolepyruvate is converted to the more stable keto form, while at the same time being subject to oxidative breakdown. The breakdown would shift the equilibrium so that the keto indolepyruvate is converted back to the enol form, which is broken down, leading to the disappearance of the keto form (Fig. 5.29).

Further evidence of the breakdown of indolepyruvate has been provided here, in the detection and identification of some of these breakdown products using ^{1}H-NMR and ^{13}C-NMR. One of the breakdown products identified was indoleacetic acid, which is most often described as a plant growth hormone [223]. Indeed, indoleacetic acid has been previously described as a spontaneous breakdown product of indolepyruvate [192, 224, 225]. However, the process by which indoleacetic acid is generated from

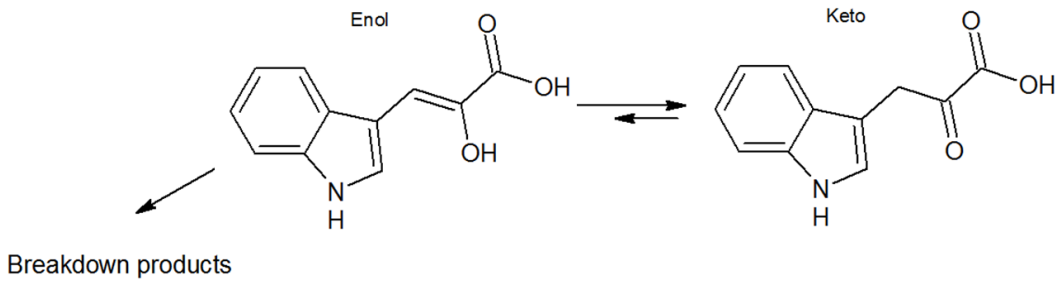

Figure 5.29. Diagram of the proposed enol-keto tautomerism of indolepyruvate. Indolepyruvate is crystallised in its enol tautomer state. When dissolved in an aqueous solution, it converts to its keto tautomer. The presence of oxidising factors such as oxygen cause the enol form to breakdown, pulling the equilibrium from the keto to the enol form, until indolepyruvate is entirely broken down.

indolepyruvate is unclear, as the decarboxylation reaction required for this process is normally catalysed enzymatically. Interestingly, indoleacetic acid was only detected after the original fraction containing the unknown aldehyde was acidified. The first compound extracted was likely an aldehyde derivative of indolepyruvate, as it contained a characteristic aldehyde peak at 10 ppm (^{1}H-NMR) and 190 ppm (^{13}C-NMR). Interestingly, several papers describe the conversion of indolepyruvate to indoleacetaldehyde to indoleacetic acid [203, 223], but all the mechanisms described are based on enzymatic conversion processes rather than free radical attack from oxidative species. While a pathway from indolepyruvate to indoleacetic acid may not be clear, there is evidence at least that both hydroxyphenylpyruvate and phenylpyruvate undergo oxidative degradation to their aldehyde derivatives, hence the conversion of indolepyruvate to a compound such as indoleacetaldehyde is entirely possible [198]. Politi et al. have published on a free radical based mechanism, which generates kynurenic acid from indolepyruvate breakdown [222]. Kynurenic acid was not identifiable in the spectra obtained here, but it is possible it could be present as the third, unidentified compound in the spectra (bio_pb_2c). It is also possible that compounds similar to those discovered by Chowdhury et al. were generated [185], but this remains to be determined.

5.3.5 MIF can weakly tautomerise the enol to keto conversion of indolepyruvate.

The pro-inflammatory cytokine MIF has previously been demonstrated to be both a phenylpyruvate and hydroxyphenylpyruvate tautomerase [141]. It has been shown here that MIF may also act as a tautomerase of indolepyruvate, though to a much lesser extent than that for the aforementioned aromatic ketoacids. Although the exact function of this tautomerase activity remains unclear, one study has shown the abolition of the tautomerase activity by insertion of an extra residue at the active site of the enzyme eliminated its glucocorticoid regulatory activity [204]. Other research has shown that only the N-terminal tail of the enzyme is required to bind a downstream CD74 receptor to mediate cellular responses, and that the tautomerase activity is redundant [226]. To date, no natural host metabolite has been found for MIF and the purpose of its tautomerase function remains a mystery, while the hunt for a suitable metabolite continues.

It was noted that hydroxyphenylpyruvate, phenylpyruvate, and now indolepyruvate, are each substrates for MIF, and all three aromatic ketoacids are produced and excreted in large quantities by bloodstream form *T. brucei*. The reported K_m of MIF for hydroxyphenylpyruvate and phenylypyruvate is quite high (2.4 mM and 6 mM, respectively), and would only be relevant at high concentrations of these aromatic ketoacids [141]. It could be possible that the highly conserved MIF is exploited by the parasite during host invasion and parasite proliferation. MIF is secreted by macrophages and other immune cells, and functions to down-regulate the anti-inflammatory effects of the glucocorticoids, and so its production is associated with an increase in the inflammatory response. An increase in the inflammatory response would be detrimental to *T. brucei* and possibly also to the host. It has already been demonstrated that indolepyruvate can act to dampen the innate inflammatory response [172]. If the tautomerase function is important for the regulatory functions, it could be possible that during parasitemia the excreted aromatic ketoacids act to inhibit MIF function, and in doing so, reduce the severity of the host inflammatory response. The data shown here indicate that this is unlikely to be the case for indolepyruvate, but it could be possible for hydroxyphenylpyruvate and phenylypyruvate, or indeed all three compounds in a concerted manner. It has been demonstrated that the hypoxia-inducible factor,

HIF1-α, has an important role in signalling the up-regulation of MIF [227, 228]. It is tempting to speculate that indolepyruvate could down-regulate MIF through its inhibition of HIF1-α signalling. Indolepyruvate has already been shown to be capable of down-regulating HIF1-α [172].

The only work that has been carried out with *Trypanosoma*, however, has indicated that MIF acts to exacerbate the parasites pathogenesis. Stijlemens et al. demonstrated that in the absence of MIF or during reduction of MIF activity, inflammatory marker expression was decreased and liver damage was reduced, as was *T. brucei* pathogenicity development [229]. Additional studies by the same group have shown that MIF activity acts to increase detrimental hemodilution during chronic infection of the host [230]. Interestingly, it is noted here that the researchers observed a decrease in the expression of IFN-γ, TNF-α, and IL-6, though not IL-10, whereas indolepyruvate and hydroxyphenylpyruvate were found to inhibit IL-6 and TNF-α by the Molecular Immunology group (page 216), as was the secretome of *T. gambiense* [207]. Again, it is plausible that through HIF1-α and/or MIF, these aromatic ketoacids could act to suppress the innate inflammatory response. It remains difficult to reconcile this speculative role for aromatic ketoacids and MIF in inflammation suppression, with the evidence of the contribution of MIF to *T. brucei* pathogenicity in the host. Perhaps in the absence of the secretion of aromatic ketoacids in MIF$^{+/+}$ WT mice the resulting inflammatory response would be considerably worse? This remains to be seen.

Additionally, aromatic ketoacids and MIF could play a role in the regulation of the CNS inflammatory response. The three aromatic ketoacids discussed here can cross the BBB [173], as can *T. brucei*. Not only was MIF found to be expressed at significant background levels in the CNS, but upon LPS induction MIF mRNA expression was vastly increased, more so than other cytokines, and a corresponding increase in IL-1β, IL-6, and TNF-α occurred. Again, all three of these cytokines were found to have a reduced expression in response to aromatic ketoacid treatment when LPS treated, compared to the absence of aromatic ketoacids. It could be possible here that these aromatic ketoacids inhibit MIF activity and consequently reduce cytokine expression.

MIF tautomerase activity could act to promote the availability of aromatic ketoacids.

As has been discussed, indolepyruvate, hydroxyphenylpyruvate, and phenylpyruvate are all unstable in aqueous solutions and under oxidising conditions. In aqueous solvents each aromatic ketoacid undergoes enol to keto tautomerisation, followed by degradation to other indole derivatives. Crucial to the research on the ability of indolepyruvate to dampen aspects of the innate immune response [172], it has been shown here that keto indolepyruvate will persist in solution for a minimum of a 12 hour period, perhaps longer, before decaying to other products. During infection this degradation is unlikely to be problematic, as continual degradation is balanced by continual aromatic ketoacid production by *T. brucei*. However, it is important to suggest the possibility that the MIF enol to keto tautomerase activity could be exploited to keep the aromatic ketoacids in their keto state during parasite infection, which is less prone to degradative oxidation [221]. The Inflammation research group have observed that indoleacetic acid, likely a product of indolepyruvate breakdown shown here, does not reduce pro-IL-1β production in LPS activated macrophages (personal communication, Sarah Corcoran).

5.3.6 Conclusions.

T. brucei cASAT is responsible for the deamination of aromatic amino acids, and subsequent production of aromatic ketoacids. These aromatic ketoacids are secreted at significant rates by the parasite, and can be detected at significantly elevated amounts in the blood (up to sub-mM concentrations, shown here) and urine of the infected host [111]. Interestingly, the availability of aromatic amino acids appears to be the limiting factor in the rate of secretion of these ketoacids. NMR has revealed that indolepyruvate is the sole secreted product from the deamination of tryptophan by TbcASAT. A possible role for the secreted aromatic ketoacids in host immunomodulation was proposed, as previous research indicated indolepyruvate could have neuromodulatory and antioxidative properties [173, 180], and *T. gambiense* has been shown to secrete proteins that could regulate immune response [207]. In addition, the three aromatic ketoacids were shown to have anti-inflammatory properties for UV irradiated hairless mice[187]. In murine BMDMs only indolepyruvate produced by *T. brucei* was found to suppress

pro-IL-1β production, possibly via hydroxylation of HIF-1α, in an AhR independent manner. A similar reduction in pro-IL-1β production was observed in mixed glial cells with indolepyruvate only. In addition, all three aromatic ketoacids were found to suppress TNF-α, IL-6, and IL-10, to different degrees. All three aromatic ketoacids were also found to induce HO-1 expression. HO-1 has been shown to dampen inflammation in various tissues of an infected host, while promoting survival and proliferation of the parasite [215–217]. It appears that this is the first time that direct HO-1 inducers derived from a parasite has been described. Further work, such as *T. brucei* infection studies in mice models need to be carried out to establish if this is the case *in vivo*. It is apparent that the aromatic ketoacids have roles in regulating the host inflammatory response, though the purposes of this regulation remain somewhat speculative.

In agreement with previous research, it has been demonstrated here that indolepyruvate breaks down under oxidative conditions [193, 198, 224]. However, while the conversion from enol to keto form of indolepyruvate was shown to be reasonably fast, the subsequent loss of the keto form is gradual, and takes place over a 12 - 16 hour period. The AHADH assay revealed that under standard cell culture conditions, no keto indolepyruvate is detectable after 24 hours. At this stage, indolepyruvate has likely, though not yet confirmed, degraded into indoleacetaldehyde and/or subsequently indoleacetic acid. Another breakdown product that was observed, but remains unidentified, but could be related to those described by Chowdhury et al. [185]. The results obtained by Tivendale et al. on the stability of indolepyruvate are contrary to the vast amount of literature describing its breakdown; given their lack of transparent experiment methodology, it seems reasonable that their results were somehow obtained in the absence of an oxidative source (such as air) [186]. Precisely how indolepyruvate breakdown occurs chemically is not understood, as such reactions are normally facilitated enzymatically [202].

T. brucei excretes the keto tautomers of aromatic ketoacids, in considerable quantities. The pro-inflammatory cytokine MIF has been shown to be an enol to keto tautomer of hydroxyphenylpyruvate, phenylpyruvate, and now as a weak tautomer of indolepyruvate [141]. No natural substrate for this tautomeric activity has been found, but MIF could be relevant during a trypanosomal infection, either by being inhibited by the aromatic ketoacids when present at high concentrations, or acting to keep the

aromatic ketoacids in their more stable keto state. MIF has been shown to increase the immunopathogenicity of *T. brucei* infections, and its absense has proved beneficial to the host [229].

Chapter 6

Final Discussion.

6.1 Current and new understandings.

Trypanosomes are very adaptable in their metabolic functions, and vary in their ability to catabolise amino acids and glucose, their secretion of differing metabolic end products, or even the presence/absence of a functional Krebs cycle and/or oxidative phosphorylation [84]. Even more surprisingly, this diversity can be reflected during the life cycle stage of a single species, as is the case with bloodstream form and procyclic form *T. brucei*. Following the completion of the sequencing of both the *T. brucei* and *T. cruzi* genomes in 2005 [231, 232], a vast effort has been made to establish the functions of genes in both species. The repertoire of metabolically associated proteins such as transporters and enzymes identified comprises of up to 9,000 genes, 2,000 of which have designated EC numbers [231]. The role of a cytoplasmic aspartate aminotransferase (cASAT) which appears to be essential in the bloodstream form, but not the procyclic form, of *T. brucei* has been examined here.

6.1.1 A metabolic role for TbcASAT in bloodstream form *T. brucei*.

Two ASAT genes have been identified in *T. brucei*, which encode mitochondrial and cytoplasmic enzymes (page 74). In most organisms, both ASATs act as a key link in the glutamate-malate shuttle where they exchange NAD^+ and NADH using α-ketoacids across the mitochondrial inner membrane. Such a function could not occur in bloodstream form *T. brucei* as only the cytosolic form (TbcASAT), and not mASAT, is expressed by these cells [98]. In addition, bloodstream form cells lack a Krebs cycle and instead regenerate NADH through a plant-like alternative oxidase [72]. In procyclic *T. brucei*, a partial Krebs cycle seems to exist, as well as most elements of an electron transport chain [49, 83]. Here the mitochondrial ASAT (TbmASAT) may play a role in the partial Krebs cycle of procyclic cells by conventional transfer of NADH, perhaps with or without the co-function of TbcASAT. However, procyclic cells also express and alternative oxidase that can be used for oxidation of NADH. The reduction in TbcASAT activity by RNAi was lethal to bloodstream form cells, which is a strange result in terms of the traditional view of ASATs role in most eukaryotes. It may be that reduction of TbcASAT activity in procyclic cells could be compensated

by the remaining activity of TbmASAT, which is not possible in bloodstream cells. The reasons why knockdown of TbcASAT is lethal in bloodstream form cells remain unclear. TbcASAT had been implicated in a possible methionine recycling pathway [99], which would function to supply precursors for polyamine biosynthesis. The synthesis of polyamines are essential for the growth of *T. brucei*, as uptake of polyamines from the parasites extracellular environment are generally inefficient [233]. Demand for polyamines in *T. brucei* is high, in particular for spermidine and putrescine, which are required for the synthesis of trypanothione, a thiol that is used for protection against oxidative stress [233, 234]. Methionine regenerated by KMTB transamination would be converted to s-adenosylmethionine, which would be further used for polyamine synthesis (page 24) [101]. However, in light of recent studies, and data obtained here, this cycle seems not to function in this capacity in *T. brucei*. A strong indication of this was the lack of glucose derived carbons in labelling experiments performed by Creek et al. [77]. In the ^{15}N-tryptophan mass spectrometry experiments performed here, very little labelling of methionine was detected. While KMTB cannot be precluded as a suitable substrate for TbcASAT, as previously demonstrated [99], it was subsequently shown that TbcASAT exhibited 3 times higher affinity for α-ketoglutarate than KMTB [98]. The TbcASAT kinetic data provided here builds upon this, in finding that TbcASAT had a 4 - 7 fold increase in affinity (K_m) for oxaloacetate compared to α-ketoglutarate as an amino acceptor from tryptophan or phenylalanine (page 99). If oxaloacetate was the *de facto* substrate for TbcASAT, its transamination would produce aspartate, which could be required for both purine and pyrimidine biosynthesis in bloodstream form *T. brucei*, as outlined in Fig. 6.1 [77].

T. brucei, like most protozoa, lack the ability to synthesise purine rings *de novo*, and so must salvage purines from their surrounding host environments through the expression of a multitude of life cycle stage specific purine transporters [235]. Although highly specific and non-specific transporters exist, salvaged purines can ultimately be converted from any one nucleobase or nucleoside to another. In this case, a source of aspartate would be important for the interconversion of AMP and IMP, where it provides a nitrogen group through adenylosuccinate, which is converted to AMP (Fig. 6.2). In culture conditions and *in vivo*, however, this suggested contribution may only be minor. Creek at al. have reported significant uptake of inosine and guanosine from culture media, and low uptake of hypoxanthine, meaning that adenylosuccinate

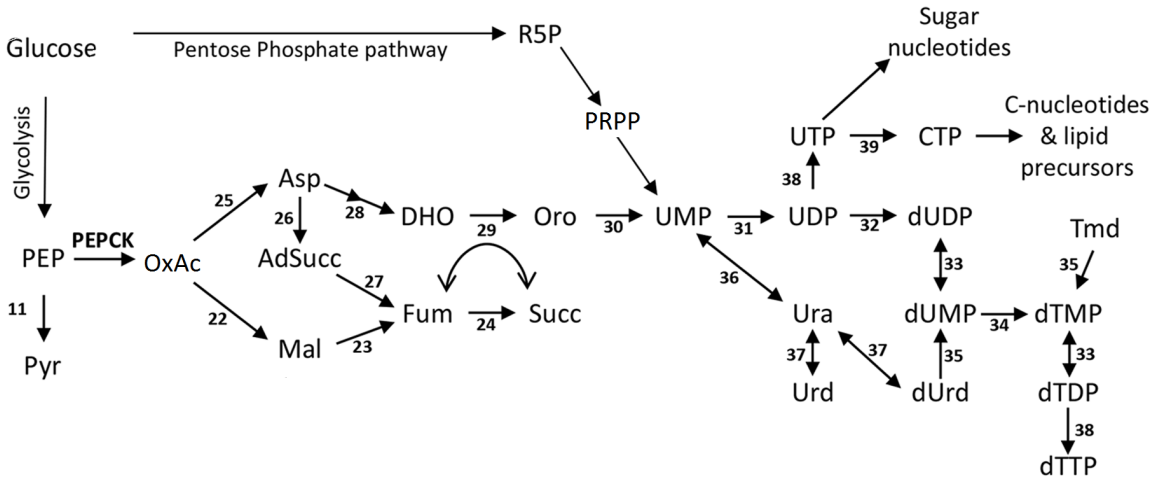

Figure 6.1. The metabolic pathways of glucose-derived oxaloacetate in *T. brucei*. Aspartate generated from oxaloacetate by TbcASAT enters both pathways for purine salvage/recycling and pyrimidine biosynthesis in bloodstream form *T. brucei*. Metabolites; phosphoenolpyruvate (PEP), pyruvate (Pyr), oxaloacetate (OxAc), malate (Mal), fumarate (Fum), succinate (Succ), **aspartate (Asp)**, adenylosuccinate (AdSucc), dihydroorotate (DHO), orotate (Oro) uracil (Ura), uridine (Urd), deoxyuridine (dUrd), thymidine (Tmd). Enzymes; pyruvate kinase (11), malate dehydrogenase (22), fumarase (23), NADH-dependent fumarate reductase (24), **aspartate aminotransferase (25)**, adenylosuccinate synthase (26), adenylosuccinate lyase (27), aspartate carbamoyltransferase & dihydroorotase (28), dihydroorotatedehydrogenase (29), orotate phosphoribosyltransferase & orotidine 5-phosphate decarboxylase (30), nucleoside diphosphatase (31), ribonucleoside-diphosphate reductase (32), thymidylate kinase (33), thymidylate synthase (34), thymidine kinase (35), uracil phosphoribosyltransferase (36), uridine phosphorylase (37), nucleoside diphosphate kinase (38), cytidine triphosphate synthase (39). Figure modified from [77].

interconversion is not likely to be the primary source of AMP or IMP. Indeed, supplementation of culture media performed here with adenosine seemed to delay cell death rather then restore a growth phenotype. Furthermore, though the HMI-9 media used in the cASAT RNAi experiments lacks guanosine or inosine, it contains a high concentration of hypoxanthine ($\approx$ 1 mM) which can be inter-converted to IMP or GMP as required by the parasite.

Where TbcASAT catalysed aspartate generation may be crucial then is in pyrimidine biosynthesis. While high affinity transporters for pyrimidines exist in both bloodstream and procyclic *T. brucei*, they appear to be expressed in such minor amounts that most of pyrimidines in the parasite are proposed to be synthesised de novo from precursor UMP, which can be converted to other pyrimidines [236]. Only uracil has been

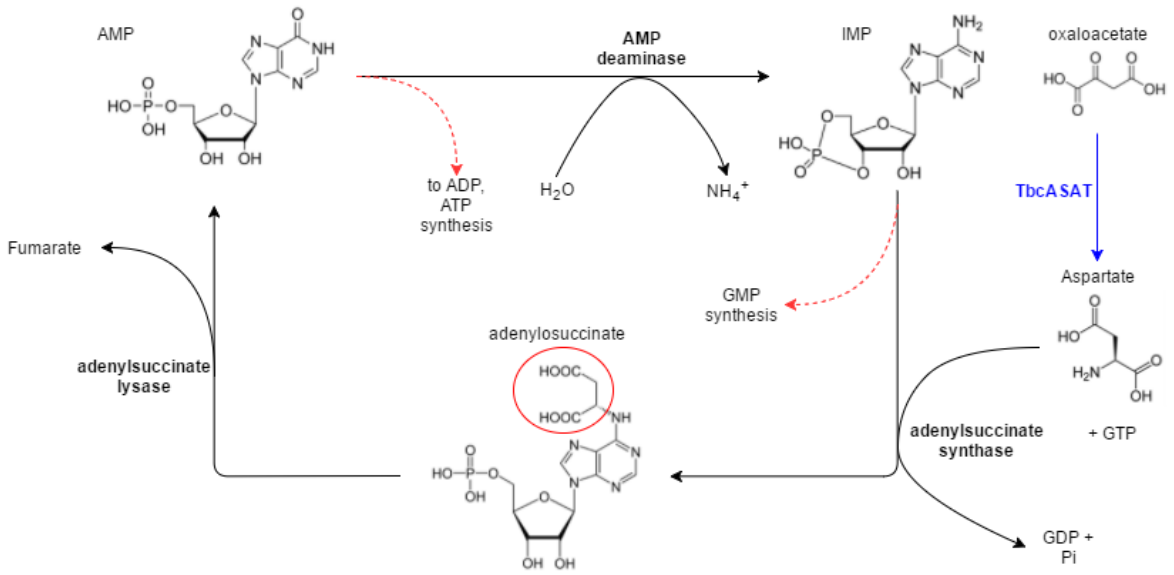

Figure 6.2. The purine nucleotide cycle in bloodstream form *T. brucei*. Aspartate generated from oxaloacetate by TbcASAT is used to convert inosine monophosphate (IMP) to adenylosuccinate, which can be further converted to adenosine monophosphate (AMP), and back to IMP. IMP and AMP produced here could be used to replenish ATP and GMP.

observed to be transported into bloodstream form *T. brucei* at appreciable amounts [237]. In contrast to purines, *T. brucei* can fully synthesise pyrimidines including their ringed substructures [235]. Several studies suggest that the activity of the pyrimidine biosynthetic pathway is crucial for the viability of the parasite, in lieu of pyrimidine salvage. For example, all the enzymes required for UMP synthesis are present, including aspartate carbamoyltransferase, which could act to feed glutamine derived N-carbamoyl-L-aspartate into dihydroorotate [238]. Dihydroorotate is converted to orotate by dihydroorotate dehydrogenase (DHODH). When this enzyme was subjected to RNAi knock down, bloodstream form *T. brucei* grew as normal in standard culture media (HMI-9) [239]. However, when exogenous pyrimidine supplies in the media were removed, cell growth was significantly reduced. Perhaps most tellingly, *T. brucei* orotate phosphoribosyltransferase and orotidine 5-phosphate decarboxylase (position 30, Fig. 6.1) fusion knockout cells were viable in the presence of exogenous pyrimidines, but cell death was rapidly onset in the absence of exogenous pyrimidines. This indicates that pyrimidine biosynthesis is required for cell growth and that in the absence of biosynthesis, pyrimidines must be salvageable from external sources [240]. The dependency on the transport of uracil was again highlighted by the increase in uracil uptake and increased expression of uridine phosphorylase in pyrimidine deprived *T.*

brucei. Surprisingly, however, both thymidine kinase (TK) and cytidine deaminase appear to be required for synthesis of thymine nucleotides, in contrast to their expected redundancy for roles in thymidine salvage [241]. Activity of either enzyme should not be required as de novo biosynthesis of deoxynucleotides should compensate for their loss, yet TK conditional null cells could not be rescued in the presence of exogenous pyrimidine sources. It is not immediately obvious as to why TK is essential, it may be that the pyrimidine pathway is more complex than previously thought.

The knockdown of TbcASAT was performed under standard culture conditions similar to those of Arakaki et al. [239]. However, whilst their RNAi knockdown of DHODH had little effect on the bloodstream form cells under these conditions, the knockdown of TbcASAT was lethal to bloodstream form cells (page 120). It was initially suspected that TbcASAT RNAi could be lethal because of its *combined* role in pyrimidine biosynthesis and nucleotide salvage. Ablation of TbcASAT activity would disrupt the supply of aspartate to key processes in both pathways; aspartate ultimately used for UMP synthesis in pyrimidine biosynthesis (positions 29 and 30, Fig. 6.1), and aspartate used to synthesise adenylosuccinate from IMP in a purine salvage pathway (Fig. 6.2). Knockdown of PEPCK also supported this view. Creek et al. found, to their surprise, that bloodstream form *T. brucei* cell growth was arrested, and ^{13}C-labelling of aspartate, uracil, and UMP was significantly reduced when PEPCK expression was down-regulated [77]. In addition, *T. brucei* appears to lack the ability to internalise aspartate, with no transport of the α-amino acid being observed by bloodstream form *T. brucei* [94], and no depletion in media following bloodstream form *T. brucei* culture [93]. It is also likely that aspartate, a negatively charged amino acid, cannot be passively taken up from culture media against the negative plasma membrane potential of *T. brucei* [242]. So it is probable that the bloodstream stage of the parasite at least relies on the biosynthesis of aspartate from oxaloacetate by TbcASAT to some extent. Though only preliminary, the ^{15}N-tryptophan mass spectrometry data provided here suggests that amino groups enter both uracil and adenosine. Qualitative images of the induced cASAT RNAi cells revealed that induced cells did not develop multiple nuclei or kinetoplast, suggesting cell death was due to growth arrest rather than failure of cytokinesis, which is line with observations that in the absence of available pyrimidines, DNA synthesis is majorly disrupted and chromosome synthesis is halted [240]. In stark contrast, attempts to rescue growth with adenosine supplementation were not

successful, and HMI-9 media contains suitable supplies of pyrimidines that have been demonstrated to rescue growth defects in almost every case where de novo pyrimidine biosynthesis is disrupted [237, 239, 240, 243].

In light of this, it can only be certain that TbcASAT is probably required for its deamination function, and perhaps for the consequential production of aspartate from oxaloacetate. Detection of ^{15}N-labelled adenosine and uracil suggests that TbcASAT does at least partially contribute to each of the pyrimidine biosynthesis and exogenous purine salvage pathways under normal conditions *in vitro*. It has already been suggested that aspartate could be important in generating asparagine. Asparagine is important for both protein synthesis and nitrogen homoeostasis, as was demonstrated in asparagine synthetase (AS) knockdown cells [177]. These cells had impaired growth, which was restored in the presence of external asparagine. Again, however, the TbcASAT knockdown lethality is confusing, as HMI-9 media also contains asparagine which would have been expected to rescue knockdown cell growth, as was observed previously [177]. No obvious mechanisms exist within *T. brucei* to explain the ^{15}N-labelling of leucine/isoleucine and valine, bar the possibility of the involvement of a putative branched-chain amino acid aminotransferase (Tb927.2.4590) [151, 244].

Perhaps aspartate is required for protein synthesis. The relative uptake of the majority of amino acids supplied in culture by bloodstream form *T. brucei* is low or does not occur (Fig. 6.3) [93], and so aspartate could act as an uncharacterised point of entry for protein synthesis. Indeed, cASAT gene knockout slowed the growth rates of *A. thaliana*, most likely through disruption of essential amino acid biosynthesis [245, 246]. However, *T. brucei* seems to lack almost all genes required for the classical synthesis of these essential amino acids based on searches of the TrypanoCyc database [244, 247]. On an intriguing note, two recent studies have highlighted the unexpected importance of aspartate biosynthesis in human cell lines with inhibited mitochondrial respiration [248, 249]. Birsoy et al. demonstrated that upon inhibition of ETC function, GOT1 (cASAT) knockout is lethal to cells, but growth can be rescued by supplementation with high concentrations of exogenous aspartate in combination with over-expression of an aspartate transporter [249]. Sullivan et al. obtained almost identical results in human cancer cell lines with inhibited ETC, and further demonstrated imbalances in purine pools in the absence of aspartate. Both studies suggest that the lack of ETC

produced electron acceptors (such as NAD^+) prevents normal production of aspartate from glutamate in these cells, and so cells reverse flux direction of GOT1 to synthesis aspartate for protein, RNA, and DNA synthetic purposes. These studies highlight the possible complexity of the role for aspartate in other cells, including *T. brucei*. Experiments that could be conducted to further investigate the proposed metabolic functions of TbcASAT are outlined in section 6.2.

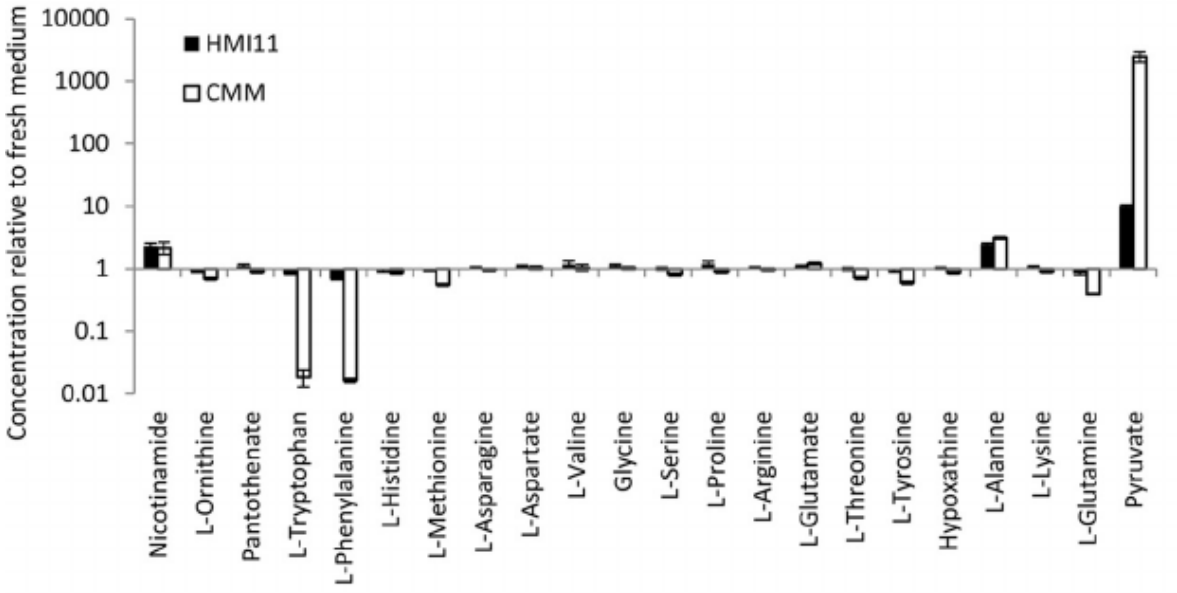

Figure 6.3. The relative changes in select metabolites in spent media following bloodstream form *T. brucei* culture..

The majority of amino acids remain unchanged in abundance, indicating no uptake or no net change in uptake/output. There is a large decrease in available phenylalanine and tryptophan, and moderate decreases in methionine, threonine, tyrosine, and glutamine. Figure modified from [93].

6.1.2 *T. brucei* secreted aromatic ketoacids could have an important role in host-parasite interactions.

Is TbcASAT unusual in its broad specificity?

It has been demonstrated that TbcASAT is a broad-specificity aminotransferase, with high specific activities for aromatic amino acids and oxaloacetate. One of the most important questions raised by this demonstration is what is the significance of this substrate preference? And does this preference play an important function for *T. bru-*

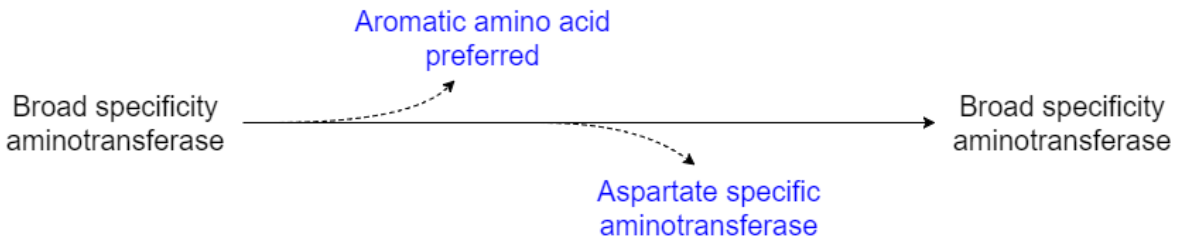

Figure 6.4. The possible evolutionary divergence of ASAT.

The original broad substrate ASAT could have diverged in three ways; ASAT that became specific for aspartate e.g. in vertebrates, ASAT that became more specific for aromatic amino acids e.g. trypanosomal cASAT, or ASAT that remained broad in their specificities e.g. bacterial ASAT [143].

cei? Numerous examples exist of both broad and narrow specificity aspartate aminotransferases [98, 131, 142, 143, 146, 148, 149]. It appears to be a general rule that ASAT from higher organisms, such as vertebrates, tend to be more substrate specific preferring to use aspartate or glutamate as a substrate, with weakened abilities in using other substrates. Jensen et al. note that specificity appears to be selected for in higher organisms, as primitive enzymes could have been more broad in their substrate selectivity [143]. In trypanosomatids, a mix of both broad and selective aminotransferase have been described [96, 98, 150, 161, 250]. It was noted by Berger et al. that even amongst the broad specificity ASATs, TbcASAT was unusually broad in its transamination abilities [99]. Marciano et al. further demonstrated that TbcASAT, but not TbmASAT, had a particularly high specific activity for aromatic amino acids, more so than that for aspartate [98]. It could be possible that broad specificity aminotransferases first arose, after which some aminotransferase became specialised for utilisation of aspartate, e.g. for functions such as the glutamate-malate shuttle. Other aminotransferase remained very broad in their specificities having no particular selective pressures, or in the case of *T. brucei* became specialised in their ability to use aromatic amino acids (Fig. 6.4) [143]. Given that the aromatic ketoacids do not appear to be further catabolised in bloodstream form *T. brucei*, and that aromatic amino acids are amongst the lowest concentrated amino acid in the human bloodstream (each $\leq$ 100 μM) [93, 94], the explanation for these preferences was not clear at first. The data presented here now indicates that the preference for use of aromatic amino acids by *T. brucei* TbcASAT may have arisen as a consequence of a need to modulate host immune functions, as first proposed by Ackerman et al. [108].

It had been established that *T. brucei* infected animals had reduced levels of circulating free aromatic amino acids [109], and increased excretion of aromatic ketoacids in urine [110, 111]. Several key pieces of new data have been demonstrated here; for the first time an increased elevation of aromatic ketoacids in the host sera as a result of *T. brucei* infection has measured and reported, NMR studies have confirmed that indolepyruvate is produced by TbcASAT deamination of tryptophan and excreted by the parasite, and the rates of secretion of aromatic ketoacids by *T. brucei* have been ascertained. This clarifies that increased aromatic ketoacids in the host are a product of *T. brucei* metabolism, and not a host metabolic response to infection. It had been suggested that host expressed indoleamine 2,3-dioxygenase (IDO) could be responsible for the reduction of tryptophan observed during *T. brucei* infection, as its inhibition in infected mice lead to a 10-fold increase in parasite numbers, presumably due to increased availability of tryptophan [251]. A more recent study monitoring host global metabolic changes in mice in response to *T. brucei* infection found a parasitemia-correlated increase in both hydroxyphenylpyruvate and phenylpyruvate [252]. The authors suggest that this increase in aromatic ketoacids could be due to a host enzymatic response, but they did not investigate this. Elsewhere, a study with the malarial parasite *Plasmodium yoelii* suggests that during parasitic infection up-regulation of IDO is in fact responsible for a decrease in free tryptophan in the host, and a corresponding increase in circulating kynurenine, a tryptophan metabolite [253]. However, neither IDO mRNA or protein levels in the host were assessed in this study, so it remains possible that the parasite was responsible for the observed effects (though they inhibit IDO activity pharmacologically). Indeed, it is noted that the related *P. falciparum* expresses an ASAT with the ability to effectively utilise aromatic amino acids in transamination reactions [99, 154], so it is possible that this parasite could also secrete aromatic ketoacids, though this has not been reported in the literature. Politi et al. have reported that indolepyruvate is an inhibitor of IDO, so perhaps some of the hosts ability to regulate tryptophan concentration is lost [173]. In the case of these studies, it is likely that the host can modulate tryptophan levels during infection; however, the dramatic decrease in concentrations of circulating free aromatic amino acids [93, 109, 251], especially tryptophan, and increase in aromatic ketoacids may be primarily due to uptake and metabolism by the parasite. TccASAT was also able to utilise aromatic amino acids preferentially with oxaloacetate, though it does not secrete aromatic ketoacids due to the activity of its MDH-related AHADH enzyme [139]. It has been suggested

that in *T. cruzi* the function of AHADH is to convert aromatic ketoacids to aromatic lactates, a process that would regenerate NAD^+ from NADH [101, 139]. The possibility of an immunological role for the corresponding aromatic hydroxyacids during *T. cruzi* infection cannot be ruled out. However, at least one of these products, indolelactate, had no effect on IL-1β regulation in murine BMDMs.

T. brucei secreted aromatic ketoacids modulate elements of the host immune response.

The production of aromatic ketoacids was noted by Berger et al., but were suggested to be a necessary byproduct of methionine regeneration from KMTB [101], but this pathway seems to not function in *T. brucei* [77, 93, 106]. Alternative roles were considered, originally suggested by Ackerman and Seed, whereby aromatic ketoacids (tryptophol) secreted by *T. brucei* may have a role in the immunodepression observed in the parasite infected hosts [108]. It is also possible that disruption of aromatic amino acid levels and secretion of aromatic ketoacids may affect biogenic amine pools [109].

T. brucei, and indeed other African trypanosomes, remain constantly exposed to the immune system during their vascular life stage in the host. The parasite has evolved immune avoidance mechanisms to prevent clearance by the host, most notably by expressing a VSG coat on its surface [35]. Evidence that the parasite can secrete factors that modulate the immune response has been demonstrated recently [117, 207]. A trypanosome suppressive immunomodulatory factor (TSIF) secreted by *T. brucei* can induce TNF-α and NO production by macrophages, which in turn may block T cell proliferation [117]. The secretome of *T. gambiense* has been shown to diminish the production of TNF-α, IL-6, and IL-10, as well as impair maturation of LPS-induced murine macrophages [207], though whether proteins are truly secreted is not clear - cell integrity was suggested to be evident by the absence of VSG in mass spectrometry analysis, but no other proteins were examined. Additionally, the Coomassie stained SDS gels of the secretome provided by these researchers appear to be very similar in composition to what would be expected of whole cell lysates. *T. brucei* has been shown to secrete extracellular vesicles (EVs) that contain virulence-associated proteins. These EVs have the ability to transfer SRA protein from *T. rhodesiense* to APO-L1 susceptible *T. brucei*, conferring resistance to APO-L1 lysis in these cells [254]. They

also appear to be able to transport an *T. brucei* adenylate cyclase, which could act to reduce TNF-α secretion by regulating cAMP pathways in the host immune cells [254, 255]. The related *T. congolense* has been shown to profoundly depress the production of IL-1 and IL-2 in murine models [119]. In contrast, IL-1 seems to be markedly increased in mice infected with *T. brucei* [120]. It has been demonstrated that one of the primary products generated by TbcASAT and consequently excreted by *T. brucei*, is the aromatic ketoacid indolepyruvate. Indolepyruvate is a potent antioxidant and has been implicated in the modulation of sleep cycles during clinical trials [173, 180]. It has also been shown to prevent UV-B induced damage in mice [187], an effect that was also observed for phenylpyruvate and hydroxyphenylpyruvate. The results here show that *T. brucei* secreted indolepyruvate is capable of suppressing elements of the host innate inflammatory response, through down-regulation of IL-1β [172]. It is speculated here, though it has yet to be demonstrated, that this suppressive mechanism may function at the peaks of parasitemia, to prevent inflammatory shock in the host when burdened with such high parasite loads. This would benefit the host, and in turn allow the parasite to further proliferate (Fig. 6.5). The aromatic ketoacid concentrations recorded in the blood of *T. brucei* infected rats and used for *in vitro* BMDM treatments are only likely to be experienced at the peaks of parasitemia, as evidenced by the studies here on indolepyruvate breakdown (page 181). In support of this idea, Wang et al. could not detect the presence of aromatic ketoacids in chronically infected mice with a *T. brucei* strain that exhibited low parasitemia [256]. When a more virulent *T. brucei* strain that could reach high levels of parasitemia was used, however, significant quantities of hydroxyphenylpyruvate and phenylpyruvate were detected in the urine of infected mice [252]. The use of different strains of these parasites that differ in their pathogenesis may explain the disparity between the results of many of these studies [119, 120, 252, 256].

Initial studies to examine the roles these aromatic ketoacids may play in the CNS during infection with *T. brucei* were also undertaken. In the latter stages of trypanosomiasis, the parasite enters the CNS through unknown mechanisms, leading to a marked increase in neuropathological conditions [22]. This stage may persist for weeks or months, depending on the subspecies. How then does the parasite persist in the CNS without immediately causing an acute and detrimental immune response? It has been noted that cytokines associated with both innate and adaptive immune

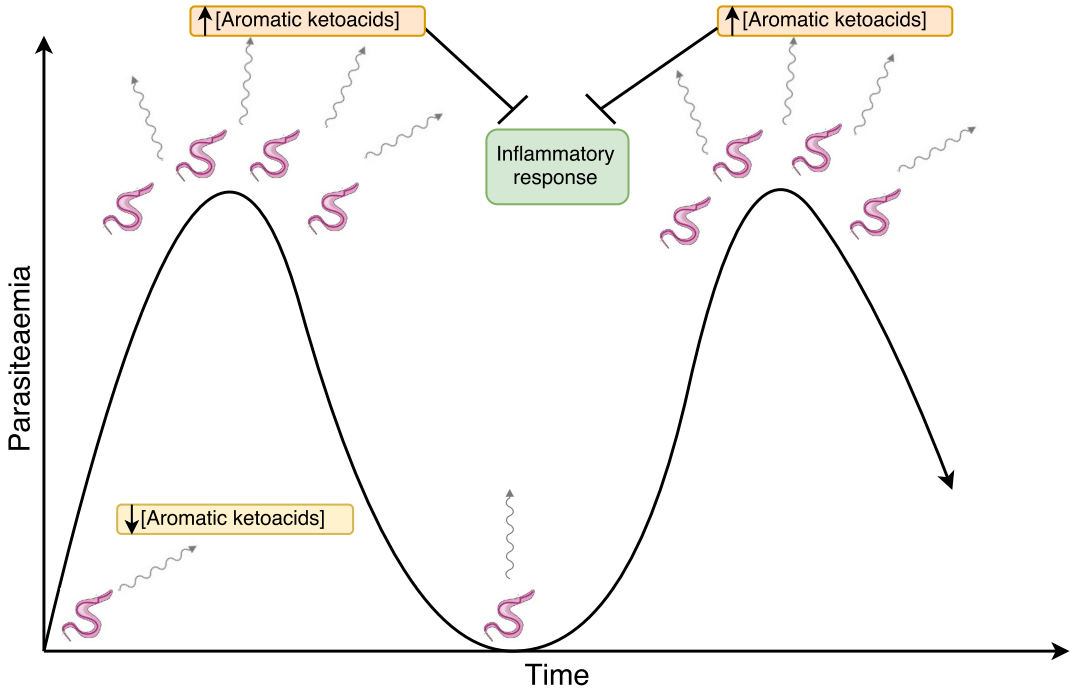

Figure 6.5. The suggested inflammatory response dampening mechanism of *T. brucei* secreted aromatic ketoacids.

At low levels of parasitemia, the corresponding amounts of secreted aromatic ketoacids circulating in the host are low. As parasite numbers rise, so do the concentrations of aromatic ketoacids. The raised aromatic ketoacid concentration may act to dampen components of the host innate immune system, preventing an excessive inflammatory response.

responses are up-regulated in the brains of *T. brucei* infected mice [210], therefore the CNS is clearly capable of mounting a robust immune response to the parasite. The data obtained here demonstrate that aromatic ketoacids can down-regulate the expression of inflammatory cytokines in murine mixed glial cells *in vitro*. Moreover, it was discovered that heme oxygenase-1 (HO-1) is potently induced by all three aromatic ketoacids. HO-1 is believed to act as a protectant against oxidative stress, and has been shown to have some protective effects for the host during *T. cruzi*, *Leishmania*, and *Plasmodium* infection [215–217]. Again, it is tempting to speculate that *T. brucei* secreted aromatic ketoacids may dampen the host inflammatory response during infection, thereby prolonging the survival of the parasite and the host during CNS invasion. It is also possible that circulating aromatic ketoacids suppress the immune cells of the CNS prior to invasion of the parasite, as they can cross blood-brain barrier [173, 219].

The dramatic decrease in aromatic amino acids may also play a role in immune suppression. Newport et al. notes a severe decrease in plasma tryptophan concentrations in *T. gambiense* infected voles, and a notable decrease in tyrosine in the brain of infected voles (tryptophan not measured) [109, 257]. Tryptophan starvation has been shown to reduce the effectiveness of both $CD8^+$ and $CD4^+$ T-cell responses [258]. Rodgers et al. had described a mechanism where the pharmacological inhibition of the production of neurotoxic metabolites of the kynurenine pathway in the brain led to reduced inflammation severity in late stage CNS infection with *T. brucei* [259]. It could also be possible that this pathway is inhibited by *T. brucei* uptake of tryptophan in a similar manner, depriving the pathway of precursor tryptophan. In support of this idea, Vincent et al. failed to identify many metabolites of the kynurenine pathway in the tryptophan-depleted CSF of infected humans [260].

Indolepyruvate: an unstable molecule stabilised by MIF?

The instability of indolepyruvate under oxidative conditions has been examined, indicating that it breaks down and forms other, semi-identified compounds. Key to these studies, it has been demonstrated that indolepyruvate may persist for many hours before degrading completely, and that at least one of its degradation products does not appear to have any immune regulatory function (indoleacetic acid). This discussion has been outlined previously (pages 217 & 222), but it could be possible that indolepyru-

vate, as well as hydroxyphenylpyruvate and phenylpyruvate, are maintained as their ketonic tautomers *in vivo* through the tautomerase function of MIF. This would allow them to persist for longer and potentially dampen the host inflammatory response. It is also possible that the circulating aromatic ketoacids act to inhibit MIF slightly during infection, reducing its pro-inflammatory effects. The relevance of the MIF tautomerase activity remains unknown, though MIF has been shown to exacerbate the inflammatory response in *T. brucei* infected mice [229, 230].

6.1.3 Aromatic ketoacids and the elusive Stumpy Induction Factor (SIF).

In the bloodstream of mammalian hosts, the *T. brucei* population is pleomorphic, being comprised of two distinct cell types; the long slender proliferating cells and short non-dividing stumpy cells [261]. Stumpy cells are pre-adapted for uptake by the tsetse fly and for further differentiation into procyclic form cells within the fly. In the bloodstream of the host a subset of long slender cells are induced to differentiate into stumpy cells in a density dependent manner, termed quorum sensing [262]. This process is triggered when SIF levels released by the long slender cells reach a critical threshold, typically at high parasitemia. Commitment to differentiation is irreversible, and is accompanied by vast changes in the proteome and kinome of the parasite [263]. Despite recent progress in unravelling the mechanisms of differentiation, identification of the SIF remains elusive. For example, it has long been known that the stumpy to procyclic transition can be stimulated *in vitro* by the Krebs cycle intermediate cis-aconitate and by lowering the culturing temperature to 27 ^{o}C [47]. Monomorphic bloodstream form cells can also be stimulated to differentiate directly into procyclic cells in this manner. SIF is known to be a small ($<$ 500 Da) parasite-derived molecule(s) and is heat stable, persisting in culture for several weeks at 37 ^{o}C [264]. Recently, two studies have reported on a number of small molecular weight molecules that are capable of inducing some level of bloodstream to procyclic or stumpy differentiation [265, 266]. Both of these studies screened thousands of compounds for molecules capable of inducing differentiation, with successful molecules detected and screened by a modified procyclin locus reporter assay [266], or a modified PAD1 expression cell line [265]. One compound, DDD00015314, was found to induce partial differentiation of pleomorphic

long slender bloodstream cells to a cell with a stumpy-like phenotype [265]. Given that high concentrations of aromatic ketoacids (up to 0.55 mM) are detectable at high levels of parasitemia in infected hosts and that bloodstream *T. brucei* is capable of excreting large quantities of aromatic ketoacids, both demonstrated here, could one or all of these aromatic ketoacids be the unidentified SIF? Other researchers have noted that aromatic ketoacids accumulate in culture media over time [93]. Both hydroxyphenylpyruvate and phenylpyruvate are heat stable, at least over short periods (page 188). All three aromatic ketoacids are between 150 - 210 Da in mass. Early investigations into the ability of these aromatic ketoacids to induce bloodstream form to stumpy form progression have been performed in the lab with a pleomorphic Antat 1.1 line. Differentiation was monitored by detecting PAD1 expression, a transporter that is specifically expressed by stumpy cells [267]. As yet, no obvious inductive effects have been observed. However, it is possible that unsuitable concentrations of aromatic ketoacids were used in these early screens. Wenzler et al. noted that the dose response curves of the compounds in their screens were bell-shaped rather than sigmoidal, indicating that high doses of the compounds were inhibitory to cell differentiation [266]. The aromatic ketoacids were screened at 0.25 - 1 mM concentrations, 5 - 20 times higher than the concentrations of compounds used in other screens [265]. It is also possible that the aromatic ketoacids are required to signal in unison to induce differentiation. This possibility has been previously suggested by Vassella et al. [264]. Finally, a number of breakdown products of indolepyruvate have been partially identified here. Whilst this would seem to preclude indolepyruvate as a suitable candidate for SIF, Chowdhury et al. have described some complex diindole structures that can be generated from indolepyruvate [185]. These indole structures are not too dissimilar structurally to the trypanosome differentiation-inducing compounds identified elsewhere [265, 266]. More thorough investigations will be conducted into the possible roles of aromatic ketoacids as potential SIF(s).

6.2 Conclusions and future work.

Several key investigations to solidify the metabolic function of TbcASAT and the secretion of aromatic ketoacids remain to be undertaken to establish the roles suggested here. Given the lower than expected levels of ^{15}N-labelled tryptophan in the metabolomics experiment, every effort should be made to repeat this experiment with higher ^{15}N-

tryptophan concentrations (and removal of supplemented phenylalanine and tyrosine), to confirm that TbcASAT is used to generate aspartate for pyrimidine biosynthesis and purine salvage. This role for cASAT is likely to be important during an *in vivo* infection, where circulating concentrations of purine and pyrimidines are low [268], though it is redundant under standard *in vitro* culture conditions. The inability to rescue the growth phenotype of cASAT RNAi cells cannot be directly explained, though it must be related to a need for the parasite to generate aspartate. This could be investigated further; ectopic expression of an aspartate transporter could be used to attempt to rescue the growth defect in these cells. This could clarify whether or not aspartate is required by *T. brucei*. Interestingly, *T. cruzi* can uptake aspartate from its environment, though a specific transporter has not been identified [269].

It has been suggested here that the N-terminal of TccASAT may play an important role in its broad-specificity. There are ongoing efforts to crystallise TbcASAT, in addition to future generation of cASAT structures for related trypanosomes e.g *T. congolense*, for comparative purposes. Evidence of a lack of a methionine recycling pathway in *T. brucei* has been further provided, and it was demonstrated that aromatic ketoacids can suppress elements of the inflammatory responses of the host. However, and crucially, all experiments conducted so far have been performed under *in vitro* conditions. It is of the utmost importance that similar experiments be carried out in *in vivo* models. Work is currently being undertaken to generate pleomorphic cell lines expressing either AHADH^{in} or constitutively expressed AHADH vectors, as well as attempts to generate dual *cASAT* knockout cells (that will express a 'rescue' copy of ASAT and will not secrete aromatic ketoacids). The proposed model of suppression of the inflammatory responses would be expected to be reflected by a decrease in the survival times of hosts containing the aforementioned modified pleomorphic cell lines, compared to a wild type cell line producing normal amounts of aromatic ketoacids. The breakdown products of indolepyruvate need to be fully characterised, as does their relevance to the immune responses of the infected host. The striking induction of HO-1 by all three aromatic ketoacids suggests they should be investigated as possible therapeutics. The production of aromatic ketoacids from aromatic amino acids has been demonstrated, but the quantification of the amounts of aromatic amino acids directed into aromatic ketoacid production has not been performed. Presumably these aromatic amino acids would also be required for other biosynthetic purposes, in addition

to aromatic keto acid secretion.

It has been demonstrated that TbcASAT activity is crucial to the survival of only the bloodstream form of *T. brucei*, seemingly through its generation of aspartate from glucose-derived oxaloacetate, which the cells cannot uptake from their extracellular environment. This aspartate could then be used for both pyrimidine biosynthesis and purine salvage. It is possible that this dual role in both pathways explains the lethality of TbcASAT knockdown, as neither activity on its own would seem sufficient to lead to loss of parasite viability. However, cASAT RNAi was not expected to be lethal when these cells were cultured under standard *in vitro* conditions due to the ability to salvage purines and pyrimidines from culture media. The preference for aromatic amino acids may have evolved as a mechanism to produce and secrete aromatic ketoacids, which has been shown can down-regulate elements of the host inflammatory response. It is proposed that this function is most likely relevant at the peaks of parasitemia observed in natural *T. brucei* infections.

Bibliography

1. Stevens, J., Noyes, H., Schofield, C. & Gibson, W. The molecular evolution of trypanosomatidae. *Advances in Parasitology* **48,** 1–53 (2001).

2. Piontkivska, H. & Hughes, A. L. Environmental kinetoplastid-like 18S rRNA sequences and phylogenetic relationships among Trypanosomatidae: Paraphyly of the genus Trypanosoma. *Molecular and Biochemical Parasitology* **144,** 94–99 (May 2005).

3. Gruby, D. Recherches et observations sur une nouvelle espace d'haematozoaire, Trypanosoma sanguinis. *The Academy of Sciences* **17,** 1134–1136 (3rd July 1845).

4. Steverding, D. The history of African trypanosomiasis. *Parasites & Vectors* **1,** 1–8. ISSN: 1756-3305 (Aug. 2008).

5. Cox, F. E. History of sleeping sickness (African trypanosomiasis). *Infectious Disease Clinics of North America* **18,** 231–245. ISSN: 0891-5520 (June 2004).

6. Bruce, D. *Preliminary Report on the Tsetse Fly Disease or Nagana, in Zululand.* (Durban, Bennett & Davis., 1895).

7. Stephens, J. & Fantham, H. B. On the Peculiar Morphology of a Trypanosome from a Case of Sleeping Sickness and the Possibility of Its Being a New Species (T. rhodesiense). *Proceedings of the Royal Society of London B: Biological Sciences* **83,** 28–33. ISSN: 0962-8452 (Oct. 1910).

8. Bruce, S.-G. D. Classification of the African Trypanosomes pathogenic to man and domestic animals. *Transactions of the Royal Society of Tropical Medicine and Hygiene* **8,** 1–22. ISSN: 0035-9203 (Nov. 1914).

9. Stevens, J. R., Noyes, H. A., Dover, G. A. & Gibson, W. C. The ancient and divergent origins of the human pathogenic trypanosomes, Trypanosoma brucei and T. cruzi. *Parasitology* **118 (Pt 1),** 107–16. ISSN: 0031-1820 (1999).

10. Haag, J., O'hUigin, C. & Overath, P. The molecular phylogeny of trypanosomes: evidence for an early divergence of the Salivaria. *Molecular and Biochemical Parasitology* **91,** 37–49. ISSN: 0166-6851 (Mar. 1998).

11. Stevens, J. & Gibson, W. The Molecular Evolution of Trypanosomes. *Parasitology Today* **15,** 432–437. ISSN: 0169-4758 (Nov. 1999).

12. Fraga, J. *et al.* Phylogenetic analysis of the Trypanosoma genus based on the heat-shock protein 70 gene. *Infect Genetics Evol* **43,** 165–172. ISSN: 1567-1348 (2016).

13. Stevens, J. & Gibson, W. The Evolution of Salivarian Trypanosomes. *Memórias do Instituto Oswaldo Cruz* **94,** 225–228. ISSN: 0074-0276 (Mar. 1999).

14. Simpson, A. G., Gill, E. E., Callahan, H. A., Litaker, R. W. & Roger, A. J. Early Evolution within Kinetoplastids (Euglenozoa), and the Late Emergence of Trypanosomatids. *Protist* **155,** 407–422. ISSN: 1434-4610 (Dec. 2004).

15. Capewell, P., Cooper, A., Clucas, C., Weir, W. & Macleod, A. A co-evolutionary arms race: trypanosomes shaping the human genome, humans shaping the trypanosome genome. *Parasitology* **142,** 108–119 (Mar. 2014).

16. Kennedy, P. G. Clinical features, diagnosis, and treatment of human African trypanosomiasis (sleeping sickness). *The Lancet Neurology* **12,** 186–194. ISSN: 1474-4422 (2013).

17. Vanwalleghem, G. *et al.* Coupling of lysosomal and mitochondrial membrane permeabilization in trypanolysis by APOL1. *Nature Communications* **6,** 8078. ISSN: 2041-1733 (Aug. 2015).

18. Gibson, W. Sex and evolution in trypanosomes. *International Journal for Parasitology* **31,** 643–647. ISSN: 0020-7519 (May 2001).

19. Uzureau, P. *et al.* Mechanism of Trypanosoma brucei gambiense resistance to human serum. *Nature* **501,** 430–434. ISSN: 0028-0836 (2013).

20. Genovese, G. *et al.* Association of Trypanolytic ApoL1 Variants with Kidney Disease in African Americans. *Science* **329,** 841–845. ISSN: 0036-8075 (Oct. 2010).

21. Hamilton, P. B., Gibson, W. C. & Stevens, J. R. Patterns of co-evolution between trypanosomes and their hosts deduced from ribosomal RNA and protein-coding gene phylogenies. *Molecular Phylogenetics and Evolution* **44,** 15–25. ISSN: 1055-7903 (July 2007).

22. Barrett, M. P. *et al.* The trypanosomiases. *The Lancet* **362,** 1469–1480 (Mar. 2003).

23. Vanhamme, L. *et al.* Apolipoprotein L-I is the trypanosome lytic factor of human serum. *Nature* **422,** 83–87 (Mar. 2003).

24. Raper, J., Portela, M. P. M., Lugli, E., Frevert, U. & Tomlinson, S. Trypanosome lytic factors: novel mediators of human innate immunity. *Current Opinion in Microbiology* **4,** 402–408 (Jan. 2001).

25. Sutherland, C. S., Yukich, J., Goeree, R. & Tediosi, F. A Literature Review of Economic Evaluations for a Neglected Tropical Disease: Human African Trypanosomiasis (Sleeping Sickness). *PLOS Neglected Tropical Diseases* **9,** e0003397 (2015).

26. Brun, R., Blum, J., Chappuis, F. & Burri, C. Human African trypanosomiasis. *The Lancet* **375,** 148–159. ISSN: 0140-6736 (Oct. 2010).

27. Truc, P. *et al.* Atypical Human Infections by Animal Trypanosomes. *PLoS Neglected Tropical Diseases* **7,** e2256 (2013).

28. Vreysen, M. J., Seck, M. T., Sall, B. & Bouyer, J. Tsetse flies: Their biology and control using area-wide integrated pest management approaches. *Journal of Invertebrate Pathology* **112,** S15–S25. ISSN: 0022-2011 (2013).

29. Cecchi, G., Mattioli, R., Slingenbergh, J. & Rocque, D. S. Land cover and tsetse fly distributions in sub Saharan Africa. *Medical and veterinary Entomology* **22,** 364–373. ISSN: 1365-2915 (Aug. 2008).

30. Stich, A., Abel, P. M. & Krishna, S. Human African trypanosomiasis. *BMJ (Clinical research ed.)* **325,** 203–6 (Feb. 2002).

31. Torr, S. & Vale, G. Know your foe: lessons from the analysis of tsetse fly behaviour. *Trends in Parasitology* **31,** 95–99. ISSN: 1471-4922 (2015).

32. Enyaru, J. *et al.* Evidence for the occurrence of Trypanosoma brucei rhodesiense sleeping sickness outside the traditional focus in south-eastern Uganda. *Annals of tropical medicine and parasitology* **93,** 817–22. ISSN: 0003-4983 (1999).

33. Picozzi, K. *et al.* Sleeping sickness in Uganda: a thin line between two fatal diseases. *BMJ* **331,** 1238–1241. ISSN: 0959-8138 (May 2005).

34. Simarro, P., Franco, J., Diarra, A. & Jannin, J. Epidemiology of human African trypanosomiasis. *Clinical Epidemiology* **6,** 257–275. ISSN: 1179-1349 (2014).

35. Borst, P. Antigenic Variation and Allelic Exclusion. *Cell* **109,** 5–8. ISSN: 0092-8674 (Feb. 2002).

36. Fairlamb, A. H. Chemotherapy of human African trypanosomiasis: current and future prospects. *Trends in Parasitology* **19,** 488–494. ISSN: 1471-4922 (Mar. 2003).

37. Njiru, Z. *et al.* African trypanosomiasis: Sensitive and rapid detection of the sub-genus Trypanozoon by loop-mediated isothermal amplification (LAMP) of parasite DNA. *International Journal for Parasitology* **38,** 589–599. ISSN: 0020-7519 (Aug. 2008).

38. Bern, C. Antitrypanosomal Therapy for Chronic Chagas' Disease. *The New England Journal of Medicine* **364,** 2527–2534. ISSN: 0028-4793 (Nov. 2011).

39. Babokhov, P., Sanyaolu, A. O., Oyibo, W. A., Fagbenro-Beyioku, A. F. & Iriemenam, N. C. A current analysis of chemotherapy strategies for the treatment of human African trypanosomiasis. *Pathogens and Global Health* **107,** 242–252. ISSN: 2047-7724 (2013).

40. Khare, S. *et al.* Proteasome inhibition for treatment of leishmaniasis, Chagas disease and sleeping sickness. *Nature* **537,** 229–233. ISSN: 0028-0836 (2016).

41. Unitingtocombatntds.org. *The London Declaration - Uniting to Combat NTDs.* [Online; accessed 10-October-2016]. 2016.

42. Hide, G. History of sleeping sickness in East Africa. *Clinical microbiology reviews* **12,** 112–25. ISSN: 0893-8512 (1999).

43. Allsopp, R. Options for vector control against trypanosomiasis in Africa. *Trends in Parasitology* **17,** 15–19. ISSN: 1471-4922 (Jan. 2001).

44. Magez, S., Caljon, G., Tran, T., Stijlemans, B. & Radwanska, M. Current status of vaccination against African trypanosomiasis. *Parasitology* **137,** 2017–2027. ISSN: 0031-1820 (Oct. 2010).

45. Sharma, R. *et al.* The heart of darkness: growth and form of Trypanosoma brucei in the tsetse fly. *Trends in parasitology* **25,** 517–24. ISSN: 1471-4922 (Sept. 2009).

46. Cross, G. A., Wirtz, L. & Navarro, M. Regulation of vsg expression site transcription and switching in Trypanosoma brucei. *Molecular and Biochemical Parasitology* **91,** 77–91. ISSN: 0166-6851 (1998).

47. Matthews, K. R. & Gull, K. Commitment to differentiation and cell cycle reentry are coincident but separable events in the transformation of African trypanosomes from their bloodstream to their insect form. *Journal of Cell Science* **110 (Pt 20),** 2609–18. ISSN: 0021-9533 (1997).

48. Roditi, I. & Lehane, M. J. Interactions between trypanosomes and tsetse flies. *Current Opinion in Microbiology* **11,** 345–351. ISSN: 1369-5274 (Aug. 2008).

49. Van Hellemond, J., Opperdoes, F. & Tielens, A. The extraordinary mitochondrion and unusual citric acid cycle in Trypanosoma brucei. *Biochemical Society Transactions* **33,** 967–971. ISSN: 0300-5127 (May 2005).

50. Fenn, K. & Matthews, K. R. The cell biology of Trypanosoma brucei differentiation. *Current Opinion in Microbiology* **10,** 539–546. ISSN: 1369-5274 (July 2007).

51. Langousis, G. & Hill, K. L. Motility and more: the flagellum of Trypanosoma brucei. *Nature Reviews Microbiology* **12,** 505–518. ISSN: 1740-1526 (2014).

52. Gull, K. The Cytoskeleton of Trypanosomatid Parasites. *Annual Review of Microbiology* **53,** 629–655. ISSN: 0066-4227 (1999).

53. Kohl, L., Robinson, D. & Bastin, P. Novel roles for the flagellum in cell morphogenesis and cytokinesis of trypanosomes. *The EMBO Journal* **22,** 5336–5346. ISSN: 1460-2075 (Mar. 2003).

54. Yaeger, R. *Protozoa: Structure, Classification, Growth, and Development.* 1273 (1996).

55. Fernandes, O. *et al.* Brazilian isolates of Trypanosoma cruzi from humans and triatomines classified into two lineages using mini-exon and ribosomal RNA sequences. *The American journal of tropical medicine and hygiene* **58,** 807–11. ISSN: 0002-9637 (1998).

56. Prata, A. Clinical and epidemiological aspects of Chagas disease. *The Lancet Infectious Diseases* **1,** 92–100. ISSN: 1473-3099 (Jan. 2001).

57. Martins, A. V. *et al.* Biology of Trypanosoma cruzi: An update. *Infectio* **16,** 45–58. ISSN: 0123-9392 (2014).

58. Schmunis, G. A. & Yadon, Z. E. Chagas disease: A Latin American health problem becoming a world health problem. *Acta Tropica* **115,** 14–21. ISSN: 0001-706X (Oct. 2010).

59. Perez-Molina, J. A., Perez, A. M., Norman, F. F., Monge-Maillo, B. & Lopez-Velez, R. Old and new challenges in Chagas disease. *The Lancet. Infectious diseases.* ISSN: 1473-3099 (2015).

60. Bern, C. Chagas' Disease. *The New England journal of medicine* **373,** 456–66 (2015).

61. Rabinovich, J. E., Wisnivesky-Colli, C., Solarz, N. D. & Gurtler, R. E. Probability of transmission of Chagas disease by Triatoma infestans (Hemiptera: Reduviidae) in an endemic area of Santiago del Estero, Argentina. *Bulletin of the World Health Organization* **68,** 737 (1990).

62. Rassi, A., Rassi, A. & Marin-Neto, J. A. Chagas disease. *The Lancet* **375,** 1388–1402. ISSN: 0140-6736 (Oct. 2010).

63. Malik, L. H., Singh, G. D. & Amsterdam, E. A. The Epidemiology, Clinical Manifestations, and Management of Chagas Heart Disease. *Clinical Cardiology* **38,** 565–569. ISSN: 1932-8737 (2015).

64. Malik, L. H., Singh, G. D. & Amsterdam, E. A. Chagas Heart Disease: An Update. *The American journal of medicine.* ISSN: 0002-9343 (2015).

65. Gomes, Y. M., Lorena, V. & Luquetti, A. O. Diagnosis of Chagas disease: what has been achieved? What remains to be done with regard to diagnosis and follow up studies? *Memorias do Instituto Oswaldo Cruz* **104,** 115–121. ISSN: 0074-0276 (Sept. 2009).

66. Nardy, A. F., Freire-de-Lima, C. G. & Morrot, A. Immune Evasion Strategies of Trypanosoma cruzi. *Journal of Immunology Research* **2015,** 1–7. ISSN: 2314-8861 (2015).

67. Schofield, C. & Maudlin, I. Trypanosomiasis control. *International Journal for Parasitology* **31,** 615–620. ISSN: 0020-7519 (Jan. 2001).

68. Dias, J., Silveira, A. & Schofield, C. The impact of Chagas disease control in Latin America: a review. *Memórias do Instituto Oswaldo Cruz* **97,** 603–612. ISSN: 0074-0276 (Feb. 2002).

69. Tyler, K. & Engman, D. The life cycle of Trypanosoma cruzi revisited. *International Journal for Parasitology* **31,** 472–481. ISSN: 0020-7519 (Jan. 2001).

70. Michels, P. A., Bringaud, F., Herman, M. & Hannaert, V. Metabolic functions of glycosomes in trypanosomatids. *Biochimica et Biophysica Acta (BBA)-Molecular Cell Research* **1763,** 1463–1477 (June 2006).

71. Riviere, L. *et al.* Acetate produced in the mitochondrion is the essential precursor for lipid biosynthesis in procyclic trypanosomes. *Proceedings of the National Academy of Sciences.* ISSN: 0027-8424 (Sept. 2009).

72. Bringaud, F., Riviere, L. & Coustou, V. Energy metabolism of trypanosomatids: Adaptation to available carbon sources. *Molecular and Biochemical Parasitology.* ISSN: 0166-6851 (June 2006).

73. Mazet, M. *et al.* Revisiting the Central Metabolism of the Bloodstream Forms of Trypanosoma brucei: Production of Acetate in the Mitochondrion Is Essential for Parasite Viability. *PLoS Neglected Tropical Diseases* **7,** e2587 (2013).

74. Haanstra, J. R. *et al.* Compartmentation prevents a lethal turbo-explosion of glycolysis in trypanosomes. *Proceedings of the National Academy of Sciences* **105,** 17718–17723. ISSN: 0027-8424 (Aug. 2008).

75. Bakker, B. M. *et al.* Compartmentation protects trypanosomes from the dangerous design of glycolysis. *Proceedings of the National Academy of Sciences* **97,** 2087–2092. ISSN: 0027-8424 (2000).

76. Vertommen, D. *et al.* Differential expression of glycosomal and mitochondrial proteins in the two major life-cycle stages of Trypanosoma brucei. *Molecular and Biochemical Parasitology* **158,** 189–201. ISSN: 0166-6851 (Aug. 2008).

77. Creek, D. J. *et al.* Probing the metabolic network in bloodstream-form Trypanosoma brucei using untargeted metabolomics with stable isotope labelled glucose. *PLoS pathogens* **11,** e1004689. ISSN: 1553-7366 (Mar. 2015).

78. Gilbert, R. J., Klein, R. A. & Miller, P. G. The role of threonine in the metabolism of acetyl coenzyme a by Trypanosoma brucei brucei. *Comparative biochemistry and physiology. B, Comparative biochemistry* **74,** 277–81. ISSN: 0305-0491 (1983).

79. Cronín, C. N., Nolan, D. P. & Voorheis, P. H. The enzymes of the classical pentose phosphate pathway display differential activities in procyclic and bloodstream forms of Trypanosoma brucei. *FEBS Letters.* ISSN: 0145-7938 (1989).

80. Achcar, F., Kerkhoven, E. J. & Barrett, M. P. Trypanosoma brucei: meet the system. *Current Opinion in Microbiology* **20,** 162–169. ISSN: 1369-5274 (Aug. 2014).

81. Kovarova, J. & Barrett, M. P. The Pentose Phosphate Pathway in Parasitic Trypanosomatids. *Trends in parasitology* **32,** 622–34. ISSN: 1471-4922 (2016).

82. Maugeri, D. A. & Cazzulo, J. J. The pentose phosphate pathway in Trypanosoma cruzi. *FEMS Microbiology Letters* **234,** 117–123. ISSN: 1574-6968 (May 2004).

83. Chaudhuri, M., Ajayi, W. & Hill, G. C. Biochemical and molecular properties of the Trypanosoma brucei alternative oxidase. *Molecular and Biochemical Parasitology* **95,** 53–68. ISSN: 0166-6851 (1998).

84. Tielens, A. G. & Hellemond, J. J. v. Surprising variety in energy metabolism within Trypanosomatidae. *Trends in Parasitology* **25,** 482–490. ISSN: 1471-4922 (Oct. 2009).

85. Coustou, V. *et al.* ATP generation in the Trypanosoma brucei procyclic form: cytosolic substrate level is essential, but not oxidative phosphorylation. *The Journal of biological chemistry* **278,** 49625–35. ISSN: 0021-9258 (Mar. 2003).

86. Besteiro, S., Barrett, M. P., Riviere, L. & Bringaud, F. Energy generation in insect stages of Trypanosoma brucei: metabolism in flux. *Trends in Parasitology* **21,** 185–191. ISSN: 1471-4922 (May 2005).

87. Weelden, S. W. H. v. *et al.* Procyclic Trypanosoma brucei Do Not Use Krebs Cycle Activity for Energy Generation. *Journal of Biological Chemistry* **278,** 12854–12863. ISSN: 0021-9258 (Apr. 2003).

88. Weelden, S. W. H. v., Hellemond, J. J. v., Opperdoes, F. R. & Tielens, A. G. M. New Functions for Parts of the Krebs Cycle in Procyclic Trypanosoma brucei, a Cycle Not Operating as a Cycle. *Journal of Biological Chemistry* **280,** 12451–12460. ISSN: 0021-9258 (Apr. 2005).

89. Cazzulo, J. J. Intermediate metabolism inTrypanosoma cruzi. *Journal of Bioenergetics and Biomembranes* **26,** 157–165. ISSN: 0145-479X (1993).

90. Maugeri, D. A., Cannata, J. J. & Cazzulo, J.-J. Glucose metabolism in Trypanosoma cruzi. *Biochemical Society. Essays Biochem.* **51,** 15–30. ISSN: 0071-1365 (Oct. 2011).

91. Tielens, A. & Hellemond, J. V. Differences in Energy Metabolism Between Trypanosomatidae. *Parasitology Today* **14,** 265–272. ISSN: 0169-4758 (1998).

92. D'Andrea, G. Classifying amino acids as gluco(glyco)genic, ketogenic, or both. *Biochemical Education* **28,** 27–28. ISSN: 1879-1468 (Jan. 2000).

93. Creek, D. J. *et al.* Metabolomics Guides Rational Development of a Simplified Cell Culture Medium for Drug Screening against Trypanosoma brucei. *Antimicrobial Agents and Chemotherapy* **57,** 2768–79. ISSN: 0066-4804 (June 2013).

94. Marie-Pierre, H. *Amino acid transporters in Trypanosoma brucei brucei.* PhD thesis (University of Glasgow, May 2001), 190.

95. Coustou, V. *et al.* Glucose-induced Remodeling of Intermediary and Energy Metabolism in Procyclic Trypanosoma brucei. *Journal of Biological Chemistry* **283,** 16342–16354. ISSN: 0021-9258 (June 2008).

96. Spitznagel, D. *et al.* Alanine aminotransferase of Trypanosoma brucei–a key role in proline metabolism in procyclic life forms. *The FEBS journal* **276,** 7187–99. ISSN: 1742-4658 (Sept. 2009).

97. Steiger, R. F., Opperdoes, F. R. & Bontemps, J. Subcellular Fractionation of Trypanosoma brucei Bloodstream Forms with Special Reference to Hydrolases. *European Journal of Biochemistry* **105,** 163–175. ISSN: 1432-1033 (1980).

98. Marciano, D. *et al.* Biochemical characterization of stage-specific isoforms of aspartate aminotransferases from Trypanosoma cruzi and Trypanosoma brucei. *Molecular and Biochemical Parasitology* **161,** 12–20. ISSN: 0166-6851 (Sept. 2008).

99. Berger, L. C., Wilson, J., Wood, P. & Berger, B. J. Methionine Regeneration and Aspartate Aminotransferase in Parasitic Protozoa. *Journal of Bacteriology* **183,** 4421–4434. ISSN: 0021-9193 (Aug. 2001).

100. Chatterjee, A. N. & Ghosh, J. J. Transaminases of Leishmania donovani, the Causative Organism of Kala-azar. *Nature* **180,** 1425–1425. ISSN: 0028-0836 (1957).

101. Berger, B. J., Dai, W. W., Wang, H., Stark, R. E. & Cerami, A. Aromatic amino acid transamination and methionine recycling in trypanosomatids. *Proceedings of the National Academy of Sciences of the United States of America* **93,** 4126–30. ISSN: 0027-8424 (1996).

102. Stibbs, H. H. & Seed, J. R. Chromatographic evidence for the synthesis of possible sleep-mediators inTrypanosoma brucei gambiense. *Experientia* **29,** 1563–1565. ISSN: 0014-4754 (Dec. 1973).

103. Stibbs, H. H. & Seed, J. R. Metabolism of tyrosine and phenylalanine in Trypanosoma brucei gambiense. *International Journal of Biochemistry* **6,** 197–203. ISSN: 0020-711X (1975).

104. Montemartini, M., Santome, J., Cazzulo, J. J. & Nowicki, C. Production of aromatic α-hydroxyacids by epimastigotes of Trypanosoma cruzi, and its possible role in NADH reoxidation. *FEMS Microbiology Letters* **118,** 89–92. ISSN: 1574-6968 (May 1994).

105. Backlund, P. S. & Smith, R. A. Methionine synthesis from 5'-methylthioadenosine in rat liver. *The Journal of biological chemistry* **256,** 1533–5. ISSN: 0021-9258 (1981).

106. Hasne, M. & Barrett, M. P. Transport of methionine in Trypanosoma brucei brucei. *Molecular and Biochemical Parasitology* **111,** 299–307. ISSN: 0166-6851 (Dec. 2000).

107. Stibbs, H. H. & Seed, J. R. Further studies on the metabolism of tryptophan inTrypanosoma brucei gambiense: Cofactors, inhibitors, and end-products. *Experientia* **31,** 274–278. ISSN: 0014-4754 (1975).

108. Ackerman, S. B. & Seed, J. R. The effects of tryptophol on immune responses and it implications toward trypanosome-induced immunosuppression. *Experientia* **32,** 645–7. ISSN: 0014-4754 (1976).

109. Newport, G. R., Page, C. R., Ashman, P. U., Stibbs, H. H. & Seed, J. R. Alteration of Free Serum Amino Acids in Voles Infected with Trypanosoma brucei gambiense. *The Journal of Parasitology* **63,** 15. ISSN: 0022-3395 (1977).

110. Hall, J. E. & Seed, J. R. Increased urinary excretion of aromatic amino acid catabolites by Microtus montanus chronically infected with Trypanosoma brucei gambiense. *Comparative Biochemistry and Physiology Part B: Comparative Biochemistry* **77,** 755–760. ISSN: 0305-0491 (Jan. 1984).

111. Sawalhy, A. E., Seed, J. R., Hall, J. E. & Attar, H. E. Increased Excretion of Aromatic Amino Acid Catabolites in Animals Infected with Trypanosoma brucei evansi. *The Journal of Parasitology* **84,** 469. ISSN: 0022-3395 (1998).

112. Morrison, L. J., Marcello, L. & McCulloch, R. Antigenic variation in the African trypanosome: molecular mechanisms and phenotypic complexity. *Cellular Microbiology* **11,** 1724–1734. ISSN: 1462-5822 (Dec. 2009).

113. Stockdale, C., Swiderski, M. R., Barry, J. D. & McCulloch, R. Antigenic variation in Trypanosoma brucei: joining the DOTs. *PLoS biology* **6,** 185. ISSN: 1544-9173 (July 2008).

114. Stijlemans, B. *et al.* Immune Evasion Strategies of Trypanosoma brucei within the Mammalian Host: Progression to Pathogenicity. *Frontiers in Immunology* **7,** 233 (2016).

115. Silva, M. Induced cytokine network during experimental African trypanosomiasis. *International Journal of Interferon, Cytokine and Mediator Research* **3,** 71–78. ISSN: 1179-139X (Dec. 2011).

116. Baral, T. N. Immunobiology of African Trypanosomes: Need of Alternative Interventions. *Journal of Biomedicine and Biotechnology* **2010,** 1–24. ISSN: 1110-7243 (2010).

117. Gomez-Rodriguez, J. *et al.* Identification of a Parasitic Immunomodulatory Protein Triggering the Development of Suppressive M1 Macrophages during African Trypanosomiasis. *Journal of Infectious Diseases* **200,** 1849–1860. ISSN: 0022-1899 (Sept. 2009).

118. Taylor, K. A. Immune responses of cattle to African trypanosomes: protective or pathogenic? *International Journal for Parasitology* **28,** 219–240. ISSN: 0020-7519 (Feb. 1998).

119. Mitchell, L. A., Pearson, T. W. & Gauldie, J. Interleukin-1 and interleukin-2 production in resistant and susceptible inbred mice infected with Trypanosoma congolense. *Immunology* **57,** 291–6. ISSN: 0019-2805 (1986).

120. Sileghem, M., Darji, A., Hamers, R. & Baetselier, D. P. Modulation of IL-1 production and IL-1 release during experimental trypanosome infections. *Immunology* **68,** 137–9. ISSN: 0019-2805 (1989).

121. Laemmli, U. K. Cleavage of Structural Proteins during the Assembly of the Head of Bacteriophage T4. *Nature* **227,** 680–685. ISSN: 0028-0836 (1970).

122. Medina-Acosta, E. & Cross, G. A. Rapid isolation of DNA from trypanosomatid protozoa using a simple 'mini-prep' procedure. *Molecular and biochemical parasitology* **59,** 327–9. ISSN: 0166-6851 (1993).

123. Wirtz, E., Leal, S., Ochatt, C. & Cross, G. A. A tightly regulated inducible expression system for conditional gene knock-outs and dominant-negative genetics in Trypanosoma brucei. *Molecular and Biochemical Parasitology* **99,** 89–101. ISSN: 0166-6851 (Mar. 1999).

124. Wickstead, B., Ersfeld, K. & Gull, K. Targeting of a tetracycline-inducible expression system to the transcriptionally silent minichromosomes of Trypanosoma brucei. *Molecular and Biochemical Parasitology* **125,** 211–216. ISSN: 0166-6851 (Feb. 2002).

125. Livak, K. J. & Schmittgen, T. D. Analysis of Relative Gene Expression Data Using Real-Time Quantitative PCR and the $2^{(\Delta\Delta Ct)}$ Method. *Methods* **25,** 402–408. ISSN: 1046-2023 (2001).

126. Sunter, J., Wickstead, B., Gull, K. & Carrington, M. A new generation of T7 RNA polymerase-independent inducible expression plasmids for Trypanosoma brucei. *PloS one* **7,** e35167 (Dec. 2012).

127. Schmid-Burgk, J. L., Schmidt, T., Kaiser, V., Honing, K. & Hornung, V. A ligation-independent cloning technique for high-throughput assembly of transcription activator–like effector genes. *Nature biotechnology* **31,** 76–81. ISSN: 1087-0156 (2013).

128. Aslanidis, C. & Jong, P. J. d. Ligation-independent cloning of PCR products (LIC-PCR). *Nucleic acids research* **18,** 6069–74. ISSN: 0305-1048 (1990).

129. Graslund, S. *et al.* The use of systematic N- and C-terminal deletions to promote production and structural studies of recombinant proteins. *Protein expression and purification* **58,** 210–21. ISSN: 1046-5928 (Aug. 2008).

130. Malashkevich, V. *et al.* Crystal structure of the closed form of chicken cytosolic aspartate aminotransferase at 1.9 A resolution. *Journal of molecular biology* **247,** 111–24. ISSN: 0022-2836 (1995).

131. Rhee, S. *et al.* Refinement and Comparisons of the Crystal Structures of Pig Cytosolic Aspartate Aminotransferase and Its Complex with 2-Methylaspartate. *Journal of Biological Chemistry* **272,** 17293–17302. ISSN: 0021-9258 (1997).

132. Bornhorst, J. A. & Falke, J. J. *Purification of proteins using polyhistidine affinity tags* 245–254 (2000).

133. Kruger, N. J. The Bradford method for protein quantitation. *Methods in molecular biology (Clifton, N.J.)* **32,** 9–15. ISSN: 1064-3745 (1994).

134. Consortium, S. G. *et al.* Protein production and purification. *Nature Methods* **5,** 135–146. ISSN: 1548-7091 (Aug. 2008).

135. Britton, H. T. S. & Robinson, R. A. CXCVIII.-Universal buffer solutions and the dissociation constant of veronal. *J. Chem. Soc.* 1456–1462 (1931).

136. McFarland, J. *The investigation of two novel proteins of cellular and metabolic significance in Trypanosoma brucei.* PhD thesis (School of Biochemistry and Immunology, Trinity College Dublin., Jan. 2016), 280.

137. Bergmeyer, H. U. & Bernt, E. *Methods of Enzymatic Analysis (Second Edition), Volume 3* 2302 (1974).

138. Nowicki, C. & Cazzulo, J. J. Aromatic amino acid catabolism in trypanosomatids. *Comparative biochemistry and physiology. Part A, Molecular & integrative physiology* **151,** 381–90. ISSN: 1095-6433 (Nov. 2008).

139. Franke, M. C. C., Vernal, J., Cazzulo, J. J. & Nowicki, C. The NAD-linked aromatic α-hydroxy acid dehydrogenase from Trypanosoma cruzi. *European Journal of Biochemistry* **266,** 903–910. ISSN: 1432-1033 (Dec. 1999).

140. Bergmeyer, H., Scheibe, P. & Wahlefeld, A. Optimization of methods for aspartate aminotransferase and alanine aminotransferase. *Clinical chemistry* **24,** 58–73. ISSN: 0009-9147 (1978).

141. Rosengren, E. *et al.* The macrophage migration inhibitory factor MIF is a phenylpyruvate tautomerase. *FEBS Letters* **417,** 85–88. ISSN: 1873-3468 (Nov. 1997).

142. Mehta, P. K., Hale, T. I. & Christen, P. Aminotransferases: demonstration of homology and division into evolutionary subgroups. *European Journal of Biochemistry* **214,** 549–561. ISSN: 1432-1033 (1993).

143. Jensen, R. A. & Gu, W. Evolutionary recruitment of biochemically specialized subdivisions of Family I within the protein superfamily of aminotransferases. *Journal of bacteriology* **178,** 2161–71. ISSN: 0021-9193 (1996).

144. Shrawder, E. & Martinez-Carrion, M. Evidence of phenylalanine transaminase activity in the isoenzymes of aspartate transaminase. *The Journal of biological chemistry* **247,** 2486–92. ISSN: 0021-9258 (1972).

145. Vernal, J., Cazzulo, J. J. & Nowicki, C. Isolation and partial characterization of a broad specificity aminotransferase from Leishmania mexicana promastigotes. *Molecular and Biochemical Parasitology* **96,** 83–92. ISSN: 0166-6851 (Oct. 1998).

146. Bujacz, A., Rutkiewicz-Krotewicz, M., Nowakowska-Sapota, K. & Turkiewicz, M. Crystal structure and enzymatic properties of a broad substrate-specificity psychrophilic aminotransferase from the Antarctic soil bacterium Psychrobacter sp. B6. *Acta Crystallographica Section D: Biological Crystallography* **71.** ISSN: 1399-0047 (Mar. 2015).

147. Blankenfeldt, W., Montemartini-Kalisz, M., Kalisz, H. M., Hecht, H. & Nowicki, C. Crystal structure of trypanosoma cruzi tyrosine aminotransferase: Substrate specificity is influenced by cofactor binding mode. *Protein Science* **8,** 2406–2417. ISSN: 1469-896X (1999).

148. Han, Q., Robinson, H., Cai, T., Tagle, D. A. & Li, J. Biochemical and structural characterization of mouse mitochondrial aspartate aminotransferase, a newly identified kynurenine aminotransferase-IV. *Bioscience Reports* **31,** 323–32. ISSN: 0144-8463 (Oct. 2011).

149. Placzek, S. *et al.* BRENDA in 2017: new perspectives and new tools in BRENDA. *Nucleic Acids Research* **45,** D380–D388. ISSN: 0305-1048 (Jan. 2017).

150. Marciano, D., Maugeri, D. A., Cazzulo, J. J. & Nowicki, C. Functional characterization of stage-specific aminotransferases from trypanosomatids. *Molecular and biochemical parasitology* **166,** 172–82. ISSN: 0166-6851 (Aug. 2009).

151. Aslett, M. *et al.* TriTrypDB: a functional genomic resource for the Trypanosomatidae. *Nucleic Acids Research* **38,** D457–D462. ISSN: 0305-1048 (Oct. 2010).

152. Brun, R., Hecker, H. & Lun, Z.-R. Trypanosoma evansi and T. equiperdum: distribution, biology, treatment and phylogenetic relationship (a review). *Veterinary Parasitology* **79,** 95–107. ISSN: 0304-4017 (Oct. 1998).

153. Abendroth, J. *et al.* Structures of aspartate aminotransferases from Trypanosoma brucei, Leishmania major and Giardia lamblia. *Acta Crystallographica Section F: Structural Biology Communications* **71,** 566–571. ISSN: 2053-230X (2015).

154. Wrenger, C. *et al.* Specific Inhibition of the Aspartate Aminotransferase of Plasmodium falciparum. *Journal of Molecular Biology.* ISSN: 0022-2836 (Nov. 2011).

155. Wen, J., Nowicki, C. & Blankenfeldt, W. Structural basis for the relaxed substrate selectivity of Leishmania mexicana broad specificity aminotransferase. *Molecular and Biochemical Parasitology* **202,** 34–37. ISSN: 0166-6851 (Aug. 2015).

156. Shi, Y. *et al.* Abnormal SDS-PAGE migration of cytosolic proteins can identify domains and mechanisms that control surfactant binding. *Protein science : a publication of the Protein Society* **21,** 1197–209. ISSN: 1469-896X (Aug. 2012).

157. Montemartini, M., Santome, J., Cazzulo, J. J. & Nowicki, C. Purification and partial structural and kinetic characterization of an aromatic L-α-hydroxy acid dehydrogenase from epimastigotes of Trypanosoma cruzi. *Molecular and Biochemical Parasitology* **68,** 15–23. ISSN: 0166-6851 (Nov. 1994).

158. Carson, M., Johnson, D., McDonald, H., Brouillette, C. & DeLucas, L. His-tag impact on structure. *Acta Crystallographica Section D: Biological Crystallography* **63,** 295–301. ISSN: 0907-4449 (July 2007).

159. Branden, C. Relation between structure and function of α/β-proteins. *Quarterly Reviews of Biophysics* **13,** 317–338 (Aug. 1980).

160. Vernal, J., Cazzulo, J. J. & Nowicki, C. Cloning and heterologous expression of a broad specificity aminotransferase of Leishmania mexicana promastigotes1. *FEMS Microbiology Letters* **229,** 217–222. ISSN: 1574-6968 (Dec. 2003).

161. Berger, B. J., Dai, W. & Wilson, J. Methionine formation from α-ketomethiobutyrate in the trypanosomatid Crithidia fasciculata. *FEMS Microbiology Letters* **165,** 305–312. ISSN: 1574-6968 (Aug. 1998).

162. Heilbronn, J., Wilson, J. & Berger, B. J. Tyrosine aminotransferase catalyzes the final step of methionine recycling in Klebsiella pneumoniae. *Journal of bacteriology* **181,** 1739–47. ISSN: 0021-9193 (1999).

163. Pirkov, I., Norbeck, J., Gustafsson, L. & Albers, E. A complete inventory of all enzymes in the eukaryotic methionine salvage pathway. *FEBS Journal* **275,** 4111–4120. ISSN: 1742-4658 (Aug. 2008).

164. Mavrides, C. & Orr, W. Multispecific aspartate and aromatic amino acid aminotransferases in Escherichia coli. *The Journal of biological chemistry* **250,** 4128–33. ISSN: 0021-9258 (1975).

165. Tangen, O., Fonnum, F. & Haavaldsen, R. Separation and purification of aromatic amino acid transaminases from rat brain. *Biochimica et Biophysica Acta (BBA) - Nucleic Acids and Protein Synthesis* **96,** 82–90. ISSN: 0005-2787 (1965).

166. Jager, J., Pauptit, R. A., Sauder, U. & Jansonius, J. N. Three-dimensional structure of a mutant E.coli aspartate aminotransferase with increased enzymic activity. *Protein Engineering, Design and Selection* **7,** 605–612. ISSN: 1741-0126 (1994).

167. Nowicki, C., Montemartini, M., Duschak, V., Santome, J. & Cazzulo, J. J. Presence and subcellular localization of tyrosine aminotransferase and p-hydroxyphenyllactate dehydrogenase in epimastigotes of Trypanosoma cruzi. *FEMS Microbiology Letters* **92,** 119–124. ISSN: 1574-6968 (Apr. 1992).

168. Voorheis, H. P. & Martin, B. R. 'Swell Dialysis' Demonstrates that Adenylate Cyclase in Trypanosoma brucei is Regulated by Calcium Ions. *European Journal of Biochemistry* **113,** 223–227. ISSN: 1432-1033 (1980).

169. Mony, B. M. *et al.* Genome-wide dissection of the quorum sensing signalling pathway in Trypanosoma brucei. *Nature* **505,** 681–685. ISSN: 0028-0836 (Jan. 2014).

170. Hall, J. E. & Seed, J. R. Quantitation of aromatic amino acid catabolites in urine of mice acutely infected with Trypanosoma brucei gambiense. *Comparative Biochemistry and Physiology Part B: Comparative Biochemistry* **69,** 791–796. ISSN: 0305-0491 (Dec. 1981).

171. Newport, G. R. & Page, C. R. Free Amino Acids in Brain, Liver, and Skeletal Muscle Tissue of Voles Infected with Trypanosoma brucei gambiense. *The Journal of Parasitology* **63,** 1060 (1977).

172. McGettrick, A. F. *et al.* Trypanosoma brucei metabolite indolepyruvate decreases HIF-1α and glycolysis in macrophages as a mechanism of innate immune evasion. *Proceedings of the National Academy of Sciences,* 201608221. ISSN: 0027-8424 (2016).

173. Politi, V., D'Alessio, S., Stazio, G. D. & Luca, G. D. Recent Advances in Tryptophan Research. *springer* **398,** 291–298 (Jan. 1996).

174. Millerioux, Y. *et al.* The threonine degradation pathway of the Trypanosoma brucei procyclic form: the main carbon source for lipid biosynthesis is under metabolic control. *Molecular Microbiology.* ISSN: 1365-2958 (2013).

175. Aranda, A. *et al.* The malate dehydrogenase isoforms from Trypanosoma brucei: Subcellular localization and differential expression in bloodstream and procyclic forms. *International Journal for Parasitology* **36,** 295–307. ISSN: 0020-7519 (Mar. 2006).

176. Vernal, J., Munoz-Jordan, J., Muller, M., Cazzulo, J. J. & Nowicki, C. Sequencing and heterologous expression of a cytosolic-type malate dehydrogenase of Trypanosoma brucei. *Molecular and Biochemical Parasitology* **117,** 217–221. ISSN: 0166-6851 (Oct. 2001).

177. Loureiro, I. *et al.* Knockdown of Asparagine Synthetase A Renders Trypanosoma brucei Auxotrophic to Asparagine. *PLoS Neglected Tropical Diseases* **7,** e2578 (Dec. 2013).

178. Lamas, B. *et al.* CARD9 impacts colitis by altering gut microbiota metabolism of tryptophan into aryl hydrocarbon receptor ligands. *Nature medicine* **22,** 598–605. ISSN: 1078-8956 (June 2016).

179. Medzhitov, R. & Janeway, C. J. Innate immune recognition: mechanisms and pathways. *Immunological Reviews* **173,** 89–97. ISSN: 1600-065X (Feb. 2000).

180. Politi, V., Luca, G. D., Gallai, V., Puca & Comin, M. Clinical Experiences with the Use of Indole-3-Pyruvic Acid. *Tryptophan, Serotonin, and Melatonin.* **467** (Jan. 1999).

181. Enanga, B., Burchmore, R., Stewart, M. & Barrett, M. Sleeping sickness and the brain. *Cellular and Molecular Life Sciences (CMLS)* **59,** 845–858. ISSN: 1420-682X (May 2002).

182. Pich, E. M., Solfrini, V., Biagini, G., Fuxe, K. & Agnati, L. F. Effects of indolepyruvic acid on sleep and food intake in the rat. *Acta Physiologica Scandinavica* **139,** 583–589. ISSN: 1365-201X (Aug. 1990).

183. Saura, J. Microglial cells in astroglial cultures: a cautionary note. *Journal of neuroinflammation* **4,** 26 (July 2007).

184. Otterbein, L. E., Soares, M. P., Yamashita, K. & Bach, F. H. Heme oxygenase-1: unleashing the protective properties of heme. *Trends in Immunology* **24,** 449–455. ISSN: 1471-4906 (Aug. 2003).

185. Chowdhury, G. *et al.* Structural identification of Diindole agonists of the aryl hydrocarbon receptor derived from degradation of indole-3-pyruvic acid. *Chemical research in toxicology* **22,** 1905–12. ISSN: 0893-228X (Dec. 2009).

186. Tivendale, N. D., Davies, N. W., Horne, J., Ross, J. J. & Smith, J. A. Analysis of the Enol-Keto Tautomers of Indole-3-Pyruvic Acid. *Australian Journal of Chemistry.* ISSN: 0004-9425 (2014).

187. Aoki, R., Aoki-Yoshida, A., Suzuki, C. & Takayama, Y. Protective Effect of Indole-3-Pyruvate against Ultraviolet B-Induced Damage to Cultured HaCaT Keratinocytes and the Skin of Hairless Mice. *PLoS ONE* **9** (May 2014).

188. Bittinger, M. A., Nguyen, L. P. & Bradfield, C. A. Aspartate aminotransferase generates proagonists of the aryl hydrocarbon receptor. *Molecular pharmacology* **64,** 550–6 (Sept. 2003).

189. Rosengren, E. *et al.* The immunoregulatory mediator macrophage migration inhibitory factor (MIF) catalyzes a tautomerization reaction. **2,** 143–9 (1996).

190. Painter, H. & Zilva, S. The tautomeric conversion of p-hydroxyphenylpyruvic acid. *Biochemical Journal* **41,** 520 (1947).

191. Knox, W. E. & Pitt, B. M. Enzymic catalysis of the keto-enol tautomerization of phenylpyruvic acids. *The Journal of biological chemistry* **225,** 675–88. ISSN: 0021-9258 (1957).

192. Stowe, B. B. & Thimann, K. V. Indolepyruvic Acid in Maize. *Nature* **172,** 764–764. ISSN: 0028-0836 (1953).

193. Bentley, J. A., Farrar, K. R., Housley, S., Smith, G. F. & Taylor, W. C. Some chemical and physiological properties of 3-indolylpyruvic acid. *Biochemical Journal* **64,** 44–49. ISSN: 0264-6021 (Sept. 1956).

194. Schwarz, K. & Bitancourt, A. A. Further evidence of tautomerism in chromatograms of indolyl-3-pyruvic acid. *Biochemical Journal* **75,** 182–187. ISSN: 0264-6021 (Apr. 1960).

195. Yang, X., Wu, X., An, Y. & Tang, H. An NMR Study on Keto-Enol Tautomerism of Indole-3-Pyruvic Acid. **31,** 81 (Mar. 2014).

196. Bucher, T. & Kirberger, E. Uber die enol-keto-tautomerie der p-oxyphenylbrenztraubensaure. *Biochimica et Biophysica Acta* **8,** 401–406. ISSN: 0006-3002 (Jan. 1952).

197. Schwarz, K. Separation of enol and keto tautomers of aromatic pyruvic acids by paper chromatography. *Archives of Biochemistry and Biophysics* **92,** 168–175. ISSN: 0003-9861 (Jan. 1961).

198. Pitt, B. M. Oxidation of Phenylpyruvates to Aromatic Aldehydes and Oxalate. *Nature* **196,** 272–273. ISSN: 0028-0836 (1962).

199. Politi, V. *et al.* Substantially pure solid form of the enol tautomer of 3-indolylpyruvic acid for use in the treatment of central nervous system disturbances. WO Patent App. PCT/IT2003/000,275 (Nov. 2003).

200. Lin, E. C., Pitt, B. M., Civen, M. & Knox, W. E. The assay of aromatic amino acid transaminations and keto acid oxidation by the enol borate-tautomerase method. *The Journal of biological chemistry* **233,** 668–73. ISSN: 0021-9258 (1958).

201. Wishart, D. S. *et al.* HMDB 3.0–The Human Metabolome Database in 2013. *Nucleic Acids Research* **41** (2012).

202. Zhao, Y. Auxin Biosynthesis: A Simple Two-Step Pathway Converts Tryptophan to Indole-3-Acetic Acid in Plants. *Molecular Plant* **5,** 334–338. ISSN: 1674-2052 (Dec. 2012).

203. Nutaratat, P., Srisuk, N., Arunrattiyakorn, P. & Limtong, S. Indole-3-acetic acid biosynthetic pathways in the basidiomycetous yeast Rhodosporidiumpaludigenum. *Archives of Microbiology* **198,** 429–437. ISSN: 0302-8933 (Feb. 2016).

204. Lubetsky, J. B. *et al.* The tautomerase active site of macrophage migration inhibitory factor is a potential target for discovery of novel anti-inflammatory agents. **277,** 24976–82. ISSN: 0021-9258 (2002).

205. Garai, J. & Lorand, T. Macrophage Migration Inhibitory Factor (MIF) Tautomerase Inhibitors as Potential Novel Anti-Inflammatory Agents: Current Developments. *Curr Med Chem* **16,** 1091–1114. ISSN: 0929-8673 (2009).

206. Ouertatani-Sakouhi, H. *et al.* Identification and characterization of novel classes of macrophage migration inhibitory factor (MIF) inhibitors with distinct mechanisms of action. *The Journal of biological chemistry* **285,** 26581–98. ISSN: 0021-9258 (Oct. 2010).

207. Garzon, E. *et al.* The Trypanosoma brucei gambiense Secretome Impairs Lipopolysaccharide-Induced Maturation, Cytokine Production, and Allostimulatory Capacity of Dendritic Cells. *Infection and Immunity* **81,** 3300–3308. ISSN: 0019-9567 (2013).

208. Nyakundi, J. N., Crawley, B. & Pentreath, V. W. The relationships between endotoxins, nitric oxide and inflammatory cytokines in blood and intestinal tissues in experimental Trypanosoma brucei brucei infections. *Parasitology* **124,** 597–604. ISSN: 0031-1820 (Feb. 2002).

209. Bentivoglio, M. & Kristensson, K. Tryps and trips: cell trafficking across the 100-year-old blood–brain barrier. *Trends in Neurosciences* **37,** 325–333. ISSN: 0166-2236 (June 2014).

210. Masocha, W., Amin, D. N., Kristensson, K. & Rottenberg, M. E. Differential Invasion of Trypanosoma brucei brucei and Lymphocytes into the Brain of C57BL/6 and 129Sv/Ev Mice. *Scandinavian Journal of Immunology* **68,** 484–491. ISSN: 1365-3083 (Nov. 2008).

211. Daulouede, S. *et al.* Human Macrophage Tumor Necrosis Factor (TNF)-α Production Induced by Trypanosoma brucei gambiense and the Role of TNF-α in Parasite Control. *Journal of Infectious Diseases* **183,** 988–991 (2001).

212. Magez, S. *et al.* Specific uptake of tumor necrosis factor-alpha is involved in growth control of Trypanosoma brucei. *The Journal of cell biology* **137,** 715–27. ISSN: 0021-9525 (1997).

213. Hunter, C. A., Gow, J. W., Kennedy, P. G., Jennings, F. W. & Murray, M. Immunopathology of experimental African sleeping sickness: detection of cytokine mRNA in the brains of Trypanosoma brucei brucei-infected mice. *Infection and immunity* **59,** 4636–40. ISSN: 0019-9567 (1991).

214. Geiger, A. *et al.* Escaping Deleterious Immune Response in Their Hosts: Lessons from Trypanosomatids. *Frontiers in Immunology* **7** (May 2016).

215. Gutierrez, F. R. *et al.* Haeme oxygenase activity protects the host against excessive cardiac inflammation during experimental Trypanosoma cruzi infection. *Microbes and Infection* **16,** 28–39 (2014).

216. Luz, N. F. *et al.* Heme Oxygenase-1 Promotes the Persistence of Leishmania chagasi Infection. *The Journal of Immunology* **188,** 4460–4467. ISSN: 0022-1767 (May 2012).

217. Epiphanio, S. *et al.* Heme Oxygenase-1 Is an Anti-Inflammatory Host Factor that Promotes Murine Plasmodium Liver Infection. *Cell Host & Microbe* **3,** 331–338. ISSN: 1931-3128 (May 2008).

218. Ivashkiv, L. B. & Donlin, L. T. Regulation of type I interferon responses. *Nature reviews. Immunology* **14,** 36–49 (2014).

219. Rothhammer, V. *et al.* Type I interferons and microbial metabolites of tryptophan modulate astrocyte activity and central nervous system inflammation via the aryl hydrocarbon receptor. *Nature medicine* **22,** 586–97. ISSN: 1078-8956 (June 2016).

220. Ward, F. W. The Fate of Indolepropionic Acid in the Animal Organism. *Biochemical Journal* **17,** 907–915. ISSN: 0264-6021 (1923).

221. Bartolini, B., Corniello, C., Sella, A., Somma, F. & Politi, V. *Developments in Tryptophan and Serotonin Metabolism* 601–608 (Mar. 2003).

222. Politi, V., Lavaggi, M. V., Stazio, G. D. & Margonelli, A. Kynurenine and Serotonin Pathways. **294,** 515–518 (Jan. 1991).

223. Auxin Biosynthesis: Are the Indole-3-Acetic Acid and Phenylacetic Acid Biosynthesis Pathways Mirror Images? *Plant physiology* **171,** 1230–41 (2016).

224. Henderson, J. H. M. Biological Activity of Degradation Products of Indolepyruvic Acid. *Nature* **205,** 702–703. ISSN: 0028-0836 (Feb. 1965).

225. Tam, Y. Y. & Normanly, J. Determination of indole-3-pyruvic acid levels in Arabidopsis thaliana by gas chromatography-selected ion monitoring-mass spectrometry. *Journal of Chromatography A* **800,** 101–108. ISSN: 0021-9673 (Mar. 1998).

226. Fingerle-Rowson, G. *et al.* A Tautomerase-Null Macrophage Migration-Inhibitory Factor (MIF) Gene Knock-In Mouse Model Reveals That Protein Interactions and Not Enzymatic Activity Mediate MIF-Dependent Growth Regulation. *Molecular and Cellular Biology* **29,** 1922–1932. ISSN: 0270-7306 (Sept. 2009).

227. Shah, Y. M. *et al.* Hypoxia-Inducible Factor Augments Experimental Colitis Through an MIF Dependent Inflammatory Signaling Cascade. *Gastroenterology* **134,** 2036–2048. e3 (Aug. 2008).

228. Fu, H., Luo, F., Yang, L., Wu, W. & Liu, X. Hypoxia stimulates the expression of macrophage migration inhibitory factor in human vascular smooth muscle cells via HIF-1α dependent pathway. *Bmc Cell Biol* **11,** 1–13. ISSN: 1471-2121 (2010).

229. Stijlemans, B. *et al.* MIF Contributes to Trypanosoma brucei Associated Immunopathogenicity Development. *PLoS Pathogens* **10,** e1004414. ISSN: 1553-7366 (2014).

230. Stijlemans, B. *et al.* MIF-Mediated Hemodilution Promotes Pathogenic Anemia in Experimental African Trypanosomosis. *PLOS Pathogens* **12,** e1005862. ISSN: 1553-7374 (2016).

231. Berriman, M. *et al.* The genome of the African trypanosome Trypanosoma brucei. *Science (New York, N.Y.)* **309,** 416–22 (May 2005).

232. El-Sayed, N. M. *et al.* The Genome Sequence of Trypanosoma cruzi, Etiologic Agent of Chagas Disease. *Science* **309,** 409–415. ISSN: 0036-8075 (May 2005).

233. Willert, E. & Phillips, M. A. Regulation and function of polyamines in African trypanosomes. *Trends in Parasitology* **28,** 66–72. ISSN: 1471-4922 (Feb. 2012).

234. Bachi, C. J., Vergara, C., Garofalo, J., Lipschik, G. Y. & Hutner, S. H. Synthesis and Content of Polyamines in Bloodstream Trypanosoma brucei. *Journal of Eukaryotic Microbiology* **26,** 484–488. ISSN: 1550-7408 (Aug. 1979).

235. Koning, H. P. d., Bridges, D. J. & Burchmore, R. J. Purine and pyrimidine transport in pathogenic protozoa: From biology to therapy. *FEMS Microbiology Reviews* **29,** 987–1020. ISSN: 1574-6976 (Nov. 2005).

236. Gudin, S. *et al.* Trypanosoma brucei: A survey of pyrimidine transport activities. *Experimental Parasitology* **114,** 118–125. ISSN: 0014-4894 (Oct. 2006).

237. Ali, J. A. M. *et al.* Pyrimidine Salvage in Trypanosoma brucei Bloodstream Forms and the Trypanocidal Action of Halogenated Pyrimidines. *Molecular Pharmacology* **83,** 439–453 (Feb. 2013).

238. Hammond, D. J. & Gutteridge, W. E. UMP synthesis in the kinetoplastida. *Biochimica et Biophysica Acta (BBA) - General Subjects* **718,** 1–10. ISSN: 0304-4165 (Sept. 1982).

239. Arakaki, T. L. *et al.* Characterization of Trypanosoma brucei dihydroorotate dehydrogenase as a possible drug target; structural, kinetic and RNAi studies. *Molecular Microbiology* **68,** 37–50. ISSN: 1365-2958 (Apr. 2008).

240. Ali, J. A. M. *et al.* Pyrimidine biosynthesis is not an essential function for Trypanosoma brucei bloodstream forms. *PLoS ONE* **8** (Mar. 2013).

241. Leija, C. *et al.* Pyrimidine Salvage Enzymes Are Essential for De Novo Biosynthesis of Deoxypyrimidine Nucleotides in Trypanosoma brucei. *PLOS Pathogens* **12,** e1006010. ISSN: 1553-7366 (Nov. 2016).

242. Nolan, D. P. & Voorheis, H. P. The mitochondrion in bloodstream forms of Trypanosoma brucei is energized by the electrogenic pumping of protons catalysed by the F1F0-ATPase. *European journal of biochemistry / FEBS* **209,** 207–16. ISSN: 0014-2956 (1992).

243. Ong, H. B., Sienkiewicz, N., Wyllie, S., Patterson, S. & Fairlamb, A. H. Trypanosoma brucei (UMP synthase null mutants) are avirulent in mice, but recover virulence upon prolonged culture in vitro while retaining pyrimidine auxotrophy. *Molecular Microbiology* **90,** 443–455. ISSN: 1365-2958 (2013).

244. Shameer, S. *et al.* TrypanoCyc: a community-led biochemical pathways database for Trypanosoma brucei. *Nucleic acids research* **43,** D637–44 (2014).

245. Schultz, C. J., Hsu, M., Miesak, B. & Coruzzi, G. M. Arabidopsis mutants define an in vivo role for isoenzymes of aspartate aminotransferase in plant nitrogen assimilation. *Genetics* **149,** 491–9. ISSN: 0016-6731 (1998).

246. Torre, F. d. l., Canas, R. A., Pascual, M. B., Avila, C. & Canovas, F. M. Plastidic aspartate aminotransferases and the biosynthesis of essential amino acids in plants. *Journal of Experimental Botany* **65,** 5527–5534. ISSN: 0022-0957 (Oct. 2014).

247. Jander, G. & Joshi, V. Aspartate-Derived Amino Acid Biosynthesis in Arabidopsis thaliana. *The Arabidopsis book / American Society of Plant Biologists* **12,** e0121 (Jan. 2009).

248. Sullivan, L. B. *et al.* Supporting Aspartate Biosynthesis Is an Essential Function of Respiration in Proliferating Cells. *Cell* **162,** 552–563. ISSN: 0092-8674 (July 2015).

249. Birsoy, K. *et al.* An Essential Role of the Mitochondrial Electron Transport Chain in Cell Proliferation Is to Enable Aspartate Synthesis. *Cell* **162,** 540–551. ISSN: 0092-8674 (July 2015).

250. Nowicki, C. *et al.* Recombinant tyrosine aminotransferase from Trypanosoma cruzi: structural characterization and site directed mutagenesis of a broad substrate specificity enzyme. *Biochimica et Biophysica Acta (BBA) - Protein Structure and Molecular Enzymology* **1546,** 268–281. ISSN: 0167-4838 (Jan. 2001).

251. Vincendeau, P. *et al.* Importance of L-Tryptophan Metabolism in Trypanosomiasis. **467,** 525–531 (Jan. 1999).

252. Li, J. V. *et al.* Metabonomic Investigation of Single and Multiple Strain Trypanosoma brucei brucei Infections. *The American Journal of Tropical Medicine and Hygiene* **84,** 91–98. ISSN: 0002-9637 (Jan. 2011).

253. Tetsutani, K., To, H., Torii, M., Hisaeda, H. & Himeno, K. Malaria parasite induces tryptophan-related immune suppression in mice. *Parasitology* **134,** 923–930. ISSN: 1469-8161 (July 2007).

254. Szempruch, A. J. *et al.* Extracellular Vesicles from Trypanosoma brucei Mediate Virulence Factor Transfer and Cause Host Anemia. *Cell* **164,** 246–257. ISSN: 0092-8674 (Jan. 2016).

255. Salmon, D. *et al.* Adenylate Cyclases of Trypanosoma brucei Inhibit the Innate Immune Response of the Host. *Science* **337,** 463–466. ISSN: 0036-8075 (Dec. 2012).

256. Wang, Y. *et al.* Global metabolic responses of mice to Trypanosoma brucei brucei infection. *Proceedings of the National Academy of Sciences* **105,** 6127–6132. ISSN: 0027-8424 (Apr. 2008).

257. Newport, G. R. & III, C. R. Free Amino Acids in Brain, Liver, and Skeletal Muscle Tissue of Voles Infected with Trypanosoma brucei gambiense. *The Journal of Parasitology* **63,** 1060. ISSN: 0022-3395 (1977).

258. Fallarino, F. *et al.* The Combined Effects of Tryptophan Starvation and Tryptophan Catabolites Down-Regulate T Cell Receptor γ-Chain and Induce a Regulatory Phenotype in Naive T Cells. *The Journal of Immunology* **176,** 6752–6761. ISSN: 0022-1767 (June 2006).

259. Rodgers, J., Stone, T. W., Barrett, M. P., Bradley, B. & Kennedy, P. Kynurenine pathway inhibition reduces central nervous system inflammation in a model of human African trypanosomiasis. *Brain* **132,** 1259–1267. ISSN: 0006-8950 (Sept. 2009).

260. Vincent, I. M. *et al.* Metabolomics Identifies Multiple Candidate Biomarkers to Diagnose and Stage Human African Trypanosomiasis. *PLOS Neglected Tropical Diseases* **10,** e0005140 (2016).

261. Mony, B. M. & Matthews, K. R. Assembling the components of the quorum sensing pathway in African trypanosomes. *Molecular Microbiology* **96,** 220–232. ISSN: 1365-2958 (Apr. 2015).

262. Reuner, B., Vassella, E., Yutzy, B. & Boshart, M. Cell density triggers slender to stumpy differentiation of Trypanosoma brucei bloodstream forms in culture. *Molecular and Biochemical Parasitology* **90,** 269–280. ISSN: 0166-6851 (1997).

263. Domingo-Sananes, M. R., Szoor, B., Ferguson, M. A., Urbaniak, M. D. & Matthews, K. R. Molecular control of irreversible bistability during trypanosome developmental commitment. *The Journal of cell biology* **211,** 455–68. ISSN: 0021-9525 (Oct. 2015).

264. Vassella, E., Reuner, B., Yutzy, B. & Boshart, M. Differentiation of African trypanosomes is controlled by a density sensing mechanism which signals cell cycle arrest via the cAMP pathway. *Journal of cell science* **110 (Pt 21),** 2661–71. ISSN: 0021-9533 (1997).

265. MacGregor, P. *et al.* High-Throughput Chemical Screening for Antivirulence Developmental Phenotypes in Trypanosoma brucei. *Eukaryotic Cell* **13,** 412–426. ISSN: 1535-9778 (Mar. 2014).

266. Wenzler, T. *et al.* A new approach to chemotherapy: drug-induced differentiation kills African trypanosomes. *Scientific Reports* **6,** 22451. ISSN: 2045-2322 (Mar. 2016).

267. Dean, S., Marchetti, R., Kirk, K. & Matthews, K. R. A surface transporter family conveys the trypanosome differentiation signal. *Nature* **459,** 213–217. ISSN: 0028-0836 (May 2009).

268. Traut, T. W. Physiological concentrations of purines and pyrimidines. *Molecular and Cellular Biochemistry* **140,** 1–22. ISSN: 0300-8177 (1994).

269. Canepa, G. E. *et al.* Aspartate transport and metabolism in the protozoan parasite Trypanosoma cruzi. *FEMS Microbiology Letters* **247,** 65–71. ISSN: 1574-6968 (May 2005).

Appendix

A The nucleotide sequences of *T. brucei* and *T. cruzi* cASAT ORFs.

A.1 The ORF of *T. brucei* cASAT (Tb927.10.3660).

```
ATGTCCAGGCCCTTTAAGGACTTAGCACCCGTTCCATTGGACCCCGTCTT          50
TGGTCTAGCGAGGGCTGCAAAGGCCGCCCCAGAACCGAAGGCGGATCTCG         100
TTATTGGTGCCTACCGCGACCAAAACGGGTTGCCGTATCCATTAAAAGTA         150
GTGCGGAAGGCTGAGCGGCGCATTGTGGACATGGGCCTTGATAAAGAGTA         200
CCCACCCATGACTGGTCTTCTTAACTTTGTTGAAGAAGCTGTAAAACTCG         250
CCTACGGCAATACGGTGCCATTGGAGCGTATCGCCGCCTCGCAGGGTCTC         300
AGCGGCACCGGCTCGCTTAGCCTTGGAGCCACGCTCCTCAGGCAGGTGGT         350
ACCTGAAGATACCCCCGTGTATGTTTCAAATCCCACATGGTCAAACCACG         400
TATCAATATTCGGAATTGTGGGTCACAAAAATATCCGTGAATACCGTTAC         450
TACAGTCCCAGCACCCATGAGCTGGACTTCGTTGGCCTCATTGAAGATCT         500
GAACGTGGCCCCTCAGGGGAGTATTATTGTGCTGCACGCATGTGCCCATA         550
ACCCCACTGGTGTGGATCCAAGCAAAGATCAGTGGGCAACCATCGCCGAT         600
GTATTTGTTGAACGTAAATTGATTCCCTTCTTCGACTCCGCCTACCAGGG         650
TTTTGCATCCGGCAGTCTCGACGAGGACGCCTACGCCATCCGCCACTTTG         700
CAAAGAGAGGGATGGAAATGCTACTTGCACAGTCCTTTTCCAAGAACATG         750
GGTTTGTATGCCGAACGTGTTGGTGTGATTTCTGCTGTCGTTTCGGATGC         800
TTCAAGGAAGGAGGCCGTGCGGAGCCGCCTTGAGGTGATCGCCCGTTCCT         850
ATTACTCAACCCCACCTGTACATGGCGCTCGCATCGCTCACCTCGTGATG         900
AGTGACAAAGAACTCCGCGCAGAATGGGAGCAGGAACTCAAGGAGATGGT         950
GAACCGCGTCCGAAGCATGCGTCAAGGTGTTTATGAAGGGCTGATGAAAC        1000
TCGGTACTCCCGGCACTTGGGAGCACATCATCAACCAGAAGGGTATGTTC        1050
TCTTATATGGGACTTTCAAGGCCTCAGTGCGAAAGGTTGTGCGAGAAGCG        1100
CGTTTTTGTGCTGCCTGTCGGCCGCGCCAACCTCGCAGCGTTAACGCCCT        1150
CAACAATGGATTTTCTGGTCAAGTCGATTGACGATGTTGTCCGACACGTG        1200
CGTAACAAGTAG       1212
```

A.2 The ORF of *T. cruzi* cASAT (TcCLB.503841.70).

```
ATGGCGATCCGATGCCTCTGGAACAACATTGCTGCCCTCCCAGCAGACCC          50
CATTTTTTCTGCTTCTTTGGTTGCGAAGAAAGCACCAGAACCAAAAGCAG         100
ACCTCATTATTGGCGCCTACCGTGATGCGGAAGGCCACCCATACCCCCTA         150
AATGTTGTAAGAAAAGCAGAACAACGCCTTCTGGAAATGAATGCCGACAA         200
GGAGTACCTACCAATGTCAGGGTATGCGCCCTTCATTGAAGAGTCTTTGA         250
AGATTGCTTATGGGGACAGTGTGGCGCGTGAAAATGTGGTGGGCATACAG         300
GGACTGAGCGGCACAGGGTCACTCAGTATTGGAGCGTGTTTCCTCGCCCG         350
TGTACTCTCGCGCGACACTCCTGTGTACATTTCCGATCCGACGTGGCCAA         400
ACCACTACGCTGTTATGGCCGCGGCAAATCTGACCGACTTACGCAAGTAC         450
CGTTACTACGACAACGCCAAACGTTGCATTGACTTTGATGGTCTTTTAGA         500
AGACCTCAACGGGGCGCCGGAGGGCAGTATTGTGATCCTGCATGCCTGTG         550
CACATAATCCGACAGGTATGGACCCGACCCACGAACAATGGGCCAAAATT         600
TTGGAGGTTTTCCAGGCGCGTCGTCTCATTCCCTTCTTTGACTCTGCATA         650
TCAGGGATATGCCACCGGAAGCCTTGATAATGACGCCTATTCGATTCGTC         700
TCTTTGCACGACAAGGGATGGAAATGCTTCTTGCACAGTCCTATTCAAAG         750
AATATGGGCCTGTACGCAGAGCGTGTGGGTGTCTGCTCCATTGTCACAGC         800
CAACCCAAAGAAGGCACCGTTGATTAAGTCGCAGCTTGAAACGATCGTAC         850
GTAGCCAATATTCCACTCCACCGGCTCACGGTGCTCGAGTGGCGTACCTC         900
GTCTTGAGCGACCCTGAACTTCGTGCAGGGTGGGAGCAGGAGTTGCGAGT         950
AATGTCGACGCGTGTGCTCGAAATGCGCCAAGCTTTGTACGATGGCCTCA        1000
AGAGACTCGGTACCCCTGGCTCCTGGGAACATATTATTCAGCAGGTTGGA        1050
ATGTTTTCATATCTTGGTCTCACGAAGGCCCAGTGTGAAAAACTTATTGA        1100
AAGGCGTGTCTTTGTACTCCCATCCGGACGTGCAAACATGGCTGGTCTAA        1150
CAAAAAGGTCAGTGGAACTGCTTGTAAAAGGCATCGACGAGGTGGTAAGA        1200
ACCGTCACGGAATGA       1215
```

B The amino acid sequences of *T. brucei* and *T. cruzi* cASAT.

B.1 The amino acid sequence of *T. brucei* cASAT (TbcASAT).

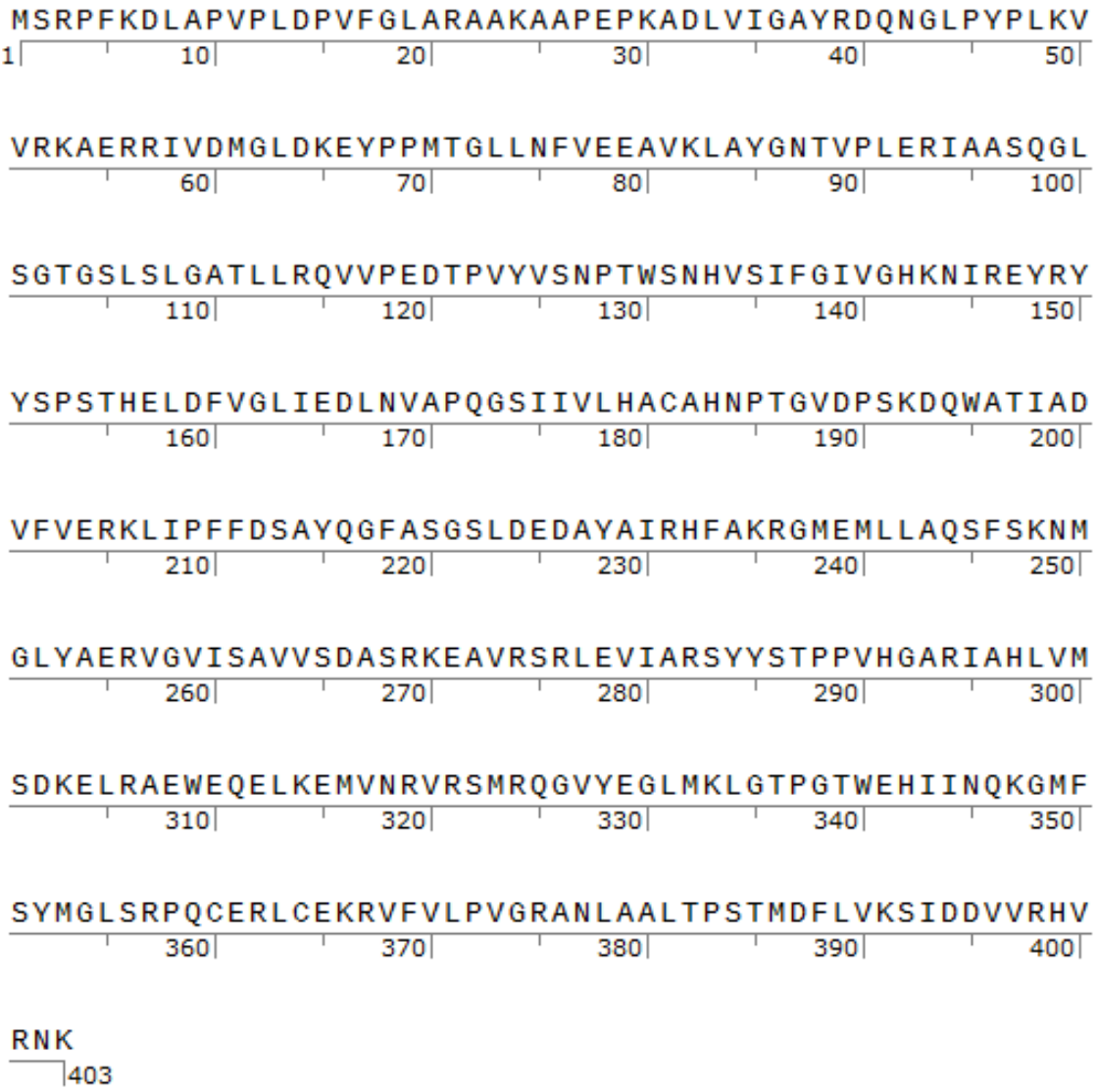

B.2 The amino acid sequence of *T. cruzi* cASAT (TccASAT).

```
MAIRCLWNNIAALPADPIFSASLVAKKAPEPKADLIIGAYRDAEGHPYPL
1|        10|        20|        30|        40|        50|

NVVRKAEQRLLEMNADKEYLPMSGYAPFIEESLKIAYGDSVARENVVGIQ
        60|        70|        80|        90|       100|

GLSGTGSLSIGACFLARVLSRDTPVYISDPTWPNHYAVMAAANLTDLRKY
       110|       120|       130|       140|       150|

RYYDNAKRCIDFDGLLEDLNGAPEGSIVILHACAHNPTGMDPTHEQWAKI
       160|       170|       180|       190|       200|

LEVFQARRLIPFFDSAYQGYATGSLDNDAYSIRLFARQGMEMLLAQSYSK
       210|       220|       230|       240|       250|

NMGLYAERVGVCSIVTANPKKAPLIKSQLETIVRSQYSTPPAHGARVAYL
       260|       270|       280|       290|       300|

VLSDPELRAGWEQELRVMSTRVLEMRQALYDGLKRLGTPGSWEHIIQQVG
       310|       320|       330|       340|       350|

MFSYLGLTKAQCEKLIERRVFVLPSGRANMAGLTKRSVELLVKGIDEVVR
       360|       370|       380|       390|       400|

TVTE
    404
```

C The nucleotide & amino acid sequences of *T. cruzi* AHADH.

C.1 The ORF of *T. cruzi* AHADH (TcCLB.506937.10).

```
ATGTTTTTTGAAGGTGCATGCGCGAAGGTGGTCGTCTCGGGGGCGGCCGG        50
CCAAGTTGGGTACGCATTACTCCCCCTCATTGCCGGCGGCCGCATGTTGG       100
GTCCCAATCAACATCTGCAGCTGAACCTGCTCGATATTGAGCCCGCCATG       150
AAATGTCTTGAGGGGATACGTGCGGAACTCATGGACTGTGCCTTCCCACT       200
GCTGGACCGTGTTGTCATCACGCACAAACCGGCGGTGGCCTTTGAGAATG       250
TTGATATCGCCATTCTCTGTGGCTCGTTTCCGGCCAAACCCGGCACGCTG       300
CGGAGGGATCTCCTGCAGAAAAATGCCGCAATTTTTTCAGAACATGGGCG       350
TCTTTTGGGTGAATTGGCCAGTAAAGACTGCCACGTGTGTGTTGTGGGCA       400
ATCCTGTCAACACCAATGCCCTTGTTCTTTTGAATGCCTCGAACGGGAAA       450
ATCAAGCCGAAGAACGTGTCGGCGCTTACGCGACTGGACCACAACCGTTC       500
GCTTGCGCTTGTGGCAGAGCGAGCCAATGCTCATGTTCGAGATGTCAAGA       550
ACTGTATTATTTGGGGAAACCACAGCGGTACACAAGTCCCGGATGTTAAC       600
AGCGCCACTGTGAGAGGCGTCCCTGTGCGAGAAGCGATAAAGGATGACGC       650
GTACTTTGATGGAGAATTTATGACAACTGTGCAGCAACGCGGGTATGAGA       700
TTATTCGGTGGCGCGGCAACTCTTCGGCTCTTTCTGCCGCAAATGCCGCT       750
GTTGACCAAGTGCACGACTGGGTTCTTGGTACGCCAACGGGGACACATGT       800
TTCCATGGCTGTGTATTCCGATGGTAACCCATACGGTGTGCCACCAGGCC       850
TTGTCTTCTCCTTCCCCGTGACATGCAGCGGAGGTGAGTGGCAGTTTGTC       900
GAGAATGCGTGTGTTACGCCGAGTGTGGCGAAACATTTGGCTGCCACCAC       950
CAAAGAGTTGGAAGAGGAACGGTCGGAGTCGCTGTCTTTGGCATTGTAA       999
```

C.2 The amino acid sequence of *T. cruzi* AHADH.

D The nucleotide sequences of Trypanosomatida and Higher Eukaryote cASAT ORFs.

>T.gambiense Tbg972.10.4560
MSRPFKDLAPVPLDPVFGLARAAKAAPEPKADLVIGAYRDQNGLPYPLKVVRKAERRI
VDMGLDKEYPPMTGLLNFVEEAVKLAYGNTVPLERIAASQGLSGTGSLSLGATLLRQV
VPEDTPVYVSNPTWSNHVSIFGIVGHKNIREYRYYSPSTHELDFVGLIEDLNVAPQGS
IIVLHACAHNPTGVDPSKDQWATIADVFVERKLIPFFDSAYQGFASGSLDEDAYAIRH
FAKRGMEMLLAQSFSKNMGLYAERVGVISAVVSDASRKEAVRSRLEVIARSYYSTPPV
HGARIAHLVMSDKELRAEWEQELKEMVNRVRSMRQGVYEGLMKLGTPGTWEHIINQKG
MFSYMGLSRPQCERLCEKRVFVLPVGRANLAALTPSTMDFLVKSIDDVVRHVRNK

>T.evansi TevSTIB805.10.3890
MSRPFKDLAPVPLDPVFGLARAAKAAPEPKADLVIGAYRDQNGLPYPLKVVRKAERRIV
DMGLDKEYPPMTGLLNFVEEAVKLAYGNTVPLERIAASQGLSGTGSLSLGATLLRQVVP
EDTPVYVSNPTWSNHVSIFGIVGHKNIREYRYYSPSTHELDFVGLIEDLNVAPQGSIIV
LHACAHNPTGVDPSKDQWATIADVFVERKLIPFFDSAYQGFASGSLDEDAYAIRHFAKR
GMEMLLAQSFSKNMGLYAERVGVISAVVSDASRKEAVRSRLEVIARSYYSTPPVHGARI
AHLVMSDKELRAEWEQELKEMVNRVRSMRQGVYEGLMKLGTPGTWEHIINQKGMFSYMG
LSRPQCERLCEKRVFVLPVGRANLAALTPSTMDFLVKSIDDVVRHVRNK

>T.rangeli TRSC58_05843
MSAKSLWDGINSLPPDAIFAIAAEAKKAPQPKADLIIGAYRDADGRPYPLKVVRKAERR
LLEMNLDKEYLPMAGYGPLIEESMKLIYGNSVPRENLVGAQGLSGTGSLCLGAFFISRV
LSPKTPVYISNPTWPNHYAVMSAAGMTDLRQYRYYDETRRRLNFEGLMEDLRAAPAGSV
VILHACAHNPTGMDPSHAQWGEMAELFRTHRLIPFFDSAYQGYATGSLENDAYAVRLFA
QQGMEMLVAQSYSKNMGLYAERVGVCSIVTANPAKAPMIKVQLEHVARSLYSSPPAHGA
RVAHLVLSDPELRSEWEAELCGMAQRVQEMRQDVYNGLKQRGTPGNWEHVVRQVGMFSY
LGLNKAQCARLAEKRVFVLASSRANMASLTKHTTGLLVDAIDDVVRDVTLASQGESTGA
AAKM

>T.congolense TcIL3000_10_2990
MATFSRNVTAIPRDSTFALAATAKAAPPPKVDLIIGAYRDENGLPYPLRAVRKAERRIV
DMGLDKEYSPMRGLSHFIEEALKLAYGADAPMERIAAIQSLSGTGALSLGATLLAQILP
NGTPVYVSNPTWPNHPSVFSIVGHKDVREYRYYDSTTRSLDFSGFIADLQAAPAGSIVV
LHACAHNPTGVDPTKEQWAAIADVFLAKKLVPFFDMAYQGFASGNFDEDAYSVRLFQSK
GMEMLLAQSFSKNMGLYGERVGVCSVVVKDPARKDPVLSRLECIGRSYYSTAPLHGARV
AHLVMSDKELRAEWEQEVREMVSRIKNMRKAVYDGLVERKTHGSWEHIITQKGMFSYLG
LSRPQCQRLIEKKCFVMPTSRANMAALTPHTVDFFITSVDEVVRQFRSA

>T.grayi DQ04_04421000
MTSFWENVKAAVPDAIFALALEAKNAPEPKADLIIGAYRDPEGRPYPLQVVRKAEKLLVV
DIKPEKEYLPMSGYQPFIDEAVKLAYADSVPRERVAAVQGLSGTGSLSLGACFLAQLMPR
DVVVYISDPTWPNHYAVMRAAGLTNTRTYRYYNAATRSLDIEGLLADLRAAPERSIVILH
ACAHNPTGVDPTHAQWEQIAEVFKARQLIPFFDSAYQGYATGNLDEDAYAIRLFARQGME
MLVAQSFSKNMGLYSERVGACSVVVSNPEKAAAVKANLETVARSYYSNPPAHGARLAHLV
LSDKTMRKEWEDELRGMAARVLEMRKDVYDGLTKRGTPGTWDHVLSQVGMFSYLGLTKAQ
CEKLVEKRVFVLPSGRANMAGLTKASVQLLVDAIDEVVRAAPSQ

>T.vivax TvY486_1003700
MTSIFKDLEPAPRDPILALSLDARAAKEPKADLIIGAYRDEEGRPYPLQVVRKAEQRL
ISMGLDREYLPMFGHGPFIEEATKMAYGDSVPMERVVGAQGLSGTGSLSLGAHLLCRV
LPADTAVYVSTPTWPNHYAVFRAAGLKNIREYRYYDPKTRRLDFEGLIEDLKAAPAGS
IVVLHACAHNPTGVDPTKEQWQKIADVCKSGRLTPFFDSAYQGYATGSLVNDVYSVRL
FAKMGLEIVLAQSFAKNMGLYCERVGVCSVAVSDASKTAAIRACFESIARSFYTTPPA
HGARVAHLVLSDPELRKEWEEELGKMVKRVQAMRRAVYDGLKKRGTPGTWEHVIDQIG
MFSYLGLTEEQCLKLREKRVFVLNSGRANMAALTHASVDVVVKAIDEVVRETQGK

>T.equiperdum SCU71015.1
MSRPFKDLAPVPLDPVFGLARAAKAAPEPKADLVIGAYRDQNGLPYPLKVVRKAERRI
VDMGLDKEYPPMTGLLNFVEEAVKLAYGNTVPLERIAASQGLSGTGSLSLGATLLRQV
VPEDTPVYVSNPTWPNHVSIFGIVGHKNIREYRYYSPSTHELDFVGLIEDLNVAPQGS
IIVLHACAHNPTGVDPSKDQWATIADVFVERKLIPFFDSAYQGFASGSLDEDAYAIRH
FAKRGMEMLLAQSFSKNMGLYAERVGVISAVVSDASRKEAVRSRLEVIARSYYSTPPV
HGARIAHLVMSDKELRAEWEQELKEMVNRVRSMRQGVYEGLMKLGTPGTWEHIINQKG
MFSYMGLSRPQCERLCEKRVFVLPVGRANLAALTPSTMDFLVKSIDDVVRHVRNK

>L.mexicana LmxM.34.0820
MSTQAAMTTTERWQKIQGRAPDPIFELAKRAAAAKGPKANLVIGAYRDEQGLPYPLRVVR
KAEQLLLDMNLNYEYLPISGYQPFIDEAVKMIYGDTVELENLVAVQTLSGTGALSLGAKL
LTHVFDAEKTPIYLADPTWPNHYSIVKAAGWKDIRTYAYYDHKTLGLDFEGMKKDILAAP
DGSVFLLHQCAHNPTGVDPSQEQWNEIASLMLAKHHQVFFDSAYQGYASGSLDTDAYAAR
LFARRGIEVLLAQSFSKNMGLYSERAGTLSLLLKDKTKRADVKSVMDSLIRAEYTCPPAH
GAHLAHLILSNNELRKEWEAELSAMAERIRTMRRTVYDELLRLQTPGRWEHVINQIGMFS
FLGLSKEQCEYCQNHNIFITLSGRANIAGLTHETALMLAQTINDAVRNVNRK

>C.fasciculata CFAC1_240033800
MSGSPTDNFDGLSALPPDSIFFTSQKAKAAQGPKADLIIGAYRDEHGCPYPLKTVRKAER
ILLDMNLDYEYLPMTGYKPFVDEATKIIYADSVAPDHLVAVQTLSGTGAVYLGAAFLAEV
YDPKTTPIYLPNPTWPNHPSILKLTGWKDIRTYNYYDPKTVALDFEGIKKDIQEAPECSV
FLLHQCAHNPTGVDPSHAQWEEIADLMLAKKHQVFFDSAYQGYASGSLDEDAFAARLFVK
KGVQFILAQSFSKNMGLYNERTGTLSVVLRNPERAAAVKTHLDLLIRANYSNPPAHGARL
VHLVLSDKELRKEWEAELAEMANRIRTMRHTVYDELKRLGTPGTWEHIINQIGMFSFLGL
SKEQCQYCQDHNVFILLSGRANMAGLTHDTALMLAKTIDEAVRTV

Figure 6. Nucleotide sequences of Trypanosomatida cASAT obtained from http://www.tritrypdb.org/.

>Mus musculus P05201
MAPPSVFAQVPQAPPVLVFKLTADFRDDPDPRKVNLGVGAYRTDESQPWVLPVVRKVEQK
IANDNSLNHEYLPILGLAEFRSCASRLVLGDNSLAIRENRVGGVQSLGGTGALRIGADFL
GRWYNGTDNKNTPIYVSSPTWENHNAVFSAAGFKDIRPYCYWDAEKRGLDLQGFLNDLEN
APEFSIFVLHACAHNPTGTDPTPEQWKQIAAVMQRRFLFPFFDSAYQGFASGDLEKDAWA
IRYFVSEGFELFCAQSFSKNFGLYNERVGNLTVVGKESDSVLRVLSQMEKIVRITWSNPP
AQGARIVAATLSDPELFKEWKGNVKTMADRILTMRSELRARLEALKTPGTWSHITEQIGM
FSFTGLNPKQVEYLVNEKHIYLLPSGRINMCGLTTKNLDYVATSIHEAVTKIQ

>Homo sapiens P17174
MAPPSVFAEVPQAQPVLVFKLTADFREDPDPRKVNLGVGAYRTDDCHPWVLPVVKKVEQK
IANDNSLNHEYLPILGLAEFRSCASRLALGDDSPALKEKRVGGVQSLGGTGALRIGADFL
ARWYNGTNNKNTPVYVSSPTWENHNAVFSAAGFKDIRSYRYWDAEKRGLDLQGFLNDLEN
APEFSIVVLHACAHNPTGIDPTPEQWKQIASVMKHRFLFPFFDSAYQGFASGNLERDAWA
IRYFVSEGFEFFCAQSFSKNFGLYNERVGNLTVVGKEPESILQVLSQMEKIVRITWSNPP
AQGARIVASTLSNPELFEEWTGNVKTMADRILTMRSELRARLEALKTPGTWNHITDQIGM
FSFTGLNPKQVEYLVNEKHIYLLPSGRINVSGLTTKNLDYVATSIHEAVTKIQ

>Gallus gallus P00504
MAASIFAAVPRAPPVAVFKLTADFREDGDSRKVNLGVGAYRTDEGQPWVLPVVRKVEQLI
AGDGSLNHEYLPILGLPEFRANASRIALGDDSPAIAQKRVGSVQGLGGTGALRIGAEFLR
RWYNGNNNTATPVYVSSPTWENHNSVFMDAGFKDIRTYRYWDAAKRGLDLQGLLDDMEKA
PEFSIFILHACAHNPTGTDPTPDEWKQIAAVMKRRCLFPFFDSAYQGFASGSLDKDAWAV
RYFVSEGFELFCAQSFSKNFGLYNERVGNLSVVGKDEDNVQRVLSQMEKIVRTTWSNPPS
QGARIVATTLTSPQLFAEWKDNVKTMADRVLLMRSELRSRLESLGTPGTWNHITDQIGMF
SFTGLNPKQVEYMIKEKHIYLMASGRINMCGLTTKNLDYVAKSIHEAVTKIQ

>Bos taurus P33097
MAPPSIFAEVPQAQPVLVFKLTADFREDPDPRKVNLGVGAYRTDDSQPWVLPVVRKVEQR
IANDSSINHEYLPILGLAEFRTCASRLALGDDSPALQEKRVGGVQCLGGTGALRIGAEFL
ARWYNGTNNKDTPVYVSSPTWENHNGVFIAAGFKDIRSYHYWDAAKRGLDLQGFLNDLEK
APEFSIFVLHACAHNPTGTDPTPEQWKQIASVMKRRFLFPFFDSAYQGFASGSLEKDAWA
IRYFVSEGFELFCAQSFSKNFGLYNERVGNLTVVAKEPDSILRVLSQMEKIVRITWSNPP
AQGARIVARTLSDPELFNEWTGNVKTMADRILTMRSELRARLEALKTPGTWNHITEQIGM
FSFTGLNPKQVEYLINEKHIYLLPSGRINMCGLTTKNLEYVATSIHEAVTKIQ

>C.fasciculata CFAC1_240033800
MSGSPTDNFDGLSALPPDSIFFTSQKAKAAQGPKADLIIGAYRDEHGCPYPLKTVRKAER
ILLDMNLDYEYLPMTGYKPFVDEATKIIYADSVAPDHLVAVQTLSGTGAVYLGAAFLAEV
YDPKTTPIYLPNPTWPNHPSILKLTGWKDIRTYNYYDPKTVALDFEGIKKDIQEAPECSV
FLLHQCAHNPTGVDPSHAQWEEIADLMLAKKHQVFFDSAYQGYASGSLDEDAFAARLFVK
KGVQFILAQSFSKNMGLYNERTGTLSVVLRNPERAAAVKTHLDLLIRANYSNPPAHGARL
VHLVLSDKELRKEWEAELAEMANRIRTMRHTVYDELKRLGTPGTWEHIINQIGMFSFLGL
SKEQCQYCQDHNVFILLSGRANMAGLTHDTALMLAKTIDEAVRTV

Figure 7. Nucleotide sequences of higher eukaryote cASAT obtained from http://www.uniprot.org/.

E ^{15}N-tryptophan mass spectrometry technical information.

Technical information modified from the quality control report provided by Glasgow Polyomics.

E.1 Analytical equipment.

Hydrophilic interaction liquid chromatography (HILIC) was carried out on a Dionex UltiMate 3000 RSLC system (Thermo Fisher Scientific, Hemel Hempstead, UK) using a ZIC-pHILIC column (150 mm × 4.6 mm, 5 μm column, Merck Sequant).

E.2 Analytical methods.

The column was maintained at 30 ^{o}C and samples were eluted with a linear gradient (20 mM ammonium carbonate in water, A and acetonitrile, B) over 26 min at a flow rate of 0.3 ml.min^{-1} as follows;

Time (min)	% A	% B
0	20	80
15	80	20
15	95	5
17	95	5
17	20	80
24	20	80

The injection volume was 10 μl and samples were maintained at 5 ^{o}C prior to injection. For the MS analysis, a Thermo Orbitrap QExactive (Thermo Fisher Scientific) was operated in polarity switching mode and the MS settings were as follows:

- Resolution 70,000.
- AGC 1e6.

- m/z range 70 - 1050.
- Sheath gas 40.
- Auxiliary gas 5.
- Sweep gas 1.
- Probe temperature 150 ^{o}C.
- Capillary temperature 320 ^{o}C.

For positive mode ionisation: source voltage +3.8 kV, S-Lens RF Level 30.00, S-Lens Voltage -25.00 (V), Skimmer Voltage -15.00 (V), Inject Flatopole Offset -8.00 (V), Bent Flatapole DC -6.00 (V). For negative mode ionisation: source voltage-3.8 kV.

The calibration mass range was extended to cover small metabolites by inclusion of low-mass calibrants with the standard Thermo calmix masses (below m/z 138), butylamine (C4H11N1) for positive ion electrospray ionisation (PIESI) mode (m/z 74.096426) and COF3 for negative ion electospray ionisation (NIESI) mode (m/z 84.9906726). To enhance calibration stability, lock-mass correction was also applied to each analytical run.